Wettability Estimation by Oil Adsorption

by

Samuel Erzuah

Thesis submitted in fulfilment of
the requirements for the degree of
PHILOSOPHIAE DOCTOR
(PhD)

University of
Stavanger

Faculty of Science and Technology
Institute of Energy Resources
2019

Preface

This thesis is submitted in partial fulfilment of the requirements for Doctor of Philosophy (PhD) degree in Petroleum Engineering at the Department of Energy Resources (Faculty of Science and Technology), University of Stavanger (UiS), Norway. This research work was predominantly carried out at NORCE Norwegian Research Centre AS (previously International Research Institute of Stavanger, IRIS). Scientific publications from this study include two conference and two journal papers. In addition, two manuscripts are also ready to be submitted to journals.

Dedicated to Nana Asonaba (Mr. Dickson Boachie)

Acknowledgements

Summary

Research related to oil reservoirs shows that wettability governs the distribution and flow properties such as relative permeability and capillary pressure. Hence, wettability is a vital parameter in reservoir multiphase flow. This has compelled numerous researchers to come up with techniques to accurately determine the wettability. Notable among these techniques include Amott method, United State Bureau of Mines (USBM) method and the flotation test. All these techniques measure a specific output to characterize the wettability. For instance, in the flotation test the wettability is characterized by the affinity of the rock/mineral sample to either the oil or the brine. In other words, the concentration of the rock/mineral sample in each phase determine the wetting preference of the sample. The existing wettability estimation techniques measure specific outputs but do not evaluate the mechanisms during the crude oil/brine/rock (COBR) interactions that triggered the observed outputs. Wettability as defined by Craig (1971) is the tendency of a fluid to adhere to a solid surface in the presence of other immiscible fluids. Hence, the aim of this PhD work was to estimate the wettability by capitalizing on the oil adhesion tendencies of the rock/mineral during Crude oil/Brine/Rock (COBR) interactions. This was accomplished using both experimental and simulation techniques.

To accomplish this, the flotation test which is one of the existing wettability characterization technique was used as the benchmark experiment to screen the rock (mineral) under the studied conditions. The rationale for selecting the flotation test is that it provides a fast and cheap wettability characterization. The contact angle measurements were also carried out to assess the wetting preferences of the mineral-fluids systems under the studied conditions. The wettability was also characterized by measuring the magnitude of oil adsorbed onto mineral surfaces using Quartz Crystal Microbalance with Dissipation (QCM-D) device. The QCM-D is a microbalance device that relies on the changes in the frequency (Δf) of a resonating crystal to measure the interactions on the sensor such as adsorption or desorption. Hence, the QCM-D technique can be used in wettability characterization. For given mineral/brine/oil systems, the QCM-D measures the change in the

frequency (Δf) which is proportional to the magnitude of the adsorbed oil (Δm_{ads}). In other words, lack of oil adsorption is depicted by negligible change in the frequency ($\Delta f \approx 0$ Hz) of the oscillating crystal. On the other hand, the higher the reduction in the frequency of the resonating crystal, the higher the magnitude of the adsorption. This was attributed to the added mass resulting from the adsorption due to the polar oil component in the crude oil unlike the n-decane. Prior to qualifying the QCM-D device as a wettability characterization tool, the QCM-D technique was confronted with numerous challenges notably corrosion, dissolution of the sensor coating (sensor etching), fluid trapping inside the flow-cell and the salt precipitation. The detail description of these challenges and how they were mitigated have been discussed in the later part of the thesis.

To understand the wetting preferences of the minerals during the flotation and QCM-D test, the COBR interactions were studied via Surface Complexation Modelling (SCM). The SCM was used to evaluate the oil adhesion tendencies resulting from the attractive bond existing between the mineral-brine and the oil-brine interfaces. Similar surface reactions and their reaction constants for numerous surfaces (oil and brine) have been reported in literature. Hence, the plan was to use these existing SCM data to better understand the experimental results. It can be concluded that, the SCM could explain the oil adhesion tendencies of the mineral during the flotation tests and the QCM-D experiments. The advantage of the SCM technique is that, it can also predict the mechanisms that led to the oil adhesion such as direct adhesion of carboxylate ($>COO^-$) onto positive mineral sites or by divalent cations (Ca^{2+} & Mg^{2+}) bridging. Hence, the SCM can be used to screen potential injection water compositions to assess their effect on the oil recovery efficiency. Moreover, the SCM technique was successfully used to predict the trend in zeta potential measurement from literature.

The application of SCM was extended to predict wettability of mineral mixtures and reservoir rocks. For the studied sandstone rocks, and mineral mixtures, it was observed that the wettability was inclined towards the mineral with largest surface area provided the calcite contents is low. However, as the calcite content increases, the wetting preferences of the rock is dictated by the calcite content and not the

dominant surface area. In addition, the SCM technique has successfully been used to assess the mechanisms during spontaneous imbibition in chalk with carbonated water (CW). The SCM technique has also been successfully used to capture the trend in some existing wettability data using the Amott and the USBM techniques. The SCM technique has also been used to capture the trend during contact angle measurements using Drop Shape Analyzer (DSA) device.

The SCM technique can be described as a fast and cheap technique of estimating the wettability. This is because, the properties and the qualities of the rock-fluids in question are used as input into the model. The challenge is that the current model is based on batch reactions. Hence, the future plan is to develop a robust in-situ wettability simulator by incorporating into the existing model, the kinetics of the minerals (e.g. dissolution rate) and their distribution in the reservoir rock.

List of Publications

I. Erzuah, Samuel; Fjelde, Ingebret; Omekeh, Aruoture Voke (2017). Wettability Characterization Using the Flotation Technique Coupled with Geochemical Simulations. In: *19th European Symposium on Improved Oil Recovery/IOR Norway 2017*. European Association of Geoscientists and Engineers. ISBN 978-94-6282-209-2

II. Erzuah, Samuel; Fjelde, Ingebret; Omekeh, Aruoture Voke (2019). Wettability Estimation by Surface Complexation Simulations. *SPE Reservoir Evaluation & Engineering Journal* **22** (02): 509-519. SPE-185767-PA.

III. Erzuah, Samuel; Fjelde, Ingebret; Omekeh, Aruoture Voke (2018). Challenges Associated with Quartz Crystal Microbalance with Dissipation (QCM-D) as a Wettability Screeening Tool. *Oil & Gas Science and Technology–Revue d'IFP Energies nouvelles* **73**: 58.

IV. Erzuah, Samuel; Fjelde, Ingebret; Omekeh, Aruoture Voke (2018). Wettability Estimation by Oil Adsorption Using Quartz Crystal Microbalance with Dissipation QCM-D. Society of Petroleum Engineers. doi:10.2118/190882-MS.

V. Erzuah, Samuel; Fjelde, Ingebret; Omekeh, Aruoture Voke. Effect of the Intrinsic Properties of Reservoir Rock Minerals on Wettability via Surface Complexation Modelling (SCM). Manuscript.

VI.   Erzuah, Samuel; Fjelde, Ingebret; Omekeh, Aruoture Voke. Surface Complexation Modelling (SCM) as a New Wettability Screening Tool versus the Existing Techniques. Manuscript.

Table of Contents

List of Figures

List of Tables

List of Symbols

A_1	Area under the secondary drainage curve
A_2	Area under the imbibition curve
A_{eff}	Effective surface area of the rock
C	Mass sensitivity constant of the sensor ($ng\ cm^{-2}\ Hz^{-1}$)
F	Faraday constant ($C\ mol^{-1}$)
I_{AH}	Amott-Harvey Index
I_o	Displacement by oil index
I_{o-w}	Wettability index from flotation tests
I_w	Displacement by water index
N_A	Avogadro's constant ($6.022140857\times10^{23}\ mol^{-1}$)
R	Universal gas constant ($m^3\ Pa\ K^{-1}\ mol^{-1}$)
T	Temperature (K^{-1})
V_{osp}	Volume of oil produced after spontaneous imbibition of water into the core (ml)
V_{od}	Volume of oil produced after force imbibition of water into the core (ml)
V_{wsp}	Volume of water produced after spontaneous imbibition of oil into the core (ml)
V_{wd}	Volume of water produced after force imbibition of oil into the core (ml)
V_b	Volume of brine (ml)
V_o	Volume of oil (ml)
W	USBM wettability index
W_T	Total weight of minerals (g)
W_{O-W}	Total weight of oil-wet minerals (g)
W_{W-W}	Total weight of water-wet minerals (g)
Z	Surface charge
">"	Denotes surface groups either oil or mineral surfaces
f_{ref}	Reference FW frequency signal (Hz or s^{-1})
f_{ads}	Frequency signal with the adsorbed film (Hz or s^{-1})
ΔD	Change in dissipation (ppm)
Δf	Change in resonant frequency (Hz or s^{-1})
Δm_{ads}	Mass of the adsorbed film ($\mu g/cm^2$)
n	Frequency harmonic number (Dimensionless)
t_q	Thickness of the quartz sensor (cm)
Δt_{ads}	Thickness of the adsorbed film (nm)

Abbreviations

BP	Bond Product (Dimensionless)
BPV	Back-pressure valve
COBR	Crude oil/brine/rock
DSA	Drop Shape Analyzer
DW	Distilled water/deionized water
FW	Formation water
M_w KOH	Molecular weight of KOH (56.105 g/mol)
LSW	Low Salinity Water
PSR	Pseudo-Sandstone Rock
QCM-D	Quartz Crystal Microbalance with Dissipation
QHPT	High Pressure High Temperature QCM-D device
SCM	Surface Complexation Modelling
SRR	Sandstone Reservoir Rock
STO	Stock Tank Oil
TAN	Total Acid Number (mg KOH/g oil)
TBN	Total Base Number (mg KOH/g oil)
TBP	Total Bond Product (Dimensionless)
USBM	United State Bureau of Mines

Greek

θ	Contact angle (degrees, º)
σ_A	Adhesion tension
σ_{os}	Interfacial tension (IFT) at the oil-solid interface
σ_{ws}	Interfacial tension (IFT) at the water-solid interface
σ_{ow}	Interfacial tension (IFT) at the oil-water interface
ρ_q	Density of the quartz crystal (g/cm^3)
v_q	Shear wave velocity of the quartz crystal (cm/s)
μ_q	Shear modulus of the quartz crystal (g cm^{-1} s^{-2})
f_o	Resonance frequency (Hz)
ψ	Electric potential

Part I

1   Introduction

In reservoir multiphase flow, wettability is a crucial parameter that governs the fluid phase distribution and flow properties in the oil reservoir (Anderson 1986b; Anderson 1986c; Morrow 1990). Research has shown that wettability governs the electrical properties, capillary pressure, relative permeability, irreducible saturation and other Enhanced oil Recovery (EOR) processes (Anderson 1986a; Anderson 1986b). In other words, the wettability of the reservoir rock is a vital parameter in optimizing oil recovery by drive fluid (Buckley et al. 1989; Radke et al. 1992). For instance, Morrow (1990) reported that waterflooding in a strongly oil-wet medium is less efficient due to early breakthrough. On the contrary, waterflooding in a water-wet medium leads to late breakthrough time (Morrow 1990). To add to the above, Cockcroft et al. (1989) reported that the wetting preferences of the reservoir rock is an inevitable parameter that is considered during the selection of field development options and the oil recovery potential.

Due to the role of wettability on oil recovery, numerous techniques have been developed to measure wettability. The Amott and the United State Bureau of Mine (USBM) methods are the oil and gas industry accepted wettability estimation techniques (Anderson 1986a). These existing techniques predict the wettability by measuring a specific output such as the total volume of fluid spontaneously and forcibly imbibed by a core (Amott method) and the area under the capillary pressure curve (USBM). Nonetheless, mechanisms during the crude oil/brine/rock (COBR) interactions that triggered the observed outputs are not evaluated by these techniques. The aim of this PhD work was to estimate the wettability by capitalizing on the oil adhesion tendencies of the minerals.

According to Craig (1971), wettability is the tendency of oil to spread on or adhere to the surface of a solid in the presence of another immiscible fluids. Since water is the most abundant fluid on earth, it is assumed that prior to the crude oil accumulating into the reservoir, the formation water is the main reservoir fluid. Hence, the original wettability of the reservoir rock can be said to be strongly water-wet. Research has shown that the

adsorption of polar oil component onto the pore walls of the reservoir rock will lead to less water-wet state (Hui & Blunt 2000). Wettability only becomes significant after crude oil accumulation into the reservoir. Numerous researchers have reported that direct contact of the crude oil with the pore walls of the reservoir rock can lead to a less water-wet condition (Hui & Blunt 2000; Rao & Maini 1993). Busireddy and Rao (2004) reported that the adsorption of polar oil components in the crude oil is controlled by numerous forces such as van der Waals, hydration and electrostatic forces. On the other hand, Buckley et al. (1989) reported that lack of oil adhesion can be attributed to the expansion of the double layer. Thus, stabilizing the water film existing between the rock-brine and oil-brine interfaces. In this PhD work, the emphasis was placed on the role of the attractive electrostatic forces existing between the rock-brine and oil-brine interfaces on oil adhesion.

1.1   Motivation and objectives

Prior to the crude oil accumulation into the reservoir, the formation water (FW) is assumed to be the only fluid existing in the reservoir. In the absence of crude oil in the reservoir, the FW is the only fluid available to wet the surface of the reservoir. Hence, the reservoir rock can be termed water-wet. However, after the crude oil accumulation into the reservoir, there exist multiphase flow in the reservoir. Now the question, which of these fluids (FW or crude oil) will adhere to the surface of the reservoir rock arises. Thus, the term wettability. Wettability according to Craig (1971) is the tendency of a fluid to spread on or adhere to a solid surface in the presence of other immiscible fluids. Consequently, for multiphase flow in an oil reservoir, if the magnitude of the oil retained on the reservoir rock surface can be measured, the wetting preferences of the reservoir rock can be determined.

The main aim of this PhD study is to estimate wettability via oil adsorption using both experimental and simulation techniques.
- ✓ To accomplish this, the flotation test will be used as the reference wettability screening tool to characterize the wetting preferences of the crude oil/Brine/Rock (COBR) systems used in this study. The flotation test relies on the affinity of the reservoir rock to either the brine (FW) or the oil.

✓ In addition, contact angle measurements will also be employed to characterize the wetting tendencies of the COBR systems using Drop Shape Analyzer (DSA) device.

✓ Furthermore, Quartz Crystal Microbalance with Dissipation (QCM-D) device will also be used to measure the magnitude of oil adsorption onto mineral surfaces during COBR interactions. This will be accomplished by capitalizing on the changes in frequency (Δf) of the resonating sensor to estimate the magnitude of oil adsorption.

✓ To add to the above, the wetting preferences during the experimental methods (flotation test and QCM-D technique) will also be predicted using Surface Complexation Modelling (SCM). The SCM technique relies on the electrostatic attraction existing between the oil-brine and mineral brine-interfaces to estimate the oil adhesion tendencies of the minerals.

✓ Finally, the oil-brine and mineral-brine interactions for some laboratory experiments from literature (e.g. zeta potential measurement, spontaneous imbibition test, Amott and USBM wettability measurements) will also be predicted to validate the SCM technique.

1.2 Structure of the thesis

This thesis is divided into two sections namely, Part I and Part II. In the Chapter 1 of Part I, the focus of this PhD studies is introduced after which the background is also presented. In addition, the compelling factor to undertake this study is presented next. The fundamental studies on wettability estimation is presented in Chapter 2. These includes overview of wettability and its effect on oil recovery, factors controlling wettability, and the effect of surface forces on oil adhesion. The existing techniques of estimating wettability is presented next. This is then followed by the description of the principles surrounding the proposed wettability technique namely, wettability estimation by Surface Complexation Modelling (SCM) and wettability estimation by oil

adsorption using Quartz Crystal Microbalance with Dissipation (QCM-D). Chapter 3 also focuses on the methods employed during the PhD studies namely flotation test, QCM-D technique, SCM approach and the contact angle measurements. In addition, the challenges confronted during the qualification of the QCM-D technique as a wettability characterization tool and how they were averted are also presented in this chapter. Chapter 4 gives a detailed description of Surface Complexation Modelling (SCM) and how it models wettability. The entire chapter 4 is dedicated for SCM technique of wettability estimation. This is due to its fast but cheap wettability characterization approach. Although SCM is not new in the oil and gas industry, its application in wettability estimation is yet to be fully exploited in the oil and gas industry. In this chapter, the focus is on modelling experimental results using SCM. Chapter 5 talks about the main results and discussions. The experimental results will be presented first followed by their simulated counterparts. Since the flotation test is the reference experiment, its results will be presented first followed by the QCM-D before that of the contact angle measurements. Note that, the simulated experimental results via SCM will also be presented together with their respective experimental results. The last chapter of Part I (Chapter 6) focuses on the conclusions and the future work before presenting the list of references (Chapter 7). The published and unpublished papers based on this study are also appended in Part II of the thesis.

2   Theory

In this chapter, some of the basic concept related to wettability will be elucidated. This include but not limited to overview of wettability, effect of wettability on oil recovery, factors that governs wettability and the role of surface forces in oil adhesion. In addition, the existing techniques of estimating wettability will be discussed prior to proposing the rationale behind the studied wettability techniques.

2.1   Wettability and its effect on oil recovery

Wettability is an essential parameter in reservoir multiphase flow due to its role in the oil recovery efficiency. It is defined as the ability of a fluid to preferentially wet a solid surface in the presence of other immiscible fluids (Craig 1971). Research has shown that wettability controls rock-fluid properties such as electrical properties, relative permeability, irreducible saturations, waterflood behavior and many flow properties in the oil reservoir (Anderson 1986b; Anderson 1986c, 1987; Torsaeter 1988). During waterflooding, it has been shown that early breakthrough occurs in strongly hydrophobic medium as compared to strongly hydrophilic medium (Raza et al. 1968) as illustrated in Figure 1. Numerous researchers have reported that rock-fluid properties can indirectly be linked to the wetting preferences of the reservoir rock minerals as observed in well logs (Cockcroft et al., 1989; Desbrandes et al., 1990; Desbrandes & Gualdron, 1987). In view of this, comprehensive studies have been carried-out to understand the role of wettability in oil recovery and the factors that governs the wetting preferences of reservoir rock minerals. In line with this, some of the findings from the existing wettability techniques will be discussed in this section.
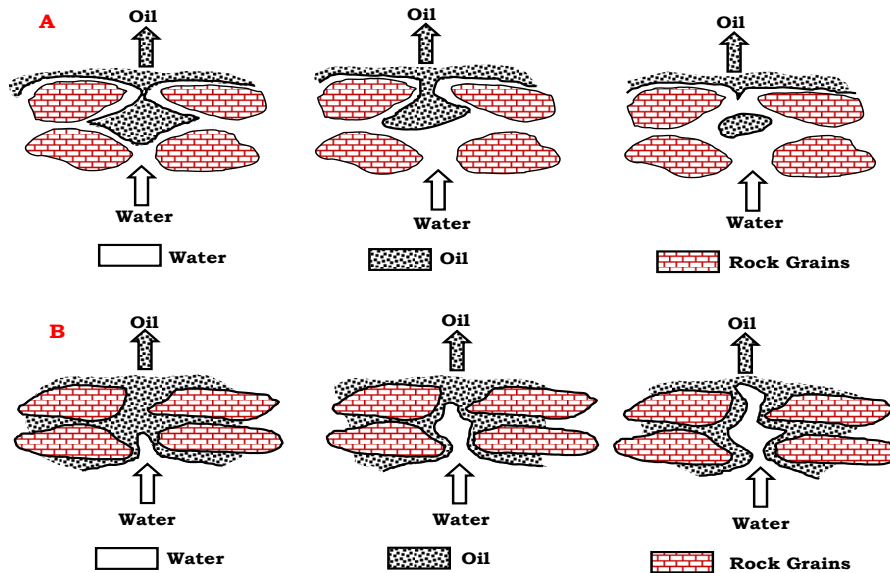
Figure 1: Effect of wettability on breakthrough time during waterflooding. Late breakthrough occurs for strongly hydrophilic rock (Section A) while early breakthrough occurs in hydrophobic medium (Section B). Redrawn after Raza et al. (1968).

2.2   Factors that controls wettability

Research has shown that numerous factors governs wettability. These factors include but not limited to ionic composition of the brine, the mineralogical composition of the rock and oil chemistry (Anderson 1986a; Buckley et al. 1989).

2.2.1   Mineralogical composition

Minerals are the building blocks of rocks (Plummer et al. 1994). Hence, the intrinsic properties of a rock-brine system such as surface charge and surface area is dictated by the predominant mineral (either surface area or mass fraction) in the rock. For instance, above pH 2 silicate-brine interfaces are mainly negatively charged while calcite-brine interface on the other hand are mostly positively below pH 9.5 (Buckley & Liu 1998). It has been reported by numerous researchers that the surface-active components in both rock (minerals) and the crude oil surfaces can interact with each other during COBR interactions (Buckley et al. 1998;

Cuiec 1975). Hence above pH 2, cationic oil component can be adsorbed directly onto silicate surface due to the unlike charges. In a similar vein, anionic oil component can be adsorbed onto the calcite surface at pH below 9.5. To add to the above, numerous rock-brine interactions such as sorption, adsorption, precipitation, desorption, and dissolution are bound to occur prior to the crude oil accumulation. To replicate the wetting preferences of the reservoir rock, these interactions prior to the crude oil accumulation into the reservoir should not be ignored.

2.2.2   Crude oil composition

Like the mineralogy of the rock, the crude oil composition also has a pronounced effect on the wetting properties of the reservoir rock. Saturates, Aromatic, Resins and Asphaltenes (SARA) are the dominant components in the crude oil composition (Fan et al., 2002). Moreover, it has been reported that the surface-active components in the crude oil are concentrated in the heavy end fractions such as asphaltene and resins (Dubey & Waxman 1991). Buckley et al. (1998) stipulated that crude oil can also be characterized using the Total Acid Number (TAN), Total Base Number (TBN) and the API gravity. It has also been reported that the polar oil component in the crude oil can be acidic, basic or non-ionic (Dubey & Doe 1993).

2.2.3   Ionic composition of brine

Comprehensive studies have been carried out on the effect of ionic composition of the brine on oil adhesion (Buckley & Liu 1998; Buckley et al. 1998). For instance, it has been reported that ions such as Ca^{2+} and Mg^{2+} can bridge oil-brine and rock-brine interfaces with negatively charges, thereby leading to oil adhesion (Buckley & Liu 1998). This has led to an increase in smart water and low salinity water (LSW) research with the mindset of getting an optimal composition of the injected brine that has the tendency to optimize the oil recovery.

2.3   Effect of Surface Forces on oil adhesion

During COBR interaction, surface forces such as electrostatic, Van der Waals and hydration forces can lead to oil adsorption onto reservoir rock

(Busireddy & Rao 2004). For instance, Rao and Maini (1993) stipulated that in order to release and mobilize adsorbed oil to flow with the injected brine, the surface forces that led to the oil adsorption must be exceeded. With respect to this, comprehensive studies have been carried out on the role of electrostatic forces on oil adhesion (Brady & Krumhansl 2012b; Brady et al. 2012).

2.4   Existing wettability estimation techniques

Remarkable strides have been made by numerous researchers in the pursuit of fast, cheap and accurate wettability estimation techniques. For instance, Gomes et al. (2008) estimated the wetting preferences of reservoir rock sample using Special Core Analysis (SCAL) approach. According to Anderson (1986a), these techniques are either qualitative or quantitative. The qualitative wettability characterization techniques provide relatively quick but approximate wettability estimates. Anderson (1986a) reported that the qualitative techniques include but not limited to flotation method, microscope examination method, glass slide method, capillary pressure curve method, relative permeability curve method, reservoir log method, nuclear magnetic resonance method and dye adsorption approach.

Unlike the qualitive wettability estimation techniques, the quantitative counterparts are relatively time-consuming approach of characterizing the wettability and they assign numerical value to the wettability measurement (Anderson 1986a). These techniques include Amott test, United State Bureau of Mines (USBM) method and the contact angle measurement technique. In this section, the qualitative approach will be presented first followed by its quantitative counterpart.

2.4.1 Qualitative wettability techniques

The qualitative techniques are fast approaches of estimating the wettability. Nevertheless, they do not assign numerical values to the wettability estimate.

2.4.1.1 **Flotation test**

The flotation test relies on the affinity of the reservoir rock (mineral) sample to either the brine or the oil phase. The rationale behind the flotation test is to replicate the rock-fluids interaction prior to and after the crude oil accumulation into the reservoir. The flotation test is recommended for strongly wetted system (Anderson 1986a). The flotation test is confronted with limitations such as particles size and density. Mwangi et al. (2013), characterized the wetting preferences of the rock (mineral) samples under different reservoir conditions using the flotation test. The flotation test was used as the reference experiment to characterize the rock-fluids systems used in the PhD work. Detailed flotation test procedure is presented in Chapter 4 under the method section and it is similar to the ones reported in literature (Dubey and Doe 1993; Mwangi et al. 2013).

2.4.1.2 **Microscope examination method**

Microscope examination method is a visual examination approach of characterizing wettability by describing the fluid distribution around the pore surface via a microscope (Anderson 1986a). This technique is very important in assessing the effect of wettability alteration chemicals during Crude Oil/Brine/Rock (COBR) interactions at the pore scale (Anderson 1986a).

2.4.1.3 **Glass slide method**

The glass slide method is hinged on the rate at which the wetting phase displaces the non-wetting phase (Anderson 1986a). In this technique, the glass slide is assumed to be a replica for the reservoir rock. According to Anderson (1986a), the glass slide is aged in their respective fluids (crude oil and brine) simultaneously by suspending it in a transparent vessel containing both brine and crude oil. At the end of the ageing period, the glass slide is then dipped into the brine phase to determine the wetting state. If the brine quickly displaces the crude oil from the glass slide, it can be described as water-wet. On the other hand, if the brine slowly displaces the crude oil from the glass slide, then it is an oil-wet.

2.4.1.4   **Capillary pressure curve method**

According to Anderson (1986), the capillary pressure curve can serve as the basis for the USBM technique and it measures the work required to forcibly imbibe the core plug with fluids (either oil or brine). The area under the oil-drive and that of the water-drive reflects the work required. In other words, the smaller the area under the fluid-drive in question, the less work it requires to displace the other phase and vice-versa. Figure 2 illustrates the areas under the capillary pressure curve after both brine and oil drive for water-wet (Figure 2A) and oil-wet (Figure 2B) cores respectively. It can be observed from Figure 2 that the work required to displace the non-wetting phase by the wetting fluid is small as depicted by the area under the curve (A_2 & A_1 of Figure 2A & 2B respectively).
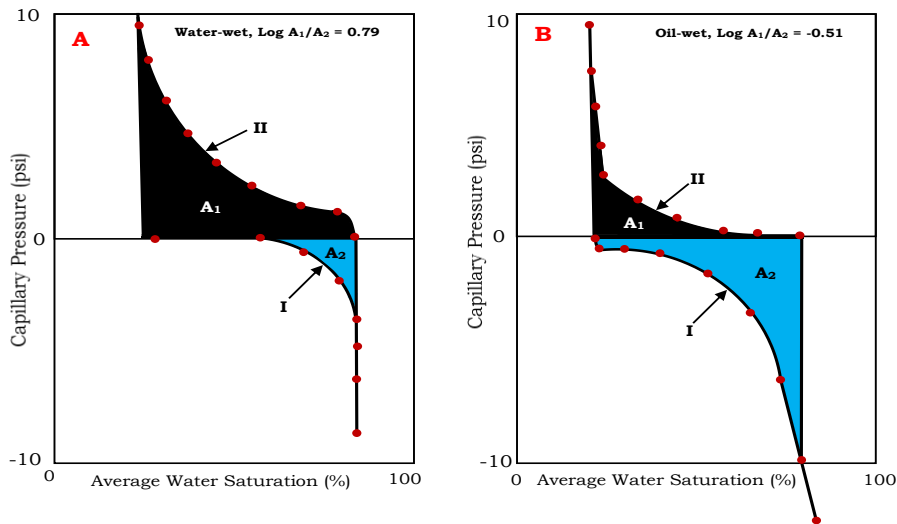
Figure 2: Capillary pressure curve technique of estimating the wettability for water-wet and oil-wet cores. Section A depicts untreated core (water-wet) while Section B represents core treated with organochlorosilanes (oil-wet). Schematic redrawn after (Donaldson et al. 1969). NB. I denotes brine drive while II depicts oil drive.

For neutrally-wet cores, the area under the capillary pressure curve during the oil drive is approximately the same as that of the brine drive as illustrated in Figure 3. In other words, the work required to displace one fluid (i.e. either the oil or water) with the other is the same and hence, the core has equal affinity to both fluids.
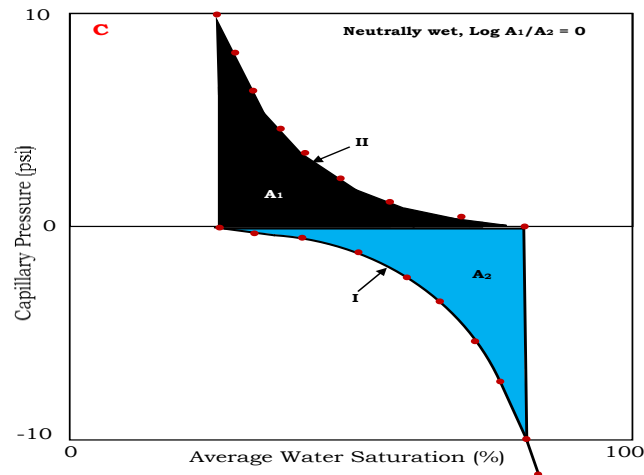
Figure 3: Capillary pressure curve for a neutral wet core. The core is pretreated with oil for 324 hours at 140°F rendering it neutrally-wet. Schematic redrawn after (Donaldson et al. 1969). NB. I depicts brine drive while II represents the oil drive.

2.4.1.5 **Reservoir log method**

The reservoir log technique capitalizes on the electrical properties of the formation fluids (oil and brine) to estimate the wetting preference of the reservoir rock (Anderson 1986a). In other words, if the pore spaces are filled with brine, the resistivity log readings are lower as compared to an oil filled pore space. For instance, if a resistivity log is run before and after injecting wettability alteration agents into the reservoir, the changes in the wetting preferences of the reservoir rocks can be inferred from the two logs.

2.4.1.6 **Nuclear Magnetic Resonance (NMR) method**

As reported by Anderson (1986a), the NMR estimates the fractional wettability by capitalizing on the thermal (longitudinal) relaxation time of the water protons (hydrogen) in the porous media. To accomplish this, the sample is expose to a strong magnetic field prior to introducing it to a weaker magnetic field. For the NMR, the greater the fraction of the oil-wet fraction, the longer the relaxation time. Hence, the slower the relaxation rate and vice-versa.

2.4.1.7 **Dye adsorption method**

The dye adsorption method as its name implies estimates the wettability by capitalizing on the adsorption tendency of a dye (methylene blue) by the water (Anderson 1986a). In other words, this method is hinged on the assumption that the wetting fluid will only spread on or adheres to the surface of the rock if it has affinity for it. For water-wet system, the dye will be adsorbed to the water film on the pore walls of the rock. On the other hand, the dye will not be adsorbed to any oil film if present on the rock surface. Hence, the fractional wettability can be characterized by using the dye adsorption technique.

2.4.2 Quantitative wettability techniques

Unlike the qualitative wettability characterization approach, the quantitative wettability technique on the other hand assigns numerical value to the wettability measurement.

2.4.2.1 **Amott technique**

The Amott method employs both spontaneous imbibition and forced displacement to estimate the average wettability of the core (Anderson 1986a). In other words, the Amott test is hinged on the ease with which the wetting phase displaces the non-wetting phase via spontaneous and forced imbibition. The Amott test procedure include;

   I. The core is saturated with brine and drained to irreducible water saturation (S_{wi}) with the oil.

  II. With the core at S_{wi}, it is then completely submerged in a container filled with brine (imbibing fluid) and the volume that was spontaneously imbibed (V_{wsp}) by the core is recorded (Figure 4A).

 III. More brine is forcefully imbibed into the core and its volume (V_{wf}), recorded (Figure 4B).

 IV. With the core now at irreducible oil saturation (S_{or}), the core is then completely submerged in a container filled with oil (displacing fluid) and the volume that was spontaneously imbibed (V_{osp}) by the core is recorded (Figure 5A).

V.   More oil is forcefully imbibed into the core and its volume (V_{of}), recorded (Figure 5B).
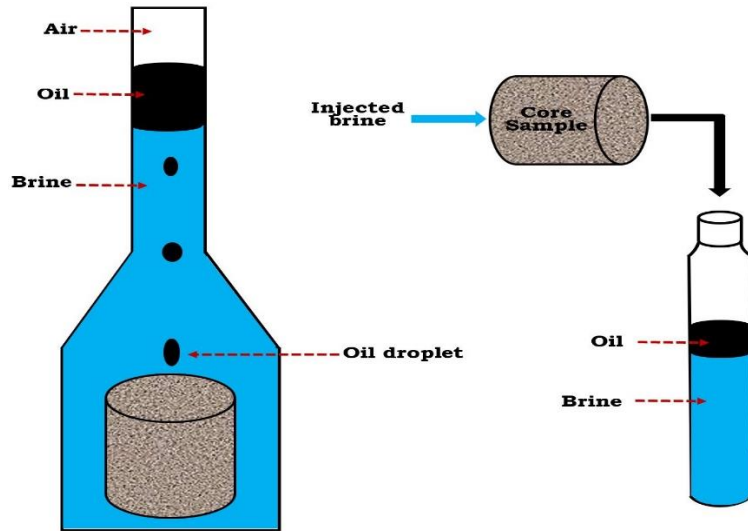
Figure 4: Spontaneous imbibition (left) and forced imbibition (right) by water. Redrawn after (Amott 1959).

The total volume of the brine imbibed by the core (V_{wt}) becomes

$$V_{wt} = V_{wsp} + V_{wf} \tag{1}$$

In a similar vein, the total volume of the oil imbibed by the core (V_{ot}) during the reverse imbibition process becomes

$$V_{ot} = V_{osp} + V_{of} \tag{2}$$
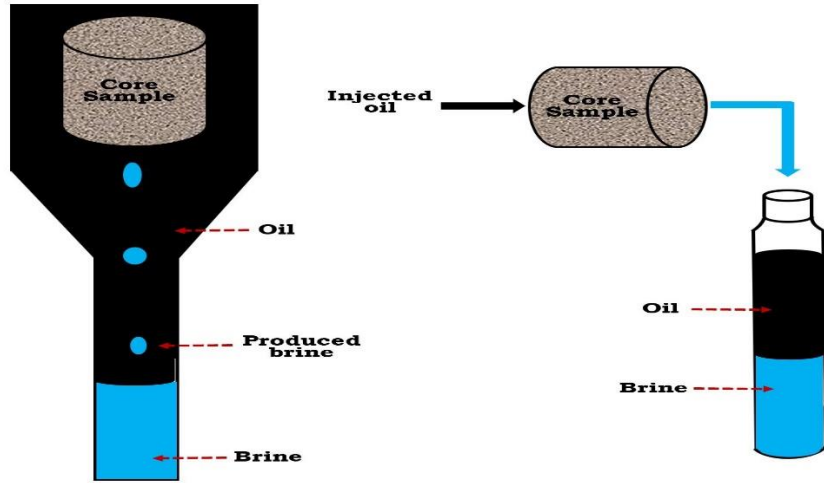
Figure 5: Spontaneous imbibition (left) and forced imbibition (right) by oil. Redrawn after (Amott 1959).

The Amott test measures the wettability from both the displacement by water index (I_w) and that of the oil index (I_o). The I_w and I_o is given respectively by the relations;

$$I_w = \frac{V_{wsp}}{V_{wt}} = \frac{V_{odsp}}{V_{ot}} \tag{3}$$

$$I_o = \frac{V_{osp}}{V_{ot}} = \frac{V_{wdsp}}{V_{wt}} \tag{4}$$

Where

V_{odsp} is the volume of oil displaced during the spontaneous imbibition of water ($V_{odsp} = V_{wsp}$)

V_{wdsp} is the volume of brine displaced during the spontaneous imbibition of oil ($V_{wdsp} = V_{osp}$)

For $I_w \neq 0$ (positive displacement with water) and $I_o = 0$; implies water-wet system.

For $I_o \neq 0$ (positive displacement with oil) and $I_w = 0$; implies oil-wet system.

Displacement by water index (I_w) and that of the oil index (I_o) are combined into a relative displacement index called the Amott-Harvey index (I_{AH}) and it is given by the relation;

$$I_{AH} = I_w - I_o = \frac{V_{odsp}}{V_{ot}} - \frac{V_{wdsp}}{V_{wt}} \tag{5}$$

NB. Positive I values (+I) depicts a completely water-wet system whiles negative I values (-I) portrays a completely oil-wet system. If the value of I is zero (I = 0), it implies a neutrally-wet system.

2.4.2.2   **United State Bureau of Mines (USBM) method**

The USBM technique employs the capillary pressure relationships (Figures 2 & 3) to estimate wettability by measuring the work required to forcefully imbibe the core with the fluids (Anderson 1986a; Donaldson et al. 1969). The procedure for the USBM method is given as;

   I.   The core is saturated with brine and drained with oil to irreducible water saturation (S_{wi}). I.e. Primary (initial) drive is established.
  II.   With the core now at S_{wi}, it is then completely submerged in a container filled with brine (imbibing fluid) for spontaneous imbibition to take place.
 III.   More brine is then injected into the core until it reaches irreducible oil saturation (S_{or}).
  IV.   With the core now at irreducible oil saturation (S_{or}), the core is then completely submerged in a container filled with oil (displacing fluid)
   V.   More oil is then injected into the core until it reaches irreducible water saturation (S_{wi}).

$$W = \log\left(\frac{A_1}{A_2}\right) \tag{6}$$

Where

W = USBM wettability index

A_1 = Area under the secondary drainage curve

A_2 = Area under the imbibition curve

Note that, for strongly water-wet systems, W = "+∞" while for strongly oil-wet systems, W = "-∞". For neutrally-wet systems, W= 0.

2.4.2.3 **Contact angle method**

Compared to the Amott and USBM, the contact angle technique is less time consuming and hence it is one of the easiest wettability characterization technique (Anderson 1986a). However, the contact angle technique measures the wettability on a single mineral crystal. The contact angle technique is related to the interfacial energies of the rock-fluid system via the Young's equation. For instance, the Young's equation oil/water/solid system is given by

$$\sigma_{os} - \sigma_{ws} = \sigma_{ow}cos\theta = \sigma_A \tag{7}$$

Where

σ_A Adhesion tension
σ_{os} Interfacial tension (IFT) at the oil-solid interface
σ_{ws} Interfacial tension (IFT) at the water-solid interface
σ_{ow} Interfacial tension (IFT) at the oil-water interface
θ Contact angle measurement

Note that for positive adhesion tension ("+"σ_A), implies water-wet system while negative adhesion tension ("-"σ_A), depicts oil-wet system. If the adhesion tension is zero ("~0"σ_A), it signifies neutrally-wet system.
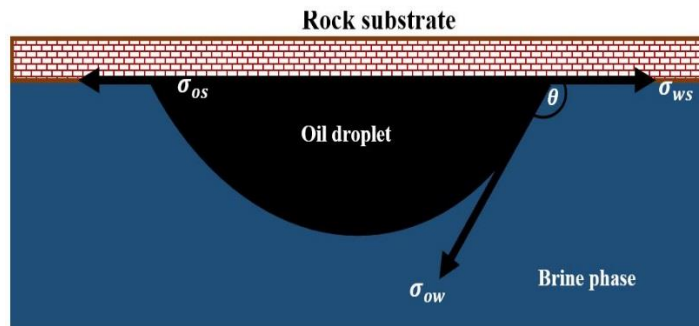
Figure 6: Analogy of the contact angle measurement through the brine phase.

If the contact angle measurement is less than 90° ($\theta < 90°$), it implies water-wet medium whereas contact angle measurement greater than 90° ($\theta > 90°$) implies oil-wet.
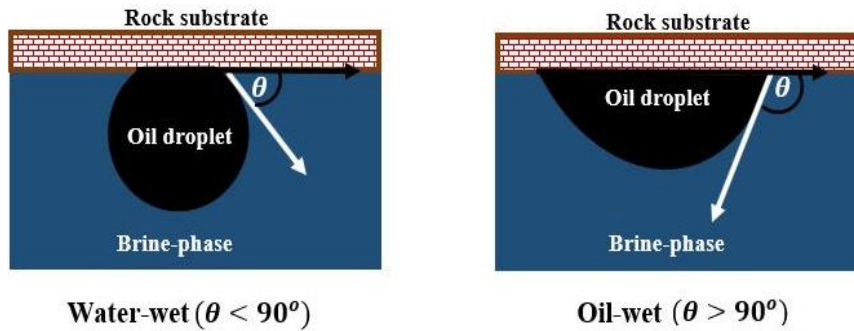
Figure 7: Contact angle measurement analogy for water-wet (left) and oil-wet (right).

2.5 Hypothesis

All the existing wettability characterization techniques measure a specific output such as total volume of the wetting and non-wetting fluids imbibed by the core in the case of the Amott test. Nonetheless, the mechanisms during rock-fluid interactions are not evaluated. In this PhD work, the plan is to estimate the wettability of reservoir rocks by exploiting the wetting preferences of the minerals mainly in contact with the flowing fluids phases. In other words, this PhD work seeks to estimate the wettability of minerals using oil adsorption approach.

To achieve this, the flotation test which is one of the existing wettability characterization technique was used as the benchmark wettability technique to screen the wetting preferences of the mineral (rock) samples under the desired reservoir conditions. The COBR interactions during the flotation test was also assessed via Surface Complexation Modelling (SCM). In addition, oil adsorption onto minerals surfaces were also assessed using Quartz Crystal Microbalance with Dissipation (QCM-D). Detail description of the SCM and the QCM-D techniques are presented in the next chapter (Chapter 3).

Theory

18

3 Proposed Wettability Estimation Techniques

If a magnet is passed over a container filled with both magnetic and non-magnetic materials, it could be observed that the metallic materials will be attracted to the magnet while the non-magnetic counterpart will remain in the container. The affinity of the magnetic materials to a magnet can be attributed to the attractive magnetic forces existing between the two materials unlike the non-magnetic counterpart. From the law of magnetism, like pole repels while unlike poles attracts. Hence, repulsive magnetic forces exist between two magnets of similar polarity and vice-versa. In a similar vein, we intend to estimate the wettability by understanding the oil adsorption during COBR interactions on minerals surfaces. This was accomplished using Surface Complexation Modelling (SCM) and Quartz Crystal Micro-balance with Dissipation (QCM-D). The SCM technique will be presented first followed by the QCM-D approach.

3.1 SCM Technique

Surface Complexation Modelling (SCM) according to Goldberg (2013) is a chemical model that gives molecular description of surface adsorption phenomenon using an equilibrium approach by exploiting the charge balance, mass balance, chemical reactions and equilibrium constant. Mineral and oil surfaces dissociate when they are exposed to brine thereby resulting in the generation of surface charge and potential across the interfaces. Comprehensive studies on the dissociated surfaces and their interactions with ions in the brine have been studied by numerous researchers. In this PhD work, the existing SCM data from literature were used to estimate the wettability.

3.1.1 Motivation for the SCM technique

The motivation for the SCM technique of wettability estimation stems from our quest to understand the COBR interactions during the flotation test. It has been reported that surface forces such as electrostatic,

hydration and Van der Waals forces dictates the adhesion of polar oil component in the crude oil onto minerals (rock) surfaces (Busireddy and Rao 2004). Emphasis was placed on the role of the attractive electrostatic forces existing between the oil-brine and rock-brine interfaces on oil adsorption via SCM.

Anionic minerals have high affinity to cationic oil components while cationic minerals have high affinity to anionic oil components (Buckley & Liu 1998). Hence, if both the reservoir rock (minerals) and the oil interfaces have similar charges, bridging by divalent ion with dissimilar charge (cations or anions) can lead to oil adhesion. To better understand the oil adhesion tendencies of the reservoir rock (minerals) during the flotation test, the COBR interactions during the flotation test were assessed via SCM. The oil adhesion mechanisms onto both anionic and cationic surfaces is illustrated in Figure 8.

ANIONIC SURFACE   **CATIONIC SURFACE**

= Positive sites on the mineral surface

= Negative sites on the mineral surface

= Basic oil component

= Divalent cations in FW

= Divalent anions in FW

= Acidic oil component
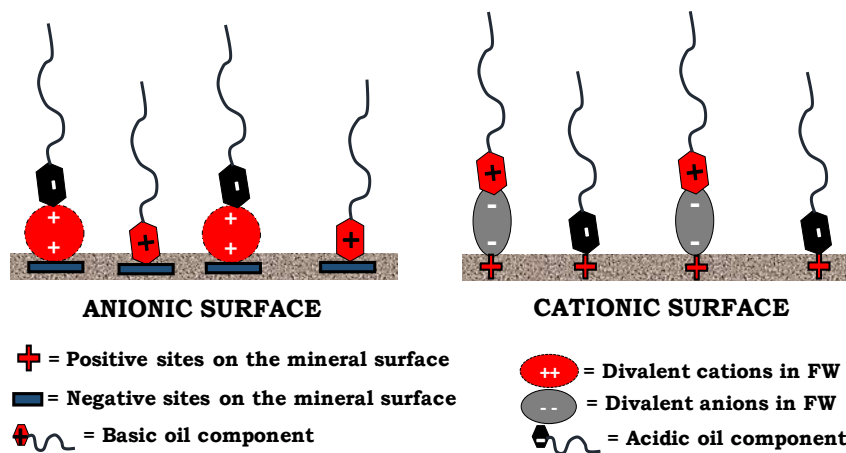
Figure 8: Oil adhesion onto anionic and cationic Surfaces.

3.1.2   Overview of SCM technique

Surface Complexation Modelling (SCM) is a thermodynamic approach of simulating adsorption phenomena by capitalizing on the surface reactions and their reaction constants of the surfaces (oil and mineral) involved (Brady & Krumhansl 2012a; Goldberg 2013; Koretsky 2000). Koretsky (2000) reported that the availability of nutrient in soils, the

global cycling of elements, the formation of ore deposits, transportation and transformation of contaminats (i.e. metallic and organic) are all dictated by the complexation reactions at the mineral-water interface. It has been reported that, the mineral-water interface adsorption can be predicted by numerous empirical and semi-empirical models such as the the Langmuir isotherm, simple ion exchange models and Freundlich isotherm (Koretsky 2000). Nonetheless, these models have their limitations. Koretsky (2000) reported that the structure of the adsorbed species and the surface charge that led to the adsorption process were not accounted for in these models especially the isotherm. Hence, the need for a more robust adsorption model that can overcome the limitations inherent in the existing empirical and semi-empirical adsorption models. This resulted in Surface Complexation Modelling (SCM) and it includes the Constant Capacitance Model (CCM), the Diffuse Layer Model (DLM), Tripple Layer Model (TLM) and Charge Distribution MUltiSite Ion Complexation (CD-MUSIC) model (Koretsky 2000; Wolthers et al. 2008). Like the formation of complexes in solution, the formation of complexes on surfaces can be modelled based on the surface species, chemical reactions, charge balances, mass balances and thermodynamic equilibrium constants (Goldberg 2013). Four main characteristics permeate through all the Surface Complexation Models (Dzombak & Morel 1990). According to Dzombak and Morel (1990), these features includes;

- o Irrespective of the silicate mineral involved, the SCMs assume that the silicate surfaces can be describes as flat plane of surface hydroxyl sites. The reactions at these surface hydroxyl sites can also be described by equations. For instance, surface protonation reactions on silicate mineral surfaces can be written as,

$$> SOH + H_{aq}^+ \leftrightarrow > SOH_2^+ \qquad (8)$$

- o For all the SCMs, the mass law equations are used to describe surface reactions (e.g. protonation, deprotonation, ligand and metal sorption) regardless of the mineral surfaces involved. The mass law equation for the surface protonation reactions described in Eqn 8 becomes;

$$K^{int} = \frac{\{>SOH_2^+\}}{\{>SOH\}\{H_{aq}^+\}} \tag{9}$$

Where $\{> SOH_2^+\}$, $\{> SOH\}$ and $\{H_{aq}^+\}$ depicts the activities of those species.

o All the SCMs assume variable charge resulting from chemical reactions at the mineral surface. For instance, at pH of the pristine point of zero charge (pH$_{ppzc}$), the surface charge of a mineral is zero (Sverjensky 1994). If the pH is below the pH$_{ppzc}$, the mineral surface becomes cationic while the mineral surface exhibits anionic charge if the pH is above pH$_{ppzc}$ (Sverjensky 1994). Sverjensky attributed this to the reaction of the surface hydroxyl groups with either H$^+$ or OH$^-$.

o In all the SCMs, the effect of the surface charge on the apparent (measured) equilibrium constants (K^{app}) can be estimated. The intrinsic equilibrium constants (K^{int}) can be estimated from the measured equilibrium constants (K^{app}) using the columbic (electrostatic) correction factor as given by the relation;

$$K^{int} = K^{app} exp \left(\frac{-zF\psi(x)}{RT} \right) \tag{10}$$

Where
z   Surface charge
F   Faraday constant
$\psi(x)$ Electric potential as a function of the distance from the mineral surface (x)
R   Universal gas constant
T   Temperature

Though, there are some common characteristics permeating through all the SCMs, nonetheless each model is unique. Goldberg (2013) reported that the location and surface configuration of the adsorbed ions at the solid-solution interface distinguish one model from the other. According to Sverjensky and Sahai (1996), the differences in the SCMs can be attributed to;

- o The description of the electric double layer
- o The electric potential (ψ) calculation
- o Treatment of the surface sites as either completely homogeneous (single site models) or as heterogeneous (multi-site models).

Butt (2006) reported that, the electric double layer is composed of inner and outer parts. The Stern layer is the innermost part of the electric double layer while the Gouy or diffuse layer forms the outermost layer of the double layer (Butt 2006). Considering interface of a carbonate mineral-water (Figure 9), the complex formed can be either an inner sphere or outer sphere complexes based on the location and the configuration of the adsorbed ion on the mineral surface (Goldberg 2013; Butt 2006; Wolthers et al. 2008).
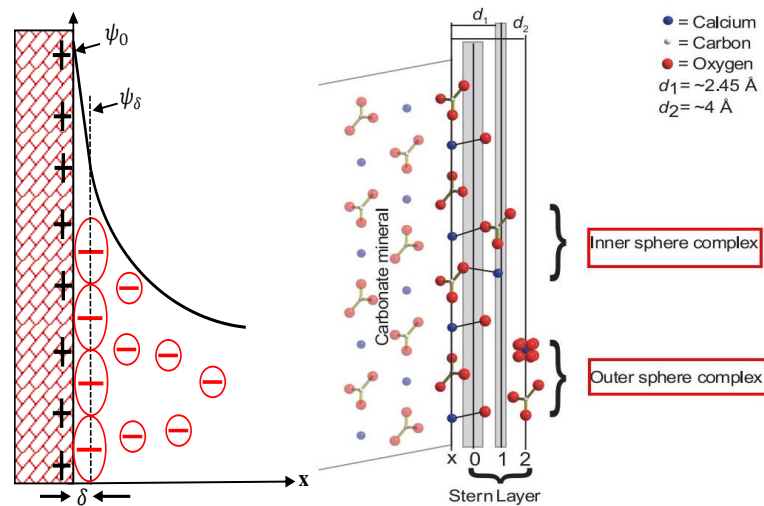
Figure 9: Simplified version of the Stern layer. The Stern layer on the left was redrawn after Butt (2006) while that of the carbonate mineral-water after Wolthers et al. (2008).

Constant Capacitance Model (CCM) and Diffuse Layer Model (DLM)

If the configuration of the adsorbed ions on a surface during solid-solution interactions occured on a single surface plane, the complex formed is termed an inner-sphere complex (Goldberg 2013). Examples of inner-sphere complexes models include the Constant Capacitance

Model (CCM) and the Diffuse Layer Model (DLM) as illustrarted in Figure 10. For CCM and DLM, the adsorption of ions onto the solid-solution interface occurs on a single plane (Koretsky 2000) as illustrated in Figure 10. The distinction between the CCM and the DLM is that the adsorbed plane of ions are counterbalance by a single plane of counterions and diffuse ion "swarm" of counterions respectively.
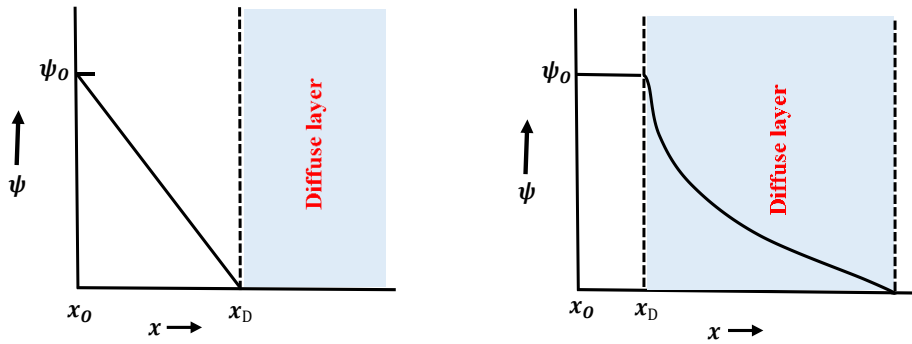
Figure 10: Constant Capacitance Model (CCM) and Diffuse Double Layer (DLM). CCM (left) and DLM (right), redrawn after Koretsky (2000).

Triple Layer Model (TLM)

Contrary to the single plane adsorption of ions in the CCM and DLM, the adsorption of ions occurs on two separate planes for the TLM with the charge balance provided by a diffuse ion "swarm" (Koretsky 2000). In other words, the adsorption of ion onto the solid-solution interfaces can lead to the formation of both inner-sphere and outer-sphere complexes. Since the DLM is one of the simplest electric double layer models and can accurately describe the surface reactions, it was employed in this PhD study.
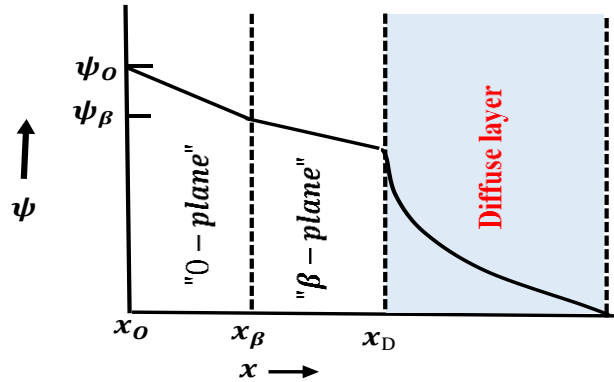
Figure 11: Triple layer Model (TLM). Redrawn after Koretsky (2000).

Numerous surface reactions and their reaction constants of mineral-brine systems have been carried out by numerous researchers (Brady & Krumhansl 2012a; Brady & Krumhansl 2012b; Brady et al. 2012; Gu & Evans 2007; Sverjensky & Sahai 1996, 1998; Van Cappellen et al. 1993; Wolthers et al. 2008). In-depth surface complexation studies have also been carried out for kaolinite, hematite, zircon, quartz, goethite, nepheline, magnetite, talc, chlorite, muscovite, montmorillonite, albite, anorthite, microline, rutile, gibbsite and almandine (Chen & Brantley 1997; Sverjensky & Sahai 1996, 1998; Wieland et al. 1994). For carbonate minerals such as siderite, rhodochrosite, calcite, dolomite and magnesite, comprehensive surface complexation modelling have also been reported by several authors (Pokrovsky et al. 1999; Van Cappellen et al. 1993; Wolthers et al. 2008). To add to the above, the surface reactions and the reaction constants for oil-brine interface have also been studied by Brady and Krumhansl (2012b). Several authors have used the available SCM data from literature to either predict experimental results or to better understand laboratory data. For instance, precipitation reactions of polymer at high surface coverage has also been reported in literature (Katz and Hayes 1995).

3.1.3 Application of SCM in wettability studies

Buckley and Liu (1998) reported that during COBR interactions, electrical charges exist on the oil-brine and the rock-brine interfaces. For example, if the rock-brine and the oil-brine interfaces have like charges, repulsive electrostatic forces are bound to exist between the two interfaces. Thus, maintaining a thick water film leading to lack of oil adsorption and hence water-wet state. On the other hand, attractive electrostatic forces are bound to exist between oil-brine and rock-brine interfaces with unlike charges, thereby leading to oil adsorption. SCM simulates the electrostatic forces existing between the oil-brine and rock-brine interfaces during COBR interactions by capitalizing on the available SCM data from literature.

To accomplish this, the COBR interactions during the various laboratory experiment works were simulated via a geochemical solver, PHREEQ-C. The mineral-brine interactions during the experimental works have also been modelled in the past by similar chemical reactions from numerous researchers (Katz & Hayes 1995; Song et al. 2017). Comprehensive studies have also been carried out on the possible surface complexes formed between important ions (e.g. Ca^{2+} and Mg^{2+}) and the mineral surfaces (Sverjensky & Sahai 1996, 1998; Goldberg 2013; Koretsky 2000; Wolthers et al. 2008). In addition, Brady & Krumhansl (2012a) have also carried out comprehensive studies for some oil-brine systems. To model the COBR interactions via PHREEQ-C, the surface reactions and the reaction constants for the surfaces (oil and minerals) were used as input into the SCM.

3.2 QCM-D Technique

Quartz Crystal Micro-balance with Dissipation (QCM-D) technique is a real time micro scale (10^{-6}) measurement of molecular adsorption (Chandrasekaran et al. 2013; Chen et al. 2015; Dudášová et al. 2008; Ekholm et al. 2002; Feiler et al. 2007; Keller & Kasemo 1998). The QCM-D technique relies on the changes in the frequency (Δf) and the dissipation (ΔD) signals of a resonating crystal to estimate the mass of the adsorbed components (Ekholm et al. 2002). The change in dissipation (ΔD) measures the energy loss by the resonating sensor due to the adsorbed film. For instance, monitoring the dissipation signal can

unravel the mechanical (viscoelastic) properties of the adsorbed film (Feiler et al. 2007; Keller & Kasemo 1998). Keller and Kasemo (1998) reported that if the Δf and ΔD are measured real-time; the adsorption process can be characterized.

3.2.1 Motivation for QCM-D technique

Unlike the flotation test which relies on the affinity of the minerals to either the brine or the oil to characterize the wettability; the QCM-D technique on the other hand, estimates the wetting preferences of minerals by measuring the magnitude of the oil adsorbed during COBR interactions. In other words, the wettability is dictated by the tendency of the mineral to adsorb oil as observed in the SCM technique. Considering the injection sequence, Fluid#1(reference fluid)/Fluid#2 (test fluid)/Fluid #1, if the change in frequency (Δf) of the reference fluid (Fluid #1) prior to and after the injection of the test fluid (Fluid#2) is negligible ($\Delta f \approx 0$), it depicts lack of adsorption of the test fluid components on the sensor as illustrated in Figure 12.
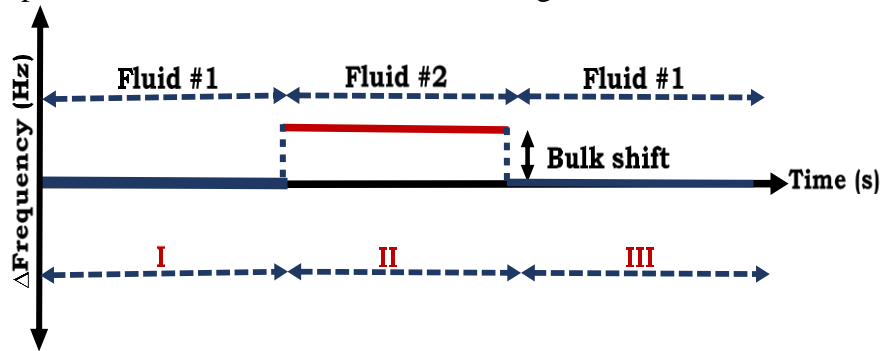
Figure 12: Lack of oil adsorption analogy during QCM-D experiments. The negligible change in frequency ($\Delta f \approx 0$) of the sensor during Fluid #1/Fluid #2/ Fluid #1 injection sequence depicts lack of oil adsorption. NB. Fluid #1is the reference fluid while Fluid #2 is the test fluid (oil).

On the other hand, if the change in the reference fluid frequency signal prior to and after the injection of the test fluid (Fluid#2) during the injection sequence Fluid#1(reference fluid)/Fluid#2 (test fluid)/Fluid #1 is less than zero ($\Delta f < 0$) depicting oil adsorption as shown in Figure 13. The change in frequency (Δf) can be attributed to the added mass resulting from the adsorption. NB. For the QCM-D studies, the sign

conversion is that if the change in frequency (Δf) between consecutive injection fluids is negative (Δf < 0), it depicts adsorption while positive change in frequency (Δf > 0) also depicts desorption. On the other hand, if the change in frequency is approximately zero (Δf ≈ 0), it implies that neither adsorption nor desorption has taken place.
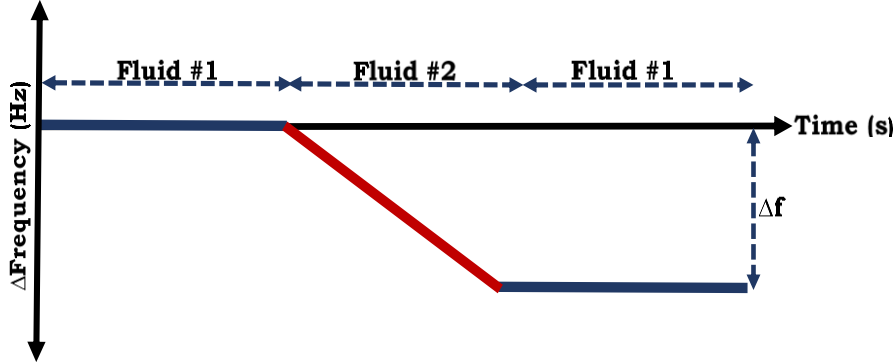
Figure 13: Analogy of oil adsorption during QCM-D experiments. The magnitude of oil adsorbed onto the mineral surface is proportional to the change in frequency of the oscillating crystal (Δf < 0). NB. Fluid #1 is the reference fluid while Fluid #2 is the test fluid (oil).

3.2.2 *Potential application of QCM-D in wettability estimation*

Wettability is the tendency of a fluid to preferentially wet a solid surface in the presence of another immiscible fluids (Craig 1971). Hence, if the magnitude of the adsorbed oil can be measured, the wettability can be characterized based on the adhered oil during the mineral/brine/oil interactions. In other words, the mass of the adsorbed film and its thickness (Δm_{ads} and Δt_{ads}) during the QCM-D test can be used to characterize the wettability. Based on the Sauerbrey equation, numerous authors (Ekholm et al. 2002; Feiler et al. 2007; Kubiak et al. 2015; Lu & Czanderna 2012) have estimated the magnitude of the adsorbed oil (Δm_{ads}) using the relation;

$$\Delta m_{ads} = -\frac{1}{2}\left(\frac{\rho_q v_q}{f_o{}^2 n}\right)\left(f_{ads} - f_{ref}\right) = -\frac{C\Delta f}{n} \qquad (11)$$

where

Δm_{ads}	Mass of the adsorbed film (ng/cm^2)
ρ_q	Density of quartz crystal (2.65g/cm^3)
v_q	Shear wave velocity (334000cm/s)
f_{ref}	Reference frequency signal, Hz
f_{ads}	Adsorbed film frequency, Hz
f_o	Resonance frequency (4.95MHz)
Δf	Change in frequency (Hz)
n	Frequency harmonic number (n = 1, 3, 5, 7 etc.)
C	Mass sensitivity constant (C $\approx$ 18 ngcm^{-2}Hz^{-1})

In a similar vein, the thickness of the adsorbed film (Δt_{ads}) can also be used to characterize the wetting preferences of mineral surfaces. For a given sensor, the ratio of the change in the frequency signal after the adsorption to its nominal signal prior to the adsorption should be equal to that of the thickness (Lu & Czanderna 2012). This can be used to estimate the adsorbed film thickness (Δt_{ads}) as depicted in Eqn. 12.
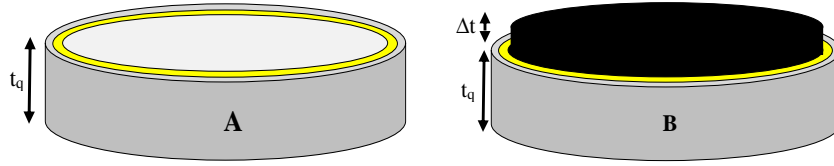
Figure 14: Sensor thickness analogy. Sensor thickness prior to and after the oil adsorption (Sections A and B respectively). Change in the thickness of the adsorbed film (Δt) to the thickness of the quartz crystal (t_q) prior to the oil adsorption is proportional to the ratio of the changes in the frequency of the oscillating crystal (Δf) after the oil adsorption to the resonance frequency of the quartz crystal.

Mathematically, the magnitude of the adsorbed film thickness (Δt_{ads}) is given by the relation;

$$\Rightarrow \frac{\Delta t}{t_q} = - \frac{\Delta f}{f_q}$$

$$\Rightarrow \Delta t = - \left(\frac{\Delta f}{f_q}\right) t_q = - \left(\frac{1}{2f_o}\sqrt{\frac{\mu_q}{\rho_q}}\right)\left(\frac{f_{ads}-f_{ref}}{f_{ref}}\right) \qquad (12)$$

Since f_{ref} is an integral multiple of f_o (i.e. $f_{ref} = nf_o$), Eqn (12) can be re-written as;

$$\Rightarrow \Delta t = - \left(\frac{1}{2f_o} \sqrt{\frac{\mu_q}{\rho_q}}\right) \left(\frac{f_{ads} - nf_o}{nf_o}\right)$$

$$\Rightarrow \Delta t = - \left(\frac{1}{2f_o{}^2} \sqrt{\frac{\mu_q}{\rho_q}}\right) \left(\frac{\Delta f}{n}\right) \tag{13}$$

where

μ_q Shear modulus of quartz crystal (2.947×10^{11} gcm^{-1}s^{-2})

The QCM-D has the potential to be used as wettability characterization tool. Nonetheless, the working conditions of the conventional QCM-D device is 200ºC but at 1 atmosphere. The volatile components in the crude oil will boil out at high temperatures. Hence, the need for a QCM-D device that can operate at high temperature and high pressure. Biolin Scientific (Frölunda, Sweden) provided the solution to our problem by supplying a high pressure, high temperature prototype QCM-D device (QHPT vessel) for this study. Detailed description of the QHPT vessel is discussed in the next section.

3.2.3 Overview of the QHPT vessel

Contrary to the conventional QCM-D device with only one fluid occupying the flow-cell chamber at a given time, the QHPT vessel on the other hand can accommodate two fluids in the flow-cell at any given time. These fluids are the system and test fluids as illustrated in Figure 15B. The system fluid occupies the flow-cell chamber beneath the sensor whereas the space above the sensor (deposition area) is occupied by the test fluids. The rationale behind the use of the system fluid (non-conductive fluids) was to insulate the back electrode thereby preventing short circuiting during the injection of the conductive fluids (e.g. brine). In addition, the two immiscible fluids (system and test fluids) in the flow-cell chamber help to minimize differential pressure build-up across the sensor, thereby preventing the fragile sensor from cracking.

30
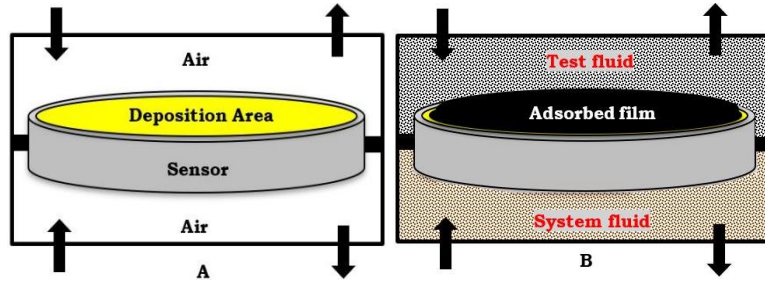
Figure 15: Schematic of the high-pressure, high-temperature QCM-D (QHPT) vessel. Sections A and B depict the QHPT vessel prior to and after the injection of the test and system fluid respectively. Note that the arrows depict the direction of flow into and out of the flow-cell.

3.2.3.1 Proposed application of QHPT device in oil adsorption

For a more realistic studies of oil adsorption onto mineral surfaces, the rock-fluids interactions prior to and after the crude oil accumulation into the reservoir was replicated using QCM-D device. In other words, the formation water (FW) was injected to serve as the reference fluid prior to injecting the Stock Tank Oil (STO). The FW was then re-injected after the injection of the STO. The magnitude of the adsorbed oil was estimated from the change in the FW frequency signals (Δf) before and after the injection of STO. The initial QCM-D experimental set-up for oil adsorption is illustrated in the Figure 16.
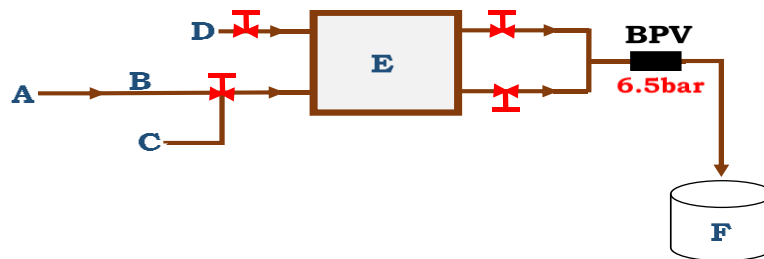
Where
A   Reference Brine injection point
B   Stainless-steel flowline
C   Test fluid (oil) injection point
D   System fluid injection point
E   Stainless-steel flow-cell
F   Effluent
BPV   Back Pressure Valve

Figure 16: QCM-D initial experimental set-up to investigate oil adsorption.

Nonetheless, the QCM-D technique was confronted with numerous challenges during the early experimental stages. These challenges and how they were averted will be discussed in the next section.

3.2.4 QCM-D challenges and mitigations

Corrosion, sensor etching (sensor coating dissolution), fluid trapping and salt precipitation were some of the challenges confronted during the qualification of the QCM-D as wettability characterization tool. A brief description of these challenges and how they were mitigated are presented in the subsequent sections. More details on the challenges and mitigations of the QCM-D can be found in Paper III.

3.2.4.1 **Corrosion challenge and its mitigation**

The QCM-D technique detects the magnitude of the adsorbed component by measuring the changes in the frequency (Δf) of the oscillating sensor during the fluid injection sequence. Figure 17 shows a typical QCM-D response with the original set-up (Figure 16). From Figure 17, it can be observed that during the injection of the deionized water (DW), the changes in both frequency ($\Delta f \approx 0 Hz$) and dissipation ($\Delta D \approx 0$ ppm) were negligible (Section I of Figure 17). On the other hand, during the injection of the FW (with salinity 97308 ppm), the change in frequency ($\Delta f \neq 0 Hz$) and dissipation ($\Delta D \neq 0$ ppm) were relatively high (Section II of Figure 17). The added mass is the reason for the relatively high frequency attenuation and the high energy loss (dissipation) by the sensor. Since stainless steel components dominated the initial experimental set-up, the added mass was attributed to corrosion resulting from high salinity brine (pH $\approx$ 5.9) coupled with relatively high temperature (65°C).
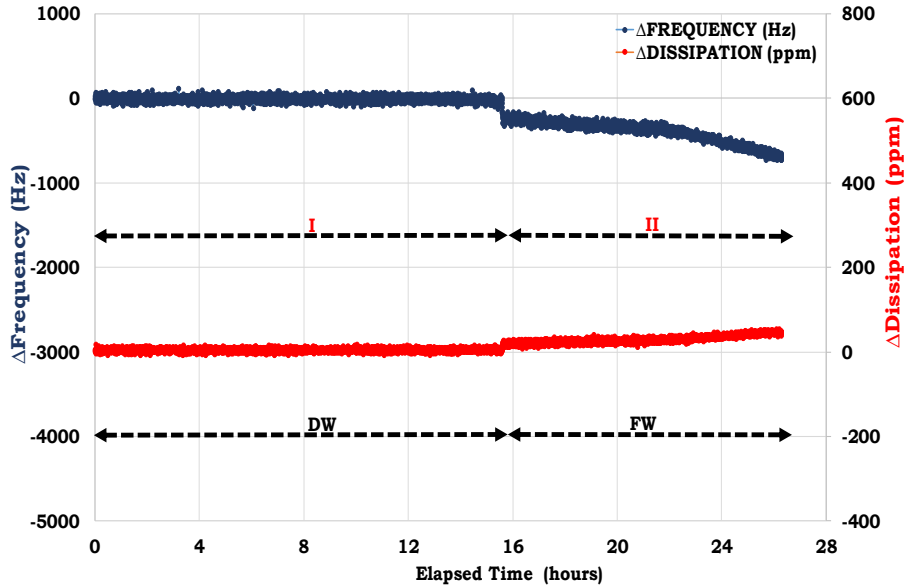
Figure 17: Corrosion challenge resulting from stainless steel components in the initial experimental set-up. The reduction in the frequency signal during the FW injection stage was due to the deposition of corroded materials as confirmed by the dissipation signals

To confirm this hypothesis, the FW samples were stored in both stainless steel and titanium piston-cells (at 23ºC) for approximately a week. At the end of this test, it was observed that the colour of the FW stored in the stainless piston-cell has changed from colourless to yellowish while that in the titanium piston-cell remained colourless. To add to the above, the original FW and the FW stored in both the stainless steel and titanium piston-cell were analysed using an Inductive Coupled Plasma (ICP) analytical technique to assess the elemental compositions of the FW under the studied conditions. It was observed that, the iron (Fe) content of the FW stored in the stainless-steel piston cell was higher (8.2 mg/l) as compared to both the titanium (<0.1 mg/l) and the original FW (<0.1 mg/l). Hence, confirming that corrosion challenge can be mitigated using titanium and non-metallic components such as polyether ether ketone (PEEK).

3.2.4.2 **Sensor etching and its mitigation**

After the corrosion challenge was mitigated, it was observed that the frequency signals became abnormally high at relatively constant dissipation (Section II of Figure 18). This was linked to the dissolution of the sensor coating (originally 50 - 100 nm thick) leading to loss in mass of the sensor. Thus, compelling the sensor to oscillate at abnormally high frequency but at constant dissipation. This phenomenon is termed "sensor etching".
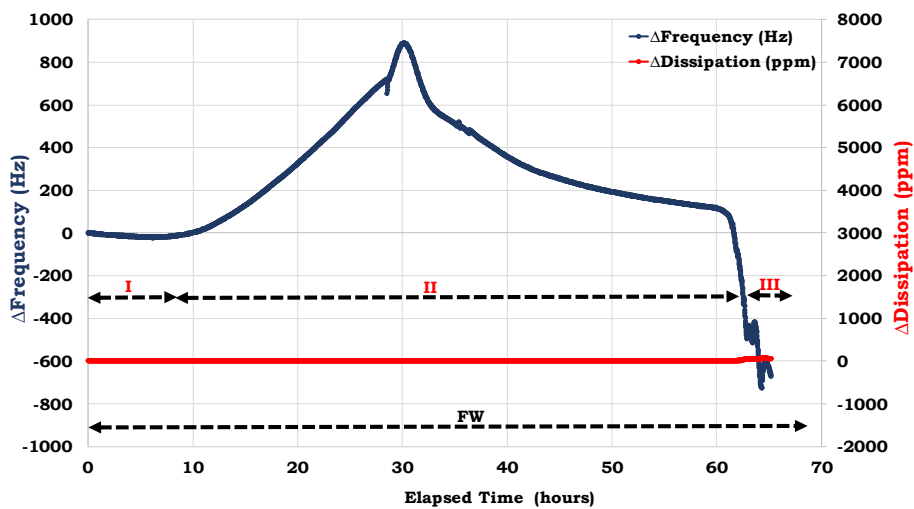
Figure 18 : Sensor etching due to the dissolution of the mineral coatings. This is attributed to the concentration gradient between the injected FW and the coatings on the minerals.

This challenge was mitigated by establishing equilibrium between the injected brine and the respective minerals coated on the sensor. This was accomplished by injecting the brine through a pre-column filled with similar minerals as coated on the sensor to ensure that equilibrium was established prior to injecting the brine onto the sensor as illustrated in Figure 20. Hence, the sensor etching was mitigated by injecting the brine through a pre-column filled with similar mineral as the coatings on the sensor.

3.2.4.3 **Fluid trapping and its mitigation**

After resolving the corrosion and sensor etching challenges, the next hurdle was fluid trapping inside the flow-cell. This was observed in the form of prolonged oil adsorption during the re-injection of FW after the injection of STO (Section III of Figure 19). However, the fluid trapping effect was not observed during the injection of FW/n-decane/FW injection sequence. This is because unlike the STO with polar oil component, the n-decane has no surface-active component and hence, the observed result.
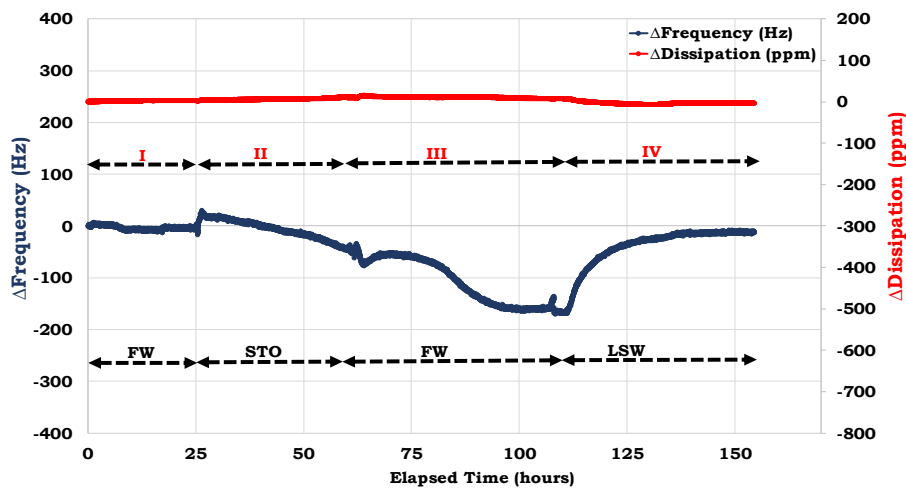
Figure 19: Fluid trapping during FW/STO/FW injection sequence.

Since the fluids (oil and brine) were trapped due to the differences in densities, and the current flow-cell design of the QHPT vessel, the flow-cell was rotated to optimize fluid displacement. In other words, the flow-cell was rotated to maximize the expulsion of the previous fluid in the flow-cell with the current injection fluid by capitalizing on their density contrast.

3.2.4.4 **Salt precipitation and its mitigation**

The final challenge that was encountered was precipitation of salt due to temperature difference. This challenge was averted by performing the

experiment in a constant temperature set-up such as oven. The final experimental set-up for oil adsorption studies is illustrated in Figure 20.

3.2.4.5 QCM-D experimental set-up with resolved challenges

The final experimental set-up is devoid stainless-steel components. Pre-column and a constant temperature system (e.g. oven) are required. To prevent the boiling out of the volatile components in the STO, a back pressure of 6.4 bar was also placed at the effluent as illustrated in Figure 20.
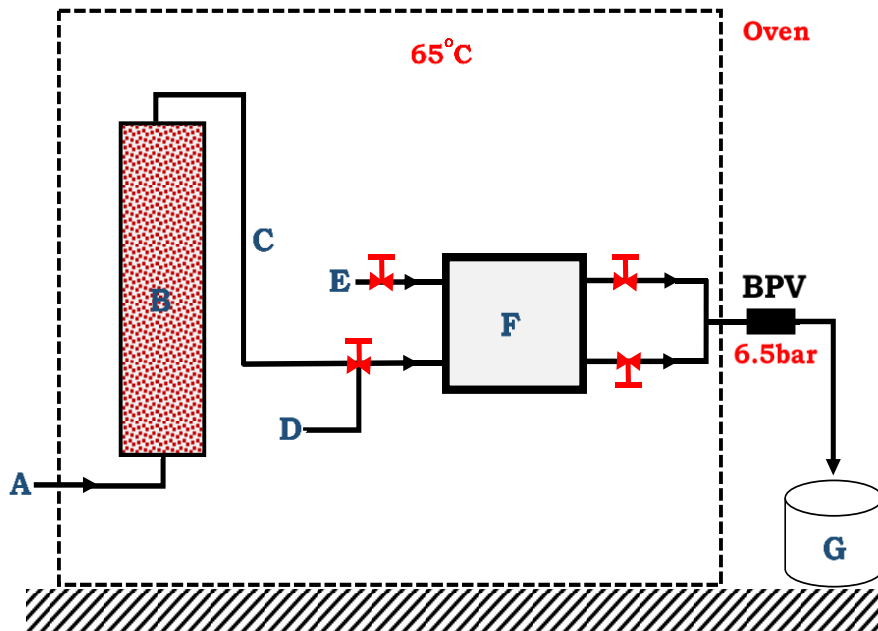
Where
A   Reference brine injection point
B   Pre-column
C   PolyEther Ether Ketone (PEEK) tubing
D   Test fluid injection point
E   System fluid injection point
F   Titanium QCM-D flow-cell
G   Effluent
BPV   Back Pressure Valve

Figure 20: QCM-D experimental set-up

4   Methods

Both experimental and simulation techniques were employed in these studies. The experimental results were compared with their simulated counterparts before meaningful conclusions were drawn. Minerals (mineral mixtures) and rock samples (outcrop and reservoir rocks) were utilized during the experimental work. Furthermore, the COBR interactions during the experiments were also simulated via a geochemical simulator, PHREEQ-C – version 3.3 (Parkhurst & Appelo, 2013).

4.1   Experimental methods and materials

Three experimental methods were utilized to investigate the wetting preferences of the mineral (rock) samples under the studies rock-fluid systems. The experimental methods considered includes;

  I.   Flotation test
 II.   Quartz Crystal Microbalance with Dissipation (QCM-D) test
III.   Contact Angle measurement method

The flotation test was carried out for two North Sea sandstone rocks. Prior to that, the flotation test was also performed for the main dominant minerals in the studied sandstone rocks such as quartz, albite, illite, montmorillonite and calcite. Moreover, mineral-mixtures (Pseudo-Sandstone Rock, PSR) were also prepared to assess the effect of increasing surface area on wettability by increasing the illite content (PSR#1 and PSR#2). The effect of increasing the calcite contents on the wetting preferences were also carried out in the Pseudo-Sandstone Rock (PSR#3 and PSR#4). The mineralogical composition of Sandstone Reservoir Rock (SRR) and Pseudo-Sandstone Reservoir (PSR) can be obtained from Table 1.

During the QCM-D experiments, quartz and kaolinite sensors were employed. For the Contact angle measurements, dominant minerals in the studied sandstone rocks were used as substrates. The minerals considered include, quartz, kaolinite and calcite. In addition, the contact angle measurements were carried out on a Bentheimer sandstone rock.

The Formation Water (FW) and oil (n-decane and Stock Tank Oil, STO) compositions employed during the PhD experimental work are provided in Table 2 and Table 3 respectively. The n-decane was used as the reference oil while the STO was also employed as the test oil. The viscosities of the STO used ranges from 2.28mPa·s to 66.36mPa·s.

Mineral	SRR #1 (%)	SRR #2 (%)	PSR #1 (%)	PSR #2 (%)	PSR #3 (%)	PSR #4 (%)
Quartz	83.7	94.9	62.8	41.9	62.8	41.9
Albite	3.3	4.0	2.5	1.6	2.5	1.6
Montmorillonite	3.9	0.0	2.9	1.9	2.9	1.9
Illite	8.8	0.4	31.6	54.4	6.6	4.4
Siderite	0.0	0.5	0.0	0.0	0.0	0.0
Calcite	0.3	0.2	0.2	0.2	25.2	50.2

Table 1: Compositions of the Sandstone Reservoir Rocks (SRR) and the Pseudo-Sandstone Rock (PSR) used in the flotation test.

Ion	[a,b,c]FW#1 (mmol/L)	[c] FW#2 (mmol/L)	[a]LSW#1 (mmol/L)	[a]LSW#2 (mmol/L)
Na^+	1326.16	701.88	13.26	174.00
K^+	5.62	7.11	0.06	0.00
Mg^{2+}	17.46	23.90	0.17	0.00
Ca^{2+}	147.94	72.85	1.48	0.70
Sr^{2+}	8.44	1.65	0.08	0.00
Ba^{2+}	0.00	0.04	0.00	0.00
Cl^-	1677.67	898.69	16.78	175.50
SO_4^{2-}	0.89	3.59	0.01	0.00
Density (g/cm³) at 20ºC	1.07	1.04	0.97	0.99

Table 2 : Compositions of brine used. NB. [a] depicts the brine used during QCM-D experiments. The brine used during the contact angle measurements is depicted by [b] while [c] depicts the ionic compositions used in the flotation test.

FLUID	DENSITY (g/cm³)	TAN (mg KOH/g oil)	TBN (mg KOH/g oil)
[a]N-decane	0.74	0.00	0.00
[a]STO	0.86	0.06	0.78
[b]STO#1	0.86	0.10	1.90
[b]STO#2	0.90	0.38	2.30

Table 3 : Compositions of the oil (n-decane and Stock tank oil, STO) used in the experimental work. NB. [a] depicts the oil used during QCM-D and Contact angle measurements while [b] depicts the oil employed during the flotation test.

4.1.1 Flotation test procedure

A known weight (W_T) of the dried minerals (rock) sample was aged in the desired FW of known volume (V_b) at the designated reservoir temperature (T) for 48 hours. The brine phase was then separated and kept for later use after the ageing period. A known volume (V_o) of the oil (STO or n-decane) was added to the wet-mineral with intermittent stirring for 48 hours at the desired reservoir temperature. At the end of the ageing period, the separated brine was added to the aged mineral-oil mixture. The mineral-brine-oil mixture was then thoroughly shaken and kept at the desired reservoir temperature for 24 hours to allow the separation of the mineral into either the oil or the brine phase. The concentration of the mineral sample in each phase determines the wetting preferences.
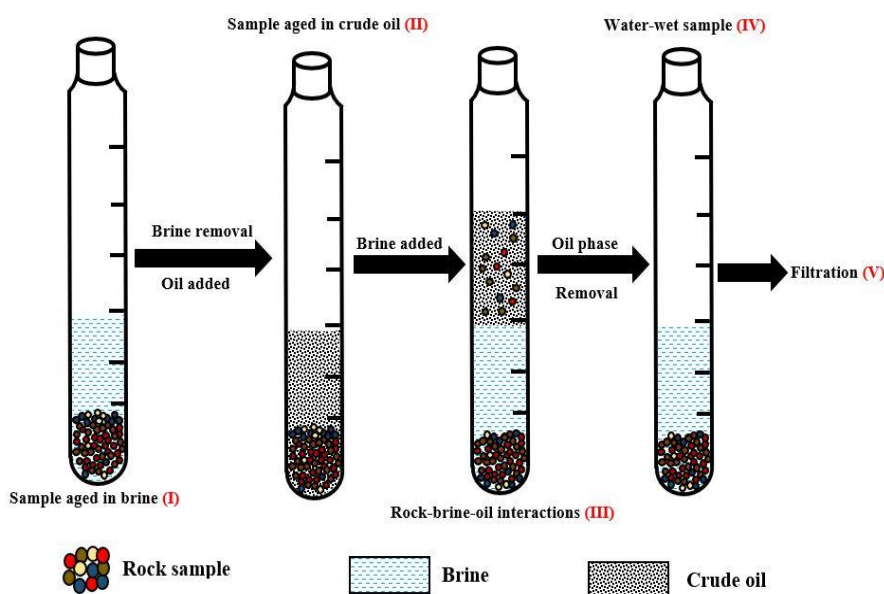
Figure 21: Schematic of the flotation test

It is more challenging to remove the adsorbed oil from the oil-wet particles than to dry the water from the water-wet mineral. Hence, the water-wet phase was filtered, and its filter cake dried until a constant weight (W_{w-w}) was achieved. The concentration of the oil-wet particles

($W_{o\text{-}w}$) is the difference between the total weight of the dried mineral (rock) sampled used (W_T) and the dried water-wet particles ($W_{o\text{-}w}$) as given by the relation;

$$W_{o-w} = W_T - W_{w-w} \tag{14}$$

Hence, the wettability with respect to the oil-wet (I_o) particles become;

$$I_{o-w} = 100\% - \left(\frac{W_{w-w}}{W_T} \, x100\%\right) \tag{15}$$

Hence, for strongly water-wet, the wettability index with respect to the oil-wet particles is negligible ($I_{o\text{-}w} \approx 0\%$) whereas that of a strongly oil-wet system is relatively high, ($I_{o\text{-}w} \approx 100\%$). The flotation test flow chart is given in Figure 21. Detail flotation test procedure can be obtained from Paper I and references there-in (Dubey and Doe, 1993; Mwangi et al. 2013; Erzuah et al. 2017)

4.1.2 QCM-D experiment procedure

The QCM-D experimental set-up for the oil adsorption studies is analogous to the schematics illustrated in Figure 20. The first step in the QCM-D test procedure is to thoroughly clean and dry the experimental set-up with nitrogen prior to mounting the sensor (either quartz or kaolinite as employed in this study). The flow-cell is then set to the desired reservoir temperature (65°C) after which the air in both the active and non-active part of the sensor were displaced with ethanol. The system fluid (n-decane in this study) was then injected to displace the ethanol from the non-active part of the flow-cell while the ethanol in the active part of the flow-cell (deposition area) was also displaced with the reference fluid (FW in this study). The back-pressure valve (BPV ≈ 0.65 MPa) was then connected and the log restarted after a stable baseline was detected. The designated fluids were injected in a sequence analogous to reservoir filling (i.e. FW/STO/FW). In other words, the reference fluid (FW) was injected prior to injecting the test fluids (n-decane or STO) as depicted by Steps I and II of Figure 22. The reference fluid (FW) was re-injected (Steps III of Figure 22) to evaluate the changes in its frequency (Δf) after injecting the test fluids (either n-decane or STO). The magnitude of the adsorbed oil can then be inferred from change in

the frequency signal (Δf) as illustrated by the Sauerbrey relation (Eqn 11). Detailed QCM-D procedure can be obtained from Papers III and IV (Erzuah et al. 2018a & 2018b).
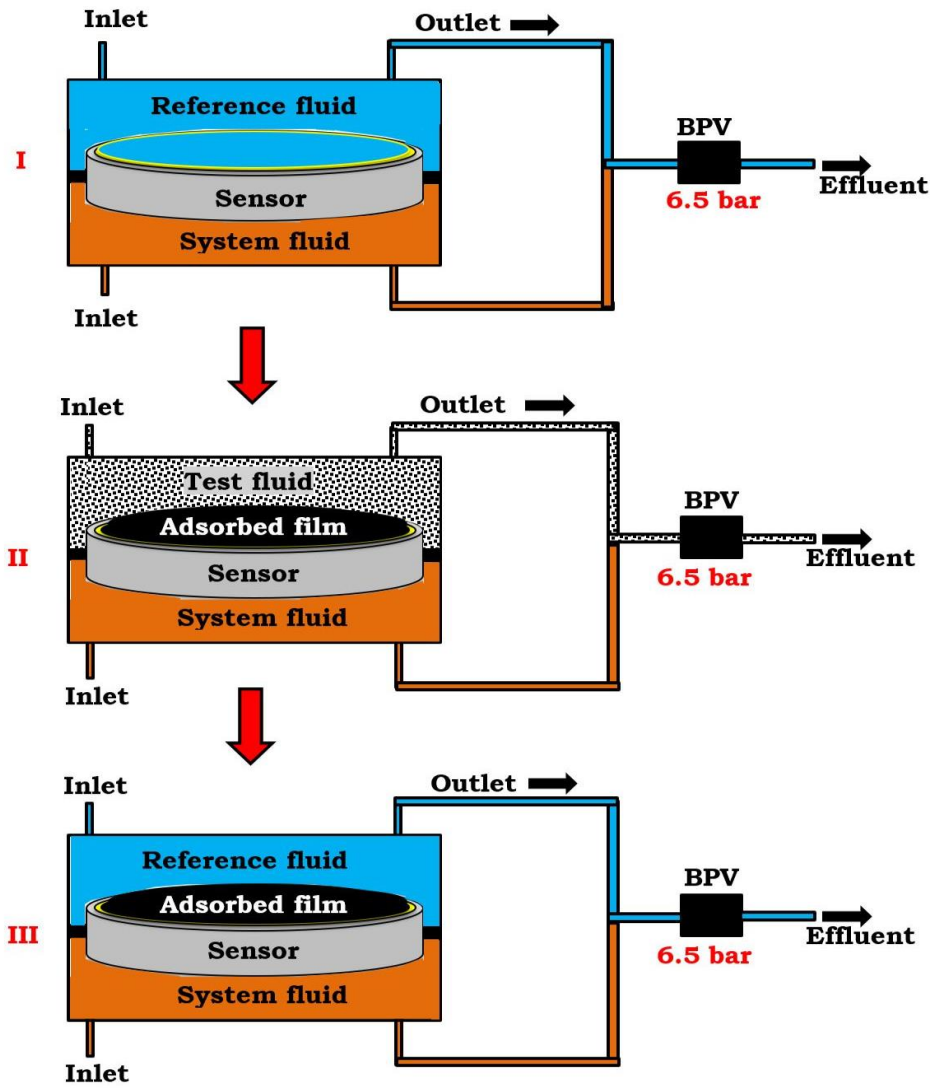
Figure 22: Detailed schematic of the QHPT flow-cell during the various injection sequence employed in the oil adsorption studies. Note that the injection sequence is analogous to the rock-fluids sequence reservoir filling. The system fluid used in this study is n-decane while the reference fluid is the brine. Finally, the test fluid is the oil phase (n-decane and STO). N-decane was employed as the reference test fluid while the desired test fluid is the STO.

4.1.3 Contact Angle Measurement procedure

The rationale behind the contact angle measurements was to replicate the rock-fluid interactions during reservoir filling. Nonetheless, mineral (rock) substrates were employed. The designated substrate was aged in a known volume of brine for 2 days at 65°C to depict the rock-brine interactions prior to crude oil accumulation. The brine phase was discarded after the ageing period. The excess brine on the substrate was removed using a centrifuge at 1000 rpm for 15 minutes. The substrate was then aged in 20 ml of the chosen oil (n-decane or STO) for 2 days at 65°C with back pressure to prevent the boiling out of the volatile oil components. The oil phase was discarded at the end of the ageing period while the excess oil on the substrate was also removed by centrifugation. The substrate was then mounted in a Drop Shape Analyzer (DSA) device and the chosen fluids (brine and oil) kept in their respective vessels.
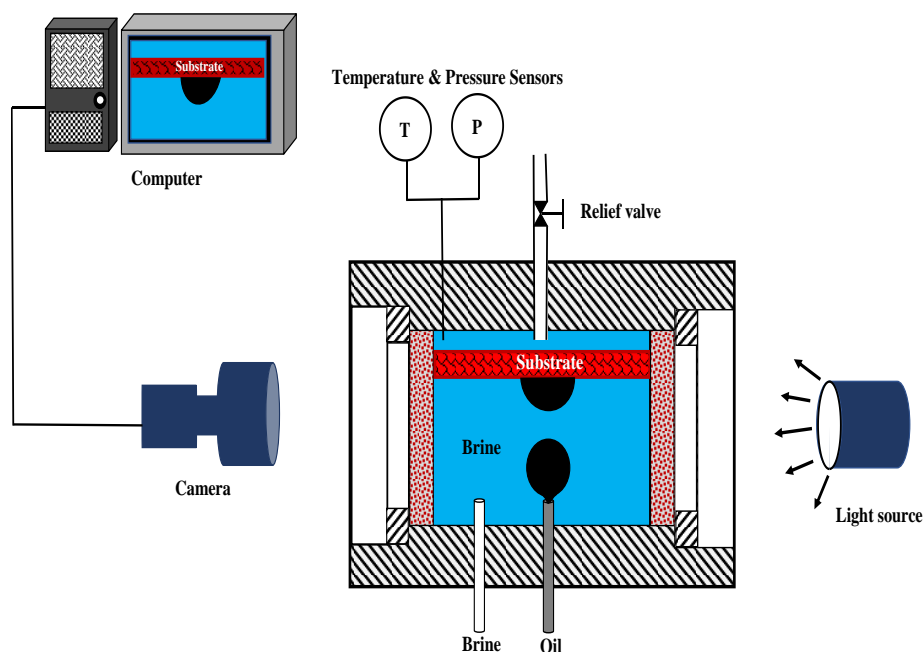
Figure 23: Contact angle measurement using Drop Shape Analyzer (DSA).

With the camera in place and all the connections to the experimental set-up secured, the desired brine is injected into the DSA chamber to displace the air in the system through the relief valve as illustrated in Figure 23.

The temperature and pressure were set to their respective values 65°C and 0.57 MPa and allowed to stabilize for at least 15 minutes. A droplet of the chosen oil is then placed on the substrate and its contact angle through the brine phase measured after a stable configuration is achieved.

4.2   Simulation approach via SCM

There is one striking similarity which spans through the developed QCM-D technique and the other existing techniques of wettability characterization such as the flotation test, USBM, Amott, contact angle etc. These techniques estimate the wettability by measuring a specific output (e.g. the magnitude of the oil adsorbed for the case of the QCM-D technique) but do not evaluate the COBR interaction mechanisms that triggered these observed effects. Numerous authors have reported that the adsorption of surface active components in the crude oil onto mineral/rock surface are governed by three main forces namely; hydration, Van der Waals, electrostatic forces (Busireddy & Rao 2004; Hirasaki 1991). To better understand the wetting preferences of the minerals/rock samples during the experimental techniques employed in this study, the COBR interactions were assessed via a geochemical simulator (PHREEQ-C). This was accomplished by capitalizing on the attractive electrostatic forces existing between the oil-brine and mineral-brine interfaces during COBR interactions via Surface Complexation Modelling (SCM). To model these experiments using a geochemical solver, the properties of the materials employed in the experiments were used as input into the SCM. The subsequent sections in this chapter will be used to shed light on how the various experiments were modelled. The modelling of the flotation test will be discussed first followed by the QCM-D experiment before that of the contact angle measurement.

4.2.1   Surface complexation : flotation test

Just as minerals have different intrinsic properties such as surface area and site densities, the crude oil also has varying intrinsic properties such as the concentration of polar functional groups. In the presence of brine these surfaces exhibit different charges ranging from anionic to cationic

(Buckley & Liu 1998). Hence, to model the flotation test via SCM, the possible COBR interactions must also be captured in the model.

4.2.1.1 Bond Product

In order for oil to be adsorbed onto a mineral/rock surfaces, the attractive electrostatic forces existing between the rock-brine and the oil-brine interfaces are analogous to Figure 24.
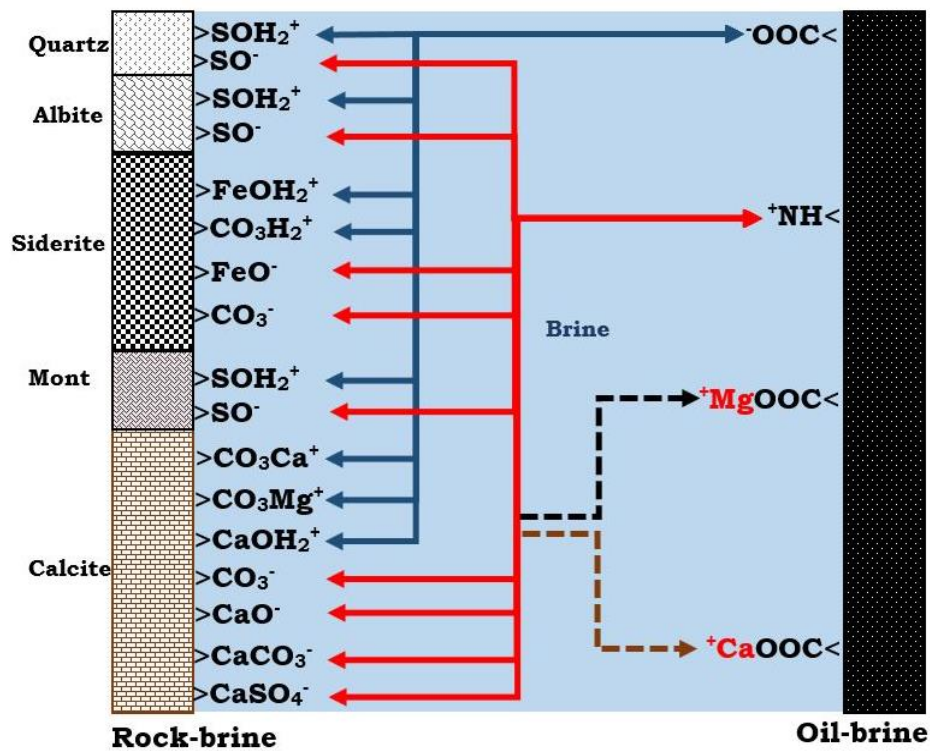
Figure 24: Analogy of the attractive electrostatic forces existing between the oil-brine and mineral-brine interfaces.

This attractive electrostatic force is represented by the Bond Product (BP) and it is the attractive electrostatic pair linkages existing between the rock site (in the rock-brine interphase) and an oil site (in the oil-brine interphase) of dissimilar charges. NB. Oil and mineral surfaces exhibit different charges ranging from cationic to anionic. Hence, for a given mineral/brine/oil interaction, the BP is the product of the mole fraction

of the oil and mineral sites with unlike charges. The sum of all the possible BP gives the Total Bond Product (TBP) and it expresses the tendency of oil to be adhered onto a mineral/rock surface. The TBP is analogous to the concentration of the oil-wet particles during the flotation test. Comprehensive studies on surface reactions and their reaction constants of various minerals have been reported in literature by numerous authors. The plan was to capitalize on these available data to better understand the experimental results.

Though, PHREEQ-C has no oil components in its database, an effective concentration of the acidic and basic oil components was incorporated into the SCM using the relation;

$$Oil\ Site\ Density\ (site/nm^2) = \frac{TAN\ or\ TBN}{M_w\ KOH}\ x\ \frac{N_A}{A_{eff}} \tag{16}$$

Where
TAN   Total Acid Number, mg KOH/g oil
TBN   Total Base Number, mg KOH/g oil
M_w KOH   Molecular weight of KOH, (56.105 g/mol)
A_{eff} Effective surface area of the mineral/rock sample, m^2/g
N_A Avogadro's Constant, ($6.022140857 \times 10^{23}$ mol^{-1})

Since the surface area available for oil adsorption is the effective surface area of the rock/mineral and hence, the effective surface area of the rock/mineral was used to estimate the oil site densities.

Surface	Site Density (site/nm^2)	Effective Surface Area (m^2/g)
Quartz	10.00	1.20
Albite	1.155	1.20
Illite	1.37	66.8
Montmorillonite	5.7	3.0
Calcite	4.90	2.00

Table 4: Properties of the dominant sandstone reservoir rock minerals used in this study. These properties include site density (site/nm^2) and the effective surface area (m^2/g). Note: The surface area and site density of quartz were obtained from Sverjensky and Sahai (1996). Albite surface area and site density were assumed to be the same as quartz. The surface area and site density for illite and montmorillonite were also obtained from Gu and Evans (2007) & Wieland et al. (1994). For calcite, the surface area (Hjuler & Fabricius, 2009) and site density (Wolthers et al. 2008).

Mineral Surface	Oil Surface	STO#1 (site/nm^2)	STO#1 (site/nm^2)	Effective Surface Area (m^2/g)
Quartz	>COOH	0.89	3.40	1.20
	>NH$^+$	16.99	20.56	1.20
Albite	>COOH	0.89	3.40	1.20
	>NH$^+$	16.99	20.56	1.20
Illite	>COOH	0.02	0.06	66.8
	>NH$^+$	0.31	0.37	66.8
Montmorillonite	>COOH	0.36	1.36	3.0
	>NH$^+$	6.79	8.23	3.0
Calcite	>COOH	0.54	2.04	2.00
	>NH$^+$	10.20	12.34	2.00

Table 5: Estimated oil site density (site/nm^2) used during the flotation tests. It was assumed that the surface area of the oil was the same as the mineral (rock) surface.

Surface Reactions	log K (25ºC)	Enthalpy (KJ/mol)
[a]Oil Surface		
>NH$^+$ ↔ >N + H$^+$	-6.0	34.0
>COOH ↔ >COO$^-$ + H$^+$	-5.0	0.0
>COOH + Ca^{2+} ↔ >COOCa$^+$ + H$^+$	-3.8	1.2
>COOH + Mg^{2+} ↔ >COOMg$^+$ + H$^+$	-4.0	1.2[g]
[b]Quartz		
>Si-O-H + H$^+$ ↔ >Si-O-H$_2^+$	-1.1	-26.4
>Si-O-H ↔ >Si-O$^-$ + H$^+$	-8.1	8.4
[c]Albite		
>Si-O-H + H$^+$ ↔ >Si-O-H$_2^+$	1.9	16.3
>Si-O-H ↔ >Si-O- + H$^+$	-8.5	1.3
[d]Illite		
>Si-O-H + H$^+$ ↔ >Si-O-H$_2^+$	7.43	24.3[h]
>Si-O-H ↔ >Si-O- + H$^+$	-8.99	18.8[i]
H$^+$ + NaX$_{ill}$ ↔ HX$_{ill}$ + Na$^+$	1.58	
[e]Montmorillonite		
>Si-O-H + H$^+$ ↔ >Si-O-H$_2^+$	5.4	24.3[h]
>Si-O-H ↔ >Si-O- + H$^+$	-6.7	18.8[i]
H$^+$ + NaX$_m$ ↔ HX$_m$ + Na$^+$	4.6	
[f]Calcite		
>CO$_3$H ↔ >CO$_3^-$ + H$^+$	-4.9	-5.0
>CO$_3$H + Ca^{2+} ↔ >CO$_3$Ca$^+$ + H$^+$	-2.8	25.7
>CO$_3$H + Mg^{2+} ↔ >CO$_3$Mg$^+$ + H$^+$	-2.2	4.5
>CaOH + H$^+$ ↔ >CaOH$_2^+$	12.2	-77.5
>CaOH ↔ >CaO$^-$ + H$^+$	-17.0	116.4
>CaOH + 2H$^+$ + CO$_3^{2-}$ ↔ >CaHCO$_3$ + H$_2$O	24.2	-90.7
>CaOH + CO$_3^{2-}$ + H$^+$ ↔ >CaCO$_3^-$ + H$_2$O	15.5	-61.6
>CaOH + SO$_4^{2-}$ + H$^+$ ↔ >CaSO$_4^-$ + H$_2$O	13.9	-72.0

Table 6: SCM input parameters for some of the dominant minerals in the studied sandstone rocks. [a] after Brady and Krumhansl (2012b) while [b] and [c] were obtained from Sverjensky and Sahai (1996, 1998). [d] was also obtained from Gu and Evans (2007), [e] after Wieland et al. (1994) and [f] from Wolthers et al. (2008). [g] Enthalpy during Mg^{2+} reaction with >COOH was assumed to be the same as that of Ca^{2+}. [h] and [i] assummed to be the same as similar reactions as kaolinite. Note. X$_{ill}$ and X$_m$ depicts the exchange sites of illite and montmorillonite respectively.

The flotation tests were predicted using the properties and quantities of the surfaces (oil and mineral) as input into the geochemical solver, PHREEQ-C.

4.2.2 Surface Complexation: QCM-D test

Like the simulation of the flotation test, the COBR interactions that led to the oil adsorption during the QCM-D experiment were also assessed via SCM. This was accomplished using similar properties and quantities of the materials used during the QCM-D experiment. In other words, similar qualities and quantities of the material used during the QCM-D experiment were also used as input into the SCM. The oil adhesion due to the electrostatic pair linkages existing between the kaolinite-brine and the oil-brine interfaces during the QCM-D experiment is illustrated in Figure 25. The magnitude of the adsorbed oil during the QCM-D experiment is analogous to the TBP.
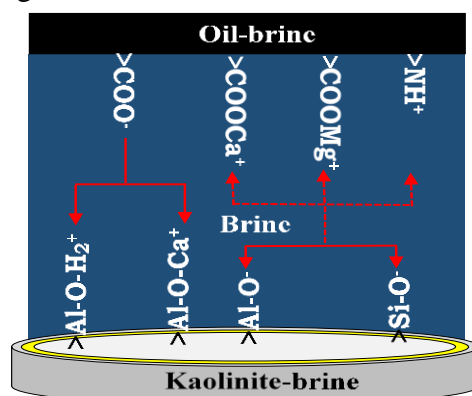
Figure 25: Analogy of oil adsorption onto kaolinite sensor. During the QCM-D experiments, the oil adhesion onto the kaolinite sensor is attributed to the electrostatic pair linkages existing between the kaolinite-brine and oil-brine interfaces.

4.2.3 SCM: Contact angle measurement modelling

Like the simulation of the COBR interactions during the flotation and QCM-D experiments, the COBR interactions at the three-phase region during contact angle measurement can also be simulated via SCM (Figure 26). In other words, the oil adhesion tendencies at the three-phase region can be used to confirm the contact angle measurements.
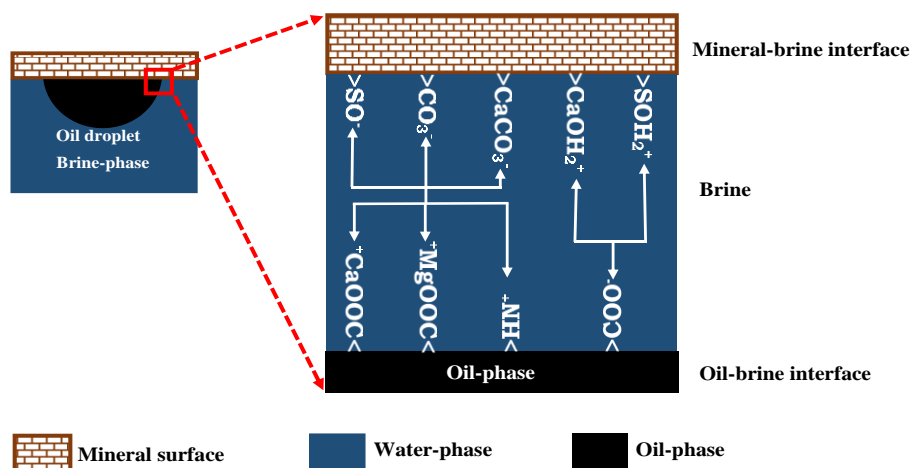
Figure 26: Analogy of oil adhesion onto mineral (rock) substrates. The mineral-brine and the oil-brine interactions at the three-phase region during contact angle measurements controls the wettability.

4.2.4 Materials employed in the prediction of literature experiments

Apart from verifying the SCM technique with the experimental work employed during these studies, the SCM technique was also used to predict laboratory experiment results from literature. The methods employed in the literature data includes zeta-potential measurements (Alotaibi & Yousef 2017), spontaneous imbibition of chalk using carbonated water (CW) and FW (Fjelde et al. 2011) and wettability estimation using the Amott and USBM (Torsaeter 1988). To predict these experiments, the properties and quantities of the materials such as the surfaces involved (mineral and oil) and the ionic composition of the brine used in the experiments were incorporated into the model.

For the zeta potential measurements, Alotaibi and Yousef (2017) employed a carbonate disk of purity greater than 99 wt% of calcium carbonate in their experiment. They also reported that the STO used was obtained from a gas oil separation plant in Saudi Arabia. In addition, the compositions of the brines used in the zeta-potential measurements are given in the Table 7. Detailed description of surface complexation during

zeta potential measurement (Alotaibi & Yousef 2017) can be obtained from Paper II.

Ions	NaCl	CaCl$_2$.6H2	MgCl$_2$.6H2O	Na$_2$SO$_4$	Smart Water	Key Ions
Na$^+$	2,266	-	-	1,865	1,824	721
Mg^{2+}	-	-	1,471	-	211	741
Ca^{2+}	-	2,080	-	-	65	228
SO$_4^{2-}$	-	-	-	3,896	429	1506
Cl$^-$	3,495	3,681	4,290	-	3,220	2,565
TDS (ppm)	5,761	5,761	5,761	5,761	5,761*	5,761
*HCO$_3^-$: 12ppm						

Table 7 : Ionic composition of the brine used in the zeta-potential measurements (Alotaibi & Yousef 2017)

Secondly, for the spontaneous imbibition experiment, the STO employed was obtained from fractured chalk field (Fjelde et al. 2011). The TAN and TBN of the STO were 0.1 mg KOH/g oil and 1.3 mg KOH/g respectively. Fjelde et al. (2011) reported that Liege core plugs were used as analog for reservoir chalk in the spontaneous imbibition experiment. The composition of the synthetic formation water used in the spontaneous imbibition experiment (FW-SI) is given in Table 8. Detailed description of surface complexation during the spontaneous imbibition experiment (Fjelde et al. 2011) can be obtained from Paper VI.

ION	FW-SI (mmol/L)	FW-WE (mmol/L)
Na$^+$	629.85	533.61
K$^+$	4.16	3.07
Mg^{2+}	22.03	6.66
Ca^{2+}	226.16	28.00
Sr^{2+}	0.00	0.00
Cl$^-$	1130.40	599.75
HCO$_3^-$	0.00	6.26

Table 8: The compositions of the brines used in the literature experiments. NB. The Ionic composition of the FW used in the spontaneous imbibition experiment (FW-SI) was obtained from (Fjelde et al. 2011) while the FW composition used in the Amott and USBM wettability estimation (FW-WE) was also obtained from (Torsaeter 1988).

Finally, for the Amott and USBM wettability measurements (Torsaeter 1988), the composition of the brine used in the experiments (FW-WE) can be obtained from Table 8. The mineralogical composition of the North Sea sandstone reservoir rock employed by Torsaeter (1988) can

also be obtained from Table 9. Note. Fields S_1, S_2 and S_3 denote the first, second and third coring depths respectively.

Mineral	Field S_1 (%)	Field S_2 (%)	Field S_3 (%)
Quartz	53.2	63.8	52.0
Plagioclase	19.2	15.0	17.7
Feldspar	16.0	11.4	8.9
Illite	1.7	2.0	4.4
Kaolinite	8.0	6.2	5.5
Iron hydroxide	0.0	0.0	0.0
Calcite	1.4	0.0	9.9
Chlorite	0.5	1.6	1.6

Table 9: Compositions of the North Sea Sandstone reservoir rock used in the Amott and USBM wettability estimation (Torsaeter 1988).

The Total Acid Number (TAN) and the Total Base Number (TBN) reported by Torsaeter (1988) in his experiments was 0.02 mg KOH/g oil and 1.1 mg KOH/g oil respectively. The oil sites densities were estimated as reported in Papers II, V and VI (Erzuah et al. 2019) while the minerals site densities (Table 10) can also be obtained from literature. The oil and mineral surface reactions and their reaction constant were also obtained from similar reaction reported in literature.

Mineral surface	Mineral Site Density (site/nm^2)	Oil Surface	Oil Site Density (site/nm^2)
Quartz	10.00	>COOH	0.18
		>NH$^+$	9.83
Plagioclase	1.16	>COOH	0.18
		>NH$^+$	9.83
Feldspar	10.00	>COOH	2.15
		>NH$^+$	118.02
Illite	1.37	>COOH	0.003
		>NH$^+$	0.18
Kaolinite	1.16	>COOH	0.02
		>NH$^+$	1.18
Iron hydroxide	10.00	>COOH	0.18
		>NH$^+$	9.83
Calcite	4.90	>COOH	0.11
		>NH$^+$	5.90
Chlorite	10.00	>COOH	0.002
		>NH$^+$	0.09

Table 10 : Oil and mineral properties of the surfaces during the Amott and USBM wettability measurements. NB. The Amott and USBM wettability measurements were predicted by incorporating into the SCM, the equivalent site densities of the surfaces (minerals and oil).

5   Results and Discussions

In this chapter some of the main results will be discussed. The flotation test results and its simulated counterpart will be presented first followed by that of the QCM-D. Next, the contact angle measurement results will be presented prior to presenting its simulated counterparts. Finally, the SCM wettability estimation technique will also be validated with existing results from literature.

5.1   Flotation test results

The flotation test results for some dominant sandstone reservoir rock minerals will be presented first prior to presenting the simulated counterpart. After which the flotation test for rock/mineral mixtures will also be presented before that of the predicted results via SCM.

5.1.1   Flotation test versus SCM results; Minerals

Each flotation test results were obtained from an average of six similar tests. The results portray that quartz is strongly hydrophilic while calcite is strongly oleophilic (Figure 27). The vertical bar depicts the experimental error during the flotation tests, and it was observed to be ±5%.
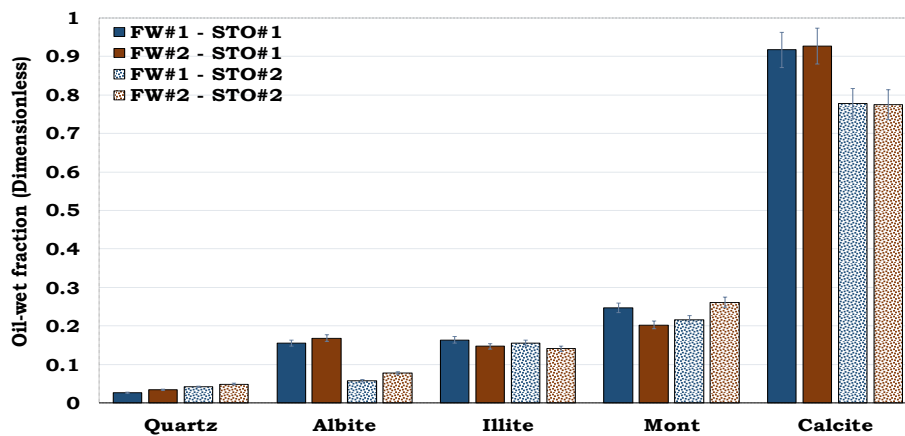
Figure 27: Flotation test results of the dominant minerals in the studied sandstone rocks. Quartz was observed to be strongly hydrophilic while calcite was strongly hydrophobic.

The predicted surface complexation (Figure 28) could capture the main trends during the flotation test results. In other words, quartz was strongly water-wet while calcite was also strongly oil-wet as observed in the flotation test.
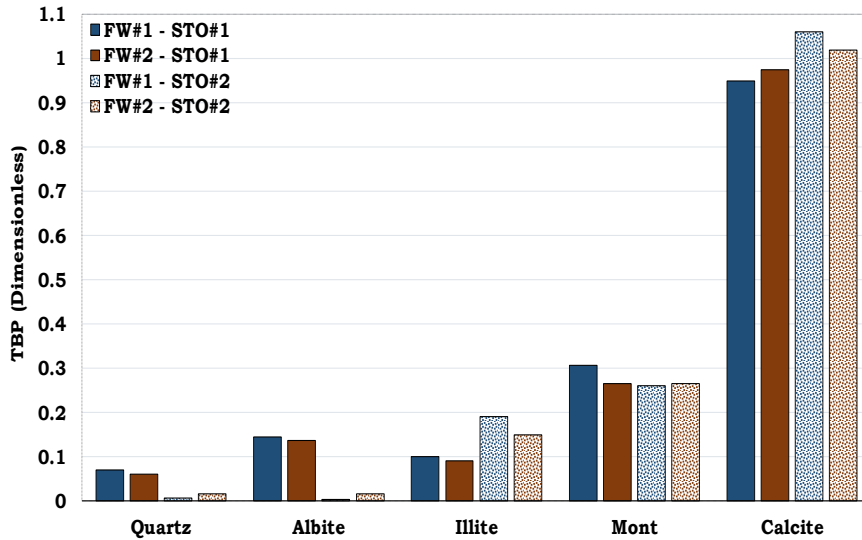
Figure 28: Simulated flotation test results of the dominant minerals in the studied sandstone rocks via SCM.

5.1.2   *Flotation test versus SCM results; Rock*

Like the flotation test results of the individual minerals, that of the reservoir rocks and mineral mixtures were also obtained from an average of six parallel experiments. From Figure 29, it can be observed that both Sandstone Reservoir Rocks (SRR #1 and SRR #2) were strongly hydrophilic while that of the mineral mixture with 50% calcite content (PSR #4) was observed to be strongly oleophilic.
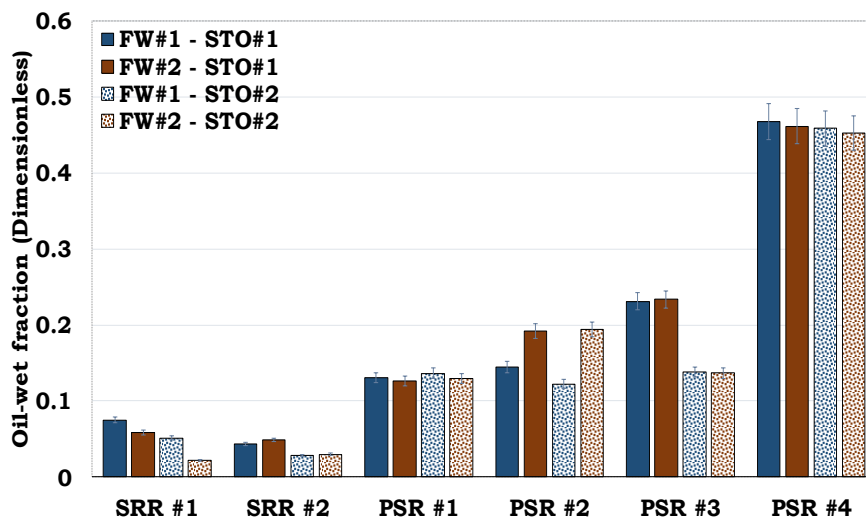
Figure 29: Flotation test results of Sandstone Reservoir Rocks (SRR) and Pseudo-Sandstone Rock (PSR). The PSR were designed to assess the effect of increasing surface area (PSR #1 and PSR #2) and calcite content (PSR #2 and PSR #4)

The results of the simulated flotation test (Figure 30) of the rock samples and mineral mixtures were in the same order as observed during the experimental results (Figure 29). This shows that the SCM could capture the trend during the flotation experiments.
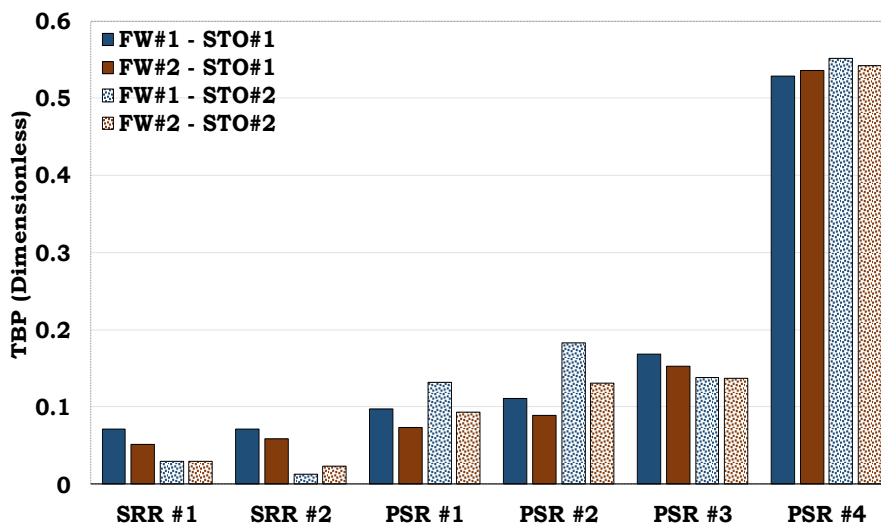
Figure 30: Predicted flotation tests of the Sandstone Reservoir Rocks (SRR) and the Pseudo-Sandstone Rock (PSR) via SCM.

5.1.3 *Oil adsorption mechanisms prediction*

The rock-brine and oil-brine interactions were also simulated to assess the mechanisms of oil adhesion onto the rock. The oil adhesion mechanisms onto the surfaces of SRR #1, PSR #2 and PSR #4 will be considered.

Oil adhesion mechanisms in SRR #1

It can be observed from Figure 31 that, divalent cation bridging dominated the oil adhesion in SRR#1. The oil adhesion was due to the bridging of the two negative surfaces, quartz-brine ($>SO^-$) and oil-brine ($>COO^-$) by divalent cations (Ca^{2+}). Direct adhesion of carboxylate ($>COO^-$) onto the positive illite sites (SOH_2^+) was the second dominant mechanism that led to the adhesion of oil onto the SRR #1. This can be attributed to the relatively high effective surface area (≈ 5.8 m^2/g) as compared to quartz (≈ 1.0 m^2/g). Though the mineralogical content of the illite was negligible (8.8%) as compared to quartz (83.7%), the intrinsic surface area of the former was higher (66.8 m^2/g) than the latter (1.2 m^2/g) and hence the observed results.
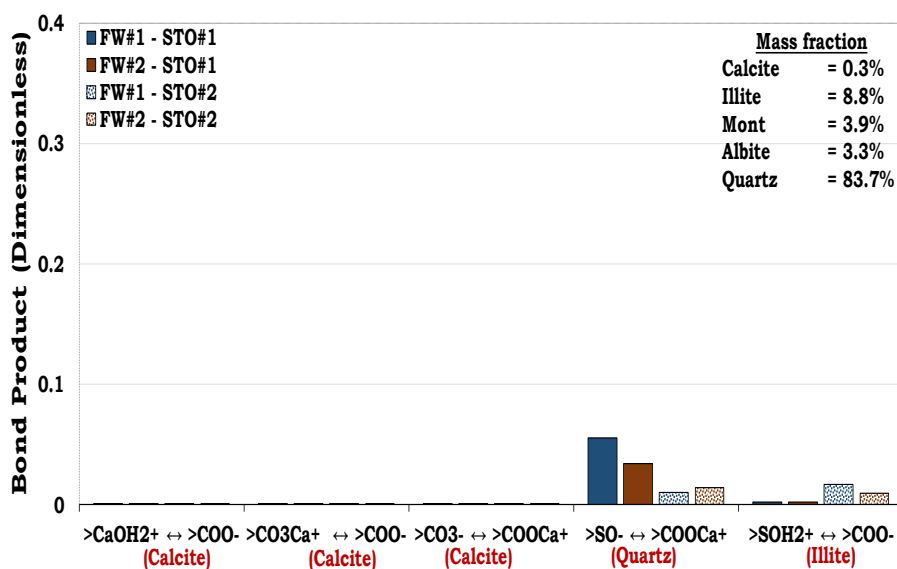
Figure 31: Mechanisms of oil adhesion onto the sandstone reservoir rock #1 (SRR#1) via SCM.

Oil adhesion mechanisms in PSR #2

The dominant oil adhesion mechanism in the PSR #2 (Pseudo-Sandstone Rock with 54.4% illite content) was direct adhesion of carboxylate (COO^-) onto the positive illite surface (SOH_2^+) as observed in Figure 32. Considering the PSR#2, the relatively high oil adhesion onto the illite as compared to quartz can be linked to the high effective surface area of the former (36.3 m^2/g) as compared to the latter (0.5 m^2/g). This explains why the oil adhesion mechanism in quartz was low (Figure 32) though, its content in the PSR #2 was relatively high (41.85%).
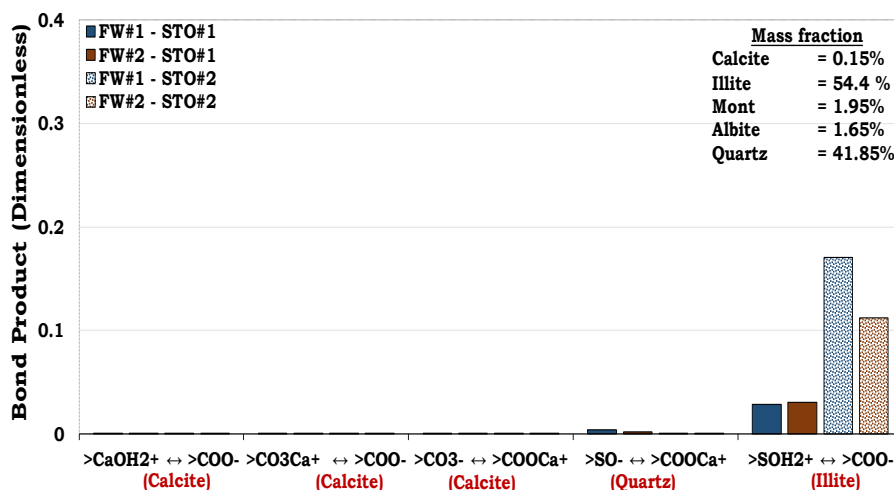
Figure 32 : Simulated oil adhesion mechanisms in the Pseudo-Sandstone Rock #2 (PSR#2) via SCM.

Oil adhesion mechanisms in PSR #4

Direct adhesion of carboxylate ($>COO^-$) onto the positive sites on the calcite and illite surfaces ($>CaOH_2^+$ and $>SOH_2^+$ respectively) occurred in the PSR #4 (Pseudo-Sandstone Rock with approximately 50% calcite content), nonetheless the latter was less distinct (Figure 33). It can also be observed from Figure 33 that, oil adhesion due to cation bridging took place in calcite ($>CO_3^- \leftrightarrow >COOCa^+$), quartz ($>SO^- \leftrightarrow >COOCa^+$), and illite ($>SOH_2^+ \leftrightarrow >COOCa^+$). Considering the oil adhesion mechanisms in SRR #1 and PSR #4, it can be concluded that the wetting preferences

of the sandstone rocks are dictated by the calcite (hydrophobic mineral) content as depicted in Figure 31 and Figure 33.
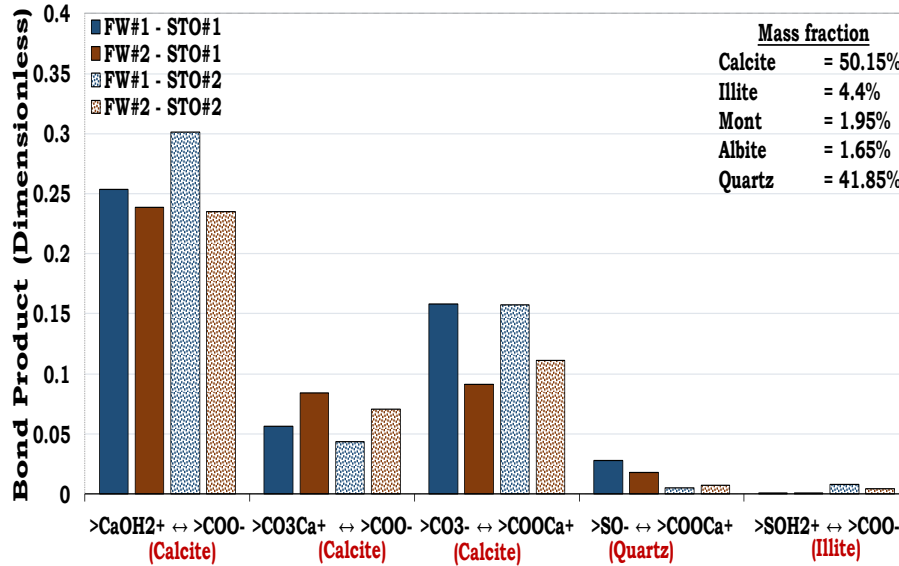
Figure 33 : Oil adhesion mechanisms in the Pseudo-Sandstone Rock #4 (PSR#4) via SCM.

5.1.4 Interfacial charge prediction

Since the oil-brine and mineral-brine interfacial charges play a vital role in electrostatic pair linkages, the interfacial charges were also simulated to assess underlying mechanisms during the oil adhesion.

Mineral-brine interface charge

The surface charge at the mineral-brine interface, which is calculated from the sum of all the surface site shows that quartz, albite and montmorillonite are mainly anionic at the studied condition with the latter being more distinct. Hence direct adhesion of the basic oil component ($>NH^+$) onto these anionic surfaces might take place if the effect of the basic surface site is not negligible. If both oil ($>COO^-$) and mineral surfaces are anionic, divalent cation (Ca^{2+} and Mg^{2+}) can bridge these surfaces leading to oil adhesion. From Figure 34, it can be observed that illite and calcite are mainly cationic and hence, direct adhesion of

56

carboxylate ($>COO^-$) onto the cationic surfaces (illite and calcite) can lead to oil adhesion.
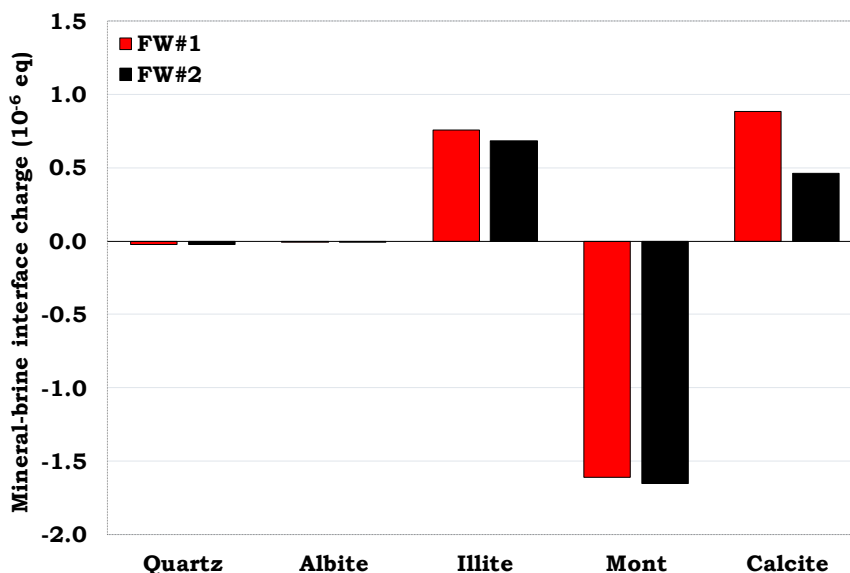
Figure 34 : Prediction of the mineral-brine interfacial charge during the flotation test via SCM.

Oil-brine interface charge

Just as the mineral-brine interface charge is very important in oil adsorption, so is the oil-brine interface charge. This is because, the oil adhesion due to the attractive electrostatic force exist between the mineral-brine and oil-brine interfaces. It can be observed from Figure 35 that, the oil-brine interface charges for the studied oil-brine systems were predominantly negative charged except for STO#2-FW#2 interface of quartz, albite and calcite. This is because, the surface area of the oil was assumed to be the same as their respective mineral surfaces. Hence, though the surface area of the oil with quartz, albite and calcite might be negatively charged, the oil-complex ($>COOCa^+$ and $>COOMg^+$) formed with the divalent cations in the brine (Ca^{2+} and Mg^{2+}) will dictate the surface charge of the oil. This was also confirmed by the high concentration of divalent ions in the FW#1 as compared to FW#2 (Table 2).
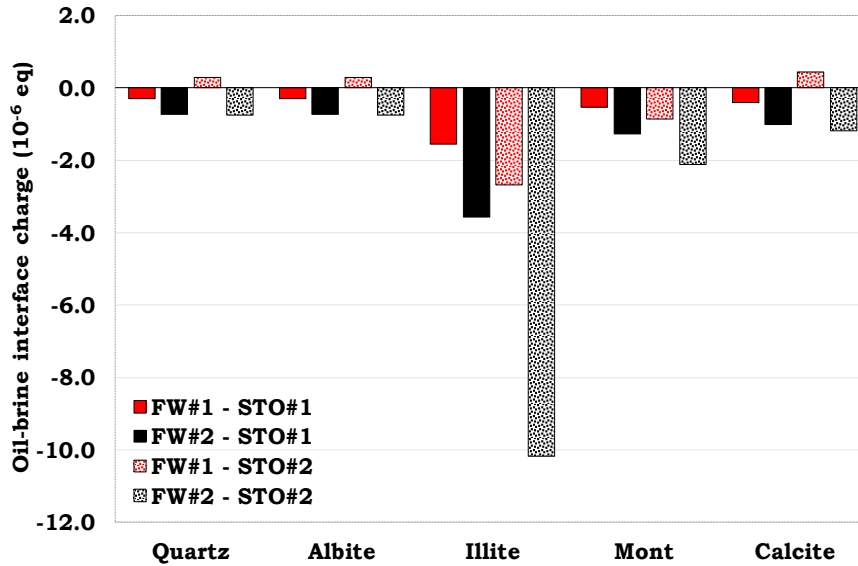
Figure 35 : Simulated oil-brine interfacial charge during the flotation tests via SCM.

5.2 QCM-D experimental results

For the QCM-D experimental results, the experiments with quartz sensor and the reference oil (n-decane) will be presented first followed by its STO counterpart (i.e. quartz: FW/N-decane/FW and FW/STO/FW injection sequences respectively). This will be followed by a similar injection sequence but with kaolinite sensor. Finally, the SCM prediction of the QCM-D experiments will also be presented.

5.2.1 Quartz/FW/N-decane

Considering the FW/n-decane/FW injection sequence with quartz sensor (Figure 36), it can be observed that the change in FW frequency (Δf) prior to and after the n-decane injection was negligible (0 Hz). This was attributed to lack of oil adsorption resulting from the absence of surface-active components in the n-decane (reference oil). From Figure 36, the bulk shift in the n-decane frequency signal (Section II of Figure 36) prior

to and after the injection of the FW is attributed to the contrast in the fluid properties such as density and viscosity.
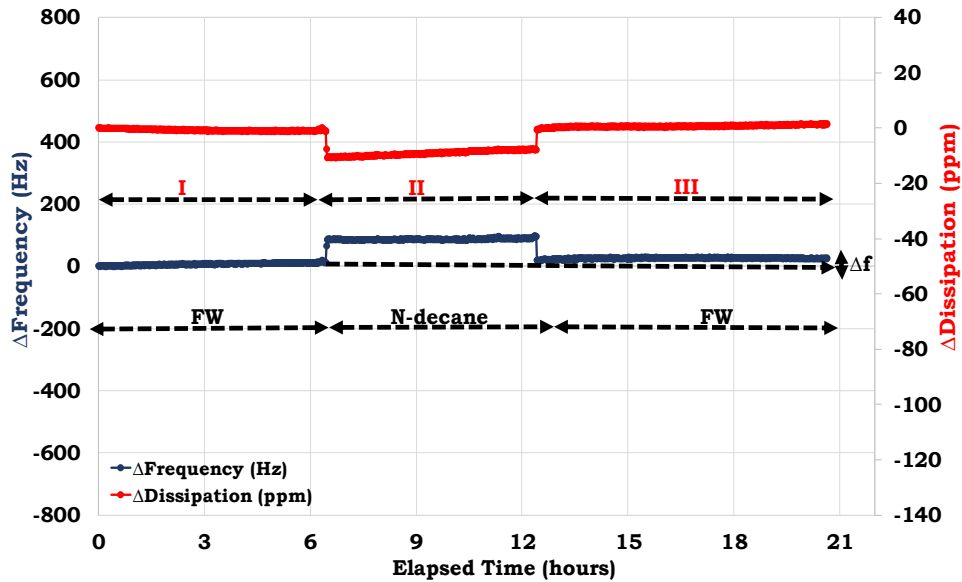
Figure 36 : Lack of oil adsorption onto the quartz sensor during FW/n-decane/FW injection sequence using QCM-D.

5.2.2 Quartz/FW/STO

Similar to the negligible change in the frequency signal (Δf) during FW/n-decane/FW injection sequence with quartz sensor (Figure 36), the FW/STO/FW injection sequence with quartz sensor (Figure 37) also resulted in no change in the frequency signal (Δf). Unlike the n-decane, the STO has surface active components in the crude oil. Nonetheless, negligible polar oil component from the STO was adsorbed onto the quartz sensor. This was confirmed by the lack of added mass onto the quartz sensor as depicted by the relatively constant frequency signals during the FW/STO/FW injection sequence Figure 37. This was linked to the strong hydrophilic nature of quartz.
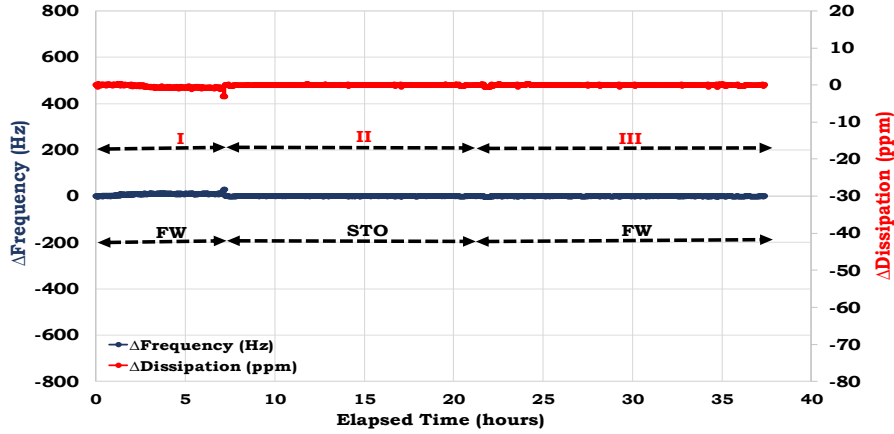
Figure 37: Negligible oil adsorption onto the quartz sensor during FW/STO/FW injection sequence using QCM-D. This is depicted by the minimal change in frequency of the quartz sensor.

5.2.3 Kaolinite/FW/N-decane

Like the FW/n-decane/FW injection sequence with quartz sensor (Figure 36), similar injection sequence with kaolinite sensor (Figure 38) also resulted in lack of oil adsorption due to the negligible change in the frequency signal (Δf).
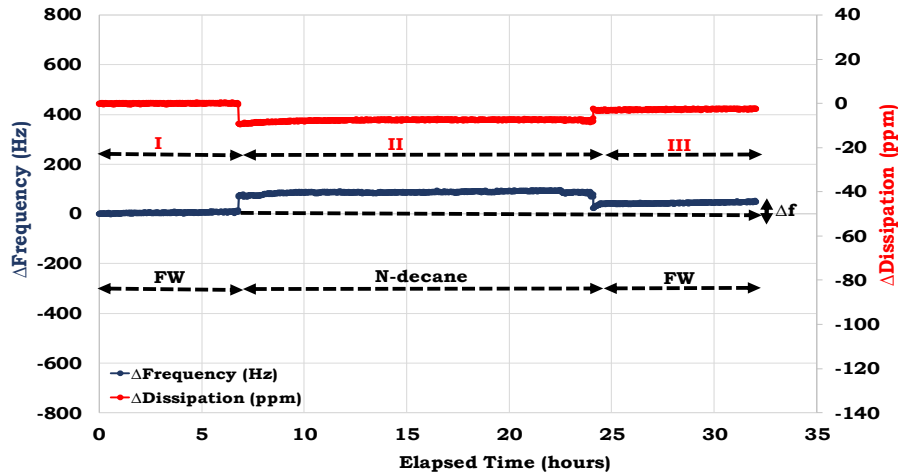
Figure 38: Minimal oil adsorption onto the kaolinite sensor during FW/n-decane/FW injection sequence using QCM-D.

60

This was credited to the lack of surface-active components in the n-decane (reference oil). The negligible energy loss by the oscillating sensor (0ppm) was due to no added mass resulting from lack of oil adsorption.

5.2.4 Kaolinite/FW/STO

Contrary to the lack of oil adsorption onto the quartz sensor during the FW/STO/FW injection sequence (Figure 37), a similar injection sequence with the kaolinite sensor resulted in oil adsorption (Figure 39). This was expressed by the relatively high change in the FW frequency signal ($\Delta f \approx 280$ Hz) before and after the injection of the STO (Figure 39). The relatively high change in the dissipation signal ($\Delta D \approx 80$ ppm) confirms the energy loss by the sensor due to the oil adsorption. Comparing the injection sequences of FW/n-decane/FW and the FW/STO/FW with kaolinite sensors (Figure 38 and Figure 39 respectively), it can be concluded that the surface active components in the crude oil is one of the key parameters that dictates the wetting state of minerals. In addition, it can be concluded that the minerals have varying wetting preferences due to their inherent properties as depicted by the FW/STO/FW injection sequence with quartz and kaolinite sensors (Figure 37 and Figure 39).
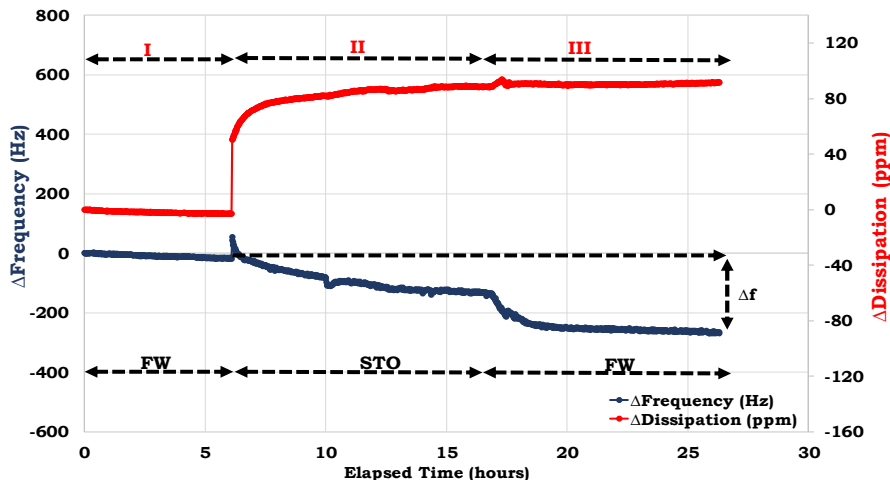
Figure 39: Oil adsorption onto the kaolinite sensor during FW/STO/FW injection sequence using QCM-D.

61

Note that for a given injection sequence, the injection was stopped only when a relatively constant frequency was achieved. For instance, during the injection STO (Section II of Figure 39), the injection was only stopped when the STO's frequency signal was relatively constant.

5.2.5 Kaolinite/LSW/STO

Unlike the relatively high oil adsorption during the FW/STO/FW injection sequence with the kaolinite sensor (Figure 39), the LSW/STO/LSW injection sequence with a similar kaolinite sensor resulted in a negligible oil adsorption as depicted in Figure 40. The lack of oil adsorption onto the kaolinite surface (Figure 40) was attributed to the low concentration of divalent cations (Ca^{2+} and Mg^{2+}) in the LSW as compared to FW (Table 2). This shows that the composition of the brine play an important role in the wetting state of the mineral in addition to the mineralogy and the composition of the oil reported earlier. Moreover, Erzuah et al. (2019) reported that divalent cations (Ca^{2+} and Mg^{2+}) in the brine can lead to oil adhesion by serving as a bridge if both the mineral-brine and the oil-brine surfaces are negatively charged.
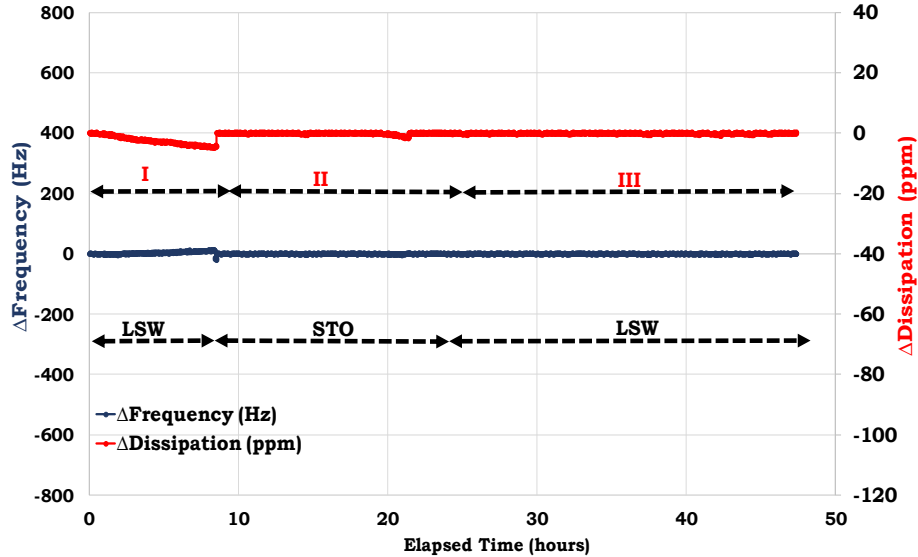
Figure 40: Negligible oil adsorption onto the kaolinite sensor during LSW/STO/LSW injection sequence using QCM-D.

It was not surprising that the oil adsorption onto the kaolinite sensor was negligible (Figure 40) due to the low Ca^{2+} concentration in LSW composition (0.70 mmol/L) as compared to the FW (174.00 mmol/L) and hence, the observed results.

5.2.6 Oil adhesion prediction during the QCM-D tests via SCM

The SCM was also used to predict the oil adhesion tendencies during the QCM-D experiments. From Figure 41, it can be concluded that the SCM could capture the oil adsorption trend of the mineral-fluid systems during the QCM-D experiments. For instance, the predicted magnitude of n-decane adhesion onto the mineral (quartz and kaolinite) surfaces were negligible (Figure 41) as confirmed by their corresponding QCM-D experiments (Figure 36 and Figure 38 respectively).
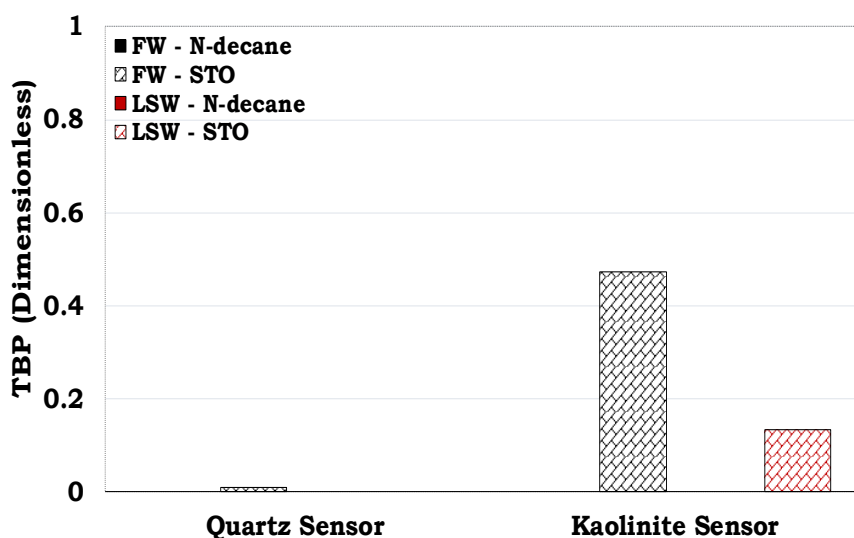
Figure 41: Predicted oil adhesion tendencies of the studied quartz and kaolinite sensors. It can be inferred that lack of oil adhesion onto the sensors with the reference fluid (n-decane) is due to the absence of surface-active components in reference fluid unlike the test fluids (STO) and hence, the observed results.

The lack of n-decane adsorption was attributed to its non-polar nature and hence, the observed results. On the other hand, the simulated mineral/brine/STO interactions during the QCM-D experiments revealed that the tendency of oil to be adsorbed onto kaolinite was higher than quartz (Figure 41) as confirmed by the QCM-D experiment results (Figure 39 and Figure 40).

5.2.6.1 **Estimated thickness (Δt_{ads}) and mass of adsorbed film (Δm_{ads})**

The oil adsorption tendencies during the QCM-D experiments and the SCM simulations were also estimated via Δt_{ads} and Δm_{ads} of the adsorbed film using the Sauerbrey equation (Eqn 11). Considering the kaolinite/FW/STO interaction during the FW/STO/FW injection sequence (Figure 39), the thickness (Δt_{ads}) and mass (Δm_{ads}) of the adsorbed film were also estimated to confirm the SCM results. For instance, the predicted thickness ($\Delta t_{ads} \approx 5.8$ nm) and mass of the adsorbed film ($\Delta m_{ads} \approx 1600$ng/cm^2) confirms that the adsorption of polar oil components onto mineral surfaces dictates the wetting preferences as supported by the QCM-D results (Figure 39).
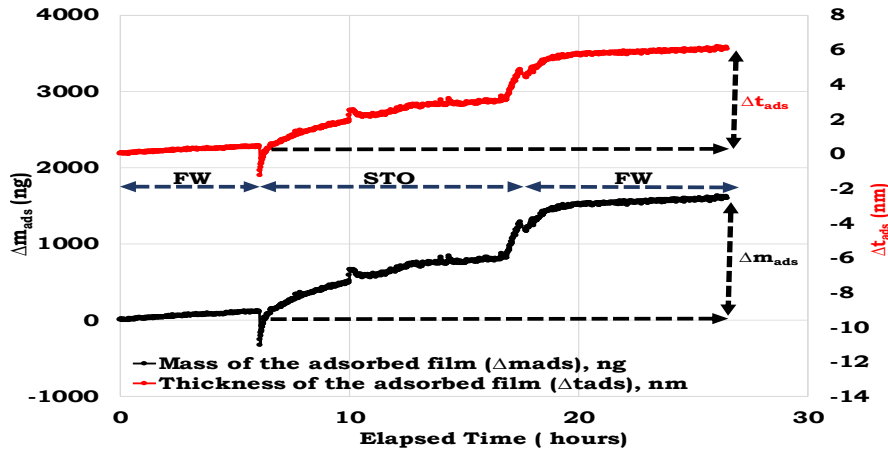
Figure 42: Calculated magnitude and thickness of the adsorbed film during the QCM-D experiment. For the kaolinite sensor, it can be inferred that the calculated increase in thickness and magnitude of the film during the FW/STO/FW injection sequence depicts oil adhesion.

Further readings on wettability estimation by oil adsorption using QCM-D can be obtained from Paper IV.

5.3 Contact angle measurements

The contact angle measurements on the mineral substrate (quartz, kaolinite and calcite) will be presented first to assess the wetting preferences of each mineral under the studied conditions. The contact angle measurement on the sandstone rock substrate will be presented next. The mineral-brine and the oil-brine interactions during the contact angle experiments were also estimated to evaluate the wetting tendencies of the minerals via SCM. This was achieved by predicting the Total Bond Product (TBP) which is the tendency of oil to be adsorbed onto a mineral or rock surface. In addition, the mechanisms that led to the oil adsorption were also assessed via SCM. Note that FW#1 (Table 2) was used as the brine phase for all contact angle measurements.

5.3.1 Mineral substrate

It can be observed from Figure 43 that, the wetting state of the minerals (quartz, kaolinite and calcite) with the reference oil (n-decane) were observed to be hydrophilic as confirmed by their low contact angle measurements ($\theta \approx 46^o, 48^o$ and 47° respectively). The observed wetting preference of the substrates with the reference oil was attributed to the lack of surface-active component in the n-decane. For the test fluid (STO), it can be observed from Figure 43 that, quartz was strongly hydrophilic ($\theta \approx 58^o$) while the calcite was strongly hydrophobic ($\theta \approx 121^o$). Kaolinite on the other hand was observed to be less hydrophilic ($\theta \approx 64^o$) than quartz ($\theta \approx 58^o$) as depicted in Figure 43. Hence, it can be concluded that the polar oil components in the crude oil has a pronounced effect on the wettability.

Surfaces	Quartz	Kaolinite	Calcite

N-decane	$\theta \approx 46^o$	$\theta \approx 48^o$	$\theta \approx 47^o$
STO	$\theta \approx 58^o$	$\theta \approx 64^o$	$\theta \approx 121^o$
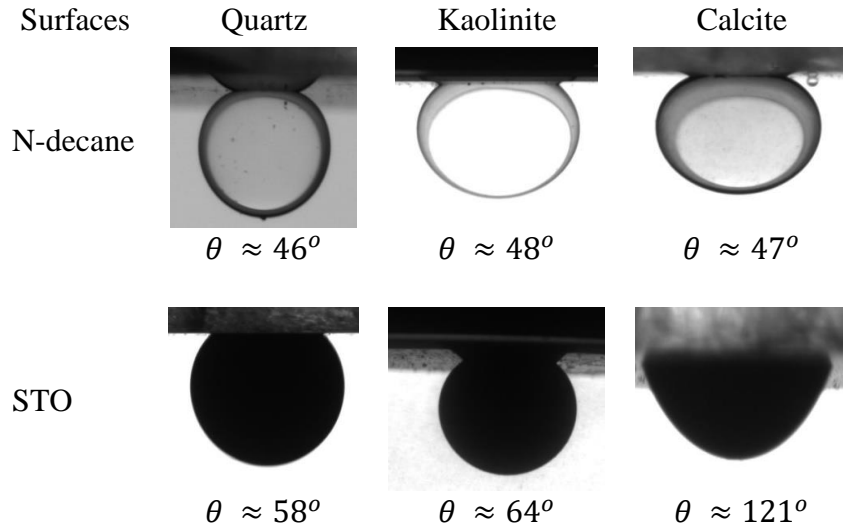
Figure 43: Mineral/oil/brine contact angle measurements using Drop Shape Analyzer (DSA) device. The reference oil for this study was n-decane while STO was used as the test fluid.

5.3.2   Bentheimer sandstone rock substrate

For the tested systems, it can be observed that the wetting state of the rock substrate for both n-decane and STO were negligible ($\theta \approx 45^o \; and \; 50^o$ respectively) and hence, the Bentheimer sandstone substrate can be said to be hydrophilic (Figure 44).

N-decane	STO

$\theta \approx 45^o$	$\theta \approx 50^o$
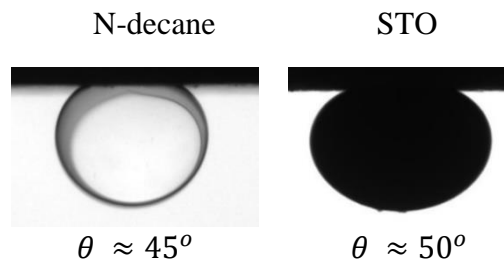
Figure 44: Bentheimer/oil/brine contact angle measurements using the Drop Shape Analyzer (DSA) device. The reference fluid for this study was n-decane while STO was used as the test fluid.

The ranking of the hydrophobicity of the studied substrate during the contact angle measurements with the STO is given as Bentheimer < quartz < kaolinite << Calcite.

5.3.3 Oil adhesion during contact angle measurement via SCM

The tendency of oil to be adsorbed onto the substrates during the contact angle measurements were also evaluated via SCM.
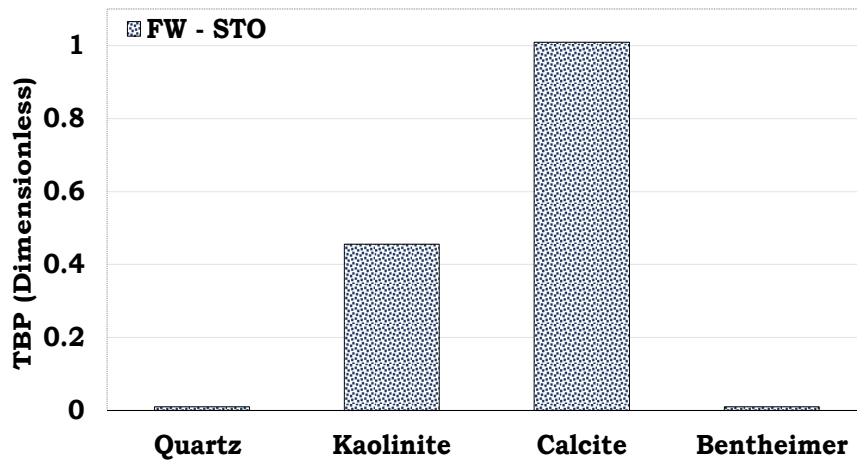
Figure 45: Oil adhesion tendencies of the minerals and rock during the contact angle measurement via SCM

The ranking of the wetting preferences of the substrates/brine/STO system via SCM was also in-line with the contact angle measurements as depicted in Figure 45.

5.3.4 Oil adhesion mechanisms during contact angle measurement

The mechanism of oil adsorption during the contact angle measurements depicts that the tendency of oil to be adsorbed onto the quartz substrate

was negligible as compared to calcite. From Figure 46, the mechanism of oil adsorption onto the quartz substrate existed between $>Si\text{-}O^- \leftrightarrow >COOCa^+$. It can also be observed from Figure 46 that the bridging of the negative kaolinite sites ($>Al\text{-}O^-$ and $>Si\text{-}O^-$) and the carboxylate ($>COO^-$) by divalent cation (Ca^{2+}) resulted in the adhesion of oil onto the kaolinite substrate.
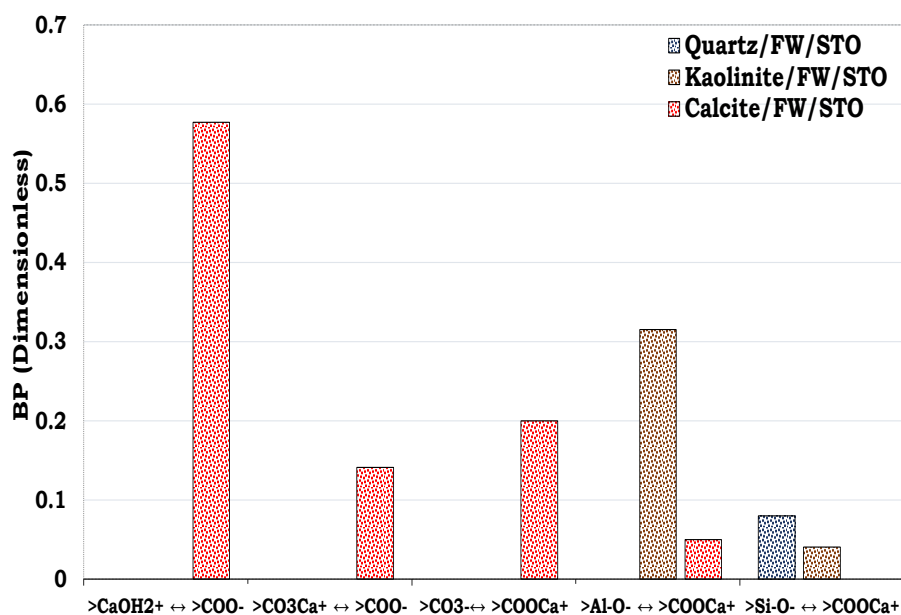
Figure 46: Predicted electrostatic pair linkages existing between the mineral-brine and the oil-brine interfaces during the contact angle measurements.

For the calcite/brine/STO system, it can be observed that the dominant oil adsorption mechanism was due to direct adhesion of carboxylate ($>COO^-$) onto the positive calcite site ($>CaOH_2^+$). In addition, bridging of the negative calcite site ($>CO_3^-$) and the carboxylate ($>COO^-$) by divalent cation such as Ca^{2+} also resulted in the adhesion of oil onto the calcite surface.

5.4 Verification of the SCM technique with literature experimental data

To validate the SCM technique as a new wettability characterization tool, there was the need to simulate the COBR interactions of literature experimental data. The data considered were zeta potential measurements of calcite-brine and oil-brine systems (Alotaibi and Yousef 2017).

In addition, the SCM technique has successfully been used to understand the mechanisms during spontaneous imbibition in chalk using Carbonated Water (CW) and Formation Water (FW) as reported in literature (Fjelde et al. 2011).

Furthermore, Amott and USBM wettability measurements for some North Sea sandstone rocks have also been predicted successfully using the SCM approach. These predictions were accomplished using the properties and quantities of the materials used in their respective experiments as inputs as reported in Table 7, Table 8, Table 9 and Table 10. However, the site densities of the mineral, surface reactions and their reaction constants are similar to the one reported in Table 4 and Table 6 respectively. The zeta potential measurements and their predicted counterpart will be presented first followed by that of the spontaneous imbibition experiment from literature and their simulated result. Finally, the wettability data from literature and their predicted counterparts will be presented.

5.4.1 Zeta potential measurements versus predictions

The oil-brine zeta potential measurements and its predictions will be presented first followed by that of the calcite-brine.

Oil-brine potential measurement versus simulation

It can be observed from Figure 47 that the SCM technique could capture the trend during zeta potential measurements from literature (Alotaibi and Yousef 2017). In other words, the zeta potential measurements and its predicted surface potential were both negative for the oil-brine system. The zeta potential is the potential at the shear plane (i.e. some

69

distance away from the mineral surface) (Butt et al. 2006), while the surface potential on the other hand is the potential at the mineral surface. Hence, the discrepancies between the zeta potential measurements and the SCM prediction is attribute to the distance of the measured potential from the surface.

Butt et al. (2006) stipulated that the double layer is thin at high salinity and hence the measured zeta potential can be assumed to the equal to the surface potential. However, this approximation become less ideal with reduction in salinity. The relatively high discrepancy between the oil-DW zeta potential measurement and the predicted surface potential is attributed to the negligible salinity of the DW.
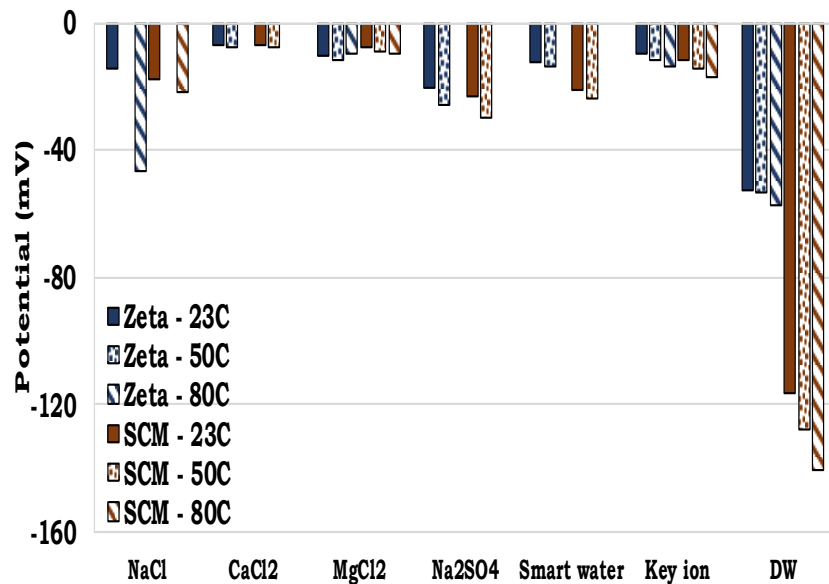
Figure 47: Zeta potential measurements of oil-brine interfaces and their simulated surface potential via SCM for different brine compositions.

Calcite-brine potential measurement versus simulation

Apart from the calcite-smart water and calcite-NaCl at 80°C, the SCM could capture the main trends during the calcite-brine zeta potential measurements (Figure 48).
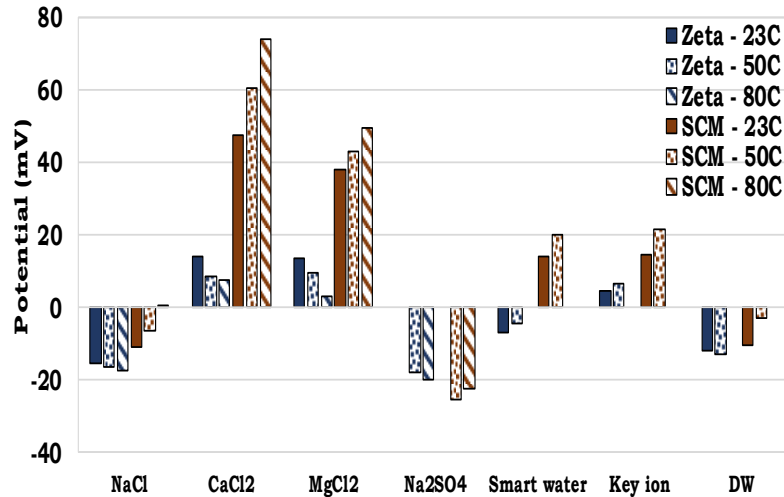
Figure 48 : Zeta potential measurements of calcite-brine interfaces and their simulated surface potential via SCM for different brine compositions.

5.4.2 CW flooding experiment versus SCM prediction

Fjelde et al. (2011) evaluated the effect of brine composition on the oil recovery efficiency. It became evident that the carbonated water (CW) improved the spontaneous imbibition of the studied chalk when compared to the formation water (FW) as depicted in Figure 49.
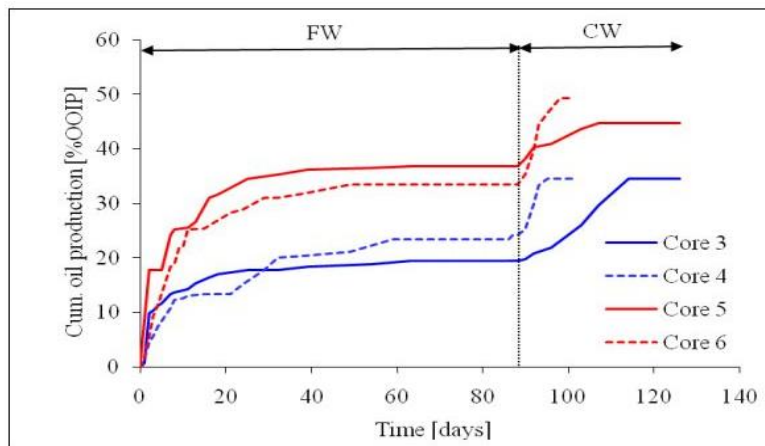
Figure 49 : Spontaneous imbibition experiment in chalk using Carbonated Water, CW (Fjelde et al. 2011).

71

Predicted oil adhesion mechanisms during the spontaneous imbibition experiment in chalk using FW and CW

The COBR interactions during the spontaneous imbibition experiment with FW and CW into the chalk (Fjelde et al. 2011) were evaluated via SCM to understand their effect on oil adhesion. To accomplish this the properties of the materials used in the experiment were also used as input into the model. 0.1 mg KOH/g oil and 1.3 mg KOH/ g oil were the respective Total Acid Number (TAN) and Total Base Number (TBN) of the crude oil used in the spontaneous imbibition experiment. In addition, the surface reaction and the reaction constants of the calcite were used as input for the chalk in the SCM since the former dominate the composition of the latter. The ionic composition of the brine used in both the spontaneous imbibition experiment and the SCM prediction are given in Table 8. The SCM estimated that the tendency of carboxylate ($>COO^-$) oil component to be adsorb onto the positive chalk surface ($>CaOH_2^+$) was the most dominant oil adhesion mechanism for both FW and CW. However, the tendency of oil to be adsorbed onto the chalk surface was higher with the FW (≈ 0.7) as compared to CW (≈ 0.4). Hence, it can be concluded that the efficiency of the oil recovery can be improved via wettability alteration as depicted in Figure 50.
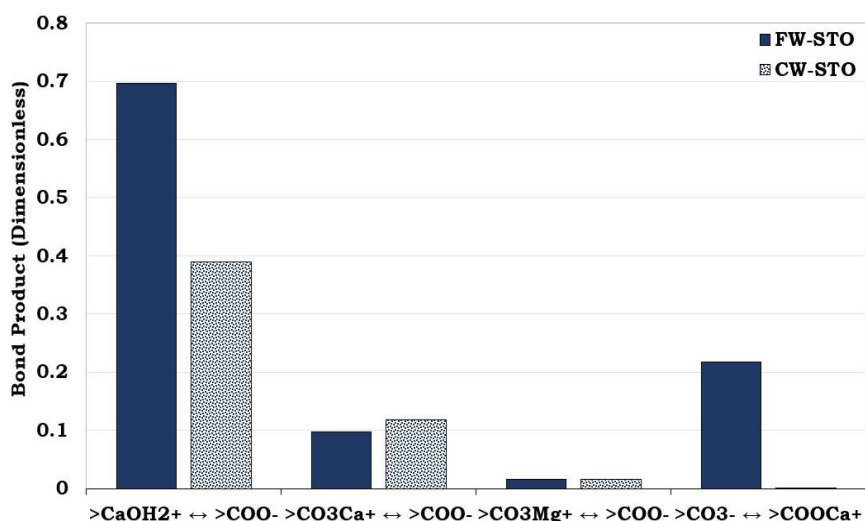
Figure 50: Simulated oil adhesion mechanisms during spontaneous imbibition in chalk with FW and CW (Fjelde et al. 2011).

5.4.3 Amott and USBM wettability measurements (Torsaeter 1988) versus SCM predictions

The measured North Sea sandstone wettability using the Amott and USBM techniques displayed different levels of hydrophilicity of the studied rocks from literature (Torsaeter 1988). It can be observed that the rock samples retrieved from the first coring depth (Field S_1 with cores A & B) were strongly hydrophilic while the second coring depth (Field S_2 with cores C & D) were observed to be the least hydrophilic. The third coring depth (Field S_3 with cores E & F) were also observed to be less hydrophilic than (Field S_1 with cores A & B) but more hydrophilic than (Field S_2 with cores C & D).
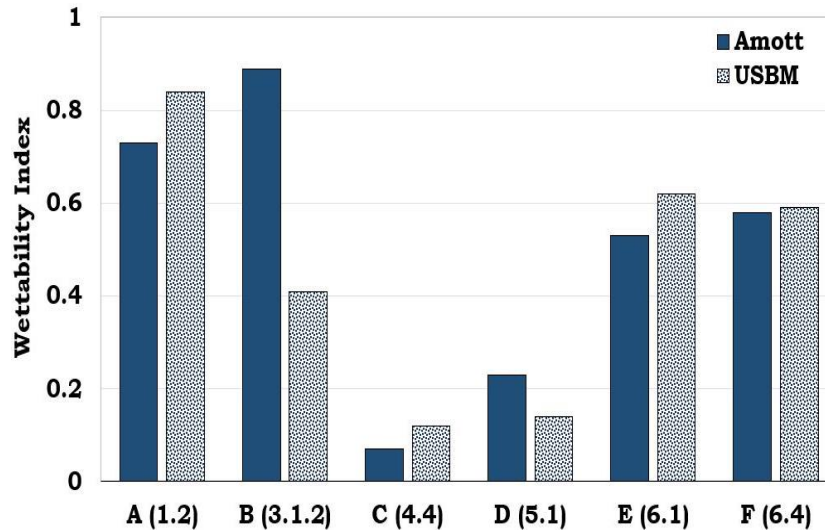
Figure 51: Wettability measurements using the Amott and USBM techniques from literature (Torsaeter 1988). Six North Sea core plugs from three depth intervals were used. First (core plugs A and B), second (core plugs C and D) and third (core plugs E and F) depth intervals.

Surface complexation: Amott and USBM experiments
Like the prediction of the spontaneous imbibition experiment (Fjelde et al. 2011), the wettability measurements using the Amott and USBM techniques (Torsaeter 1988) were also estimated using the properties of the materials employed during the experiment. In other words, the properties of the surfaces (sandstone reservoir rock and oil) were used as

input into the SCM. The oil properties used in the wettability measurement (Amott and USBM) were 0.02 mg KOH/g oil (Total Acid Number, TAN) and 1.1 mg KOH/g oil (Total Base Number, TBN). The ionic composition of the brine employed during the wettability measurement from literature is given in Table 8. The SCM results (Figure 52) agree with Amott and USBM (Figure 51) for the first (Cores A and B) and third depth (Cores E and F), but not for the second depth (Cores C and D). Note that the SCM wettability scale employed is analogous to the TBP as discussed earlier (Papers II, IV & V) and it expresses the tendency of oil to be adsorbed onto mineral surfaces. Hence, it was not surprising that the oil adhesion tendencies onto the hydrophilic surfaces were negligible. In other words, the higher the SCM wettability value (Figure 52), the less hydrophilic the surface become (Figure 51). Though, the mineral compositions for first and second depth were similar, the discrepancy between SCM and Amott and USBM results may be due to the differences in their mineral distributions in the rocks. However, information about mineral distributions was not given by Torsaeter (1988) and can not be included in the present version of the SCM-model.
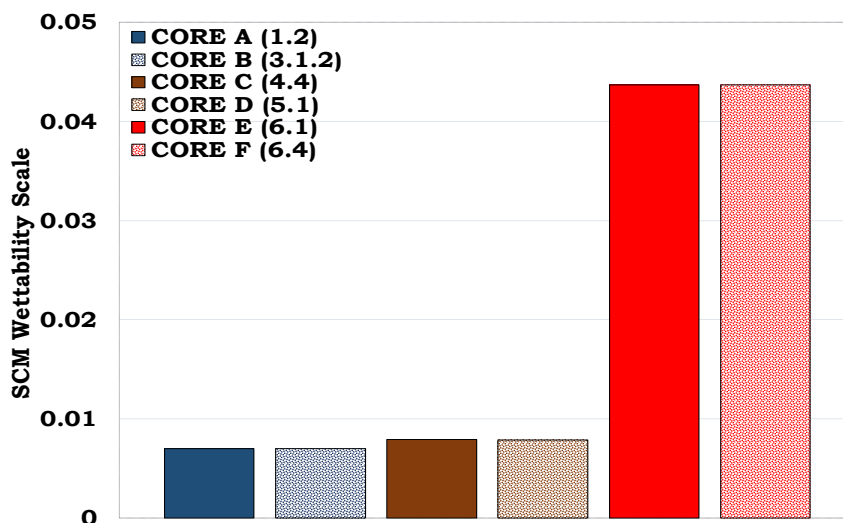
Figure 52 : Simulated Amott and USBM wettability measurements via SCM.

Predicted oil adhesion mechanisms onto the pore walls of the North Sea sandstone during the Amott and USBM wettability measurements (Torsaeter 1988)

During the Amott and USBM wettability measurements on the North Sea sandstone core plug (Torsaeter 1988), the sandstone-brine and oil-brine electrostatic pair linkages that resulted in the adhesion of oil onto the rock surface were also assessed via SCM. It can be observed that direct adhesion of carboxylate ($>COO^-$) onto the positive calcite and chlorite sites ($>CaOH_2^+$ and $>SOH_2^+$ respectively) in the sandstone rock took place. However, direct adhesion of $>COO^-$ onto $>CaOH_2^+$ was higher than that of chlorite. To add to the above, cation (Ca^{2+} and Mg^{2+}) bridging existed between the carboxylate ($>COO^-$) and the negative mineral sites in the sandstone rock ($>CO_3^-$ and SO^-) as depicted in Figure 53.
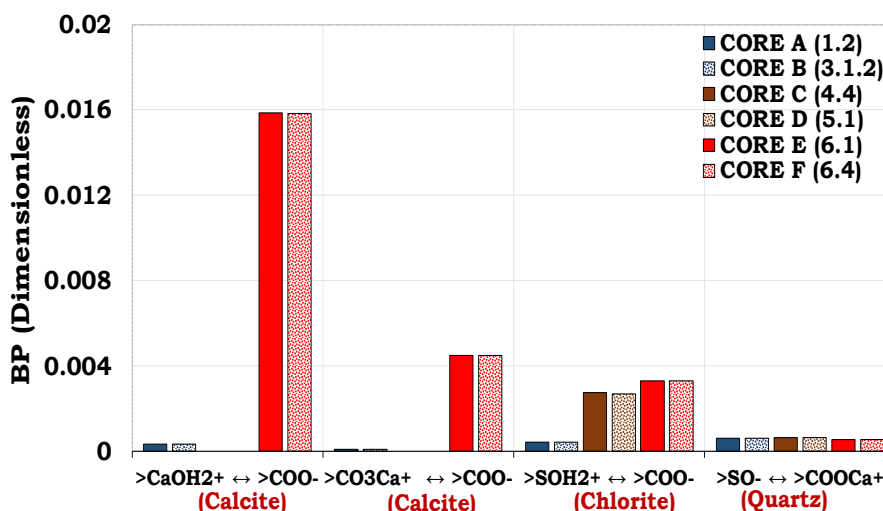
Figure 53 : Oil adhesion onto the pore walls of the core during the Amott and USBM wettability measurements. The oil adhesion was assessed via the electrostatic pair linkages existing between the mineral-brine and the oil-brine interfaces on the pore walls during the Amott and USBM wettability measurement from literature (Torsaeter 1988).

It was not surprising that the core plugs from the third coring interval were less hydrophilic as compared to first coring depth due to their

calcite content 9.9% and 1.4% respectively. This has also been confirmed in Paper V where Pseudo-Sandstone Reservoir Rocks (PSR) were prepared by increasing the content of the desired minerals such as calcite or kaolinite for a given sandstone rock. The results show that for the sandstone rock sample, increasing the calcite content increases the hydrophobicity of the rock and hence the observed results. Paper V gives a deeper insight into the effect of the mineralogical composition on oil adhesion.

5.5 Discussion

It has been shown in this study that wettability can be characterized by evaluating the oil adhesion tendencies of minerals (rocks) via both experimental and simulation techniques. The flotation test, the QCM-D method and the contact angle measurements were the experimental techniques employed in this study with the former serving as the reference experiment. In the flotation test, the water-wet minerals have affinity for the brine phase while the oil-wet mineral have affinity for the oil phase. The results of the flotation tests were in line with both the QCM-D and the contact angle measurements. Though the flotation test could screen the rock-fluid system, its limitation is that large density mineral particles can sink to the bottom of the test tube (water-wet zone) even though they might be oil-wet due to gravity. This was minimized by crushing the mineral (rock) sample before sieving to ensure uniformity of the mineral particles. However, this is not practical in reality. The flotation test can be used with same crushed rock (same particle size and density) to study the effects of fluid compositions on wettability. Detailed description of the flotation test could be obtained from Papers I and V.

Contrary to the flotation test, the QCM-D technique characterized the wettability based on the magnitude of oil adsorbed on the mineral surface. Though, the QCM-D technique is not new in the oil and gas industry, its application in wettability estimation is quite new. The use of crude oil at realistic conditions necessitated the use of a prototype QCM-D device (High-Pressure High Temperature QCM-D, QHPT) developed by Biolin Scientific, Sweden. Like most prototype devices, the QHPT

vessel was also confronted with numerous challenges namely; corrosion, sensor etching, fluid trapping and salt precipitation. Detailed description of these challenges and how they were averted can be obtained from Paper III. After resolving the challenges, the QCM-D was then used as a screening tool to evaluate the effect of injection water compositions on the efficiency of the oil recovery.

Like the flotation test and QCM-D experiments, the contact angle measurements were also used to evaluate the wetting preferences of the rock-fluid system employed in this study. This was achieved using the captive drop contact angle measurement technique via a Drop Shape Analyzer (DSA) device developed by Krüss, Hamburg, Germany. Detailed description of the captive drop contact angle measurement can be obtained from Paper VI. The limitation to the contact angle measurement is that it is carried out on mineral (rock) surfaces which might not be a true reflection of the entire rock.

To better understand these experimental results, the COBR interactions during the aforementioned experiments (i.e. flotation, QCM-D and contact angle measurements) were also assessed via SCM. The SCM technique is a fast and cheap wettability characterization technique via a geochemical solver, PHREEQ-C. This is because, the SCM estimates the wettability using properties and quantities of the surfaces (minerals and oil) unlike the conventional laboratory techniques. Some of the SCM input parameters are ionic composition of the brine, TAN & TBN of the oil, surface reactions and reaction constants of the surfaces (oil and minerals) involved, the surface area and the site densities. A remarkable advantage of the SCM technique over the flotation, the QCM-D and the contact angle measurements techniques employed in this study is that, not only does the SCM predict the wetting tendency but also the oil adhesion mechanisms that led to their observed wetting preferences. Since the SCM technique can predict the mechanisms that led to the oil adhesion, it can be used to design wettability alteration processes to improve oil recovery. For instance, if both the oil-brine and mineral-brine interfaces are negatively charged, bridging by divalent cations such as Ca^{2+} and Mg^{2+} can lead to oil adhesion. Hence, if these bridges are broken, the oil can be mobilized and produced with the injected brine. In

other words, the SCM technique can be used to design injection brine compositions that can optimize oil recovery.

The SCM technique was initially developed to characterize the wetting preferences of individual minerals. However, since reservoir rocks are composed of different minerals, mineral-mixtures of known compositions were prepared to evaluate the effect of increasing surface area and hydrophobic contents (i.e. increasing the illite and calcite contents) in a given sandstone rock sample. This was accomplished using both flotation test and SCM approach. Both the SCM and the flotation test results confirm that the wettability is inclined towards the mineral with the dominant surface area. Nonetheless, for relatively high calcite content, the wetting preferences is dictated by the calcite and not the mineral with dominant surface area (illite). Detailed description of the effect of the intrinsic properties of the rock (such as surface area and surface charge) on the wetting preferences can be obtained from Paper V.

 In addition, the SCM technique has also been successfully used to capture the trends during some laboratory experiment from literature namely zeta potential measurements, spontaneous imbibition experiment and Amott & USBM wettability characterization. The Amott and USBM wettability characterization techniques estimate the wetting preferences of core plugs by measuring specific outputs such as total volume of fluids imbibed by the core and the area under the capillary pressure curve respectively. Since these measured outputs are also affected by other factors and hence, the disparities in the Amott and USBM wettability measurements from literature (Torsaeter 1988) was not surprising even for similar rock-fluids systems (Figure 51). The SCM on the other hand, relies only on the properties of the surfaces (oil and mineral) to predict the wettability and hence for a given rock-fluids system, the wetting preferences will be the same. This was also observed in the surface complexation during the Amott and USBM wettability characterization from literature (Paper VI).

Though the SCM has successfully been used to better understand laboratory experiments, it also has some inherent limitations. For example, the SCM technique assumes that all the mineral surfaces are available for reaction. This assumption holds during surface

complexation modelling of the surface-surface interactions in the QCM-D test, contact angle measurement and flotation experiment. However, this assumption might not hold for the core and field scales due to the complex nature of the rock such as distribution of minerals in its content. Nevertheless, the mineral distributions were not accounted for in the SCM. Hence, to estimate the wettability of reservoir rock on core and field scales, the distribution of the minerals should also be incorporated into the model. In addition, the pore size and pore geometry will also influence the flow properties and hence should also be factored in the model to improve the accuracy of the SCM predictions. Moreover, since the SCM technique was based on batch reactions, the plan is to incorporate into model the kinetic of the minerals.

Results and Discussions

6 Conclusions

The SCM technique of predicting COBR interactions during laboratory experiment is a fast and cheap approach of understanding experimental data. This is because, the properties of the materials (i.e. oil and rock surfaces) are used as input into the model. The SCM technique has successfully been used to capture the trends in laboratory experimental results and they include;

- o Prediction of the oil adhesion tendencies of minerals (rocks) during the flotation test.
- o Estimation of the magnitude of oil adsorbed onto sensor (quartz and kaolinite) surfaces during QCM-D experiments.
- o Evaluating the wetting preferences of minerals and rock substrates during contact angle measurements.

The flotation test results of the studied minerals show that quartz is strongly hydrophilic while calcite is also strongly hydrophobic as confirmed by the SCM results. In addition, the attractive electrostatic pair linkages existing between the oil-brine and mineral-brine interfaces depicts that both direct adhesion of carboxylate ($>COO^-$) and cation (Ca^{2+} and Mg^{2+}) bridging can lead to the adhesion of oil onto calcite depending on the interfacial charges. On the other hand, SCM predicted that cation bridging was the only mechanism for the studied oil to be adsorbed onto quartz surface. The ranking of the hydrophobicity of the studied minerals for both the flotation test and SCM is given as quartz < albite < illite < Montmorillonite < calcite.

For the studied sandstone reservoir rock (SRR) and the pseudo-sandstone rock (PSR) with low calcite contents, their wetting preferences were inclined towards the mineral with the highest effective surface area as depicted by both the flotation test and SCM. On the contrary, the wettability was observed to be dictated by the calcite and not the mineral with the largest effective surface area if the calcite content is higher due to its strong hydrophobicity for the studied conditions. Hence, it can be concluded that the calcite content has a more pronounced effect on the wettability of the studied sandstone rock as compared to the clay content.

In addition, the SCM technique has also been successfully used to predict laboratory experiments from literature and they include;

- o Prediction of calcite-brine and oil-brine zeta potential measurements (Alotaibi and Yousef 2017)
- o Assessing the COBR interactions during spontaneous imbibition experiment with chalk using FW and CW (Fjelde et al. 2011).
- o Evaluation of Amott and USBM wettability measurements on North Sea Sandstone from literature (Torsaeter 1988).

Furthermore, wettability estimation by oil adsorption using QCM-D has also been developed. For a successfully utilization of QCM-D device as wettability characterization tool, the following precautions must be adhered to;

- o To prevent the formation and deposition of corrosion onto the sensor, non-corrosive material (such as PEEK and titanium components) should be employed if high salinity brines are used.
- o To prevent etching of the sensor resulting from equilibrium contrast between the injected brine and the sensor, a pre-column should be used. The pre-column is filled with similar minerals as coated on the sensor to establish equilibrium with the injected brine before reaching the sensor to mitigate sensor etching.
- o Constant temperature experimental set-up is required to mitigate salt precipitation resulting from contrast in temperature.
- o Since the current QCM-D flow-cell is a prototype device, it was confronted with fluid trapping challenge. Hence, the flow cell should be oriented such that the injecting fluid displaces the previously injected fluid based on their density contrast.

Finally, QCM-D has the potential to screen possible injection water composition that can optimize the oil recovery. For instance, it was observed that the tested Low Salinity Water (LSW) rendered the kaolinite sensors more water-wet as compared to the Formation Water (FW). The QCM-D results depicts that the adsorption of oil onto mineral surfaces is dictated by the mineral-fluids properties. For instance, the adsorption of n-decane onto the kaolinite was negligible while polar functional groups in the STO were also adsorbed onto the kaolinite surface.

6.1 Future work

The SCM technique has successfully been used to predict the wetting preferences of some reservoir minerals such as quartz, albite, kaolinite, montmorillonite, illite and calcite. In addition, it has also been successfully used to predict the wettability of sandstone reservoir rock sample and mineral mixtures. The plan is to extend the SCM technique to cover most of the relevant reservoir rock minerals. The current SCM technique is based on batch reaction and hence the plan is to incorporate into the existing model, the distribution of the minerals and the kinetics of surface complexation. Thereby, building a robust wettability simulator that can predict the wettability in-situ. Furthermore, the SCM technique will also be employed to better understand laboratory experiments. For instance, the surface charge from the SCM can be used as input in the calculation of contact angles. In addition, the simulations from SCM can be used as input in pore scale modelling simulation to generate capillary pressure curves if realistic pore geometry are used. The above will lead to prediction/calculation of Amott and USBM indices.

Conclusions

7   References

Alotaibi, M. B. and Yousef, A. 2017. The Role of Individual and Combined Ions in Waterflooding Carbonate Reservoirs: Electrokinetic Study. *SPE Reservoir Evaluation & Engineering* **20** (01): 77 - 86. SPE-177983-PA.

Amott, E. [1959]. Observations Relating to the Wettability of Porous Rock. Fall Meeting of Los Angeles Basin Section, Los Angeles, California, Society of Petroleum Engineers. SPE-1167-G.

Anderson, W. [1986a]. Wettability Literature Survey-Part 2: Wettability Measurement. *Journal of Petroleum Technology* **38** (11): 1246-1262. SPE-13933-PA.

Anderson, W. G. [1986b]. Wettability Literature Survey- Part 1: Rock/Oil/Brine Interactions and the Effects of Core Handling on Wettability. *Journal of Petroleum Technology* **38** (10): 20. SPE-13932-PA.

Anderson, W. G. [1986c]. Wettability Literature Survey-Part 3: The Effects of Wettability on the Electrical Properties of Porous Media. *Journal of Petroleum Technology* **38** (12): 371-378.

Anderson, W. G. [1987]. Wettability Literature Survey Part 5: The Effects of Wettability on Relative Permeability. *Journal of Petroleum Technology* **39** (11): 1453 -1468. SPE-16323-PA.

Brady, P. V. and Krumhansl, J. L. [2012a]. A Surface Complexation Model of Oil–brine–sandstone Interfaces at 100° C: Low Salinity Waterflooding. *Journal of Petroleum Science and Engineering* **81**: 171-176.

Brady, P. V. and Krumhansl, J. L. [2012b]. Surface Complexation Modeling for Waterflooding of Sandstones. *SPE Journal,* **18** (02): 214 - 218. SPE-163053-PA.

Brady, P. V., Krumhansl, J. L. and Mariner, P. E. [2012]. Surface Complexation Modeling for Improved Oil Recovery. SPE IOR Tulsa, Oklahoma, USA,, Society of Petroleum Engineers. SPE-153744-MS.

Buckley, J. and Liu, Y. [1998]. Some Mechanisms of Crude Oil/Brine/Solid Interactions. *Journal of Petroleum Science and Engineering* **20** (3 - 4): 155 -160.

References

Buckley, J., Liu, Y. and Monsterleet, S. [1998]. Mechanisms of Wetting Alteration by Crude Oils. *SPE Journal* **3** (01): 54 - 61.

Buckley, J., Takamura, K. and Morrow, N. [1989]. Influence of Electrical Surface Charges on the Wetting Properties of Crude Oils. *SPE Reservoir Engineering* **4** (03): 332 - 340. SPE-16964-PA.

Busireddy, C. and Rao, D. N. [2004]. Application of DLVO Theory to Characterize Spreading in Crude oil-Brine-Rock Systems. SPE/DOE Symposium on Improved Oil Recovery, Tulsa, Oklahoma, Society of Petroleum Engineers. SPE-89425-MS.

Butt, H.-J., Graf, K. and Kappl, M. [2006]. *Physics and Chemistry of Interfaces*. John Wiley & Sons.

Chandrasekaran, N., Dimartino, S. and Fee, C. J. [2013]. Study of the Adsorption of Proteins on Stainless Steel Surfaces using QCM-D. *Chemical Engineering Research and Design* **91** (9): 1674-1683.

Chen, Q., Xu, S., Liu, Q., Masliyah, J. and Xu, Z. [2015]. QCM-D Study of Nanoparticle Interactions. *Advances in Colloid and Interface Science,* **233** : 94-114.

Chen, Y. and Brantley, S. L. [1997]. Temperature-and pH-dependence of Albite Dissolution Rate at Acid pH. *Chemical Geology* **135** (3-4): 275-290.

Craig, F. J., [1971]. *The Reservoir Engineering Aspect of Waterflooding (Vol. 3)*. Dallas, Texas, Society of Petroleum Engineering of AIME.

Cockcroft, P., Guise, D., & Waworuntu, I. (1989). The Effect of Wettability on Estimation of Reserves. Paper presented at the SPE Asia-Pacific Conference, Sydney, Australia, 13-15 September. SPE 19484-MS.

Cuiec, L. [1975]. Restoration of the Natural State of Core Samples. Fall Meeting of the Society of Petroleum Engineers of AIME, Dallas, Texas, USA. SPE-5634-MS.

Desbrandes, R., Bassiouni, Z. A., & Gualdron, J. (1990). In Situ Formation Wettability Determination in Depleted Zones. Paper presented at the SPE Latin America Petroleum Engineering Conference, Rio de Janeiro, Brazil, 14-19 October.

Desbrandes, R., & Gualdron, J. (1987). In Situ Rock Wettability Determination with Formation Pressure Data. Paper presented at

the SPWLA 28th Annual Logging Symposium, London, England, 29 June-2 July.

Donaldson, E. C., Thomas, R. D. and Lorenz, P. B. [1969]. Wettability Determination and Its Effect on Recovery Efficiency. *SPE Journal* **9** (01): 13-20. SPE-2338-PA.

Dubey, S. and Doe, P. [1993]. Base Number and Wetting Properties of Crude Oils. *SPE Reservoir Engineering* **8** (03): 195-200. SPE-22598-PA.

Dubey, S. and Waxman, M. [1991]. Asphaltene Adsorption and Desorption from Mineral Surfaces. *SPE Reservoir Engineering* **6** (03): 389-395. SPE-18462-PA

Dudášová, D., Silset, A. and Sjöblom, J. [2008]. Quartz Crystal Microbalance Monitoring of Asphaltene Adsorption/Deposition. *Journal of Dispersion Science and Technology* **29** (1): 139-146.

Dzombak, D. A. and Morel, F. [1990]. *Surface Complexation Modeling: Hydrous Ferric Oxide*. John Wiley & Sons.

Ekholm, P., Blomberg, E., Claesson, P., Auflem, I. H., Sjöblom, J. and Kornfeldt, A. [2002]. A Quartz Crystal Microbalance Study of the Adsorption of Asphaltenes and Resins onto a Hydrophilic Surface. *Journal of Colloid and Interface Science* **247** (2): 342-350.

Erzuah, S., Fjelde, I. and Omekeh, A. 2017. Wettability Characterization Using the Flotation Technique Coupled With Geochemical Simulation. Presented at the IOR 2017- 19th European Symposium on IOR, Stavanger, Norway. 24 - 27 April.

Erzuah, S., Fjelde, I. and Omekeh, A. V. 2018a. Wettability Estimation by Oil Adsorption using Quartz Crystal Microbalance with Disipation (QCM-D). Presented at EUROPEC. Copenhagen, 11-14 June. SPE-190882-MS.

Erzuah, S., Fjelde, I. and Omekeh, A. V. 2018b. Challenges Associated with Quartz Crystal Microbalance with Dissipation (QCM-D) as a Wettability Screeening Tool. *Oil & Gas Science and Technology–Revue d'IFP Energies nouvelles* **73**: 58.

Erzuah, S., Fjelde, I. and Omekeh, A. V. 2019. Wettability Estimation by Surface Complexation Simulations. *SPE Reservoir Evaluation & Engineering Journal* **22** (02): 509-519. SPE-185767-PA.

Fan, T., Wang, J. and Buckley, J. S. [2002]. Evaluating crude oils by SARA analysis. In: *SPE/DOE Improved Oil Recovery*

Symposium, Tulsa, Oklahoma, USA, 13-17 April. SPE-75228-MS.

Feiler, A. A., Sahlholm, A., Sandberg, T. and Caldwell, K. D. [2007]. Adsorption and Viscoelastic Properties of Fractionated Mucin (BSM) and Bovine Serum Albumin (BSA) Studied with Quartz Crystal Microbalance (QCM-D). *Journal of Colloid and Interface Science* **315** (2): 475-481.

Fjelde, I., Aasen, S. and Zuta, J. [2011]. Improvement of Spontaneous Imbibition in Carbonate Rocks by CO_2-saturated Brine. IOR 2011-16th European Symposium on Improved Oil Recovery.

Goldberg, S. [2013]. Surface Complexation Modeling. *Reference Module in Earth Systems and Environmental Sciences*.

Gomes, J. S., Ribeiro, M. T., Strohmenger, C. J., Naghban, S., & Kalam, M. Z. (2008). *Carbonate reservoir rock typing-the link between geology and SCAL.* Paper presented at the Abu Dhabi International Petroleum Exhibition and Conference, Abu Dhabi, UAE, 3-6 November.

Gu, X. and Evans, L. J. [2007]. Modelling the Adsorption of Cd (II), Cu (II), Ni (II), Pb (II), and Zn (II) onto Fithian Illite. *Journal of Colloid and Interface Science* **307** (2): 317-325.

Hirasaki, G. [1991]. Wettability: Fundamentals and Surface Forces. *SPE Formation Evaluation* **6** (02): 217-226. SPE- 17367-PA.

Hui, M.-H. and Blunt, M. J. [2000]. Effects of Wettability on Three-Phase Flow in Porous Media. *Journal of Physical Chemistry,* **104** (16): 3833 - 3845.

Katz, L. E. and Hayes, K. F. [1995]. Surface Complexation Modeling: I. Strategy for Modeling Monomer Complex Formation at Moderate Surface Coverage. *Journal of Colloid and Interface Science* **170** (2): 477-490.

Keller, C. and Kasemo, B. [1998]. Surface Specific Kinetics of Lipid Vesicle Adsorption Measured with a Quartz Crystal Microbalance. *Biophysical Journal* **75** (3): 1397-1402.

Koretsky, C. [2000]. The Significance of Surface Complexation Reactions in Hydrologic Systems: a Geochemist's Perspective. *Journal of Hydrology* **230** (3-4): 127-171.

Kubiak, K., Adamczyk, Z. and Wasilewska, M. [2015]. Mechanisms of Fibrinogen Adsorption at the Silica Substrate Determined by

QCM-D Measurements. *Journal of Colloid and Interface Science* **457**: 378-387.

Lu, C. and Czanderna, A. W. [2012]. *Applications of Piezoelectric Quartz Crystal Microbalances*. Elsevier.

Morrow, N. R. [1990]. *Interfacial Phenomena in Petroleum Recovery*. CRC Press.

Mwangi, P., Thyne, G. and Rao, D. [2013]. Extensive Experimental Wettability Study in Sandstone and Carbonate-Oil-Brine Systems: Part 1–Screening Tool Development. International Symposium of the Society of Core Analysts held in Napa Valley, California, USA. SCA3013-84.

Parkhurst, D. L. and Appelo, C. 2013. Description of Input and Examples for PHREEQC Version 3.3—A Computer Program for Speciation, Batch-reaction, One-dimensional Transport, and Inverse Geochemical Calculations. Denver, Colorado, USA, U.S. Geological Survey. **6:** 497.

Plummer, C. C., David, M. and Diane, H. C. [1994]. *Physical Geology, 9th edition* McGraw-Hill Science/Engineering/Math.

Pokrovsky, O. S., Schott, J. and Thomas, F. [1999]. Processes at the magnesium-bearing carbonates/solution interface. I. A surface speciation model for magnesite. *Geochimica et Cosmochimica Acta* **63** (6): 863-880.

Radke, C., Kovscek, A. and Wong, H. [1992]. A Pore-Level Scenario for the Development of Mixed Wettability in Oil Reservoirs. SPE Annual Technical Conference and Exhibition, Washington, D.C, Society of Petroleum Engineers. SPE-24880-MS.

Rao, D. N. and Maini, B. B. [1993]. Impact Of Oil-Rock Adhesion On Reservoir Mechanics. Annual Technical Meeting, Calgary, Canada, Petroleum Society of Canada. PETSOC-93-84.

Raza, S., Treiber, L. and Archer, D. [1968]. Wettability of reservoir rocks and its evaluation. *Prod. Mon.;(United States)* **32** (4).

Song, J., Zeng, Y., Wang, L., Duan, X., Puerto, M., Chapman, W. G., Biswal, S. L. and Hirasaki, G. J. [2017]. Surface Complexation Modeling of Calcite Zeta Potential Measurements in Brines with Mixed Potential Determining Ions (Ca^{2+}, CO_3^{2-}, Mg^{2+}, SO_4^{2-}) for Characterizing Carbonate Wettability. *Journal of Colloid and Interface Science* **506**: 169-179.

References

Sverjensky, D. A. [1994]. Zero-point-of-charge prediction from crystal chemistry and solvation theory. *Geochimica et Cosmochimica Acta* **58** (14): 3123-3129.

Sverjensky, D. A. and Sahai, N. [1996]. Theoretical Prediction of Single-site Surface-Protonation Equilibrium Constants for Oxides and Silicates in Water. *Geochimica et Cosmochimica Acta,* **60** (20): 3773 - 3797.

Sverjensky, D. A. and Sahai, N. [1998]. Theoretical Prediction of Single-site Enthalpies of Surface Protonation for Oxides and Silicates in Water. *Geochimica et Cosmochimica Acta,* **62** (23-24): 3703 - 3716.

Torsaeter, O. [1988]. A Comparative Study of Wettability Test Methods Based on Experimental Results From North Sea Reservoir Rocks. SPE Annual Technical Conference and Exhibition, Houston, Texas, Society of Petroleum Engineers. SPE-18281-MS.

Van Cappellen, P., Charlet, L., Stumm, W. and Wersin, P. [1993]. A Surface Complexation Model of the Carbonate Mineral-aqueous Solution Interface. *Geochimica et Cosmochimica Acta* **57** (15): 3505-3518.

Wieland, E., Wanner, H., Albinsson, Y., Wersin, P. and Karnland, O. [1994]. A Surface Chemical Model of the Bentonite-Water Interface and Its Implications for Modelling the Near Field Chemistry in a Repository for Spent Fuel. Swedish Nuclear Fuel and Waste Management Co.

Wolthers, M., Charlet, L. and Van Cappellen, P. [2008]. The Surface Chemistry of Divalent Metal Carbonate Minerals; A Critical Assessment of Surface Charge and Potential Data Using the Charge Distribution Multi-site Ion Complexation Model. *American Journal of Science* **308** (8): 905 - 941.

Part II

Part II

Paper I

Erzuah, Samuel; Fjelde, Ingebret; Omekeh, Aruoture Voke

Paper I

Paper I

Tu P032

Wettability Characterization Using the Flotation Technique Coupled with Geochemical Simulation

S. Erzuah* (University of Stavanger), I. Fjelde (IRIS) & A.V. Omekeh (IRIS)

SUMMARY

Wettability controls the distribution of fluid phases and flow properties in oil reservoirs. Wettability characterization can be accomplished using standard techniques such as Amott-Harvey and USBM. Nevertheless, these experiments are time consuming and limited numbers are carried out for each oil reservoir. The objective is to evaluate the possibility to use the flotation technique combined with geochemical simulations for fast wettability characterization.

The flotation technique relies on the affinity of the minerals to either the brine or the oil, and was used to characterize the wettability of minerals. The amounts of oil-wet particles is determined for the mineral-brine-oil mixtures after aging the mineral in brine and oil respectively. Two formation water compositions and two stock tank oils were selected for the flotation experiments. As an introduction to this study, the wettability of six (6) minerals found in sandstone reservoir rocks were investigated by flotation test. The mineral-brine interactions such as solubility and surface complexation of minerals were modelled with the geochemical simulator PHREEQ-C, and the results were compared with their experimental counterpart. The flotation tests showed that the crude oils altered the wettability of some of the water-wet minerals to oil-wet. It was inferred that the clay minerals were less water-wet. Calcite with cationic surfaces, became more oil-wet by aging with crude oil, and this indicated direct adsorption of carboxylic acids.

Surface Complexation Modelling (SCM) results reveal that the surface charges of both quartz-brines and STOs-brine are mostly negatively charged and hence electrostatic repulsion exist between the two interfaces leading to lack of oil adhesion. Unlike quartz, the calcite-brine and the STOs-brine interfaces were positively and negatively charged respectively. Hence, direct adhesion of the polar oil components onto the calcite surface is the reason for the high oil-wet nature of calcite. This was also consistent with the total bond product which expresses the tendency of oil adhesion onto minerals surfaces. The total bond product for calcite (0.95 – 1.06) was greater than quartz (0.01 – 0.07) and hence confirming that more oil was adsorbed on the calcite surface unlike quartz. Both the SCM and the flotation test results reaveal that the calcite is strongly oil-wet while quartz is strongly water-wet.

The flotation technique combined with geochemical simulation is a promising and cheap approach of characterizing the wettability. In the flotation tests only small rock samples are required. This approach has the potential to provide fast estimation of the wettability of reservoir rocks.

Introduction

Wettability is the tendency of a fluid to preferentially wet a solid surface in the presence of another immiscible fluids (Craig 1971). Remarkable strides have been made in wettability estimation due to its profound effect on the oil recovery efficiency. In reservoir multiphase flow, wettability controls the fluid phase distribution and flow properties. Erzuah et al. (2017) emphasised on the effect of the Crude oil/Brine/Rock (COBR) interactions on wettability estimation. During COBR interactions, electrical charges exist both on the interfaces of the oil-brine and that of the mineral-brine (Buckley and Liu 1998). Dubey and Doe (1993) also reported that if the charges at the rock-brine and the oil-brine interfaces are similar, it will result in repulsion thereby maintaining a thick water film due to increase in the disjoining pressure thereby resulting in water-wet condition. On the other hand, if the oil-brine and rock-brine interfaces have unlike charges, the electrostatic force of attraction exist thereby thinning the water film resulting in a less water-wet condition. The presence of stable water film between the crude oil and the rock/mineral surface results in double-layer repulsion leading to lack of adhesion (Buckley et al., 1989). Hence, the mineralogical composition of the reservoir rock and the compositions of the fluid phases are some of the parameters that influence the wetting properties of the rock/mineral.

Minerals are the building blocks of reservoir rocks (Plummer et al., 1991) and hence the net charge of the reservoir rocks depends on the charges of the predominant minerals and the prevailing conditions in the reservoir. Prior to the crude oil accumulation into the reservoir, rock-brine interactions such as adsorption, desorption, sorption, dissolution, precipitation might have taken place. During the rock-brine interactions, some ions are lost from the brine onto the mineral surface and these processes are termed sorption and adsorption respectively (Goldberg 2013). Unlike adsorption which results in a two-dimensional structure, precipitation on the other hand is a three-dimensional structure due to the continuous adsorption of ions (Goldberg 2013). In a similar vein, the dissolution of some of the reservoir rock and/or the desorption of ions may also result in changes in the concentration of the brine. Buckley and Liu (1998) reported that silicate surfaces are negatively charged above pH 2 while calcite surfaces are positively charged for pH less than 9.5. Hence, the positively charged polar functional groups can be adsorbed onto the silicate surfaces for pH greater than 2, while negatively charged polar functional groups can be adsorbed onto the calcite surface for pH less than 9.5.

Crude oils are composed of Saturates, Aromatic, Resins and Asphaltenes (SARA) contents (Fan et al., 2002). The chemistry of the crude oil plays an essential role in the wetting properties of the rock/mineral. The API gravity, Total Acid Number (TAN) and Total Base Number (TBN) are used to characterize the crude oils (Buckley et al., 1998). Dubey and Waxman (1991) reported that most of the polar oil components are concentrated in the heavy end of the crude oil such as asphaltene and resins. Several studies have also shed light on the effect of the polar oil components adsorption on wettability (Buckley et al., 1998; Dubey and Waxman 1991; Erzuah et al., 2017). These surface-active components in the crude oil might be acidic, basic or non-ionic polar compounds (Dubey and Doe 1993). Research has shown that polar functional groups of both rock/minerals and the crude oil phase interact with each other (Buckley et al., 1998; Cuiec 1975). For instance, Buckley and Liu (1998) enumerated four (4) prominent mechanisms during COBR interactions;
 i.   polar interactions which occur if the oil and the rock surfaces are devoid of water film
 ii.   surface precipitation which is dictated by the asphaltene content of the oil
 iii. acid/base interactions due to the interfacial charges at the rock-brine and oil-brine interfaces
 iv.   charged sites and multivalent ions might also result in ion-binding interactions

Existing methods of wettability characterization

Due to the influence of oil recovery on wettability, numerous attempts have been made to characterize the wettability either qualitatively or quantitatively. According to Anderson (1986), the qualitative wettability characterization techniques include; imbibition method, relative permeability method, microscope examination, glass slide, nuclear magnetic relaxation and dye adsorption. The quantitative wettability characterization technique on the other hand includes the Amott technique, the United State Bureau of Mines (USBM) method, and Contact angle method (Anderson 1986). Unlike the contact angle method, the Amott and USBM techniques measure the average wettability of the core and hence, they are the oil and gas industry standard for wettability estimation (Anderson 1986; Mitchell et al., 1990). The challenges confronted with the oil and gas industry standards of wettability estimation is

that they are time consuming and hence expensive. Hence, the need for a cheap, fast but accurate wettability characterization. This can be accomplished using the flotation technique. Thus, the flotation technique can be used to screen possible chemical conditions in the reservoir to evaluate their effect on wettability (Mwangi et al., 2013).

Just as reservoir rocks vary due to their mineralogical compositions, so is the wettability of the reservoir rock due to the affinity of each mineral to a particular fluid phase (Buckley et al., 1998; Donaldson and Alam 2013). Prior to the crude oil accumulation, the formation water might be the most likely fluid occupying the reservoir . The rationale behind the flotation test is to mimic the wetting preference in the reservoir as a result of changing from single phase flow to multiphase flow after the crude oil accumulation. The mechanism surrounding the flotation technique is that, it relies on the affinity of each mineral to a particular fluid phase during COBR interactions. This affinity also depends on the polarity of the rock-brine and oil-brine interfaces during the COBR interactions as reported numerous authors (Erzuah et al., 2017; Mwangi et al., 2013). For instance, if the rock-brine interface is anionic, it will attract cationic components from the oil-brine interface and vice-versa. In other words, the hydrophilic minerals usually have high affinity for the brine phase while the oleophilic minerals have high affinity for the oil phase.

In this study, the objective was to evaluate the possibility to use the flotation technique combined with geochemical simulations to characterized the wettability. To accomplish this, the rock/mineral-brine interactions such as solubility and surface complexation of minerals were modelled using the geochemical simulator PHREEQ-C (Parkhurst and Appelo 2013), and compared with the flotation tests of minerals and rock.

Method
Both experimental and simulation techniques were used to characterization the wettability. This was to better understand the mechanisms surrounding the wetting preferences of the rock/minerals as observed in the flotation tests.

Flotation test
Six (6) minerals were selected for the flotation tests based on typical sandstone reservoir-rock compositions. These minerals were quartz, kaolinite, K-feldspar, montmorillonite, albite and calcite. The flotation test was also performed for a crushed reservoir rock sample to characterize the rock wettability. The mineralogical composition of the reservoir rock sample and the properties of minerals used in the flotation test are given in Table 1. Illite and chlorite found in the reservoir rock were not available as minerals, and other clay minerals were therefore selected. Two stock tank oil (STOs) and two formation waters (FWs) of varying compositions were used in the flotation test. Table 2 and Table 3 give the compositions of the oils and the FWs used in the wettability characterization.

Table 1 Mineralogical composition of the reservoir rock sample used in the flotation test.

Mineral	%Mass	Surface Area (m^2/g)	CEC (meq/kg)	Molecular Formula
Quartz	72.1	~0.1[a]		SiO_2
Illite	12.7	$65-100$[c]	200-500[c]	$K_{0.6}Mg_{0.25}Al_{1.8}Al_{0.5}Si_{3.5}O_{10}(OH)_2$
K-Feldspar	4.5	~0.1[a]		$KAlSi_3O_8$
Chlorite	7.0	$30-100$[e]	100-400[c]	$(Fe, Mg, Al)_6(Al, Si)_4O_{10}(OH)_8$
Albite	3.3	~0.1[d]		$NaAlSi_3O_8$
Calcite	0.3	2[b]		$CaCO_3$
Kaolinite	0.0	$10-38$[a]	30-150[c]	$Al_2Si_2O_5(OH)_4$
Montmorillonite	0.0	$600-800$[a]	800-1200[c]	$Ca_{.165}Mg_{.33}Al_{1.67}Si_4O_{10}(OH)_2$

Note: [a]Surface area from (Langmuir 1997), [b]after (Hjuler and Fabricius 2009), [c]after (Appelo and Postma 2004), [d]after (Chen and Brantley 1997)and [e]after (Jones 1981)

Stavanger NORWAY   The National IOR Centre of Norway   EAGE

Table 2 *Oil composition.*

FLUID	TAN (mg KOH /g oil)	TBN (mg KOH/g oil)
N-decane	0.00	0.00
STO#1	0.10	1.90
STO#2	0.38	2.30

Table 3 *Ionic compositions of the FWs.*

ION	FW#1 (mmol/L)	FW#2 (mmol/L)
Na^+	1326.16	701.88
K^+	5.62	7.11
Mg^{2+}	17.46	23.90
Ca^{2+}	147.94	72.85
Sr^{2+}	8.44	1.65
Ba^{2+}	0.00	0.04
Cl^-	1677.67	898.69
SO_4^{2-}	0.89	3.59

The flotation test procedure utilized is analogous to the bottle test procedure described by Dubey and Doe (1993) and the Modified Flotation Test procedure given by Mwangi et al. (2013). The mineral was crushed and sieved using a 53μm mesh. Approximately 0.2000g (w_I) of the sieved mineral was put into a graduated test tube, after which approximately 10.0ml of the brine was added to each graduated test tube containing the sieved mineral. The mineral-brine mixture was then thoroughly shaken and aged for 48 hours at reservoir temperature (80°C). After aging, the brine was separated from the mineral-brine mixture in order to measure the pH. The measured pH was then compared with that of the original brine.

Approximately 3.0ml of the oil was added to the test tube containing the wet mineral. The mineral-oil mixture was then aged at reservoir temperature for 48 hours with shaking every 12 hours. After ageing in the oil, the stored brine was poured into their respective oil-mineral mixture. The resulting mineral-oil-brine mixture was then thoroughly shaken and allowed to settle for 24 hours at reservoir temperature (80°C). The sunken mineral at the bottom of the test tube were considered as water-wet while those floating in the oleic phase were also considered as oil-wet (***Figure 1***)

The oil-phase and its associated mineral were then removed from the mixture. The mineral-brine mixture was then filtered on a pre-weighed filter paper and then dried in an oven at 60°C until a constant weight (w_{ww}) was achieved. The weight of oil-wet mineral (w_{ow}) was determined from the difference between the initial weight of the mineral (w_I) and the dried weight of the water-wet mineral (w_{ww}) as given by the relation $w_{ow} = w_I - w_{ww}$. Brine (10.0ml) was also filtered to serve as a reference. Three
(3) duplicates of the flotation tests are performed for each mineral and their average used as the representative wettability estimate. The flotation test procedure was also performed for the reservoir rock sample.
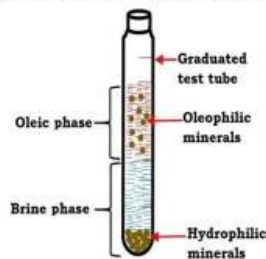
Figure 1 *Affinity of the reservoir rock/minerals to their respective fluid phase.*

Simulations

Both equilibrium and surface complexation modelling (SCM) were performed to throw more light on the wetting preferences of the rock/minerals as observed in the flotation tests. Equilibrium simulations were performed to evaluate the rock/mineral-brine interactions followed by SCM. The most and least hydrophilic minerals from the flotation tests results were considered as the candidate minerals for SCM using PHREEQ-C (Parkhurst and Appelo 2013). The diffuse electric layer model was used in the SCM due to its simplicity. In the SCM, oil and mineral surface groups were incorporated into the model to assess the effects of COBR interactions on the wetting properties. Equal amount of the FWs, STOs and the minerals as in the flotation tests were also used as input parameters in the SCM. The SCM input parameters as reported by Erzuah et al. (2017) was used.

Results and Discussions

The flotation results are presented first followed by the simulation results. Equilibrium simulations were performed first to assess the rock/mineral-brine interactions with time. Based on the flotation test and equilibrium simulation results, the most strongly hydrophilic mineral and the most strongly oleophilic mineral were considered for SCM to shed more light on their wetting mechanisms.

Flotation results

The concentration of oil-wet particles (%w) in the rock/minerals are presented first followed by the effect of TAN and TBN on the wetting properties. The COBR interactions with n-decane as the oleic phase are used as the base case experiment since it is devoid of surface-active component as compared to STOs.

Considering the silicate minerals such as quartz, K-Feldspar and albite, it can be inferred that they were predominately hydrophilic (Figure 2). The concentration of oil-wet particles in quartz was less than 5% and hence, quartz can be considered as strongly hydrophilic. The electrostatic repulsion between the mineral-brine interface and that of the oil-brine is the underlying mechanism for the strongly hydrophilic nature of the quartz (see Figure 7 in Section *Surface Complexation Simulations)*. From Figure 2, considering the concentration of oil-wet particles of quartz with n-decane (2%) and that of the STOs (3% to 5%), the effect of the polar oil component on the wetting properties can be seen clearly. K-feldspar was observed to be less hydrophilic as compared to quartz (Figure 2). For K-feldspar, the concentration of oil-wet particles with the STOs ranges between 11% to 13% while that with n-decane ranges between 4% to 5% (Figure 2). Thus, confirming the role play by the polar oil components on the wettability. Finally, the concentration of oil-wet particles in albite ranges from 6% to 17% for both FWs and STOs (Figure 2). Like K-feldspar, albite was also less hydrophilic as compared to quartz (Figure 2). Adhesion of the polar oil components onto the albite surface might have altered some of the water-wet minerals into oil-wet thus its less hydrophilic nature.

Considering the silicate clay minerals kaolinite and montmorillonite (Figure 2), it can be observed that kaolinite was less oil-wet (7% to 10%) as compared to montmorillonite (20% to 26%) under the pH of the studied systems. This can be credited to the larger reactive surface area of the montmorillonite (600

-800 m^2/g) than the kaolinite (10-38 m^2/g) as depicted in Table 1. Nonetheless, the kaolinite was slightly more oleophilic than quartz. The effect of the polar oil components on wettability became noticeable when the STOs were compared with their n-decane counterparts (Figure 2).

Calcite was the only carbonate mineral selected for the flotation test. In Figure 2, it can be inferred that calcite is strongly oil-wet (77% to 93%) as compared to the silicate minerals (2% to 26%). The most feasible explanation is that carbonate minerals have cationic surfaces for pH less than 9.5 (Buckley and Liu 1998). Hence, it became more oil-wet when aged in the crude oil due to the direct adsorption of carboxylic acids as reported by Erzuah et al. (2017).
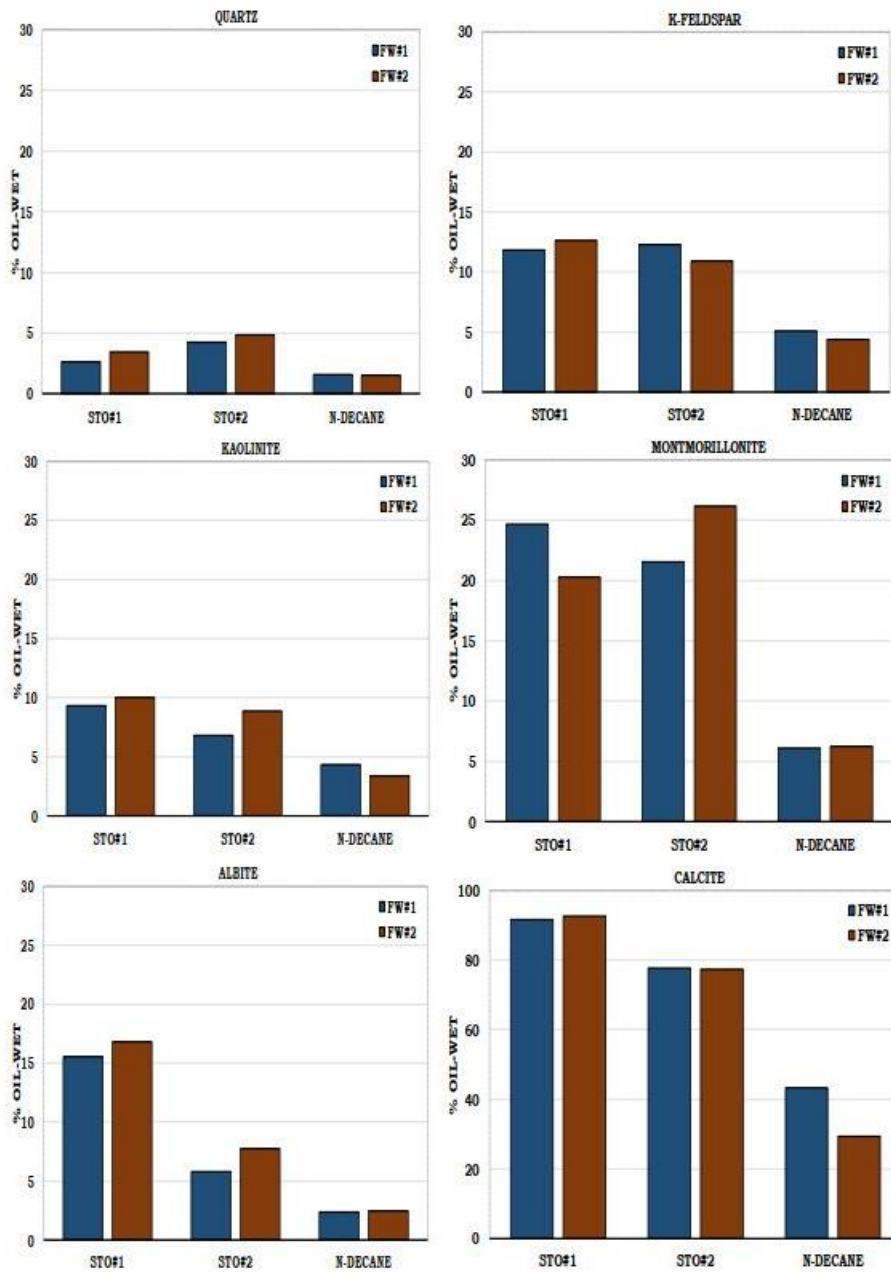
Figure 2 Oil-wet particles in each mineral during the flotation test.

Finally from Figure 2 and Table 1, it can be observed that both quartz and K-feldspar have approximately the same surface ($0.1 m^2/g$). Nonetheless, K-feldspar was less water-wet as compared to quartz. Though quartz and K-feldspar are silicate minerals, a slight change in their mineralogical composition affected their wetting properties (Figure 2). Considering the silicate clay minerals kaolinite and montmorillonite, the latter was more oil-wet than the former (Figure 2). This is due to the larger reactive surface area in montomorillonite ($600-800 m^2/g$) as compared to kaolinite ($10-38 m^2/g$), (Table 1). Considering the carbonate mineral calcite, though it has relatively small surface area ($2 m^2/g$), it was strongly oleophilic (Figure 2).

The amount of oil-wet particle in a flotation test is determined mainly by the wettability of the particle, interfacial tension, temperature and the size of the particle. In the experiments carried out the important variables are the wettability and the particle size. The particle size is expected to be the main determinant of the concentration of particles in oil phase in tests with n-decane, with smaller particles resulting in higher concentrations of the particles in n-decane phase. A comparison of the oil-wet particles in STO against the oil wet particle with n-decane will isolate the effect of wettability from the effect of particle size. The flotation results suggest that the calcite grains were smaller than the grains of the other minerals studied since it had higher concentration of oil-wet particles in n-decane. Note that the largest grain size permitted in the tests is 53μm since the minerals grains were sieved by a 53μm sieve before use.

Reservoir rock sample

For the crushed reservoir rock samples containing several minerals, it was observed that the wettability of the entire rock was rather water-wet. Quartz, albite, K-feldspar, illite, chlorite and calcite are the mineralogical constituents of the reservoir rock.

From the flotation test results (Figure 2), it can be seen that quartz, albite and K-feldspar were all water-wet with quartz being the most hydrophilic. The surface areas of albite and K-feldspar are small, and hence it can be inferred that albite and K-feldspar will also have negligible effect on the wettability of the reservoir rock. Calcite which was the most oleophilic mineral from the flotation test results (Figure 2) had negligible effect on the wettability of the entire rock (Figure 3). This was due to its insignificant reactive surface area ($2 m^2/g$) and its small percentage mass content (0.3%) in the reservoir rock (Table 1).

In addition, clay minerals like montmorillonite with large reactive surface area ($600-800 m^2/g$) and relatively oil-wet (20.2-26.2%) nature under the pH of the studied systems was absent in the reservoir rock composition. Kaolinite was also not present in the reservoir rock compositions. Nevertheless, its effect on the concentration of oil-wet particles would have been insignificant due its hydrophilic nature (Figure 2). Moreover, its relatively smaller surface area ($10-38 m^2/g$) would have also be a contributing factor. Unlike kaolinite and montmorillonite, illite and chlorite were presented in the reservoir rock sample (Table 1). From Table 1, chlorite ($30-100 m^2/g$) and illite ($65-100 m^2/g$) have relatively large reactive surface area and hence, they might have massive effect on the concentration of oil-wet particles. The wettability of the entire rock will be dictated by the minerals with the largest reactive surface area (Cuiec 1984) which would have been the chlorite and illite.

From the flotation test results (Figure 3), it was observed that the entire reservoir rock was less oil-wet (2-8%) for both STOs and FWs. From the hydrophilic nature of the reservoir rock, it can be inferred that the clay minerals such as illite and chlorite might also be hydrophilic as observed for kaolinite (Figure 2). Nevertheless, flotation tests should be carried out for illite and chlorite before better conclusions can be drawn.
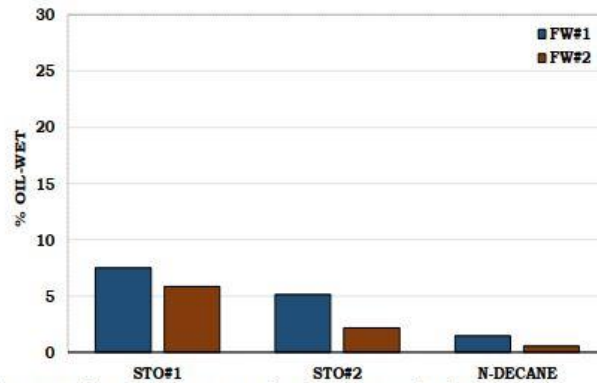
Figure 3 *Oil-wet particles in the reservoir rock sample during the flotation test.*

Effect of oil composition on wettability

The wettability was also found to be affected by the TAN and TBN of the crude oils. For both TAN and TBN, low concentrations of the oil-wet particles were recorded for n-decane (TAN = 0 & TBN= 0). This confirms the role played by the oil compositions on the wettability. The results indicate that the maximum concentration of oil-wet particles for the rock/minerals were observed when TAN was approximately 0.1 mg KOH/g oil. For TAN greater than 0.1 mg KOH/g oil, usually resulted in a reduction in the concentration of the oil-wet particles for all the rock/minerals. Exceptions were quartz with both FWs, montmorillonite with FW#2 and K-feldspar with FW#1 in which the oil-wet particles increased with increasing TAN (Figure 4).
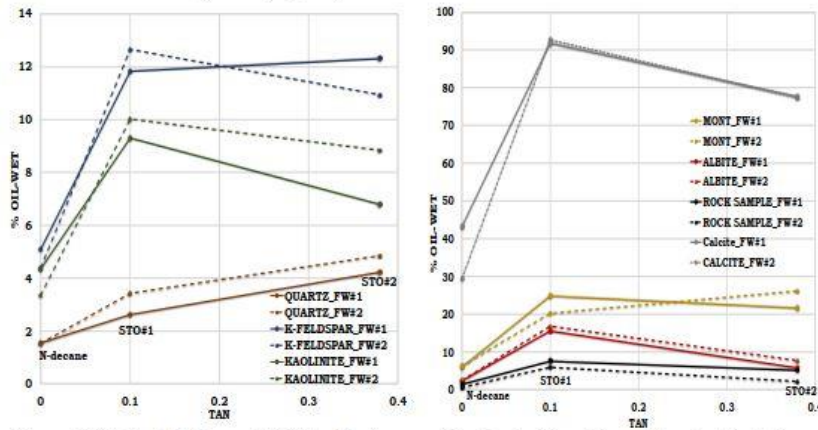
Figure 4 *Effect of TAN on wettability. The lines are for visual aid and do not translate into the actual measurement.*

The effect of TBN on wettability was similar to the trend observed in the TAN. I.e., minimum concentration of oil-wet particles were recorded with n-decane (TAN = 0 & TBN = 0) while the maximum concentration of oil-wet particles was observed for TBN of 1.90 mg KOH/g oil. For TBN greater than 1.90 mg KOH/g oil, the concentration of the oil-wet particles begins to decrease for all the rock/minerals except quartz with both FWs, montmorillonite with FW#2 and K-feldspar with FW#1 in which it increases with TBN as observed in TAN (Figure 5 & 4). Additional flotation tests results with

wide range of oil compositions are needed before meaningful conclusions can be drawn about the effects of TAN and TBN (Figure 5 & 4).
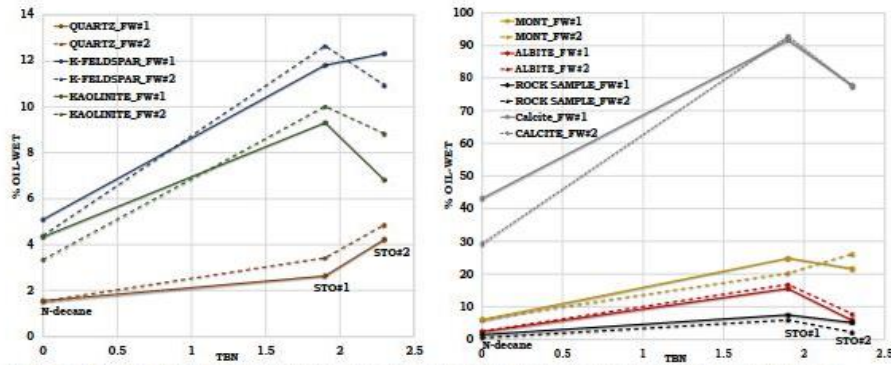
Figure 5 *Effect of TBN on wettability. The lines are for visual aid and do not translate into the actual measurement.*

Simulation results

Equilibrium simulations for all the rock/minerals were performed first to evaluate the rock/mineral-brine interactions such as dissolution and precipitation with time. Based on the flotation tests and the equilibrium simulations results, the strongly hydrophilic and the strongly oleophilic minerals were considered for surface complexation simulations.

Equilibrium Simulation results

Montmorillonite was the most reactive mineral under the pH of the studied systems with approximately 7% change in weight for both FWs. From Figure 6, it can be inferred that quartz and calcite were less reactive with the brines as compared to the other rock/minerals due to their negligible change in weight with time (-0.05% to -0.12%). The less reactive nature of the quartz and calcite, nonetheless, their flotation tests results reveal that quartz and calcite were strongly hydrophilic and strongly oleophilic respectively (Figure 2).
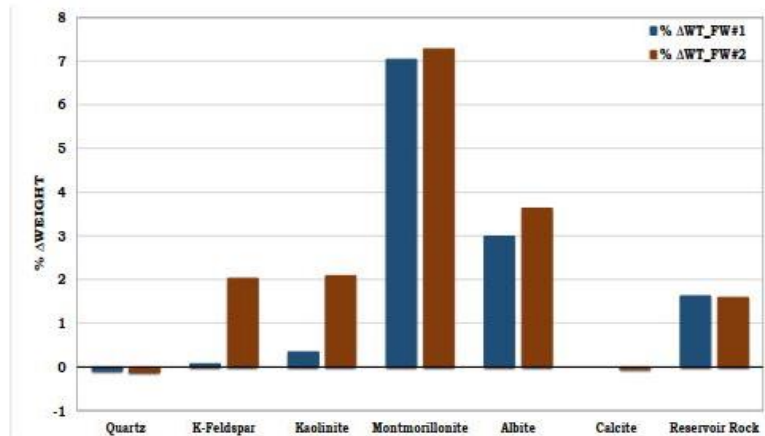
Figure 6 *Equilibrium simulations to evaluate the change in weight of the minerals with time.*

Paper I

Surface Complexation Simulations

Surface complexation simulations were performed for quartz and calcite due to their strong affinity to the brine and the oil phases respectively (Figure 2). Yet, they were the least soluble minerals under the given conditions (Figure 6). Hence, it was intriguing to evaluate the mechanism surrounding their wetting preferences using SCM. In the SCM, the surface charges of both the oil-brine and the mineral-brine interfaces were estimated to understand the possible COBR interactions. This was followed by estimating the total bond product which quantifies the tendency of oil adhesion onto minerals surfaces (Erzuah et al., 2017). Finally, the concentration of SO_4^{2-} on the calcite surface was estimated to assessed its effect on wettability.

Mineral and oil surface charges

From Figure 7, it can be observed that the calcite-brine interfaces were all positively charged while the STOs-brine interfaces were all negatively charged. Hence, direct adsorption of the negatively charged polar oil component onto the calcite surface was the contributing factor to the high concentration of oil-wet particles in calcite. This is consistent with the assertion that direct adhesion of carboxylic acid onto the calcite surface is the underlying mechanism to the strongly oleophilic nature of calcite (Zhang and Austad 2005). Quartz on the other hand was predominantly negatively charged for both the quartz-brine and STOs-brine interfaces (Figure 7). Hence, repulsive electrostatic force exists between the quartz-brine interface and that of the STO-brine due to their similar charges unlike calcite (Figure 7). This implies that direct adhesion of oil onto the quartz surface cannot take place. Hence, it can be inferred that the adhesion of oil onto a mineral surface depends on the charge at the mineral-brine interface and that of the oil-brine.
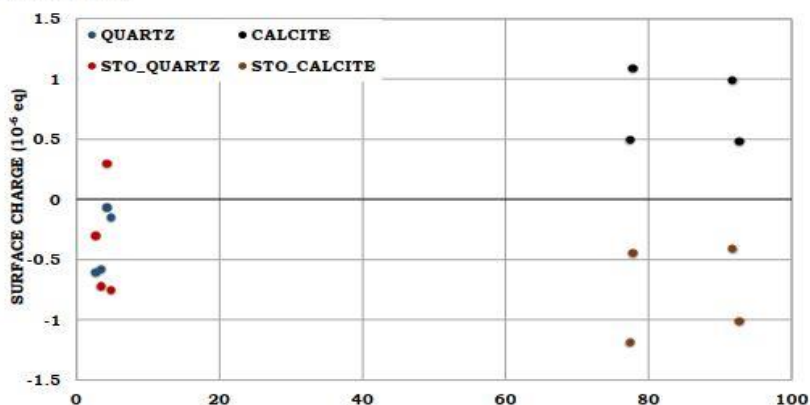
Total bond product of quartz and calcite

The total bond product is used to assess the tendency of oil adhesion onto mineral surfaces due to the attractive electrostatic pair linkages existing between the charged oil surface and that of the rock/mineral (Erzuah et al., 2017). It can be concluded that the total bond product of quartz was negligible as compared to calcite (Figure 8). This confirms that the adhesion of polar oil component onto quartz surface was negligible as compared to that of calcite. Hence, the observed wetting preferences during the flotation tests for quartz and calcite (Figure 2). Erzuah et al. (2017) also reported that cation bridging was the most likely mechanism for oil adhesion in quartz. Nonetheless the total bond product for quartz (0.01 – 0.07) was negligible as compared to calcite (0.95 – 1.06).

This confirms the assertion that negligible amount of polar oil component can be adsorbed onto the quartz surface. Hence, quartz was strongly hydrophilic while the calcite was also strongly oleophilic due to its high tendency for oil adhesion (0.95–1.06) as confirmed by their flotation tests results (Figure 2).
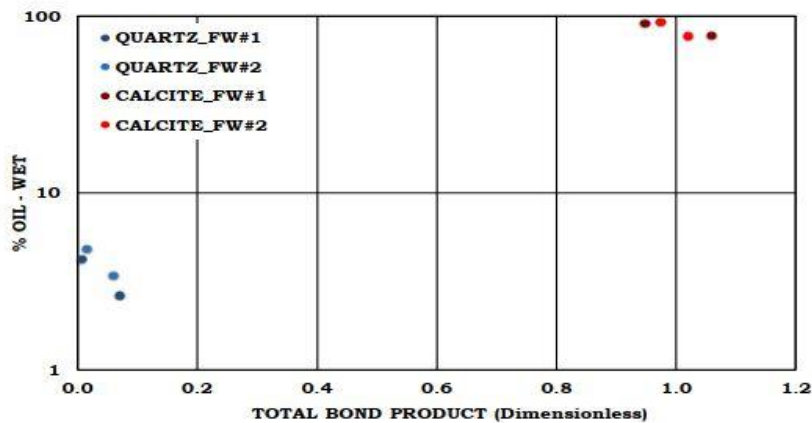
Figure 8 *Effect of Total bond product on wettability estimation.*

SO_4^{2-} concentration on calcite surface

From Figure 9, it can be inferred that bridging of polar oil components onto calcite surface by divalent anions like SO_4^{2-} has negligible effect on its oil adhesion. Calcite is cationic at pH less than 9.5 (Buckley and Liu 1998). In the flotation tests the pH were in the range 7.4-7.7 for both FWs and hence positively charged (Figure 7). From Table 3, it can be observed that the concentration of SO_4^{2-} in FW#2 (3.59 mmol/l) was greater than FW#1 (0.89 mmol/l). Nonetheless, for a given STO, the effect of SO_4^{2-} on oil adhesion in calcite was immaterial. Hence, direct adhesion of carboxylic acid onto the calcite surface is the dominant mechanism as reported by Erzuah et al. (2017).
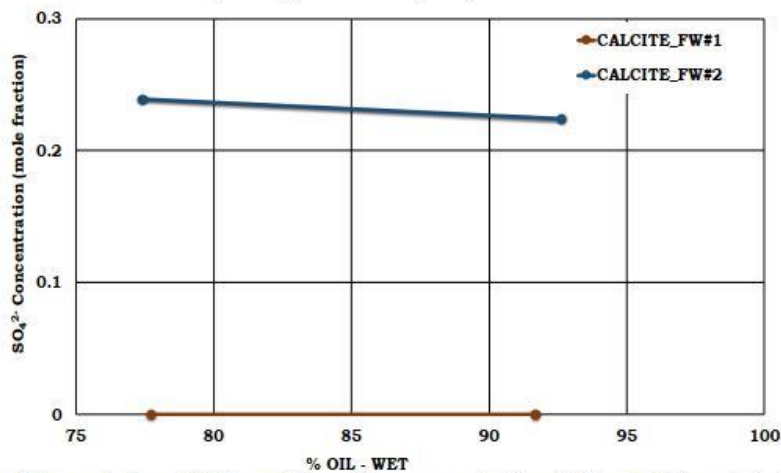
Figure 9 *Concentration of SO_4^{2-} on calcite surface vs concentration of oil-wet calcite particles in the flotation tests.*

Paper I

Conclusions

Unlike Special Core Analysis (SCAL) techniques of wettability characterization, the flotation approach is cheap and fast, and requires only smaller quantities of rock/minerals.

The ranking of the oil-wetness of the selected minerals is given as: Calcite > Montmorillonite > Albite ~ K-Feldspar >Kaolinite > Quartz. Hence, it can be concluded that calcite is strongly oleophilic while quartz is strongly hydrophilic.

From the SCM results, it can be concluded that the surface charge of the mineral-brine and the oil-brine interfaces have a huge impact in the wetting properties since they dictate the magnitude of the oil adhesion.

Based on both the flotation and simulation methods, it can be concluded that the mineralogy of the reservoir rock, the predominant surface area of the minerals, the compositions of the formation water and oil are important parameters that dictate the wetting properties.

Nomenclature

CEC	Cation Exchange Capacity (meq/kg)
COBR	Crude oil/Brine/Rock
FW	Formation Water
SCM	Surface Complexation Modelling
STO	Stock tank oil
TAN	Total acid number (mg KOH/g oil)
TBN	Total base number (mg KOH/g oil)

References

Anderson, W. [1986]. Wettability literature survey-part 2: Wettability measurement. *Journal of petroleum technology* **38**(11): 1246-1262. SPE-13933-PA. http://dx.doi.org/10.2118/13933-PA.

Appelo, C. a. J. and Postma, D. [2004]. *Geochemistry, groundwater and pollution*, CRC press.

Buckley, J. and Liu, Y. [1998]. Some mechanisms of crude oil/brine/solid interactions. *Journal of Petroleum Science and Engineering* **20**(3): 155-160. http://dx.doi.org/10.1016/S0920-4105(98)00015-1.

Buckley, J., Liu, Y. and Monsterleet, S. [1998]. Mechanisms of wetting alteration by crude oils. *SPE Journal* **3**(01): 54-61. SPE-37230-PA. http://dx.doi.org/10.2118/37230-PA.

Buckley, J., Takamura, K. and Morrow, N. [1989]. Influence of electrical surface charges on the wetting properties of crude oils. *SPE Reservoir Engineering* **4**(03): 332-340. SPE-16964-PA. http://dx.doi.org/10.2118/16964-PA.

Chen, Y. and Brantley, S. L. [1997]. Temperature-and ph-dependence of albite dissolution rate at acid ph. *Chemical Geology* **135**(3-4): 275-290. http://dx.doi.org/10.1016/S0009-2541(96)00126-X.

Craig, F. J. [1971]. *The reservoir engineering aspect of waterflooding*. Dallas, Texas, Society of Petroleum Engineering of AIME. ISBN: 978-0-89520-202-4.

Cuiec, L. [1975]. Restoration of the natural state of core samples. *Fall Meeting of the Society of Petroleum Engineers of AIME*, Dallas, Texas, USA, 28 September-1 October. SPE-5634-MS. http://dx.doi.org/10.2118/5634-MS

Paper I

Cuiec, L. [1984]. Rock/crude-oil interactions and wettability: An attempt to understand their interrelation. In: *SPE Annual Technical Conference and Exhibition*, Houston, Texas, USA, 16-19 September. SPE-13211-MS. http://dx.doi.org/10.2118/13211-MS.

Donaldson, E. C. and Alam, W. [2013]. *Wettability*, Gulf Publishing Company. Huston, Texas, USA. ISBN 13: 9781933762296.

Dubey, S. and Doe, P. [1993]. Base number and wetting properties of crude oils. *SPE Reservoir Engineering* **8**(03): 195-200. SPE-22598-PA. http://dx.doi.org/10.2118/22598-PA.

Dubey, S. and Waxman, M. [1991]. Asphaltene adsorption and desorption from mineral surfaces. *SPE Reservoir Engineering* **6**(03): 389-395. SPE-18462-PA. http://dx.doi.org/10.2118/18462-PA.

Erzuah, S., Fjelde, I. and Omekeh, A. V. [2017]. Wettability estimation by surface complexation simulations. *SPE Europec featured at 79th EAGE Annual Conference & Exhibition*, Paris, France,12-15 June. SPE-185767-MS.

Fan, T., Wang, J. and Buckley, J. S. [2002]. Evaluating crude oils by SARA analysis. In: *SPE/DOE Improved Oil Recovery Symposium*, Tulsa, Oklahoma, USA, 13-17 April. SPE-75228-MS. http://dx.doi.org /10.2118/75228-MS.

Goldberg, S. [2013]. Surface complexation modelling. *Journal of Colloid and Interface Science*.

Hjuler, M. and Fabricius, I. L. [2009]. Engineering properties of chalk related to diagenetic variations of upper cretaceous onshore and offshore chalk in the north sea area. *Journal of Petroleum Science and Engineering*, **68**(3-4): 151-170. http://dx.doi.org/10.1016/j.petrol.2009.06.005.

Jones, A. A. [1981]. Charges on the surfaces of two chlorites. *Clay Miner* **16**: 347-359. DOI: 10.1180/claymin.1981.016.4.04

Langmuir, D. [1997]. *Aqueous environmental geochemistry*, Prentice Hall Upper Saddle River, NJ. ISBN 0023674121, 9780023674129

Mitchell, A., Hazell, L. and Webb, K. [1990]. Wettability determination: Pore surface analysis. In: *SPE Annual Technical Conference and Exhibition*, 23-26 September, New Orleans, Louisiana, USA. SPE-20505-MS. http://dx.doi.org/10.2118/20505-MS.

Mwangi, P., Thyne, G. and Rao, D. [2013]. Extensive experimental wettability study in sandstone and carbonate-oil-brine systems: Part 1–screening tool development. In: *International Symposium of the Society of Core Analysts held in Napa Valley, California, USA*, 16-19 September.

Parkhurst, D. L. and Appelo, C. [2013] Description of input and examples for phreeqc version 3—a computer program for speciation, batch-reaction, one-dimensional transport, and inverse geochemical calculations. https://pubs.usgs.gov/tm/06/a43/

Plummer, C. C., McGeary, D. and Carlson, D. H. [1991]. *Physical geology*, McGraw-Hill. ISBN-13: 978-0072528152.

Zhang, P. and Austad, T. [2005]. The relative effects of acid number and temperature on chalk wettability. In: *SPE International Symposium on Oilfield Chemistry*, Society of Petroleum Engineers, 2-4 February, The Woodlands, Texas, USA. SPE-92999-MS. http://dx.doi.org/10.2118/92999-MS.

Paper II

Erzuah, Samuel; Fjelde, Ingebret; Omekeh, Aruoture Voke

Wettability Estimation Using Surface-Complexation Simulations

Samuel Erzuah, University of Stavanger and The National IOR Centre of Norway;
Ingebret Fjelde, NORCE Norwegian Research Centre AS[*] and University of Stavanger; and
Aruoture Voke Omekeh, NORCE Norwegian Research Centre AS[*] and The National IOR Centre of Norway

Summary

Wettability controls the fluid-phase distribution and flow properties in the reservoir. The ionic compositions of brine, the oil chemistry, and the reservoir-rock mineralogy have profound effects on wettability. Wettability measurement can be obtained from special core analysis (SCAL), but those data are not readily available, and the cost and time of analyzing different possible injection waters can be excessive. There is thus a need for early evaluation of wettability because it is crucial for selecting optimal field-development options. Information about wettability can be indirectly obtained from logging of other rock properties, but the uncertainty in the estimated wettability range is often high. In addition, wettability alteration by injection brines cannot be analyzed by logging. This study seeks to estimate the wettability by assessing the electrostatic interactions existing between the mineral/brine and the oil/brine interfaces using a surface-complexation model (SCM) supported with relatively simple and fast flotation experiments.

The SCM is a chemical equilibrium technique of characterizing surface adsorption phenomenon. The SCM provides a cost-effective technique of characterizing the wettability of minerals at reservoir conditions. Ionic composition of the brine and the properties of the minerals were used as input to the model. In addition, the polar oil components in the crude oil were converted into their equivalent organic acid and base concentrations to be incorporated into the model. The electric-double-layer model that was used in the SCM was the diffuse-layer model. The SCM simulation is a fast and inexpensive wettability-characterization tool if reservoir cores and crude oil required in conventional wettability measurements are not readily available.

From the flotation and SCM results, it could be concluded that the latter could capture the oil-adhesion tendencies of the former. Not only does the SCM predict the wetting tendencies of the minerals, but also it has the capacity to evaluate the mechanisms that led to their wetting preferences. For instance, the SCM results reveal that for negatively charged mineral/brine and oil/brine interfaces, divalent cations such as Ca^{2+} and Mg^{2+} can serve as a bridge between the two interfaces, thereby leading to oil adhesion. On the other hand, for positively charged mineral/brine interfaces such as calcite, direct adsorption of the carboxylic oil component was the dominant mechanism for oil adhesion. The SCM technique of characterizing wettability can be used to screen possible injection-water compositions to assess their potential to alter the wettability to more water-wet. Finally, the SCM technique could capture the trend of ζ-potential measurements from literature.

Introduction

Numerous researchers have shed light on the significance of the reservoir-rock wettability in oil recovery (Anderson 1987; Buckley et al. 1989; Radke et al. 1992). In reservoir multiphase flow, the wettability controls the fluid-phase distribution and flow properties such as relative permeability and capillary pressure (Anderson 1987; Radke et al. 1992; Wolcott et al. 1993; Longeron et al. 1995). Wettability is the tendency of one fluid to spread on or adhere to a solid surface in the presence of other immiscible fluids (Craig 1971). In reservoir multiphase flow, the wetting fluid is believed to occupy the smallest pore channels that represent the most hydrodynamically resistive pore channels, whereas the nonwetting fluid tends to occupy the largest pore channel, which is also the least hydrodynamically resistive channel (Radke et al. 1992). Various authors have also reported that direct contact of the oil with the reservoir-rock surface can alter the wettability to be more oil-wet (Hui and Blunt 2000; Rao and Maini 1993). Before the adsorbed oil can be mobilized to flow, the adhesion forces existing between the reservoir-rock surface and the adsorbed oil must be exceeded (Rao and Maini 1993).

The role played by the surface charge of the rock, the ionic composition of the formation water (FW), and the polar oil components in the crude oil is important for the crude-oil/brine/rock (COBR) interactions. During the COBR interactions, both the mineral surface and the oil/brine interface become charged because of the presence of water (Buckley et al. 1998). The charge of the crude-oil/brine interface depends on the chemistry of the flowing fluid phases (Buckley and Liu 1998; Buckley et al. 1989). Different minerals exhibit different charges, ranging from anionic to cationic. Anionic minerals have high affinity for cationic-oil components, whereas cationic minerals have high affinity for anionic-oil components. Direct adhesion of oil to the minerals can be attributed to an attractive electrostatic force existing between the oil/brine interface and the mineral surface caused by their unlike surface charges. Hence, adhesion of oil to the reservoir-rock surface is dictated by the charges at the interface during COBR interactions. Buckley et al. (1989) attributed the lack of adhesion to the presence of a stable water film between the crude oil and the mineral surface caused by the double-layer repulsion. In other words, the polar oil component will be adsorbed onto the rock surface if the film is unstable (Buckley et al. 1989). On the other hand, indirect adsorption of oil to the mineral surface can occur in the presence of divalent ions if both surfaces have similar charges. For instance, if both the mineral surface and oil are negatively charged, the divalent cations in the brine can serve as a bridge, thereby bridging the two negatively charged surfaces and making it possible for the oil to be adsorbed on mineral surfaces (Buckley and Liu 1998; Donaldson and Alam 2008). Many researchers have also studied the influence of pH on oil adhesion (Buckley and Morrow 1990; Morrow 1990). The underlying mechanisms surrounding the adhesion of a polar oil component onto the mineral surfaces are best understood by estimating the attractive electrostatic pair linkages existing between the oil/brine and mineral/brine interfaces at given reservoir conditions (Brady and Krumhansl 2012). Surface-complexation simulations can be used to evaluate the effect of the ionic composition of the FW, oil chemistry, and the mineralogical composition of the rock on oil adhesion using a geochemical model such as PHREEQ-C (Parkhurst and Appelo 2013).

Paper II

The SCM is a chemical model that provides a molecular description of adsorption phenomena using an equilibrium approach (Goldberg 2005). The SCM can be used to study the possible electrostatic pair linkages existing between the oil/brine and the mineral/brine interfaces for a given reservoir condition. The location and surface configuration of the adsorbed ion at the rock/brine interface are the main factors that distinguish the various SCMs. If the reactive surface functional group can undergo both protonation and deprotonation, such an SCM is termed the two-pK model and it includes constant capacitance, diffuse layer, and triple layer (Goldberg 2005). The electric-double-layer model that was used to estimate the electrostatic pair linkages existing between the mineral surface and the oil/brine interface was the diffuse-layer model.

Quartz, feldspars, carbonates, oxide coatings, and clay minerals are some of the typical mineralogical constituents of the sandstone reservoir rock, with the latter minerals dominating the reactive surface because of their sheet morphology and smaller grain sizes (Brady and Krumhansl 2012; Brady et al. 2012). For perfectly clean sandstone with less than 1 wt% clay contents, the effects of the clay minerals are not distinct (Brady and Krumhansl 2012; Brady et al. 2012). Polar functional groups of both crude oil and minerals can behave as either acidic or basic by donating or accepting a proton and thereby becoming negatively or positively charged, respectively (Cuiec 1975). The effect of the polar functional groups of the crude oil on wettability estimation can be simulated by incorporating equivalent concentrations of these organic acids and bases in the SCM. Brady and Krumhansl (2012) reported that the carboxylic acid and nitrogen base can be used as the analog for the oil surface groups to predict the oil surface charge, which is temperature dependent.

Surface forces such as van der Waals, hydration, and electrostatic forces govern oil adhesion on a reservoir-rock surface during COBR interactions. Because of the diversity in the reservoir-rock mineralogy and the compositions of the flowing fluid phases, a considerable number of chemical reactions can take place in oil reservoirs. In this study, the focus has been to estimate the wettability using the oil/brine and mineral/brine interactions with the SCM. The effects of the FW ionic compositions, oil chemistry, and mineralogical composition of the rock on oil adhesion were evaluated. The SCM was used to assess all the possible attractive electrostatic pair linkages that might lead to oil adhesion in reservoirs. The SCM results were compared with their corresponding flotation-test results before meaningful conclusions were drawn. **Fig. 1** illustrates the role played by the attractive electrostatic forces in oil adhesion for both anionic and cationic surfaces.
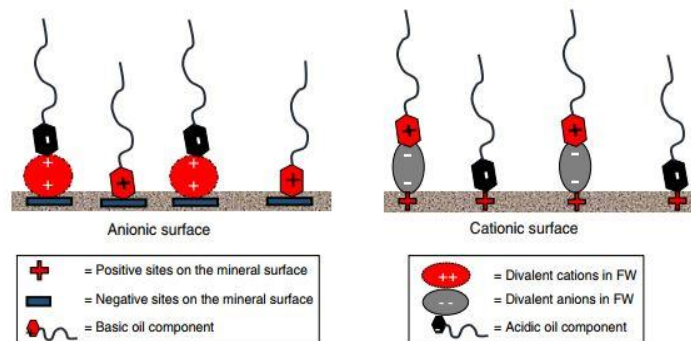
Fig. 1—Schematic illustrating the mechanisms of oil adhesion onto anionic and cationic surfaces. For cationic surfaces, direct adhesion of the anionic oil components is shown. Direct adhesion of the positively charged oil components (basic components) occurs for the anionic surfaces. In addition, bridging of the oil and mineral surfaces with similar charges by divalent ions can also occur on both cationic and anionic surfaces.

Methods

The SCM and the flotation test were used to estimate the wettability of minerals at a given reservoir condition. The simulation results were compared with their corresponding flotation-test results to assess the mechanisms that led to the wetting preferences.

Fluids and Minerals. Quartz, kaolinite, and calcite were selected because they were the dominating minerals in the studied sandstone reservoir rock. Properties of stock-tank oil (STO) and ionic compositions of synthetic FWs are given in **Tables 1 and 2,** respectively.

Fluid	Density (g/cm³) at 20°C	TAN (mg KOH/g oil)	TBN (mg KOH/g oil)
STO 1	0.86	0.10	1.90
STO 2	0.90	0.38	2.30

Table 1—Properties of STOs. KOH = potassium hydroxide.

SCM. The SCM is a chemical model that provides a molecular description of surface-adsorption phenomena using an equilibrium approach by capitalizing on the mass balance, charge balance, chemical reactions, and equilibrium constant (Goldberg 2005).

When mineral and oil surfaces contact brine, they dissociate, and a surface charge and potential are generated as a result of the dissociation and interactions between the dissociated surface and ions from the brine. These aforementioned interactions were modeled by the SCM in the form of chemical reactions that must overcome the surface potential to take place. The surface reactions and reaction parameters that are simulated in the model are given in **Table 3.** The surface charge is solved by the sum of the different surface complexes that are formed by the reactions. The surface potential is estimated from the surface charge with a diffuse-layer model. All geochemical simulations are performed with the geochemistry solver PHREEQ-C (Parkhurst and Appelo 2013). PHREEQ-C is a

geochemical solver that is widely used in groundwater chemistry and is being increasingly used to simulate reactions occurring in oil reservoirs. It is capable of performing different reactions, such as brine speciations, mineral equilibrium in brine, mineral-reaction kinetics, surface complexation, and electromigration.

Ion	FW 1 (mmol/L)	FW 2 (mmol/L)
Na^+	1326.16	701.88
K^+	5.62	7.11
Mg^{2+}	17.46	23.90
Ca^{2+}	147.94	72.85
Sr^{2+}	8.44	1.65
Ba^{2+}	0.00	0.04
Cl^-	1677.67	898.69
SO_4^{2-}	0.89	3.59
Density (g/cm^3) at 20°C	1.07	1.04

Table 2—Ionic compositions of the synthetic FWs.

Reaction	log K at 25°C	Enthalpy (kJ/mol)
Oil Surface[a]		
$=NH^+ \leftrightarrow =N + H^+$	−6.0	34.0
$=COOH \leftrightarrow =COO^- + H^+$	−5.0	0.0
$=COOH + Ca^{2+} \leftrightarrow =COOCa^+ + H^+$	−3.8	1.2
$=COOH + Mg^{2+} \leftrightarrow =COOMg^+ + H^+$	−4.0	1.2[e]
Quartz[b]		
$=Si-O-H + H^+ \leftrightarrow =Si-O-H_2^+$	−1.1	−26.4
$=Si-O-H \leftrightarrow = Si-O- + H^+$	−8.1	8.4
Calcite[c]		
$=CO_3H \leftrightarrow =CO_3^- + H^+$	−4.9	−5.0
$=CO_3 + Ca^{2+} \leftrightarrow =CO_3Ca^+ + H^+$	−2.8	25.7
$=CO_3H + Mg^{2+} \leftrightarrow =CO_3Mg^+ + H^+$	−2.2	4.5
$=CaOH + H^+ \leftrightarrow =CaOH_2^+$	12.2	−77.5
$=CaOH \leftrightarrow =CaO^- + H^+$	−17.0	116.4
$=CaOH + 2H^+ + CO_3^{2-} \leftrightarrow =CaHCO_3 + H_2O$	24.2	−90.7
$=CaOH + CO_3^{2-} + H^+ \leftrightarrow =CaCO_3^- + H_2O$	15.5	−61.6
$=CaOH + SO_4^{2-} + H^+ \leftrightarrow =CaSO_4^- + H_2O$	13.9	−72.0
Kaolinite[d]		
$=Al-O-H_2^+ \leftrightarrow =Al-O-H + H^+$	−3.0	0.0
$=Al-O-H \leftrightarrow =Al-O^- + H^+$	−3.8	32.0
$=Al-O-H + Ca^{2+} \leftrightarrow =Al-O-Ca^{2+} + H^+$	−9.7	45.0
$=Al-O-H + CaOH^+ \leftrightarrow =Al-O-CaOH + H^+$	−4.5	45.0
$=Si-O-H \leftrightarrow =Si-O- + H^+$	−7.0	32.0
$=Si-O-H + Ca^{2+} \leftrightarrow =Si-O-Ca^{2+} + H^+$	−9.7	45.0
$=Si-O-H + CaOH^+ \leftrightarrow =Si-O-CaOH + H^+$	−4.5	45.0

[a]From Brady and Krumhansl (2012) and Brady et al. (2012).
[b]From Sverjensky and Sahai (1996, 1998).
[c]Reaction contants from Van Cappellen et al. (1993).
[d]From Brady and Krumhansl (2012).
[e]Assumed to be the same as for Ca^{2+}.

Table 3—SCM input parameters.

To evaluate oil/brine/mineral interactions using the PHREEQ-C database, equivalent concentrations of the organic acids and bases in the STO were incorporated into the simulator. The surface reactions expected in the flotation test were modeled in PHREEQ-C, and similar qualities and quantities of the minerals, FW, and STO as in the flotation tests were used as input parameters. The oil and the mineral surface groups (denoted by "=") were incorporated into the model by their respective oil (=COOH, = NH) and mineral surface groups (=Si-O-H), with the symbol = denoting the surface groups. The oil and kaolinite input parameters were obtained from Brady and Krumhansl (2012) and Brady et al. (2012). The input data for the calcite were also taken from the literature: temperature-dependent reaction constants (Van Cappellen et al. 1993), site density (Wolthers et al. 2008), and surface area (Hjuler and Fabricius 2009). The quartz

surface site and surface area were taken from Sverjensky and Sahai (1996), while the enthalpy of quartz used was from a reaction similar to that of kaolinite (Sverjensky and Sahai 1998). The STO site density was obtained by converting the total acid number (TAN) and total base number (TBN) of the STO into their respective organic acid and base component with the assumption that the surface area of the oil is the same as its respective mineral surface (**Table 4**). The TAN/TBN were converted to their respective oil site density using

$$\text{Oil-site density (site/nm}^2) = \frac{\text{TAN or TBN (mg KOH/g oil)}}{\text{Mw KOH (g/mol)}} \times \frac{\text{Avogadro's number}}{\text{Surface area (m}^2/\text{g})}, \quad \dots\dots\dots\dots\dots\dots \quad (1)$$

where Mw is the molecular weight. The mineral and oil surface input parameters are given in Table 4.

Surface	Site Density (site/nm²)	Surface Area (m²/g)	Mass (g)
Quartz	10.00	1.20	0.20
=COOH/STO 1	0.89	1.20	2.59
=NH⁺/STO 1	16.99	1.20	2.59
=COOH/STO 2	3.40	1.20	2.71
=NH⁺/STO 2	20.57	1.20	2.71
Kaolinite	1.16	10.00	0.20
=COOH/STO 1	0.10	10.00	2.59
=NH⁺/STO 1	2.04	10.00	2.59
=COOH/STO 2	0.41	10.00	2.71
=NH⁺/STO 2	2.47	10.00	2.71
Calcite	4.90	2.00	0.20
=COOH/STO 1	0.54	2.00	2.59
=NH⁺/STO 1	10.20	2.00	2.59
=COOH/STO 2	2.04	2.00	2.71
=NH⁺/STO 2	12.34	2.00	2.71

Table 4—Minerals and oil surface input parameters. Note that quartz surface area and site density are from Sverjensky and Sahai (1996); kaolinite surface area and site density are from Brady and Krumhansl (2012); calcite surface area is from Hjuler and Fabricius (2009); and calcite site density is from Wolthers et al. (2008). The surface area of the oil was assumed to be the same as its respective mineral surface.

The bond product is defined as the product of the mole fraction of oppositely charged oil and mineral surfaces (Brady et al. 2015), such that the bond product is zero if all the surfaces are of the same charge and unity if the oil and mineral surfaces are oppositely charged. The bond product was calculated for quartz, kaolinite, and calcite using PHREEQ-C. **Fig. 2** illustrates the bond-product calculation with calcite as a case study. The sum of all the bond products for a given mineral is the total bond product (TBP). It is the tendency of oil to adhere onto mineral surfaces because of the attractive electrostatic pair linkages existing between the oil/brine and the mineral/brine interfaces. The ζ-potential measurements of carbonate rock from literature (Alotaibi and Yousef 2017) were also used to evaluate the model.
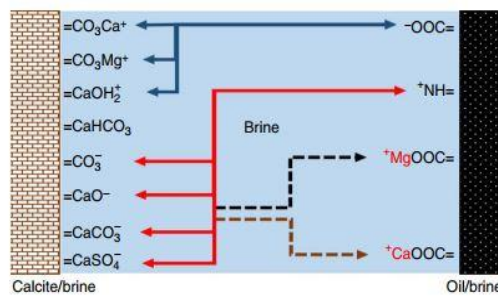
Fig. 2—Illustration of bond products caused by calcite/brine and oil/brine electrostatic interactions that led to the oil adhesion. The blue arrow depicts the direct adhesion of carboxylate (COO⁻). The red arrow illustrates the direct adhesion of the basic oil component (NH⁺). Oil adsorptions caused by the bridging of divalent cations such as Mg^{2+} and Ca^{2+} are depicted by black and brown dashed lines, respectively. TBP is the sum of all available bond products.

Flotation Test. In the flotation test, the mineral (0.2000 g) was aged in a designated FW (10.0 cm³) at 80°C for 2 days. This was to establish chemical equilibrium between the mineral and the brine. At the end of the aging period, the brine phase was removed and its pH noted and recorded. The separated brine was then kept for later use. The wet mineral was then aged for 2 days in STO (3.0 cm³) at

80°C with intermittent stirring. After aging in the oil, the separated brine phase from the previous step was added to the aged mineral/oil mixture, after which the mixture was thoroughly shaken and aged at 80°C for 1 day to allow separation. The affinity of each mineral to a particular phase determines the wettability. The water-wet phase was then filtered, and the filter cake was dried to constant weight. The concentration of the oil-wet mineral was determined as the difference between the initial weight of mineral and the weight of the dried water-wet mineral. This is because it is difficult to directly measure the weight of the oil-wet particle because of the difficulty in separating the oil-wet particles from the crude-oil phase. **Fig. 3** is a flow chart illustrating the flotation-test procedure. Details of the flotation-test procedure can be found in the literature (Erzuah et al. 2017).
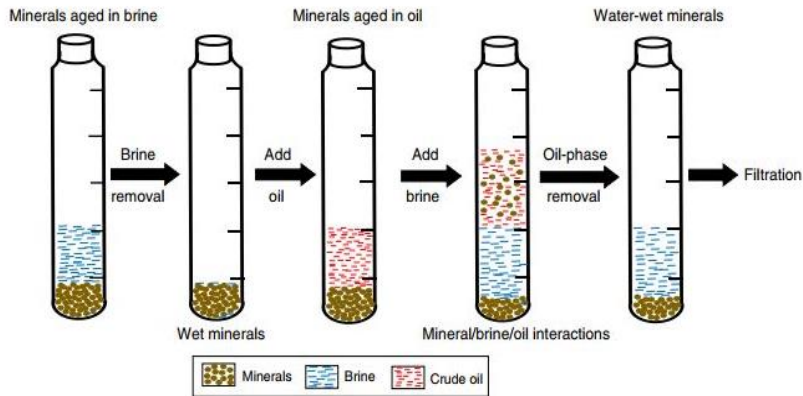
Fig. 3—Schematic depicting the flotation-test procedure.

Results and Discussions

The flotation-test results are presented first, followed by their corresponding simulation results. The SCM and the flotation-test results were then compared with each other to assess the techniques. Finally, ζ-potential measurements of calcite/brine and oil/brine interfaces from literature were also predicted with the SCM.

Flotation Experiments. Each flotation-test result was obtained from an average of six parallel experiments. The measured pH values of the studied mineral/brine systems after aging were between 7 and 8. Moreover, because the SCM results presented later in this paper captured the trend in the flotation experiments, it confirms that the conditions in the flotation experiments were close to equilibrium. From **Fig. 4,** the flotation results show that the concentration of oil-wet quartz particles was rather low, suggesting that quartz is strongly water-wet. For the kaolinite, the concentration of oil-wet particles was higher than that of quartz. Hence, it can be concluded that kaolinite is more oil-wet than quartz. This could be attributed to the higher reactive nature of kaolinite compared with quartz. The highest concentration of oil-wet particles was observed with calcite. Hence, it can be inferred that calcite is strongly oil-wet. The disparities in the flotation-test results for the different minerals are because of the varying affinities of the polar oil components in the crude oil to the different mineral sites (Table 3). Hence, the nature of the minerals, the polar components in the crude oil, and the ionic composition of the brine dictate the wetting preference of the minerals.
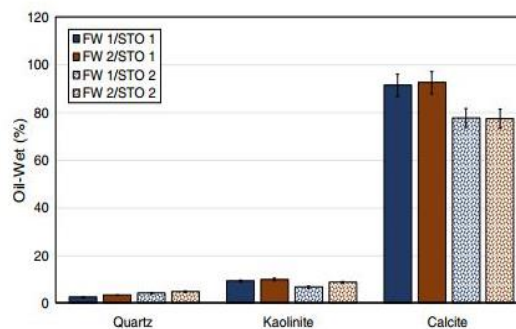
Fig. 4—Concentration of oil-wet particles during the flotation test for quartz, kaolinite, and calcite with two STOs and two FWs. Calcite was much more oil-wet than kaolinite and quartz. The vertical bars in the flotation-experiment results depict the experimental error (±5%).

SCM. The SCM was used to characterize the wettability by evaluating the oil-adhesion tendencies caused by the electrostatic pair linkages during rock/brine/oil interactions. The TBP, which depicts the tendency of a surface to adhere to oil, is presented first, followed by

the electrostatic pair linkages that led to the oil adhesion. Because the surface charges play a crucial role in oil adhesion, the mineral/brine and oil/brine interfacial charges were also estimated to evaluate the underlying mechanisms that led to the oil adhesion.

TBP. Like the flotation test, the SCM can be used to characterize wettability by estimating the tendency of oil to be adhered onto a surface using TBP. The concentration of oil-wet particles during the flotation test was estimated using SCM through the electrostatic interactions. From both the flotation test (Fig. 4) and the SCM results **(Fig. 5),** it can be concluded that quartz is strongly water-wet, whereas calcite is strongly oil-wet. Kaolinite, however, was more oil-wet than quartz, but less oil-wet than calcite.
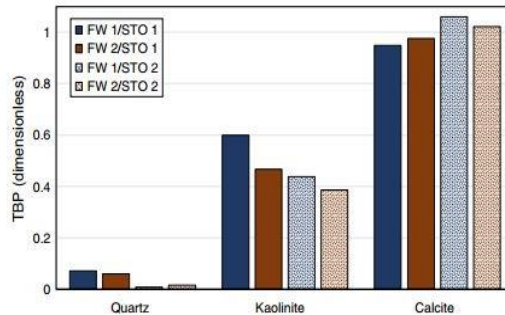
Fig. 5—Prediction of the oil-adhesion tendencies (TBP) of quartz, kaolinite, and calcite using SCM simulations with the same fluid/rock systems as the flotation experiments. Calcite shows much more oil-wet tendency with the different brine/oil formulations than kaolinite and quartz.

It can be observed that the SCM (Fig. 5) could capture the main trend of the flotation test (Fig. 4). This is because the oil/brine and mineral/brine interactions that led to the oil adhesion were modeled in the SCM using representative properties of the materials used in the flotation test. However, the TBP was relatively high for kaolinite compared with the flotation results. This could be because of the relatively high reactive surface area of the kaolinite.

Electrostatic Pair Linkage. The attractive electrostatic pair linkages that led to the oil adhesion were also estimated to assess the mechanisms of oil adhesion onto the quartz, kaolinite, and calcite surfaces. The electrostatic pair linkages for quartz are presented first, followed by kaolinite and calcite.

Quartz. From **Fig. 6,** quartz can be characterized as strongly water-wet because all the bond products were less than <0.1. This was also confirmed by the flotation-test results (Fig. 4) and the TBP (Fig. 5). From Fig. 6, the most-dominant attractive electrostatic pair linkage for quartz existed between $=Si\text{-}O^-$ and $=COOCa^+$, whereas the least-dominant electrostatic pair linkage was between $=Si\text{-}O^-$ and $=NH^+$. Hence, it can be inferred that the carboxylic acid component of the STO has a more profound effect on the wetting properties than the basic counterpart. Although not distinct for quartz, the role played by the divalent cations such as Ca^{2+} and Mg^{2+} in oil adhesion has a great effect on the wettability and how the oil recovery can be accelerated.
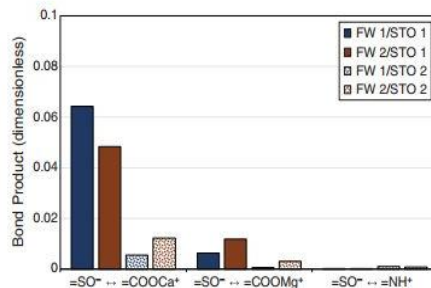
Fig. 6—Prediction of the oil-adhesion tendency of quartz using the bond product. Low oil-wet tendency in quartz, with divalent cation bridging between the negative quartz surface and the carboxylic oil component being the main adsorption mechanism in the different oil/brine combinations.

Kaolinite. For the kaolinite, the most-dominant attractive electrostatic pair linkages existed between $=Al\text{-}O^-$ and $=COOCa^+$. From **Fig. 7,** the bond product of the dominant electrostatic pair linkage in kaolinite was greater than 0.2 (approximately 0.23 to approximately 0.37), unlike quartz (<0.1). This shows that relatively more oil will be adsorbed onto the kaolinite surface than onto the quartz, and hence kaolinite is more oil-wet than quartz (Figs. 4, 5, and 6). In addition, it can be inferred from Fig. 7 that most of the dominant electrostatic pair linkages were caused by divalent-cation-bridging mechanisms. Hence, the concentration of the divalent cations such as Ca^{2+} and Mg^{2+} is crucial for oil to be adsorbed onto the kaolinite surface. From the dominant electrostatic pair linkage ($=Al\text{-}O^- \leftrightarrow =COOCa^+$), it was not surprising that the bond product with FW 1 was higher than that with FW 2 (Fig. 7) because of higher concentration of Ca^{2+} in the former than in the latter (Table 2). It can also be inferred that the basic component in the STO has a negligible role in oil adhesion compared with the carboxylic acid.
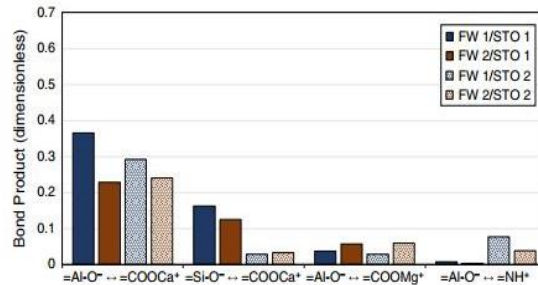
Fig. 7—Prediction of the oil-adhesion tendency of kaolinite using the bond product. Divalent cation bridging between the anionic surface sites and the carboxylic oil component is the main predicted adsorption mechanism.

Calcite. **Fig. 8** depicts the oil adhesion onto calcite surface resulting from the attractive electrostatic pair linkages existing between the calcite/brine and oil/brine interfaces. In contrast with quartz and kaolinite, in which cation bridging was the dominant electrostatic pair linkage, in calcite direct adhesion of carboxylate ($=COO^-$) onto the calcite surface ($= CaOH_2^+$) dominates the electrostatic pair linkage. This confirms the role played by the carboxylate in oil adhesion. The subsequent electrostatic pair linkages in calcite were caused by divalent ion bridging.
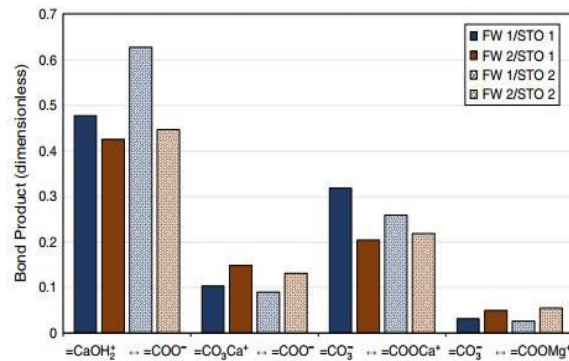
Fig. 8—Prediction of the oil-adhesion tendency of calcite using the bond product. Direct adsorption of the carboxylic oil component on the cationic calcite surface site and the divalent cation bridging between the anionic surface site and the carboxylic oil component are the main predicted adsorption mechanisms.

The bond product for the dominant electrostatic pair linkages ($= CaOH_2^+ \leftrightarrow = COO^-$) was greater than 0.4 (0.43 to approximately 0.63) compared with kaolinite (approximately 0.23 to approximately 0.37) and quartz (<0.1). This shows that calcite is strongly oil-wet compared with kaolinite and quartz.

Estimated Interfacial Charge. Because the electrostatic attraction that led to the oil adhesion exists between the mineral/brine and the oil/brine interfaces, the SCM was used to estimate the interfacial charges to elucidate the wetting properties of the minerals. The oil/brine interfacial charges are presented first, followed by the mineral/brine counterpart.

Oil/Brine Interfacial Charge. From **Fig. 9**, it can be observed that the oil/brine interfacial charges were predominantly negative apart from STO 2, which was positively charged in the presence of FW 1. The estimated positive STO 2/FW 1 interface charge was caused by the positive oil complexes formed as a result of the high concentration of divalent cations such as Ca^{2+} and Mg^{2+} in FW 1. STO 2/FW 2 was observed to be negatively charged. The difference in charge between STO 2/FW 1 and STO 2/FW 2 interfaces was because of the higher concentration of divalent cations in FW 1 compared with FW 2.

Mineral/Brine Interfacial Charge. From **Fig. 10,** it can be observed that both the quartz/brine and kaolinite/brine interfaces were negatively charged, whereas calcite/brine was positively charged. For both quartz and kaolinite, electrostatic repulsion exists between the negative mineral/brine interfaces (Fig. 9) and their predominantly negative oil/brine interfaces (Fig. 8), thereby leading to lack of oil adhesion. Figs. 6 and 7 illustrate that cation bridging can lead to oil adhesion in cases with two negatively charged surfaces. However, because the interfacial charges were insignificant for quartz compared with the kaolinite, oil adhesion by means of cation bridging was less distinct in the former (Fig. 6) than in the latter (Fig. 7). This was also confirmed by the flotation-test result (Fig. 4) and the TBP (Fig. 5). It can be concluded that the surface charge of the mineral has an overriding effect on the wetting properties compared with the oil surface charge. An electrostatic force of attraction exists between the predominantly negative oil/brine and the positive calcite/brine interfaces. It can be observed that unlike quartz (Fig. 6) and kaolinite (Fig. 7), direct adhesion of carboxylate onto the calcite surface ($= CaOH_2^+$) occurred (Fig. 8).

Ca^{2+} Oil Complexes. The Ca^{2+} can be attached to the negatively charged oil surface to form an oil complex ($=COOCa^+$). From **Fig. 11,** it can be observed that the concentration of divalent cations such as Ca^{2+} on the oil surface varies with varying FW and STO compositions. For STO 1, it can be observed that the concentration of Ca^{2+} bonded to the oil surface increases with increasing concentration of Ca^{2+} in the FW (Table 2).
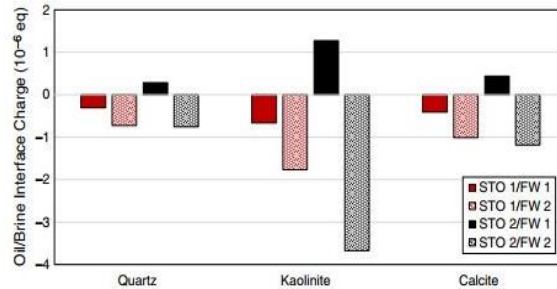
Fig. 9—Estimated oil/brine interfacial charge for quartz, kaolinite, and calcite (SCM simulations). The interfaces are negatively charged except for STO 2/FW 1, which had a higher concentration of oil complexes with divalent cations.
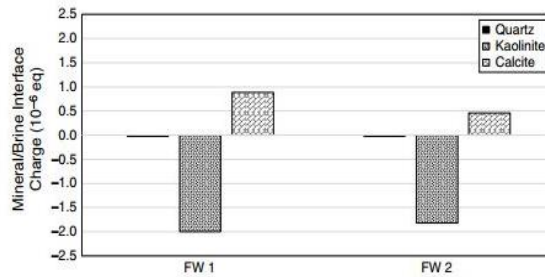
Fig. 10—Estimated mineral/brine interfacial charge (SCM simulations). The calcite surface is cationic, whereas kaolinite and quartz are anionic. However, quartz has a much lower negative charge for the two formation-water compositions than kaolinite.
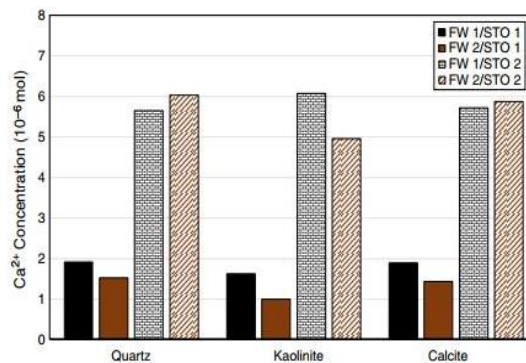
Fig. 11—Estimated concentration of Ca^{2+} bonded to the negative oil components for the different brine/oil/mineral combinations (SCM simulations). STO 2 has higher Ca^{2+} concentration on its surface.

STO 2, however, suggests otherwise, except during kaolinite/brine/oil interactions in which the concentration of Ca^{2+} bonded to the oil was higher in FW 1 than in FW 2. This suggests that the composition of the STO (Table 1) has a more dominant effect on the formation of the oil complexes than the concentration of the divalent ions in the brine. This was also confirmed by the higher Ca^{2+} concentration bonded to STO 2 than to STO 1 (Table 1).

Comparison of SCM and Flotation Experiments. The correlation between the simulation and the flotation results was performed to understand the parameters that control the wettability.

SCM vs. Flotation-Test Results. It can be seen from **Fig. 12** that the concentration of the oil-wet particles in the flotation tests is directly proportional to the TBP. It can also be inferred that calcite is strongly oil-wet, whereas quartz is strongly water-wet. Kaolinite can be described as intermediate-wet.
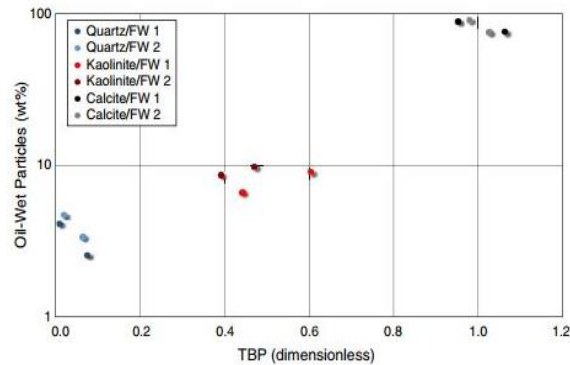
Fig. 12—Correlation between the oil-wet particles in the flotation tests (different minerals and brines) vs. the TBP predictions using SCM. Oil-wet particles in the experiments correlate with TBP.

Ca²⁺ Concentration on Mineral Surface. The concentration of Ca^{2+} on the mineral surface was proportional to the concentrations of the oil-wet particles in the flotation test, as shown in **Fig. 13.** This can be attributed to the role played by Ca^{2+} in oil adhesion. Calcite recorded the highest concentration of Ca^{2+} on its surface (approximately 0.47×10^{-6} to approximately 0.79×10^{-6} mol), whereas that of kaolinite ranges between approximately 0.01×10^{-6} and approximately 0.1×10^{-6} mol. This explains why calcite is more oil-wet than kaolinite and hence confirms the role played by divalent cations in oil adhesion.
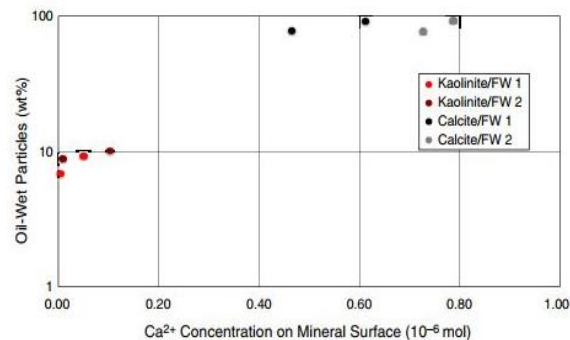
Fig. 13—Concentration of oil-wet particles in the flotation test vs. predicted Ca^{2+} concentration on the mineral surface using SCM. Higher Ca^{2+} concentration on the surface correlates with increased oil-wetness observed in the experiments.

SCM vs. Literature Experimental Data. The developed model was evaluated by predicting the oil/brine and calcite/brine ζ-potential from literature (Alotaibi and Yousef 2017). The oil/brine ζ-potential measurements and its surface-potential prediction using SCM **(Fig. 14)** are presented first, followed by the calcite/brine counterpart **(Fig. 15).** For the oil/brine interface, both the ζ-potential measurement from literature and the surface-potential prediction were all negative. However, there were some discrepancies between the SCM predictions and those from literature. These discrepancies were prominent during the oil/distilled-water (DW) ζ-potential. The high oil/DW surface-potential prediction with the SCM compared with the literature value can be attributed the difference between surface potential and ζ-potential. Note that the ζ-potential is the potential at the shear plane (some distance away from the mineral surface) (Butt et al. 2006). At high salinities the double layer is slim, and the ζ-potential can be assumed as approximately equal to the surface potential. The approximation becomes less ideal as salinity is reduced, hence the observed discrepancy between the experiment and simulation with DW.

For the calcite/brine (Fig. 15), the SCM predicted the same trend as the ζ-potential measurement from literature apart from the calcite/smartwater and calcite/sodium chloride at 80°C.

As observed in the oil/brine ζ-potential predictions (Fig. 14), the estimated calcite/brine ζ-potential was also observed to be higher than that from literature. This can also be attributed to the difference between ζ-potential and surface potential, as discussed previously. In addition, measurements of ζ-potential with calcite minerals are quite difficult and contain relatively large experimental errors (Wolthers et al. 2008). This is because the measurements are affected by the exposure of the system to carbon dioxide (CO_2) in the air (partial pressure of CO_2) and uncertainties in the equilibrium state between the minerals and brine. These uncertainties are absent in the measurements with oil, and hence the observed results.
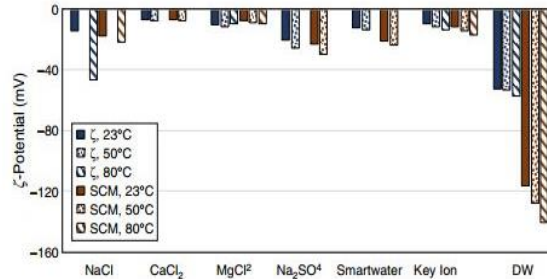
Fig. 14—Oil/brine ζ-potential measurements at different temperatures (Alotaibi and Yousef 2017) vs. its predicted surface potential (SCM). The model shows a fairly good match of experimental results except for DW, where higher surface potential is predicted.
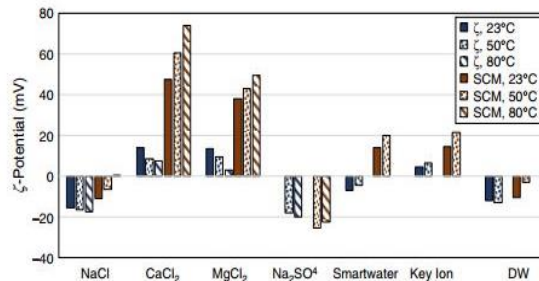
Fig. 15—Calcite/brine ζ-potential measurements at different temperatures (Alotaibi and Yousef 2017) vs. predicted surface potential (SCM). The model largely captures the trend of ζ-potential measurements with the different brines and temperature.

SCM Potential for Rock/Fluid-Interactions Studies at Reservoir Conditions. It has been shown in the study that the wettability of minerals can be estimated by SCM. This has been confirmed with wettability characterization using flotation tests. The developed SCM wettability characterization technique could capture the trend of an experimentally derived ζ-potential measurement from literature. Although the wettability of minerals can be estimated by this method, the wettability of reservoir rock on the core and field scales also depends on the mineral distribution. To estimate the wettability on these scales, it is necessary to include a description of mineral distribution in the method. The minerals that are in direct contact with the flowing fluid phases will influence the flow conditions. If the wetting properties of these minerals are known, the wettability of the reservoir rock can be estimated qualitatively. In addition, if several injection-water compositions are available for an oil reservoir, the wettability alteration during injection of these waters can be estimated qualitatively using the same technique as described in this paper.

Conclusions

The wettability estimated for quartz, kaolinite, and calcite by SCM has been found to be in agreement with the wettability characterization using the flotation tests. The oil-wetness was found to increase in the order quartz < kaolinite < calcite.

From the SCM results, direct adsorption of carboxylic acid on the positively charged calcite surfaces was the dominating wetting mechanism. For quartz and kaolinite, cation bridging was the dominating wetting mechanism.

From the simulation results, it can be concluded that the surface charge of the minerals has a more noticeable effect on oil adhesion than the charge at the oil/brine interface. For the oil, the carboxylic acid component has a more profound effect on the wetting properties of the minerals than the basic counterpart at the pH of the studied systems. Surface-complexation simulation is a cost-effective technique of estimating the wettability of the minerals in reservoir rocks. If the distribution of the dominant minerals is known, it can also be used qualitatively to estimate wettability on the core scale and the wettability distribution in oil reservoirs.

In addition, a similar method might provide a quick technique of screening the potential for injection-water compositions to alter the wettability.

Acknowledgments

References

Alotaibi, M. B. and Yousef, A. 2017. The Role of Individual and Combined Ions in Waterflooding Carbonate Reservoirs: Electrokinetic Study. *SPE Res Eval & Eng* **20** (1): 77–86. SPE-177983-PA. https://doi.org/10.2118/177983-PA.

Paper II

Anderson, W. G. 1987. Wettability Literature Survey Part 5: The Effects of Wettability on Relative Permeability. *J Pet Technol* **39** (11): 1453–1468. SPE-16323-PA. https://doi.org/10.2118/16323-PA.

Brady, P. V. and Krumhansl, J. L. 2012. Surface Complexation Modeling for Waterflooding of Sandstones. *SPE J.* **18** (2): 214–218. SPE-163053-PA. https://doi.org/10.2118/163053-PA.

Brady, P. V., Krumhansl, J. L., and Mariner, P. E. 2012. Surface Complexation Modeling for Improved Oil Recovery. Presented at the SPE Improved Oil Recovery Symposium, Tulsa, 14–18 April. SPE-153744-MS. https://doi.org/10.2118/153744-MS.

Brady, P. V., Morrow, N. R., Fogden, A. et al. 2015. Electrostatics and the Low Salinity Effect in Sandstone Reservoirs. *Energy Fuels* **29** (2): 666–677. https://doi.org/10.1021/ef502474a.

Buckley, J. S. and Liu, Y. 1998. Some Mechanisms of Crude Oil/Brine/Solid Interactions. *J. Pet. Sci. Eng.* **20** (3–4): 155–160. https://doi.org/10.1016/S0920-4105(98)00015-1.

Buckley, J. S. and Morrow, N. R. 1990. Characterization of Crude Oil Wetting Behavior by Adhesion Tests. Presented at the SPE/DOE Improved Oil Recovery Symposium, Tulsa, 22–25 April. SPE-20263-MS. https://doi.org/10.2118/20263-MS.

Buckley, J. S., Liu, Y., and Monsterleet, S. 1998. Mechanisms of Wetting Alteration by Crude Oils. *SPE J.* **3** (1): 54–61. SPE-37230-PA. https://doi.org/10.2118/37230-PA.

Buckley, J. S., Takamura, K., and Morrow, N. R. 1989. Influence of Electrical Surface Charges on the Wetting Properties of Crude Oils. *SPE Res Eng* **4** (3): 332–340. SPE-16964-PA. https://doi.org/10.2118/16964-PA.

Butt, H. J., Graf, K., and Kappl, M. 2006. *Physics and Chemistry of Interfaces*. Hoboken, New Jersey: John Wiley & Sons.

Craig, F. J. 1971. *The Reservoir Engineering Aspect of Waterflooding*, Vol. 3. Richardson, Texas: Monograph Series, Society of Petroleum Engineers.

Cuiec, L. 1975. Restoration of the Natural State of Core Samples. Presented at the Fall Meeting of the Society of Petroleum Engineers of AIME, Dallas, 28 September–1 October. SPE-5634-MS. https://doi.org/10.2118/5634-MS.

Donaldson, E. C. and Alam, W. 2008. *Wettability*. Houston: Gulf Publishing Company.

Erzuah, S., Fjelde, I., and Omekeh, A. 2017. Wettability Characterization Using the Flotation Technique Coupled With Geochemical Simulation. Presented at IOR 2017–19th European Symposium on IOR, Stavanger, Norway, 24–27 April. https://doi.org/10.3997/2214-4609.201700309.

Goldberg, S. 2005. Surface Complexation Modeling. In *Encyclopedia of Soils in the Environment*, 97–108, Elsevier. https://doi.org/10.1016/B0-12-348530-4/00558-0.

Hjuler, M. L. and Fabricius, I. L. 2009. Engineering Properties of Chalk Related To Diagenetic Variations of Upper Cretaceous Onshore and Offshore Chalk in the North Sea Area. *J. Pet. Sci. Eng.* **68** (3–4): 151–170. https://doi.org/10.1016/j.petrol.2009.06.005.

Hui, M.-H. and Blunt, M. J. 2000. Effects of Wettability on Three-Phase Flow in Porous Media. *J. Phys. Chem. B* **104** (16): 3833–3845. https://doi.org/10.1021/jp9933222.

Longeron, D., Hammervold, W. L., and Skjaeveland, S. M. 1995. Water-Oil Capillary Pressure and Wettability Measurements Using Micropore Membrane Technique. Presented at the International Meeting on Petroleum Engineering, Beijing, 14–17 November. SPE-30006-MS. https://doi.org/10.2118/30006-MS.

Morrow, N. R. 1990. Wettability and Its Effect on Oil Recovery. *J Pet Technol* **42** (12): 1476–1484. SPE-21621-PA. https://doi.org/10.2118/21621-PA.

Parkhurst, D. L. and Appelo, C. 2013. Description of Input and Examples for PHREEQC Version 3—A Computer Program for Speciation, Batch-Reaction, One-Dimensional Transport, and Inverse Geochemical Calculations. In *US Geological Survey Techniques and Methods*, Book 6, Chap. A43. Denver: US Geological Survey.

Radke, C., Kovscek, A., and Wong, H. 1992. A Pore-Level Scenario for the Development of Mixed Wettability in Oil Reservoirs. Presented at the SPE Annual Technical Conference and Exhibition, Washington, DC, 4–7 October. SPE-24880-MS. https://doi.org/10.2118/24880-MS.

Rao, D. N. and Maini, B. B. 1993. Impact Of Oil-Rock Adhesion on Reservoir Mechanics. Presented at the Annual Technical Meeting, Calgary, 9–12 May. PETSOC-93-84. https://doi.org/10.2118/93-84.

Sverjensky, D. A. and Sahai, N. 1996. Theoretical Prediction of Single-Site Surface-Protonation Equilibrium Constants for Oxides and Silicates in Water. *Geochimica Cosmochim. Ac.* **60** (20): 3773–3797. https://doi.org/10.1016/0016-7037(96)00207-4.

Sverjensky, D. A. and Sahai, N. 1998. Theoretical Prediction of Single-Site Enthalpies of Surface Protonation for Oxides and Silicates in Water. *Geochimica Cosmochim. Ac.* **62** (23–24): 3703–3716. https://doi.org/10.1016/S0016-7037(98)00262-2.

Van Cappellen, P., Charlet, L., Stumm, W. et al. 1993. A Surface Complexation Model of the Carbonate Mineral-Aqueous Solution Interface. *Geochimica Cosmochim. Ac.* **57** (15): 3505–3518. https://doi.org/10.1016/0016-7037(93)90135-J.

Wolcott, J. M., Groves, F. R. Jr., and Lee, H.-G. 1993. Investigation of Crude-Oil/Mineral Interactions: Influence of Oil Chemistry on Wettability Alteration. Presented at the SPE International Symposium on Oilfield Chemistry, New Orleans, 2–5 March. SPE-25194-MS. https://doi.org/10.2118/25194-MS.

Wolthers, M., Charlet, L., and Van Cappellen, P. 2008. The Surface Chemistry of Divalent Metal Carbonate Minerals; A Critical Assessment of Surface Charge and Potential Data Using the Charge Distribution Multi-Site Ion Complexation Model. *Am. J. Sci.* **308** (8): 905–941. https://doi.org/10.2475/08.2008.02.

Samuel Erzuah is a PhD-degree candidate at The National IOR Centre of Norway and the University of Stavanger. He is currently working on the concept of wettability estimation by oil adsorption, and has a keen interest in improved-oil-recovery studies with a focus on understanding the mechanisms during COBR interactions. Erzuah has authored or coauthored three technical papers. He holds a bachelor's degree in petroleum engineering from Kwame Nkrumah University of Science and Technology, Ghana, and a master's degree in well engineering from the University of Stavanger. Erzuah is an active SPE member and currently serves as an SPE technical editor.

Ingebret Fjelde is Chief Scientist in the Improved Oil Recovery Group at NORCE Norwegian Research Centre AS (formerly IRIS), an adjunct professor of petroleum technology at the University of Stavanger, and a project manager at The National IOR Centre of Norway. His main research interests are EOR methods in sandstone and carbonate rock (wettability alteration, low-salinity waterflooding, surfactant flooding, CO_2 flooding, new EOR methods, and combination of EOR methods), formation-damage mechanisms, and CO_2 storage. Fjelde has authored or coauthored more than 80 papers. He holds master's and PhD degrees in chemistry from the University of Bergen.

Aruoture Voke Omekeh is a research scientist at NORCE Norwegian Research Centre AS and also holds a post-doctoral-degree position at The National IOR Center of Norway. He has been with NORCE Norwegian Research Centre AS (formerly IRIS) since 2013, and works in the Improved Oil Recovery Group. Omekeh has 10 years of experience with simulation of geochemical effects of various EOR processes such as low-salinity waterflooding, waterflooding for wettability alteration, and silicate injection for in-depth diversion. His other research interests include simulation of laboratory-scale experiments of various EOR processes, CO_2 storage, and CO_2 for EOR. Omekeh holds master's and PhD degrees in reservoir engineering from the University of Stavanger and a bachelor's degree from the University of Benin, Nigeria.

Paper III

Challenges Associated with Quartz Crystal Microbalance with Dissipation (QCM-D) as a Wettability Screeening Tool (2018). *Oil & Gas Science and Technology–Revue d'IFP Energies nouvelles* **73**: 58.

Erzuah, Samuel; Fjelde, Ingebret; Omekeh, Aruoture Voke.

Paper III

REGULAR ARTICLE   **OPEN ∂ ACCESS**

Challenges associated with Quartz Crystal Microbalance with Dissipation (QCM-D) as a wettability screening tool

Samuel Erzuah[1,2,*], Ingebret Fjelde[1,2,3], and Aruoture Voke Omekeh[1,3]

[1] The National IOR Centre of Norway, P.O. Box 8600 Forus, N-4036 Stavanger, Norway
[2] The University of Stavanger, P.O. Box 8600 Forus, N-4036 Stavanger, Norway
[3] International Research Institute of Stavanger (IRIS), P.O. Box 8046, N-4068 Stavanger, Norway

Abstract. Wettability is an indispensable parameter in multiphase flow due to its profound effect in fluid phase distribution and flow properties in the oil reservoirs. One approach of unravelling the enigma associated with wettability characterization is to investigate oil adhesion onto reservoir rock surface during crude oil accumulation. This was accomplished using Quartz Crystal Microbalance with Dissipation (QCM-D) device. The QCM-D is a microbalance device that hinges on the changes in the frequency of a resonating crystal due to changes in the mass on sensor surface, precipitation, adsorption and desorption. However, this technique was confronted with numerous challenges during its early try-out. The objective of this study is to enumerate these challenges and how they were resolved. The piston-cell, valves, flow-lines and most of the experimental set-up were made from stainless steel. Hence, the high temperature coupled with high salinity brine resulted in the formation and deposition of corroded materials on the sensor. Due to the high sensitivity of the QCM-D technique, these corrosion deposits were detected *via* the high attenuation of the frequency signal as time elapsed during Formation Water (FW) injection. The second challenge was related to the dissolution of the thin sensor coatings (sensor etching) depicted by the relatively high increase in frequency signal with negligible changes in Dissipation (D). The third challenge was related to the trapping of fluids such as Stock Tank Oil (STO) inside the flow-cell. Finally, salt precipitation resulting from temperature variation during the initial experimental set-up was also observed. To resolve the corrosion challenge, all the stainless-steel components in the experimental set-up were replaced with titanium and non-metallic component such as peek materials. The sensor etching was also averted by injecting the brine through a packed column filled with similar mineral as the coatings on the sensor to attain equilibrium prior to injecting it onto the sensor. Geochemical simulation of the sensor etching was also confirmed using the geochemical simulator PHREEQ-C. Furthermore, the trapping of fluids inside the flow-cell was overcome by rotating the flow-cell to optimize the fluid displacement *via* capitalizing on their density contrast. Finally, the salt precipitation was avoided by conducting the experiment in a constant temperature experimental set-up. The QCM-D technique can be employed to estimate wettability by evaluating the tendency of the various minerals to adhere oil. The beauty of the QCM-D technique is that the surface interactions can be monitored on a real-time.

Symbols and nomenclature

BPV	Back-Pressure Valve	ΔD	Change in Dissipation (ppm)
COBR	Crude Oil/Brine/Rock	Δf	Change in frequency (Hz)
DW	Distilled Water	QHPT	High-Pressure High-Temperature QCM-D
FW	Formation Water		
LSW	Low Salinity Water		
QCM-D	Quartz Crystal Microbalance with Dissipation		
STO	Stock Tank Oil		

1 Introduction

The QCM-D is a highly sensitive weight detection and monitoring device that has permeated the fiber of modern industries such as the pharmaceutical, biomedical, oil and gas

* Corresponding author: samuel.erzuah@iris.no

industry. The QCM-D relies on the changes in the resonance frequency of the oscillating crystal to estimate the mass of the adsorbed film (Alagha et al., 2013; Chandrasekaran et al., 2013; Ekholm et al., 2002; Feiler et al., 2007; Keller and Kasemo, 1998). This is achieved by measuring the changes in the frequency (Δf) and dissipation (ΔD) with time. Aside the effect of the adsorbed film on the frequency and dissipation signal, the properties of the injected fluids such as density and viscosity also influence the signals. For instance, bulk shift in the frequency and dissipation signals occurs during the injection of two immiscible fluids of varying properties such as Formation Water (FW) and n-decane consecutively. The bulk shift in the frequency and dissipation signals has no effect in the adsorption process. Considering FW/n-decane/FW injection sequence, the constant FW frequency before and after injecting n-decane was reported by Erzuah et al. (2018) to depict lack of oil adsorption. On the other hand, adsorption/desorption onto the sensor is also depicted by a gradual decrease/increase in the frequency signal due to the added mass unlike the bulk shift in the frequency and dissipation signal resulting from the fluid properties. Erzuah et al. (2018) reported that the frequency signals of the oscillating crystal with adsorbed film is lower than prior to the adsorption during the injection sequence. The dissipation signal (ΔD) is proportional to the magnitude of the adsorbed mass. The frequency signal (Δf) on the other hands is inversely proportional to the adsorbed mass.

Numerous researchers have carried out comprehensive protein adsorption studies using QCM-D due to its role in the successful implantation of prosthetic devices in the human body (Bluemmel et al., 2007; Feiler et al., 2007). Cao et al. (2018) also investigated calcite growth rate using QCM-D. Nguyen and Elimelech (2007) have carried out comprehensive studies on the adsorption of plasmid DNA *via* QCM-D. Adsorption of cell onto various surfaces have also been carried out (Dixon, 2008). Cattanach et al. (2011) undertook corrosion monitoring under sales gas condition using QCM-D.

The intended application of the QCM-D in this presented study was to investigate oil adhesion onto reservoir rock surface. However, this technique was confronted with numerous challenges during the early try-out. The aim of this study is to enumerate these challenges and how they were averted in a chronological manner. Since the Stock Tank Oil (STO) contained volatile components, a QCM-D cell that allows higher pressure was used to avoid boiling.

2 Overview of the HPHT QCM-D device (QHPT)

The aim of this presented study has always been to qualify the QCM-D device as a wettability characterization tool. To accomplish this, the High-Pressure, High-Temperature (HPHT) QCM-D vessel (QHPT) developed by *Biolin Scientific* (Frölunda, Sweden) was employed in this study. The conventional QCM-D device can accommodate only one fluid in the flow-cell chamber at a given time. In other words, the active electrode area of the sensor is filled with the test fluid while the non-active part of the sensor is occupied by air. The QHPT vessel on the other hand can accommodate two fluids in the flow-cell chamber at a given time namely; the test and the system fluids. The test fluid occupies the active electrode area/deposition area of the sensor while the system fluid also fills the flow-cell chamber beneath the sensor (non-active part of the sensor). The system fluid used in this study was n-decane while the test fluids were crude oil and brine. The magnitude of the dissipation signal depends on the properties of the fluids occupying each side of the sensor. For instance, if air occupies both sides of the sensor as observed during the start of the experiment (Fig. 1A), the energy loss by the resonating sensor resulting from the presence of air above and beneath the sensor is negligible (~0 ppm). This is because, the properties of air such as density and viscosity are negligible. Hence, the contribution of air to the energy loss (absolute dissipation) is zero.

However, at the start of the experiment throughout this study, the system fluid used in the QHPT vessel (Fig. 1B) was n-decane while the test fluid (reference fluid) was FW. Both the n-decane and the FW have different properties (densities and viscosities) than air and hence, the energy loss by the resonating sensor due to the presence of these fluids will not be the same as in an air-filled flow-cell (Fig. 1A). In other words, the absolute dissipation value at the start of the experiment depends on the properties (density and viscosity) of fluids in the flow-cell chamber at the onset of the experiment. Nonetheless, the changes in frequency (Δf) and dissipation (ΔD) signals were used throughout this study but not their absolute values.

In an attempt to qualify the QCM-D as wettability screening tool, the challenges that were confronted and how they were averted are presented in a chronological manner.

3 Challenges

These challenges include corrosion, sensor etching, fluid trapping and salt precipitation. These challenges are presented in a sequential order as they occurred during the qualification of the QCM-D technique as a wettability screening tool.

3.1 Corrosion

The corrosion challenge is presented first followed by its mitigation protocol.

3.1.1 Corrosion challenge

The QCM-D technique is a highly sensitive weight measuring device. Hence, it has the capacity of detecting contaminants originating from the experimental set-up such as corrosion deposit. Considering Part I of Figure 2, it can be observed that the frequency and the dissipation signals were relatively stable during the injection of Distilled Water (DW), *i.e.* no change in mass on sensor. However, gradual attenuation of the frequency signal was observed during Formation Water (FW) injection Part II of Figure 2 with

Paper III
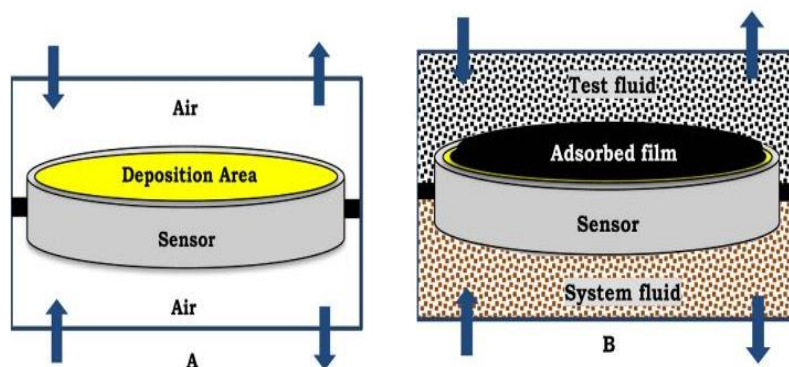
Fig. 1. Analogy of the fluids on both the active (deposition area) and non-active electrodes part of the high-pressure high-temperature QCM-D (QHPT) vessel. If air occupies both sides of the sensor (A), the energy loss (Dissipation energy) by the sensor is negligible (~0). On the other hand, if the system fluid occupies the non-active part of the sensor whiles the test fluid also occupies the active electrode part of the sensor (B). Hence, the total energy lost by the sensor is due to the presence of the fluids above and beneath the sensor in addition to the attenuation due to the adsorbed film.

a corresponding increase in the dissipation energy. Hence, it can be inferred that the additional mass due to the corrosion deposit is the reason for the observed trend (Fig. 2).

As compared to the DW signal, the attenuation of the frequency signal cannot be attributed to the presence of ion in the FW alone but rather its interactions with its environment. This was depicted by the gradual attenuation of the frequency signal describing deposition. When the flow-cell was opened, it was observed that the reduction in the frequency signal with time during the FW injection was due to the formation and/or deposition of corroded material onto the sensor. The corrosion deposit was due to the high salinity brine with pH of 5.9 coupled with high temperature in the presence of corrosive materials such as stainless steel in experimental set-up. Thus, providing a conducive condition for corrosion to take place (Fig. 2).

To confirm this hypothesis, a stainless-steel piston-cell was filled with the FW for barely a week. It can be observed from Figure 3 that a yellowish-brown substance was formed on the walls of the stainless-steel piston-cell in addition to changes in colour of the FW from colourless (Fig. 5A) to yellow (Fig. 5B). Thus, confirming that corrosion has taken place as supported by Figure 2.

3.1.2 Mitigation of the corrosion challenge

To resolve the corrosion challenge, a similar test was performed by storing the FW in titanium piston-cell for barely a week. It can be observed from Figure 4 that; no colour change was observed on the wall of the titanium piston-cell unlike in the stainless-steel (Fig. 3). Contrary to the change in colour of the FW stored in the stainless-steel piston-cell, the FW remained colourless after storing it in the titanium piston-cell (Fig. 5C). This confirms that no corrosion has taken place. Hence, the flow-cell and all the stainless-steel components in the experimental set-up were replaced with titanium and non-metallic component such as peek materials.
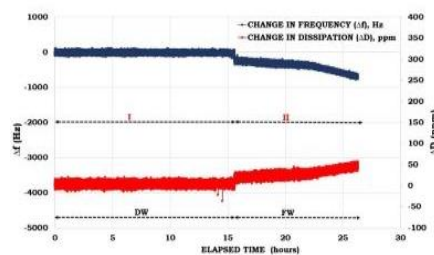
Fig. 2. Corrosion deposits originating from the experimental set-up, high temperature and the high salinity brine.

In addition, Inductive Coupled Plasma (ICP) analytical technique was employed to examine the composition of the original FW (Fig. 5A) and the FW stored in both the stainless-steel piston-cell (Fig. 5B) and that of the titanium piston cell (Fig. 5C). For the FW stored in the stainless-steel piston cell (Figs. 3 and 5B), precipitation of corrosion deposits was observed as time elapse. Hence, the sample in Figure 5B was separated into two halves. Half of this separated volume was analysed without adding hydrochloric acid (HCl) while 0.1% volume of HCl was added to the other half to dissolve the dispersed precipitate. It can be observed from Table 1 that the concentration of Fe in both the original FW and the FW stored in the titanium piston-cell was less than 0.1 mg/L (<0.1 mg/L). This confirms that the corrosion challenge can be mitigated by using the titanium piston-cell (Fig. 4) as observed in Figure 5C. On the other hand, the content of Fe in the FW stored in the stainless-steel piston cell was greater than 0.1 mg/L (>0.1 mg/L), thus confirming that corrosion has taken place.

In addition, it can also be observed that the concentration of Fe in the FW stored in the stainless-steel piston-cell (Fig. 5B) without adding HCl was relatively small (0.1 mg/L) as compared to that with HCl added

S. Erzuah et al.: Oil & Gas Science and Technology - Rev. IFP Energies nouvelles **73**, 58 (2018)
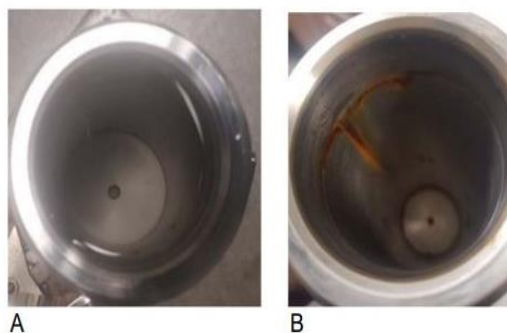
Fig. 3. Change in colour of the stainless-steel piston-cell wall before (A) and after (B) storing FW in it for 7 days. The yellowish-brown substance formed at the walls of the stainless-steel piston-cell can be linked to the corrosion formation.
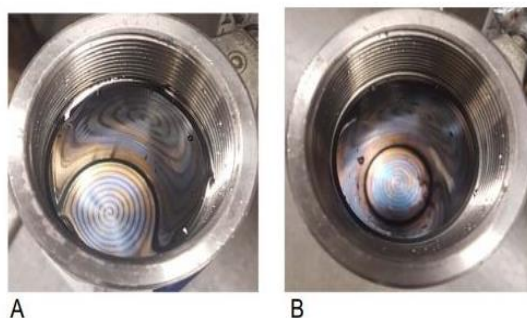
Fig. 4. Illustrate no corrosion resulting from the negligible change in colour of the wall of the titanium piston-cell before (A) and after (B) storing the FW in it for 7 days. Thus, confirming that titanium component and non-metallic component can mitigate the corrosion challenge.

(8.2 mg/L). The increase in the Fe content in the latter FW was attributed to the dissolution of the precipitated corrosion deposit with the HCl. To add to the above, it can be concluded that titanium piston-cell did not react with the FW as confirmed by the negligible titanium content (<0.04 mg/L) in all the studied FW conditions. Hence, the corrosion challenge can be mitigated by the titanium piston-cell and non-metallic components such as Polyether Ether Ketone (PEEK).

3.1.3 Experiment with resolved corrosion challenge

From Part I of Figure 6 it can be observed that no corrosion took place due to the relatively stable frequency and dissipation signal during FW injection unlike in Figure 2 with stainless-steel components. However, there was an increase in frequency of the signal with time (Part II of Fig. 6).

This was attributed to the dissolution of the coatings on the sensor with time leading to high oscillation of the resonating crystal. This challenge is termed "sensor etching". It can be observed from Part III of Figure 6 that the frequency and dissipation signals were lost as time elapsed.

4 Sensor etching

Like the presentation of the corrosion challenge, the sensor etching challenge will be presented first followed by its mitigation.

4.1 Sensor etching challenge

The QCM-D sensor is composed of quartz crystal with a thin layer (50–100 nm) of the desired mineral such as quartz and kaolinite. During the injection of high salinity brine, the coatings on the sensors were dissolved. This was depicted by the relatively high frequency signal without any significant changes in Dissipation (D). In other word, etched sensors led to reduction in mass of the crystal thereby increasing the frequency without any appreciable changes in the dissipation signal unlike during adsorption/deposition (Fig. 2). Figure 7 shows the nature of a quartz sensor before and after etching. Figures 6 and 8 also illustrate the etching of quartz and kaolinite sensors respectively during FW injection.

Unlike the quartz sensor (Fig. 6), the etching of the kaolinite sensor (Fig. 8) was very fast. In other words, the kaolinite sensor begun to etch approximately 4 h after

Fig. 5. Change in colour of the prepared FW (A) when stored in stainless steel (B) and titanium (C) piston cells respectively. The colour change in FW (B) can be attributed to corrosion formation resulting from the stainless-steel piston-cell coupled with the corrosive nature of the studied system. Since the prepared FW and the brine store in titanium piston-cell were both colourless (A and C respectively). It confirms that the corrosion challenge can be mitigated by using titanium piston-cell.

Table 1. Composition of the FW.

Element	Original FW mg/L	FW-stainless steel (without HCl) mg/L	FW-stainless steel (with HCl) mg/L	FW-Titanium mg/L
Sodium (Na)	30 600	30 800	30 100	30 500
Calcium (Ca)	5920	6010	5970	6000
Magnesium (Mg)	419	422	415	415
Barium (Ba)	0.23	0.21	0.29	0.20
Iron (Fe)	<0.1	0.1	8.2	<0.1
Strontium (Sr)	3.25	2.99	3.09	3.05
Potassium (K)	245	247	243	246
Titanium (Ti)	<0.04	<0.04	<0.04	<0.04
Sulfur (S)	31.4	31.4	30.9	31.1

the inception of the experiment (Part I of Fig. 8) as opposed to approximately 10 h in the case of the quartz sensor (Part I of Fig. 6). This confirms that the dissolution rate of kaolinite is high compared to quartz.

4.2 Mitigation of the sensor etching challenge

The sensor etching challenge was averted by injecting the brine through a pre-column filled with a similar material as the sensor coating. This was to attain equilibrium between the mineral and FW before it reaches the sensor. From Part I of Figure 9, it can be observed that no etching took place during the injection of DW. However, the sensor begun to etch during the injection of FW without packed column (Part II of Fig. 9). However, when the FW was injected through a packed column to attain equilibrium

with the coatings on the sensor, etching was averted (Part III of Fig. 9).

A completely packed sand column poses no threat to the flow of brine due to its high permeability. On the contrary, a completely packed kaolinite column will hinder the flow of brine due to its low permeability. There was therefore the need to assess a kaolinite-quartz mixture that can mitigate both etching and permit the flow of the injected brine.

Three (3) different kaolinite-quartz mixtures were considered to evaluate their effect on sensor etching. It can be concluded from Part I of Figure 10 that, if the amount of kaolinite in the mixture is small, it will lead to etching. This is because, it will take a longer time for the brine to attain equilibrium with the minerals in the pre-column. This is confirmed by Parts II and III of Figure 10 with
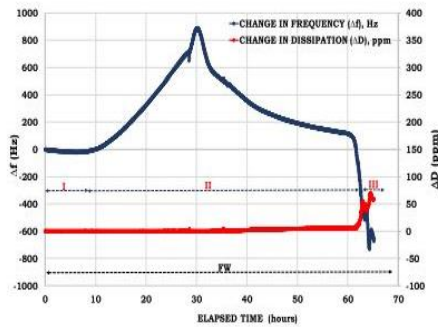
Fig. 6. QCM-D experiment with resolved corrosion challenge with using quartz sensor.
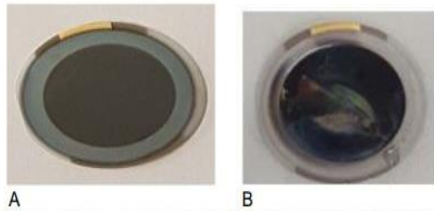
Fig. 7. Quartz sensor surface before (A) and after (B) etching.
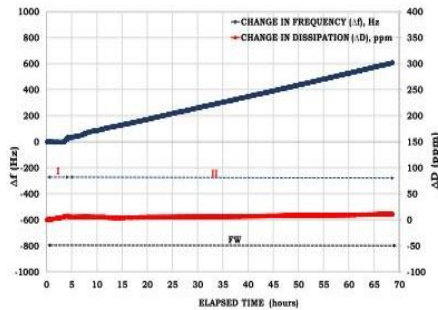
Fig. 8. Etching of kaolinite sensor due to high salinity brine coupled with high temperature (65 °C).

relatively stable frequency signal resulting from the shorter period required to reach equilibrium due to the relatively high amount of kaolinite in the mixture as compared to Part I. In addition, it can be concluded that Part II was more stable than Part III due to the relatively high amount of kaolinite in the kaolinite-quartz mixture in the former than the latter. Hence, the optimal kaolinite-quartz mixture that can mitigate etching and promoted brine injection was that of Part II of Figure 10. The sensor etching challenge and its mitigation was also confirmed by a geochemical simulator, PHREEQ-C. The geochemical simulation results confirm the dissolution of the sensor the coatings without pre-column (Fig. 11). From Figures 10 and 11, it can be
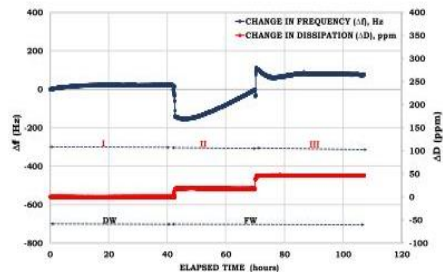
Fig. 9. Illustrates sensor etching mitigation with packed column (sand packed). Part II without and Part III with pre-column.
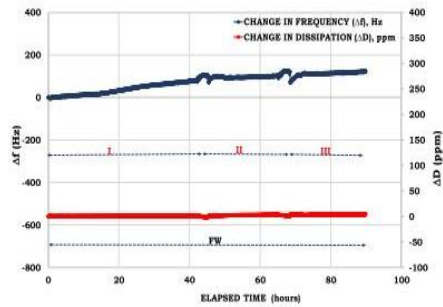
Fig. 10. Evaluating the quartz-kaolinite mixture that can curb etching with high permeability.

concluded that pre-column is needed if sensor etching is to be averted.

4.3 Experimental result with resolved sensor etching challenge

From Figure 12, it can be observed that the FW frequency signal looks relatively stable before and after the injecting *n*-decane. However, the bulk shift in the frequency signal during the injection of *n*-decane (Part II of Fig. 12) after the injection of FW is as a result of the difference in fluid properties.

Nonetheless, the bulk shift has no effect on the adsorption process. The LSW frequency and dissipation signals also look relatively stable. Thus, confirming that the sensor etching has been averted.

5 Trapping of fluids

The fluid trapping challenge was presented first followed by how it was mitigated.

5.1 Challenge with trapping of fluids inside the flow-cell

During the FW/*N*-Decane/FW/LSW/FW injection sequence (Fig. 13), the effect of the trapped fluids such as
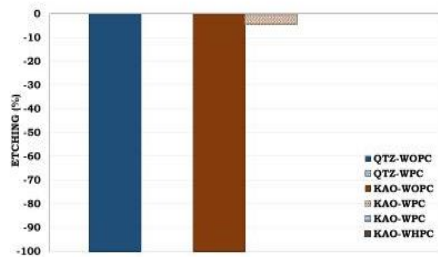
Fig. 11. Geochemical simulation of the sensor etching *via* PHREEQ-C. WOPC = Without pre-column, WPC = With pre-column, WHPC = With hybrid pre-column, QTZ = quartz sensor and KAO = kaolinite sensor.
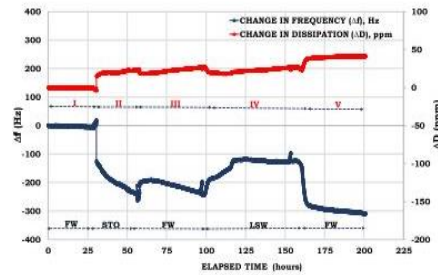
Fig. 14. Trapping of fluid inside the flow-cell due to density contrast during FW/STO/FW/LSW/FW injection sequence.
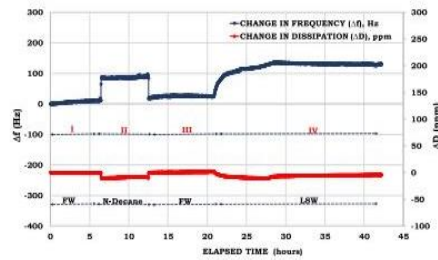
Fig. 12. FW/*N*-Decane/FW injection sequence to evaluate the mitigation of the sensor etching phenomenon.
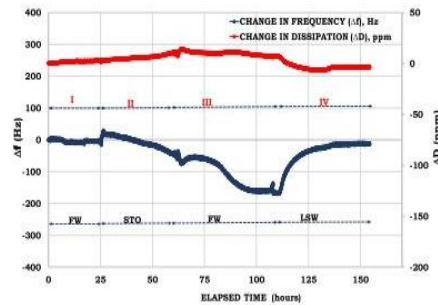
Fig. 15. Trapping of fluid inside the flow-cell due to density contrast during FW/STO/FW/LSW#1 injection sequence.
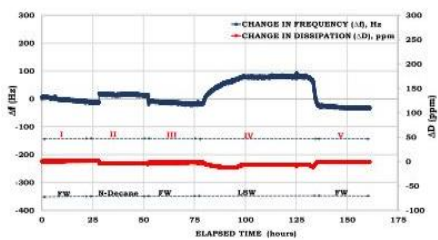
Fig. 13. Trapping of fluid inside the flow-cell due to density contrast.

the oil was not distinct due to lack of polar components in the *n*-decane. However, during the FW/STO/FW/LSW/FW injection sequence (Fig. 14 and Fig. 15), it was observed that the frequency of the FW signal after injecting STO (Part III of Fig. 14) was decreasing with time depicting adsorption as observed during the STO injection (Part II of Fig. 14).

However, the LSW frequency signal was relatively stable (Fig. 14). This can be attributed to the low concentration of divalent cations available to bridge the trapped oil during LSW injection (Part IV of Fig. 14) as compared to the FW injection (Part III of Fig. 14).

This was depicted by the attenuation of the frequency signal during the injection of the FW after the STO injection (Part III of Fig. 14). From Figure 15, it can be observed that most of the trapped STO were displaced after a prolonged injection period. This resulted in a stable frequency signal during FW injection (Part III of Fig. 15) unlike in Part III of Figure 14. In other words, it took longer time to displace most of the trapped oil from the flow-cell before the FW frequency signal became stable (Part III of Fig. 15).

5.2 Mitigation of the challenge with trapped oil inside the flow-cell

Mitigation of the trapped fluids inside the flow-cell was achieved by rotating the flow-cell to optimize the displacement of the previously injected fluid with the current one by capitalizing on their density contrast. This resulted in a fast stabilization time during the injection of FW after injecting STO. During the displacement of the FW with the oil, the flow-cell was rotated such that maximum contact was established between the sensor and the oil due to density contrast. In other words, the flow-cell was rotated in such a way that the less dense fluid rises to the top to occupy the surface of the sensor while the denser fluid moves to the bottom of the flow-cell chamber to be expelled (Fig. 16).

From Figure 17, it can be observed that during the displacement of the oil with the FW, the flow-cell was
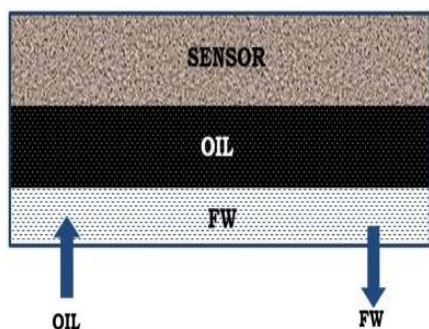
Fig. 16. Displacement of the denser fluid (FW) with the less dense fluid (oil).
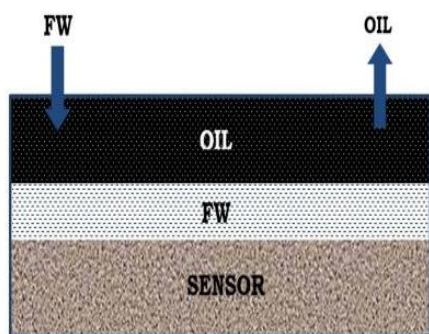
Fig. 17. Displacement of the less dense fluid (oil) with the denser fluid (FW).

rotated such that the denser fluid (FW) sink to the bottom of the flow-cell chamber to cover the sensors surface. The less dense fluid on the other hand rises to the top of the flow-cell chamber to be displaced due to density contrast.

6 Temperature

6.1 Salt precipitation challenge and its mitigation

Finally, there was also the tendency for salt precipitation resulting from temperature variation in the initial experimental set-up. This was mitigated by conducting the experiment in a constant temperature environment as depicted in Figure 18.

7 Developed QCM-D method

7.1 Experimental procedure and set-up

The QCM-D experimental procedure can be grouped into three (3) main categories namely; preparatory
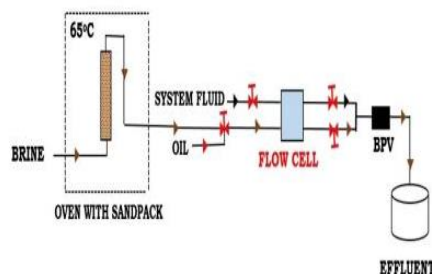
Fig. 18. Experimental set-up with QCM-D challenges resolved (BPV = Back Pressure Valve).

(pre-acquisition) stage, acquisition stage and post-acquisition stage. A schematic illustration of the QCM-D experimental set-up is shown in Figure 18.

7.1.1 Preparatory stage (pre-acquisition)

The flow-cell and the flow-lines were thoroughly cleaned with ethanol and dried with nitrogen gas to remove impurities from the system before mounting the sensor. The sensor was thoroughly cleaned with ethanol and dried with nitrogen gas before mounted into the flow cell. The temperature of the flow-cell was then set to the desired reservoir temperature (65 °C used in this study). The air in the system was displaced with ethanol using high and low flow rate intermittently. The ethanol in the non-active part of the flow-cell was displaced with the system fluid (*n*-decane) while that at the active electrode was displaced with the desired brine. Back Pressure Valve (BPV) is required at the outlet as illustrated in Figure 18 to avoid boiling of oils. The tubings from the active and the non-active parts of the sensor are connected to ensure that the pressure is the same on both sides of the sensor. This is to prevent losing the sensor through cracking.

7.1.2 Acquisition stage

The log was restarted after a stable baseline was achieved. The desired injection fluids were injected in their desired order while monitoring the frequency and the dissipation signals on real-time. When switching between fluids, the pump should be stopped with all the valves closed without stopping the data acquisition. Prior to injecting the next fluid, it should be ensured that pressure of the injecting fluid was approximately the same as in the flow-cell.

7.1.3 Post-acquisition stage

At the end of the acquisition period, the pump was stopped, and the acquisition was stopped. The BPV was then gradually disconnected to bleed off the pressure in the flow-cell. The sensor was then removed from the flow-cell and kept for latter analysis. A dummy sensor was then mounted in the flow-cell prior to injecting the cleaning fluid. The designated cleaning fluid for *n*-decane is ethanol while that of the STO is toluene followed by ethanol.
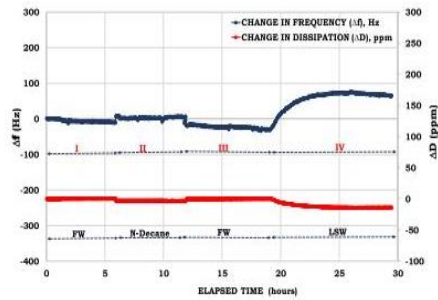
Fig. 19. Frequency and dissipation signals during FW/N-Decane/FW/LSW#1 injection sequence using quartz sensor.
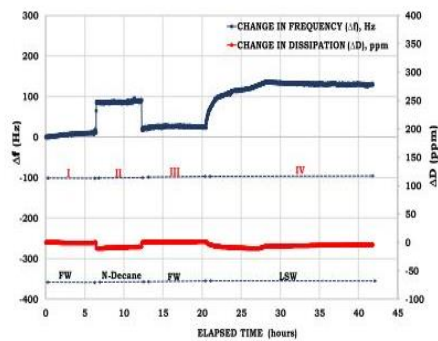
Fig. 20. Frequency and dissipation signals during FW/N-Decane/FW/LSW injection sequence using quartz sensor.
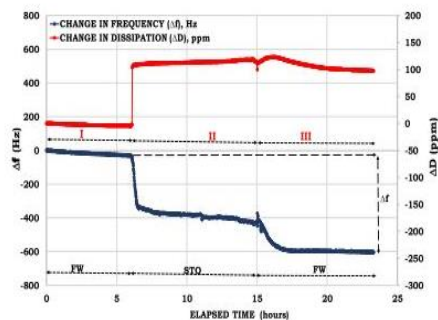
Fig. 21. Frequency and dissipation signals during FW/N-Decane/FW/LSW injection sequence using kaolinite sensor.

7.2 Results with all the challenges resolved

From Figures 19 and 20, it can be observed that the frequency and dissipation signals in an experiment with quartz sensor look relatively stable after the challenges were

resolved. In addition, the FW/N-Decane/FW/LSW injection sequence depicted the lack of oil adsorption due to the negligible change in the FW frequency signal before and after the injection of n-decane in both cases (Part III of Fig. 19 and Part III of Fig. 20).

Considering the LSW injection stage (Part IV of Fig. 19 and Part IV of Fig. 20), it can be observed that the frequency signals were approximately the same (90 Hz and 130 Hz respectively).

Figure 21 illustrates oil adhesion kinetic during FW/STO/FW injection sequence with kaolinite sensor. Some polar oil components from the STO were adsorbed onto the sensor surface. This was supported by the relatively large change in the FW frequency signal before and after injecting STO (Fig. 21) as compared to that of n-decane (Figs. 19 and 20).

7.3 Potential applications of QCM-D

The QCM-D can be employed in numerous surface interaction studies such as corrosion studies, dissolution and precipitation studies due to its high sensitivity and accuracy (Cattanach *et al.*, 2011). In other words, it has the potential to screen possible source of impurities in the laboratory experimental set-up that might lead to erroneous results. This was shown by the corrosion challenges in the presented study. It can also be used for evaluating interactions on mineral surface such as Crude Oil/Brine/Rock (COBR) interactions. Hence, it has the capabilities to be used in wettability characterization studies as presented in this paper. This method has also the potential to screen possible brine compositions and chemicals that can alter the wettability, thereby accelerating production from oil reservoirs.

8 Conclusion

A fast and promising technique for surface investigations with the potential to be used in wettability characterization studies has been developed. The QCM-D technique combined with geochemical simulations can elucidate the underlying mechanisms in experimental data. In addition, the following conclusions are drawn base on the use of the development of the QCM-D technique in the study of oil adhesion onto mineral surfaces.

(I) The experimental set-up should be composed of highly corrosion resistant materials since the brine and the high temperature used in the experiment are suitable conditions for corrosion to take place.

(II) A pre-column with the designated minerals as the sensor coatings should be included in the experimental set-up so that the brine will be in equilibrium with the surface of the sensor thereby mitigating etching. Moreover, dissolution of minerals can also be investigated by the QCM-D technique.

(III) Brine and oil are immiscible and hence, displacement of one fluid with the other is not efficient due to the difference in the densities. During the experiment, the flow-cell was rotated in a way that maximizes

the displacement of one fluid with the other. Hence, the flow-cell designed should be improved to allow efficient displacement of fluids.

(IV) To avoid the precipitation of salt, a constant temperature experimental set-up is needed.

References

Alagha L., Wang S., Yan L., Xu Z., Masliyah J. (2013) Probing adsorption of polyacrylamide-based polymers on anisotropic basal planes of kaolinite using quartz crystal microbalance, *Langmuir* **29**, 12, 3989–3998.

Bluemmel J., Perschmann N., Aydin D., Drinjakovic J., Surrey T., Lopez-Garcia M., Kesslerc H., Spatz J.P. (2007) Protein repellent properties of covalently attached peg coatings on Nanostructured Sio2-based interfaces, *Biomaterials* **28**, 32, 4739–4747.

Cao B., Stack A.G., Steefel C.I., DePaolo D.J., Lammers L.N., Hu Y. (2018) Investigating calcite growth rates using a quartz crystal microbalance with dissipation (QCM-D), *Geochim. Cosmochim. Acta* **222**, 269–283.

Cattanach K., Ramachandran S., Jovancicevic V., Sherik A. (2011) A new methodology for monitoring corrosion under sales gas conditions using the quartz crystal microbalance, *Paper presented at the CORROSION 2011.*

Chandrasekaran N., Dimartino S., Fee C.J. (2013) Study of the adsorption of proteins on stainless steel surfaces using QCM-D, *Chem. Eng. Res. Des.* **91**, 9, 1674–1683.

Dixon M.C. (2008) Quartz crystal microbalance with dissipation monitoring: enabling real-time characterization of biological materials and their interactions, *J. Biomol. Techn.* **19**, 3, 151.

Ekholm P., Blomberg E., Claesson P., Auflem I.H., Sjöblom J., Kornfeldt A. (2002) A quartz crystal microbalance study of the adsorption of asphaltenes and resins onto a hydrophilic surface, *J. Colloid Interface Sci.* **247**, 2, 342–350.

Erzuah S., Fjelde I., Omekeh A.V. (2018) Wettability estimation by oil adsorption using quartz crystal microbalance with disipation (QCM-D). *Presented at EUROPEC*, Copenhagen, 11–14 June.

Feiler A.A., Sahlholm A., Sandberg T., Caldwell K.D. (2007) Adsorption and viscoelastic properties of fractionated mucin (BSM) and bovine serum albumin (BSA) studied with quartz crystal microbalance (QCM-D), *J. Colloid Interface Sci.* **315**, 2, 475–481.

Keller C.A., Kasemo B. (1998) Surface specific kinetics of lipid vesicle adsorption measured with a quartz crystal microbalance, *Biophys. J.* **75**, 3, 1397–1402.

Nguyen T.H., Elimelech M. (2007) Adsorption of plasmid DNA to a natural organic matter-coated silica surface: kinetics, conformation, and reversibility, *Langmuir* **23**, 6, 3273–3279.

Paper IV

Wettability Estimation by Oil Adsorption Using Quartz Crystal Microbalance with Dissipation QCM-D (2018). *Presented at SPE Europec featured at 80th EAGE Conference & Exhibition. SPE-190882-MS.*

Erzuah, Samuel; Fjelde, Ingebret; Omekeh, Aruoture Voke.

Paper IV

SPE-190882-MS

Wettability Estimation by Oil Adsorption Using Quartz Crystal Microbalance with Dissipation QCM-D

Samuel Erzuah, National IOR Centre of Norway, University of Stavanger; Ingebret Fjelde, International Research institute of Stavnger, UiS, National IOR Centre of Norway; Aruoture Voke Omekeh, IRIS, National IOR Centre of Norway

Abstract

The wetting properties of the reservoir rocks are governed by the tendency of the individual minerals constituting the reservoir rock to adsorb oil during crude oil/brine/rock (COBR) interactions. To explore the oil adhesion kinetics during COBR interactions, one approach is to assess the oil adhesion tendencies of the individual minerals. The aim of this presented study was to characterize the wettability by determining the oil adhesion tendencies of the minerals using Quartz Crystal Microbalance with Dissipation (QCM-D). The kinetics of the mass (Δm_{ads}) and the thickness (Δt) of the adsorbed film were modelled mathematically using the Sauerbrey relation with the QCM-D output as input. In addition, we present Surface Complexation modelling (SCM) evaluation of possible electrostatic linkages of the studied COBR system.

The kinetics of oil adsorption during COBR interactions were prominent during Formation Water (FW)/ Stock Tank Oil (STO)/FW injection sequence with kaolinite sensor as compared to that of quartz. This was depicted by the relatively high change in the FW frequency signal (Δf) before and after the injection of STO with kaolinite sensor as compared to quartz. Negligible change in the frequency signal ($\Delta f \approx 0$) was observed during the various injection sequence with quartz sensor. This suggested that minor adsorption has taken place, thus confirming the hydrophilic nature of the quartz sensor. The mathematical modelling of the thickness (Δt) and the mass (Δm_{ads}) of the adsorbed film also reveals that kaolinite is more oil wet than quartz. This is portrayed by the relatively high magnitude of the adsorbed oil on kaolinite (Δt = 6nm - 14nm and Δm = 1600ng - 3500ng). The SCM results also confirm negligible (≈ 0.008) electrostatic pair linkage for the quartz sensor as compared to kaolinite (≈ 0.3). This shows that the tendency for oil to be adsorbed onto kaolinite sensors were relatively high as compared to quartz. The electrostatic pair linkages reveal that the dominant electrostatic pair linkage existing between the mineral- brine and the oil-brine interface was cation bridging by divalent cations such as Ca^{2+} and Mg^{2+}. Hence, it was not surprising that the FW/STO/ FW injection sequence for all the three (3) methods were relatively oil-wet as compared to similar sequence of optimum LSW composition. This was attributed to the abundance of Ca^{2+} and Mg^{2+} to bridge the two negatively charged surfaces in the former than in the latter.

Introduction

The wetting preference of a reservoir rock is an inevitable parameter in estimating the efficiency of the oil recovery by drive fluid (Buckley et al. 1989; Radke et al. 1992). Wettability is defined as the tendency of a fluid to spread on or adhere to the surface of a solid in the presence of other immiscible fluids (Craig 1971). Hence, adhesion of oil onto reservoir rock surfaces during crude oil/brine/rock (COBR) interactions play an important role in wettability estimation. Research has shown that direct contact of the crude oil with the reservoir rock surface can alter its wetting preferences towards more oil-wet (Hui and Blunt 2000; Rao and Maini 1993). The adhesion of oil onto the mineral surface depends on the attractive electrostatic force existing between the mineral-brine and the oil-brine interface (Brady and Krumhansl 2012; Brady et al. 2012; Erzuah et al. 2017). Rao and Maini (1993) reported that the attractive electrostatic forces existing between the reservoir rock surface and the adsorbed oil must be exceeded before the adhered oil can be released and mobilized to be produced with the injected brine. Lack of oil adhesion onto the reservoir rock surface was linked to the expansion of the double layer thereby resulting in a stable water film existing between the crude oil and the reservoir rock surface (Buckley et al. 1989). Various authors have espoused on some parameters that governs wettability such as the ionic composition of the brine, the surface charge of the reservoir rock minerals and the polar components in the crude oil (Buckley et al. 1989; Erzuah et al. 2017).

The aim of this presented study is to estimate the wettability by measuring the amount of oil retained on sandstone reservoir rock surface during crude oil accumulation via Quartz Crystal Microbalance with Dissipation (QCM-D). This was achieved by mimicking the reservoir fluid interaction prior to and after the crude oil accumulation on mineral surfaces. The principle behind the QCM-D is that it relies on the changes in the resonant frequency of the quartz crystal to estimate the magnitude of the adsorbed film. Measuring the changes in both the frequency (Δf) and the dissipation (ΔD) concurrently as time elapsed can be used to characterized the adsorption process (Keller and Kasemo 1998). The energy lost by the oscillating sensor due to the adsorbed mass is referred to as dissipation (ΔD) and it is directly proportional to the magnitude of the adsorbed mass. Numerous authors have reported that the viscoelastic/mechanical properties of the adsorbed film can also be investigated by monitoring the dissipation signal (Feiler et al. 2007; Keller and Kasemo 1998). Adsorption processes are surface specific and hence different surfaces exhibit diverse degree of adsorption such as monolayer and bilayer adsorption (Keller and Kasemo 1998). The underlying principle surrounding the QCM-D measurements can best be understood using the frequency response during no adsorption, adsorption and desorption analogies with different injection fluids (Figure 1 and Figure 2).
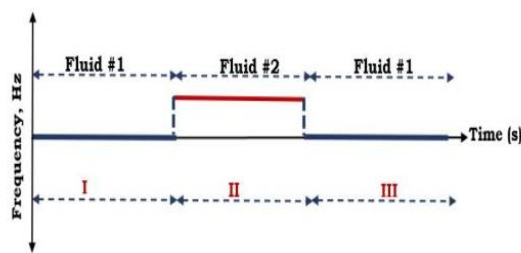
Figure 1—Analogy depicting lack of oil adsorption using QCM-DA
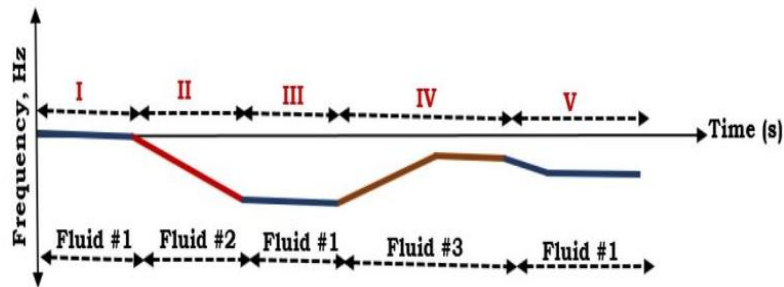
Figure 2—Adsorption and desorption of oil via QCM-D

Assume that fluids are injected in the order Fluid #1(reference fluid), Fluid #2 (test fluid) and Fluid #1 (reference fluid). The frequency signal can change when Fluid #1 is replaced with Fluid #2 due to change in fluid properties. If nothing is adsorbed on the sensor during injection of Fluid #2, the frequency signal should be the same ($\Delta f = 0$) for Fluid #1 before and after injection of Fluid #2 (Figure 1). From sections I and III of Figure 2, it can be observed that relatively large change in the frequency signal ($\Delta f \neq 0$) occurred. Thereby, depicting adsorption of some components from Fluid #2 onto the sensor (Section II of Figure 2). Considering section IV of Figure 2, it can be observed that during the injection of Fluid #3, there was a gradual increase in the frequency signal until it reached equilibrium. Higher frequency signal for Fluid #1 in Section V compared to Section III shows that the Fluid #3 has released some of the adsorbed film (Sections II and III) and hence the observed results.

Methods

Oil adhesion onto the mineral surfaces were accomplished via experimental, mathematical modelling of the thickness and mass of the adsorption. In addition, surface complexation modelling (SCM) technique as presented by Erzuah et al. (2017) was used to evaluate the mechanism that led to the oil adsorption. The experimental method was accomplished using QCM-D. The QCM-D flow-cell used in this study is the high pressure high temperature (QHPT) flow-cell developed by Biolin Scientific (Frolunda, Sweden). The operating temperature for this flow-cell is 15°C - 200°C at a maximum operating pressure of 300bar. In this study, the temperature and pressure conditions were set to 65°C and 6.4 bars respectively. N-decane was used as the system fluid while the desired injection fluids occupy the deposition area. The non- conductive system fluid will insulate the back electrode from the conductive injected brine thereby averting short circuiting. The oil adhesion onto sandstone reservoir rock was mimicked using quartz and kaolinite sensors. The oil adsorption kinetics during the experiments were also assessed using a mathematical model based on the Sauerbrey relation using the experimental data as input. The magnitude of the adsorbed film and the mechanisms that lead to the retention of oil on the mineral surface were also estimated using SCM technique as reported by Erzuah et al. (2017). Formation water (FW) and two (2) low salinity water (LSW) compositions were used to evaluate the effect of brine composition on the retention of oil. The brine was injected on the sensor via a pre-column filled with similar minerals as the coatings on the sensor to mitigate sensor etching as reported by Erzuah et al. (2018). N-decane was used as the reference oil to evaluate the effect of the polar oil component in the stock tank oil (STO) on the oil adsorption. The compositions of the brine and oil properties are given in Table 1 and Table 2 respectively.

Table 1—Properties of the brines used in the QCM-D experiments

ION	FW (mmol/L)	LSW#1 (mmol/L)	LSW#2 (mmol/L)
Na$^+$	1326.16	13.26	174.00
K$^+$	5.62	0.06	0.00
Mg^{2+}	17.46	0.17	0.00
Ca^{2+}	147.94	1.48	0.70
Sr^{2+}	8.44	0.08	0.00
Cl$^-$	1677.67	16.78	175.50
SO$_4^{2-}$	0.89	0.01	0.00
Density (g/cm^3) at 20ºC	1.07	0.973	0.985

Table 2—Properties of the oils used in the QCM-D experiments

OIL	DENSITY (g/cm3) at 20ºC	Total acid Number (TAN) (mg KOH/g oil)	Total Base Number (TBN) (mg KOH/g oil)
N-decane	0.74	0	0
STO	0.86	0.06	0.78

QCM-D experimental procedure

The QCM-D experimental procedure according to Erzuah et al. (2018) can be grouped into three stages namely; the preparatory, acquisition and post-acquisition stages. Schematic of the QCM-D experimental set-up is shown in Figure 3. During the preparatory stage, the experimental set-up such as flow-cell, flow-line and the sensor were thoroughly cleaned and dried with nitrogen. The sensor was then mounted in the flow-cell after which the temperature was set to the desired reservoir temperature (65°C in this study). The air in both the back electrode and the deposition area were displaced with ethanol. The ethanol at the back- electrode area was displaced with the system fluid (n-decane) while that at the active electrode was displaced with the designated brine (Figure 3). The outlet valves of the flow-cell were then opened after which the back-pressure valve (BPV) was connected. The log was restarted after a stable baseline was achieved. During the acquisition stage, the desired injection fluids were injected in their designated order while monitoring the frequency and the dissipation signals on real-time. The pump and the acquisition were stopped during the post-acquisition stage, after which the log was analysed. Detailed experimental procedure has been reported by Erzuah et al. (2018).
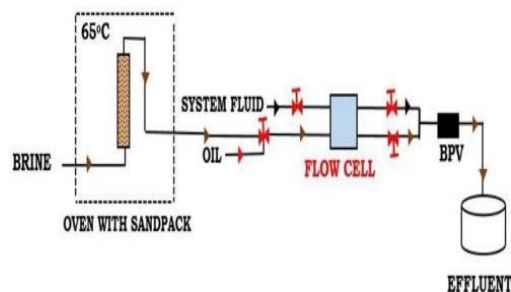
Figure 3—Schematic of the QCM-D experimental set-up

Paper IV

Mathematical modelling of the thickness and mass of the adsorption

To better understand the oil adhesion mechanisms, the mass of the adsorbed film (Δm_{ads}) and its thickness (Δt) were estimated based on the Sauerbrey relation (Ekholm et al. 2002; Feiler et al. 2007; Kubiak et al. 2015; Lu and Czanderna 2012):

$$\Delta m_{ads} = -\frac{1}{2}\left(\frac{\rho_q v_q}{f_o^2 n}\right)\left(f_{ads} - f_{ref}\right) = -\frac{C\Delta f}{n} \qquad 1$$

where

Δm_{ads} Mass of the adsorbed film, ng

ρ_q Density of quartz crystal = 2.65g/cm³

v_q Shear wave velocity = 334000cm/s

f_{ref} Reference brine frequency signal after stable baseline is detected, Hz

f_{ads} Frequency signal with the adsorbed film, Hz

f_o Resonance frequency = 4.95MHz

Δf Change in frequency, Hz

n Frequency harmonic number (n = 1, 3, 5, 7 etc.)

C Mass sensitivity constant of the crystal and it is given by the relation, 18 $ngcm^{-2}Hz^{-1}$

In a similar vein, the kinetic of the adsorbed film thickness can also be modelled as suggested by Lu and Czanderna (2012) as:

$$\frac{\Delta t}{t_q} = -\frac{\Delta f}{f_q} = Constant\ (C_t) \qquad (2)$$

$$\Rightarrow \Delta t = -\left(\frac{\Delta f}{f_q}\right)t_q = -\left(\frac{1}{2f_o}\sqrt{\frac{\mu_q}{\rho_q}}\right)\left(\frac{f_{ads} - f_{ref}}{f_{ref}}\right) = -\frac{C_t\Delta f}{f_{ref}} \qquad (3)$$

Where the additional parameters are

μ_q Shear modulus of the quartz crystal = 2.947 × 10¹¹ gcm⁻¹s⁻²

C_t Thickness of the quartz crystal in air (without any adsorbed film) and it is given by the relation, 0.033729cm

Alternatively, Eqn (2) can be expressed in terms of the fundamental frequency (f_o) as

$$\Rightarrow \Delta t\ (nm) = -\left(\frac{1}{2f_o}\sqrt{\frac{\mu_q}{\rho_q}}\right)\left(\frac{f_{ads} - f_{ref}}{nf_o}\right) = -\frac{C_{to}\Delta f}{n} \qquad (4)$$

where

C_{to} Constant representing the thickness of the quartz crystal in air (without any adsorbed film)and it is given by the relation, 6.814 × 10⁻²$nmHz^{-1}$

Surface Complexation Modelling (SCM) of the oil adsorption kinetics

To better understand the attractive electrostatic forces existing between the mineral-brine and the oil- brine interfaces during COBR interactions, SCM technique presented by Erzuah et. al (2017) was also used to evaluate the oil adsorption tendencies of the sensors during the QCM-D experiment. This was achieved by using similar properties of the materials used in the QCM-D experiment as input into the SCM model via a geochemical simulator, PHREEQ-C (Parkhurst and Appelo 2013).

Results

The QCM-D experimental results are presented first followed by the mathematical modelling result of the mass (Δm_{ads}) and the thickness (Δt) of the adsorbed film. Finally, the SCM results of the attractive electrostatic pair linkage that led to the adhesion of oil onto the sensor was also presented.

QCM-D results

The reference QCM-D experimental results with quartz sensor and the injection sequence FW/n- decane/ FW were presented first followed by its STO counterpart. The experimental results with kaolinite sensors were presented in a similar order as that of the quartz sensors. Finally, the effect of the ionic composition of the brine on oil retention was also presented. The frequency and dissipation signals presented in this study are that of the third (3rd) harmonics.

Quartz Sensor #1/FW/N-decane/FW. FW/N-decane/FW injection sequence was used as the reference experiment due to the lack of polar oil components in the reference oil (n-decane). From Figure 4, it can be observed that the change in the FW frequency signal (Δf) before (Section I) and after (Section III) the injection of the n-decane was negligible ($\Delta f \approx 0$). Thus, confirming that, the n-decane was not adsorbed onto the sensor. This can be attributed to the absence of polar component in n-decane.
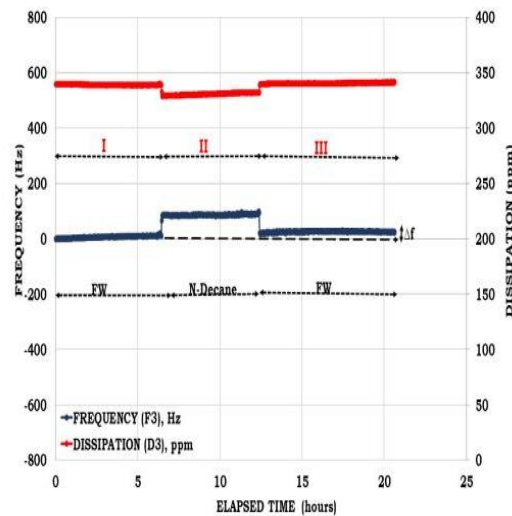
Figure 4—Frequency and dissipation signals during FW/n-decane/FW injection sequence with quartz sensor #1

Quartz Sensor #2/FW/STO/FW. Like the FW/n-decane/FW injection sequence with quartz sensor #1 which resulted in no oil adhesion (Figure 4), the FW/STO/FW injection sequence) with quartz sensor #2 also resulted in negligible oil adhesion (Figure 5). This was depicted by the neligible change in the FW frequency signal (Δf) before (Section I) and after (Section III) the injection of the STO. This can be linked to the strongly hydrophilic nature of quartz sensor thereby inhibiting oil adhesion. In other words, the lack of oil adsorption onto the sensor resulted in no attenuation in the frequency and dissipation signals due to no added mass on it.
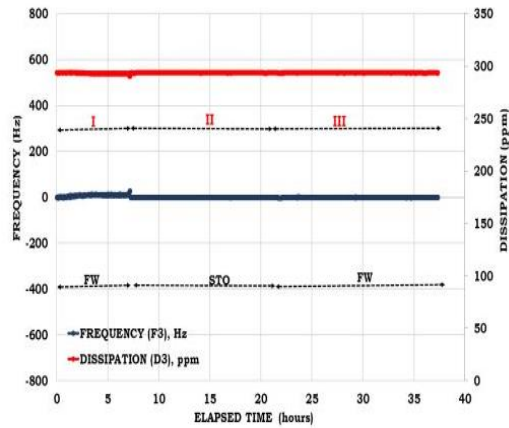
Figure 5—Frequency and dissipation signals during FW/STO/FW injection sequence with quartz sensor #2

Kaolinite Sensor #1/FW/N-decane/FW. Like the quartz sensor with relatively constant frequency and dissipation signal during FW/n- decane/FW injection sequence (Figure 4), kaolinite sensor #1 with similar injection sequence also resulted in a relatively constant frequency and dissipation signal (Figure 6). Thus, depicting lack of oil adhesion.
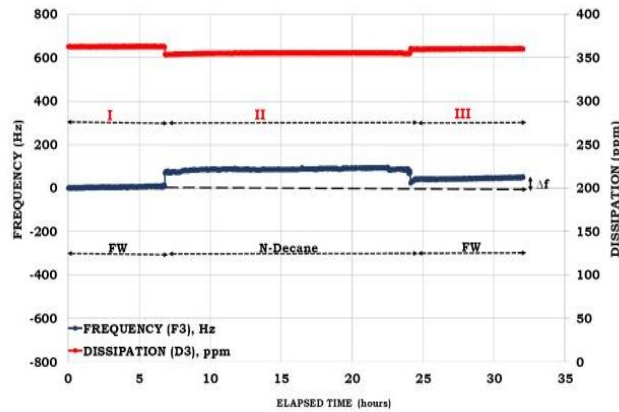
Figure 6—Frequency and dissipation signals during FW/n-decane/FW injection sequence with kaolinite sensor #1

Kaolinite Sensor #2/FW/N-decane/FW. Like the FW/n-decane/FW injection sequence for both the quartz sensor #1 (Figure 4) and kaolinite sensor #1 (Figure 6)with relative constant frequency and dissipation signals, kaolinite sensor #2 (Figure 7)with similar injection sequence also yielded approximately the same result. Thus, confirming lack of oil adsorption onto the sensors with n-decane.

Figure 7—Frequency and dissipation signals during FW/n-decane/FW injection sequence with kaolinite sensor #2

Kaolinite Sensor #3/FW/STO/FW. As compared to the FW/STO/FW injection sequence with quartz sensor #2 (Figure 5) with relatively constant frequency and dissipation signals, the FW/STO/FW injection sequence with kaolinite sensor #3 (Figure 8) on the other hand resulted in the retention of oil on the kaolinite sensors.
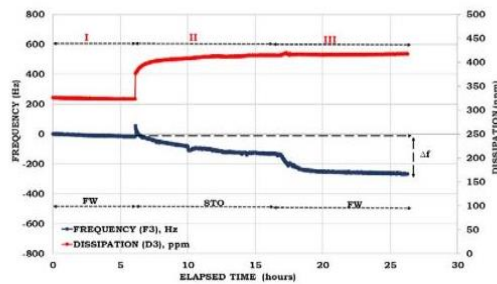
Figure 8—Frequency and dissipation signals during FW/STO/FW injection sequence with kaolinite sensor #3.

This was depicted by the relatively large change in the FW frequency ($\Delta f \approx 280\ Hz$) signal before (Section I) and after (Section III) injecting the STO. The adsorption of STO onto the kaolinite sensor #3 (Figure 8) can be attributed to the presence of polar oil component in the crude oil. This was depicted by the reduction in the frequency signal with time. In other words, the adsorbed film reduces the frequency of the oscillating crystal and hence the observed results.

Kaolinite Sensor #4/FW/STO/FW. Like FW/STO/FW injection sequence with kaolinite sensors #3 (Figure 8), the kaolinite sensor #4 (Figure 9) also resulted in adhesion of oil onto its surface. The magnitude of the adsorbed oil as depicted by the change in the FW frequency signal (Δf) before (Section I) and after (Section III) the STO injection was 340 Hz.
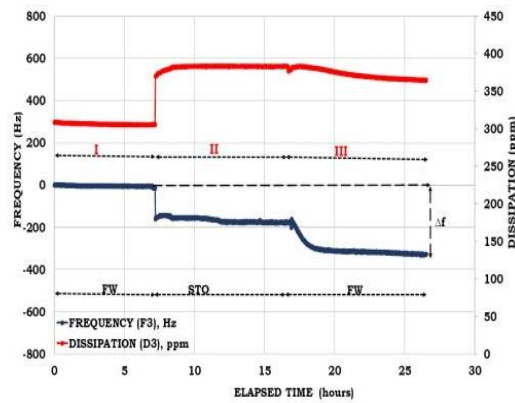
Figure 9—Frequency and dissipation signals during FW/STO/FW injection sequence with kaolinite sensor #4.

Effect of brine composition on oil adsorption

To evaluate the potential of the ionic composition of the brine to release some of the adsorbed oil to be mobilized and produced with the injected brine during low salinity waterflooding, two (2) low salinity waters (LSW#1 and LSW#2) were considered. Kaolinite sensors were used for this test due to the significance of kaolinite in reservoir rock wettability. The LSW#1 was prepared by dilute the FW by a factor of 100 (1:100) while LSW#2 composition was obtained from a low salinity plant (Table 1). The LSW/STO/LSW injection sequence was then compared to the FW/STO/FW injection sequence to assess the effect of ionic composition of the brine on oil retention.

Kaolinite Sensor #S/LSW#l/STO/LSW#l. Comparing FW/STO/FW injection sequence (Figure 8 and Figure 9) to the LSW# 1 /STO/LSWit 1 injection sequence (Figure 10), it can be observed that the magnitudes of adsorbed oil was relatively higher in the latter than the former. This shows that diluting FW might not necessarily produce LSW that can lead to improve the oil recovery. This can be linked to the presence of higher concentration of divalent cations on the clay surfaces than with FW as reported by Fjelde et al. (2017).
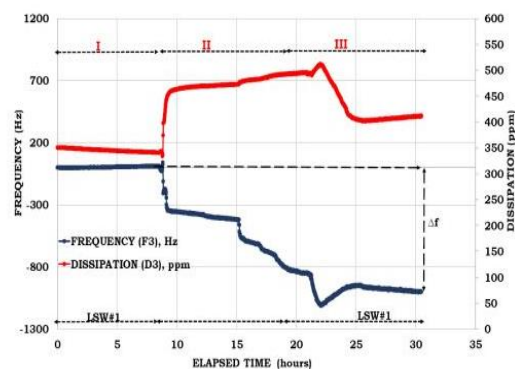
Figure 10—Frequency and dissipation signals during LSW#1/STO/LSW#1 injection sequence with kaolinite sensor#1.

Kaolinite Sensor #6/LSW#2/STO/LSW#2. Comparing the LSW#1/STO/LSW#1 injection sequence (Figure 10) to the LSW#2/STO/LSW#2 injection sequence (Figure 11), it can be observed that negligible amount of oil was retained on the latter than the former. This was confirmed by the relatively small change

in the LSW#2 frequency signal ($\Delta f \approx 0$ *Hz*)before (Section I) and after (Section III) the injection of STO as compared to LSW#1 (Figure 11 and Figure 10 respectively). This suggests that the LSW#2 (Figure 11) has the potential to release more of the adsorbed polar oil components from the surface of the sensor than LSW#1 (Figure 10). Hence, LSW#2 has the potential to be used during improved oil recovery via low salinity waterflooding.
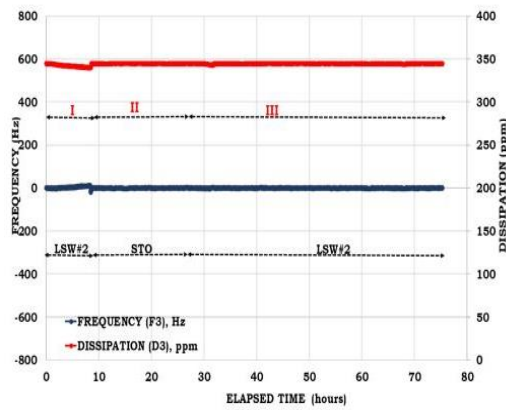
Figure 11—Frequency and dissipation signals during LSW#2/STO/LSW#2 injection sequence with kaolinite sensor #6.

Results of the mathematical modelling of the thickness (Δt) and mass (Δm_{ads}) of the adsorbed film

To appreciate the COBR interactions on the surface of the sensor, results from mathematical modelling of the thickness (Δt) and the mass of the adsorbed film (Δm_{ads}) have also been presented. Figure 12 is a mathematical modelling result of the thickness and mass of the adsorbed film during FW/STO/FW injection sequence. From Figure 12, it can be observed that both the thickness ($\Delta t \approx 5.8$ *nm*) and mass of the adsorbed film ($\Delta m_{ads} \approx 1600ng$)were relatively high after injecting the STO. Thus, confirming oil adsorption onto the sensor. The results of the thicknesses (Δt) and masses (Δm_{ads}) of the adsorbed films for the remaining sensors are summarized in Table 3.
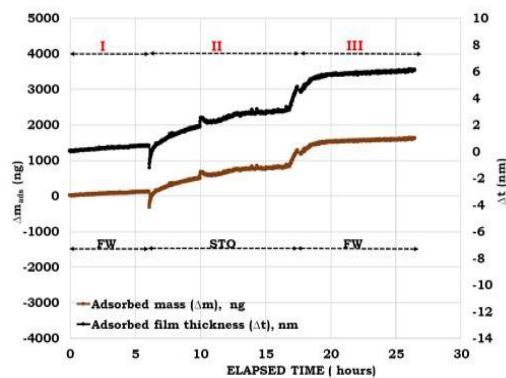
Figure 12—Mathematical modelling of the thickness and mass of the adsorbed during FW/STO/FW injection sequence with kaolimte sensor #3.

Paper IV

Table 3—Summary of the estimated thickness and masses of the adsorbed film based on the Sauerbrey relation

Sensor ID	Injection sequence	Δt (nm)	Δm_{ads} (ng)
Quartz - Sensor #1	FW/N-decane/FW	~0	~0
Quartz - Sensor #2	FW/STO/FW	~0	~0
Kaolinite - Sensor #1	FW/N-decane/FW	~1	~100
Kaolinite - Sensor #2	FW/N-decane/FW	~2	~300
Kaolinite - Sensor #3	FW/STO/FW	~5.8	~1600
Kaolinite - Sensor #4	FW/STO/FW	~7.8	~2000
Kaolinite - Sensor #5	LSW#1/STO/LSW#1	~23	~6000
Kaolinite - Sensor #6	LSW#2/STO/LSW#2	~0	~0

It can be observed from Table 3 that, the quartz sensors during FW/n-decane/FW and FW/STO/FW injection sequence were strongly hydrophilic.

In addition, for kaolinite sensor #6, it was also observed to be strongly water-wet as depicted by the negligible change in thickness ($\Delta t \approx 0$) and adsorbed mass ($\Delta m_{ads} \approx 0$) during LSW #2/STO/LSW #2 injection sequence. On the other hand, kaolinite sensor #5 was observed to be strongly oil-wet during LSW #1/STO/LSW#1 as depicted by its thickness ($\Delta t \approx 23$ nm) and adsorbed mass ($\Delta m_{ads} \approx 6000$ ng).

SCM results of the oil adsorption kinetics

To better understand the role played by the polar oil components, the ionic composition of the brine and the surface charge of the minerals on the oil adsorption, the bond product of the electrostatic interactions was assessed via SCM as reported by Erzuah et al. (2017).

Mineral-brine and oil-brine electrostatic interactions. From Figure 13, it can be observed that the dominant electrostatic pair linkage with quartz sensor was <0.01 This implies that the tendency of oil to be adhered onto quartz is negligible and thus confirming its hydrophilic nature. This was also confirmed by the relatively constant frequency signal during the FW/STO/FW injection sequence with quartz sensor (Figure 5).
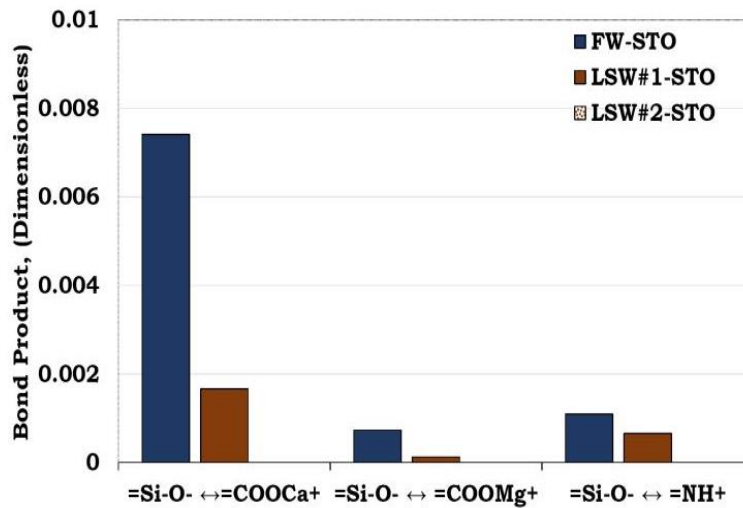
Figure 13—Bond product of the dominant electrostatic pair linkages between the quartz and oil surfaces.

Paper IV

From Table 3, the thickness and the mass of the adsorbed film was approximately zero during the FW/STO/FW injection sequence with quartz sensor. Thus, confirming the negligible oil adsorbed onto the quartz sensor.

In contrast to the quartz sensor with negligible (< 0.01) amount of oil adsorbed onto its surface (Figure 13), the kaolinite sensor on the other hand adsorbed more polar oil component (~0.3) from the STO (Figure 14). This confirms that kaolinite is more oil-wet than quartz.
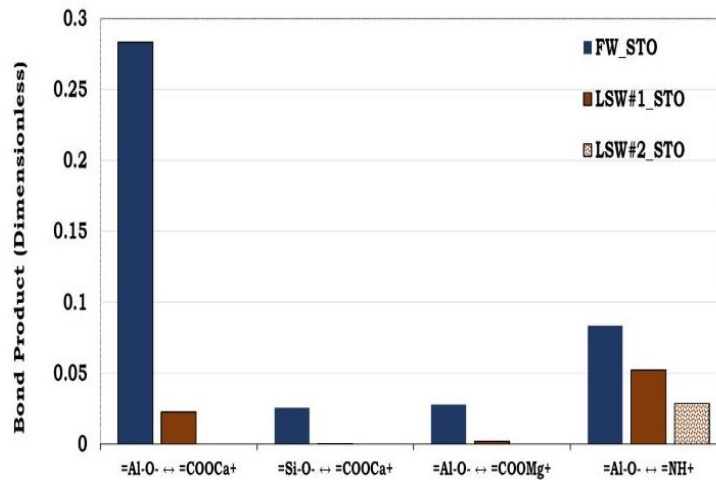
Figure 14—Bond product of the dominant electrostatic pair linkages between the kaolinite and oil surfaces.

Discussions

The SCM predicts that the main mechanism of the STO adsorption is through divalent cation bridging especially for formation water. Note that at high salinity, the surface potential is low as predicted by the DLVO (Derjaguin, Landau, Verwey, and Overbeek) theory. At this state, it is easier for the divalent cations to approach the surface and acts as a bridge for oil adsorption. At low salinity conditions, the surface potential as predicted by the SCM and DLVO theory, is expected to be high and as such prevent divalent cations from approaching the surface and acting as a bridge for oil adsorption.

The results from the SCM and experiments for kaolinite agree (in the direction of wetting) for both FW and LSW#2. LSW#2 resulted in less water surface (lower oil adsorption) when compared with FW. The experimental results show that LSW#1 in fact creates a more oil-wet situation contrary to the SCM simulations or to DLVO theory explanation. Similar less water-wet conditions of LSW#1 compared to FW (same brine and oil systems) have also been observed with other experimental methods: coreflooding experiments (Fjelde et al., 2012) and floatation test (Fjelde et al., 2017). The ability of LSW#1 to create a more oil -wet surface is explained by ion-exchange simulations (Fjelde et al., 2017). In such simulations, the surface potential of the mineral is ignored and ability of the divalent cations to bond to the surface is dependent only on its preference to the surface and on its concentration (more precisely actitivity). This shows that the ability of low salinity brine to create a less water-wet surface is very dependent on the composition of the low salinity water and not only on the ionic strength. The SCM simulations overestimates the effect of surface potential over the effect of concentration changes.

The QCM-D experimental result, adsorbed mass and thickness calculations and the SCM results demonstrated that oil adhesion onto quartz sensor is negligible as compared to that of kaolinite. Oil adhesion

Paper IV

onto the QCM-D sensors was depicted via the relatively high attenuation of the frequency coupled with relatively high dissipation. This phenomenon was more pronounced with STOs than the n- decane. This was attributed to the absence of polar oil components in the n-decane.

Unlike the LSW#1, the LSW#2 has the potential to improve the oil recovery by releasing some of the adsorbed oil and thereby alter the wettability to more water-wet. The QCM-D and SCM results confirmed the potential for the LSW#2 to alter the wettability of studied sandstones to more water-wet and thereby accelerating the oil production. Hence, dilution of FW to be used as LSW (LSW#1) during low salinity water flooding should be avoided. These ions especially the divalent ion can lead to the retention of oil onto the senor thereby hindering the oil recovery process. From the SCM results, cation bridging was the dominating wetting mechanism in both quartz and kaolinite.

Conclusion

QCM-D can be used to assess both the wetting mechanisms and the magnitude of the adsorbed film onto the minerals. Thus, providing a hint on how the wettability can be altered to optimize oil recovery. From all the three techniques employed, it can be concluded that kaolinite is more oil-wet than quartz. The method can be used to screen potential injection fluids to evaluate their tendency to alter wettability to more water-wet, thereby accelerating the oil recovery and reducing water production. The composition of low salinity water is very important due to its potential to alter wettability towards a more water-wet state.

Acknowledgement

Nomenclature

FW	Formation water
STO	Stock tank oil
TAN	Total Acid Number
TBN	Total Base Number
ΔD	Change in dissipation (dimensionless)
f_{ref}	Reference FW frequency signal after stable baseline is detected (Hz or s^{-1})
f_{ads}	Frequency signal with the adsorbed film (Hz or s^{-1})
Δf	Change in resonant frequency (Hz or s^{-1})
Δm_{ads}	Mass of the adsorbed film (μg/cm^2)
ρ_q	Density of the quartz crystal (g/cm^3)
v_q	Shear wave velocity of the quartz crystal (cm/s)
μ_q	Shear modulus of the quartz crystal (g cm^{-1} s^{-2})
f_o	Resonance frequency (Hz)
n	Frequency harmonic number (Dimensionless)
C	Mass sensitivity constant of the sensor (ng cm^{-2} Hz^{-1})
t_q	Thickness of the quartz sensor (cm)
Δt_{ads}	Thickness of the adsorbed film (nm)

References

Brady, P. V. and Krumhansl, J. L. 2012. Surface Complexation Modeling for Waterflooding of Sandstones. *SPE J*, **18** (02): 214 - 218. SPE-163053-PA. DOI: http://dx.doi.org/10.2118/163053-PA.

Brady, P. V., Krumhansl, J. L. and Mariner, P. E. 2012. Surface Complexation Modeling for Improved Oil Recovery. Presented at the SPE IOR, Tulsa, Oklahoma, USA. 14-18 April. SPE-153744-MS. DOI: http://dx.doi.org/10.2118/153744-MS.

Buckley, J., Takamura, K. and Morrow, N. 1989. Influence of Electrical Surface Charges on the Wetting Properties of Crude Oils. *SPE Res Eng* **4** (03): 332 - 340. SPE-16964-PA. DOI: http://dx.doi.org/10.2118/16964-PA.

Craig, F. J. 1971. *The Reservoir Engineering Aspect of Waterflooding. SPE Monograph Series*, Vol. **3**. Dallas, Texas, Society of Petroleum Engineering of AIME.

Ekholm, P., Blomberg, E., Claesson, P., Auflem, I. H., Sjoblom, J. and Kornfeldt, A. 2002. A Quartz Crystal Microbalance Study of the Adsorption of Asphaltenes and Resins onto a Hydrophilic Surface. *Journal of Colloid and Interface Science* **247** (2): 342–350.

Erzuah, S., Fjelde, I. and Omekeh, A. V. 2017. Wettability Estimation by Surface Complexation Simulations. Presented at the SPE Europec featured at 79th EAGE Conference and Exhibition. Paris, France, 12-15 June. DOI: 10.2118/185767-MS.

Erzuah, S., Fjelde, I. and Omekeh, A. V. 2018. Challenges Associated with Quartz Crystal Microbalance with Dissipation (QCM-D) as a Wettability Screening Tool. Presented at the IFP Energies Nouvelles, Reuil-Malmaison, France. Reuil-Malmaison, 27- 29 March.

Fjelde, I., Asen, S.M. and Omekeh. A.V. 2012. Low salinity water flooding experiments and interpretation by simulations. Presented at the Eighteenth SPE Improved Oil Recovery Symposium, Tulsa, Oklahoma, 14-18 April 2012. SPE-154142-MS. https://doi.org/10.2118/154142-MS.

Fjelde, I., Omekeh, A. V., and Haugen, P. E. 2017. Screening of The Potential for Different Injection Water Compositions to Alter Wettability to More Water-Wet. Presented at the SPE Latin America and Caribbean Mature Fields Symposium. Salvador, Bahia, Brazil, 15-16 March. SPE-184918-MS. https://doi.org/10.2118/184918-MS.

Feiler, A. A., Sahlholm, A., Sandberg, T. and Caldwell, K. D. 2007. Adsorption and Viscoelastic Properties of Fractionated Mucin (BSM) and Bovine Serum Albumin (BSA) Studied with Quartz Crystal Microbalance (QCM-D). *Journal of Colloid and Interface Science* **315** (2): 475–481. DOI: https://doi.org/10.1016/j.jcis.2007.07.029.

Hui, M.-H. and Blunt, M. J. 2000. Effects of Wettability on Three-Phase Flow in Porous Media. *Journal of Physical Chemistry*, **104** (16): 3833 - 3845.

Keller, C. and Kasemo, B. 1998. Surface Specific Kinetics of Lipid Vesicle Adsorption Measured with a Quartz Crystal Microbalance. *Biophysical Journal* **75** (3): 1397–1402.

Kubiak, K., Adamczyk, Z. and Wasilewska, M. 2015. Mechanisms of Fibrinogen Adsorption at the Silica Substrate Determined by QCM-D Measurements. *Journal of Colloid and Interface Science* **457**: 378–387.

Lu, C. and Czanderna, A. W. 2012. *Applications of Piezoelectric Quartz Crystal Microbalances.* Elsevier.

Parkhurst, D. L. and Appelo, C. 2013. *Description of Input and Examples for PHREEQC Version 3—A Computer Program for Speciation, Batch-reaction, One-dimensional Transport, and Inverse Geochemical Calculations*. Denver, Colorado, USA, U.S. Geological Survey. **6**: 497497.

Radke, C., Kovscek, A. and Wong, H. 1992. A Pore-Level Scenario for the Development of Mixed Wettability in Oil Reservoirs. Presented at the SPE Annual Technical Conference and Exhibition, Washington, D.C. 4-7 October. SPE-24880-MS. DOI: http://dx.doi.org/10.2118/24880-MS.

Rao, D. N. and Maini, B. B. 1993. Impact Of Oil-Rock Adhesion On Reservoir Mechanics. Presented at the Annual Technical Meeting, Calgary, Canada. 9 – 12 May. PETSOC-93-84. DOI: http://dx.doi.org/10.2118/93-84

Rodahl, M., Hook, F. and Kasemo, B. 1996. QCM Operation in Liquids: an Explanation of Measured Variations in Frequency and Q factor with Liquid Conductivity. *Analytical Chemistry* **68** (13): 2219–2227.

Paper V

Effect of the Intrinsic Properties of Reservoir Rock Minerals on Wettability via Surface Complexation Modelling (SCM). *Manuscript.*

Erzuah, Samuel; Fjelde, Ingebret; Omekeh, Aruoture Voke.

Paper V

Effect of Intrinsic Properties of Reservoir Rock Minerals on Wettability via Surface Complexation Modelling (SCM)

Samuel Erzuah[a,b], Ingebret Fjelde[a,b,c], Aruoture Voke Omekeh[a,c]

[a]*The National IOR Centre of Norway, N-4036 Stavanger, Norway*
[b]*University of Stavanger (UiS), N-4036 Stavanger, Norway*
[c]*NORCE Norwegian Research Centre AS, P. O. Box 8046, N-4068 Stavanger, Norway*

KEYWORDS	ABSTRACT
Surface Complexation Modelling Crude oil/brine/rock interactions Intrinsic properties Effective surface area Electrostatic attraction Hydrophilic Hydrophobic Oil adhesion Site density Total Bond Product (TBP) Wettability	Wettability is an indispensable parameter in multiphase flow due to its profound effect on fluid phase distribution and flow properties in the oil reservoir. Reservoir rocks are composed of different minerals with diverse intrinsic properties such as surface area. Hence, numerous interactions are bound to occur during Crude Oil/Brine/Rock (COBR) interactions. For instance, in the presence of brine, the surface charge of the reservoir rock minerals behaves as either anionic or cationic. In a similar vein, the charge of oil-water surface ranges from anionic to cationic. This study seeks to evaluate the effect of these intrinsic properties on the wettability of Sandstone Reservoir Rocks (SRR) and Pseudo-Sandstone Rocks (PSR) via both Surface Complexation Modelling (SCM) and flotation test. The PSR were prepared by increasing the contents of the desired minerals (illite and calcite) in the SRR to assess their intrinsic properties on the wetting preferences of the rock. The SCM technique was also used to study the COBR interactions during spontaneous imbibition of different brines in a carbonate rock. For the dominant minerals in the SRR, both the flotation tests and the SCM results shows that quartz was strongly hydrophilic while calcite was strongly hydrophobic. On the other hand, the flotation test results for the clay minerals (i.e. illite and montmorillonite) were observed to be less hydrophilic than quartz as confirmed by the SCM results. Considering the studied sandstone reservoir rocks, both the SCM and the flotation test results revealed that, the SRR were preferentially hydrophilic. Nonetheless, increasing the content of the hydrophobic minerals increases the rocks tendency to become more hydrophobic. For the dominant sandstone reservoir rock minerals with predominantly negatively charged surfaces, electrostatic repulsion exists between the mineral/brine and the oil/brine interfaces thereby resulting in negligible oil adsorption. On the other hand, more oil was adsorbed onto the calcite surface as observed in both the SCM and the flotation tests. This was attributed to the attractive electrostatic forces existing between the positively charged calcite/brine and negatively charged oil/brine interfaces. Both the SCM and flotation test results revealed that the intrinsic properties of the individual minerals such as surface area and surface charge have immense effect on the reservoir rock wettability. For the PSR with low calcite content, the wettability was inclined towards the mineral with dominant surface area. This was linked to the strong hydrophobicity of calcite as compared to the other studied minerals in the PSR. Hence, increasing the calcite content increases the hydrophobicity of the rock even if the clay minerals dominate the effective surface area. The SCM results portrayed that the dominant oil adsorption mechanism for the main sandstone minerals was divalent ions bridging. Nonetheless, direct adsorption of carboxylate was also observed in illite, montmorillonite and calcite with the latter being more pronounced.

1. Introduction

Wettability is an important parameter in multiphase flow due to its influence on fluid phase distribution and flow properties in the oil reservoirs. Research has shown that the breakthrough time during waterflooding is dictated by the reservoir rock wettability (Morrow 1990). He also reported that early water breakthrough can take place in a strongly hydrophobic media while late breakthrough occurs for strongly hydrophilic media. This was attributed to the role of wettability on flow properties such as relative permeability (Anderson 1987). Hence, inaccurate wettability estimation can affect field development option and the oil recovery processes (Cockcroft et al. 1989). Wettability is the tendency of one fluid to adhere to a solid surface in the presence of other immiscible fluids (Craig 1971). Due to the role of wettability in oil recovery, numerous techniques have been developed notably the Amott test and United State Bureau of Mines (USBM) method. Nonetheless, these techniques are expensive and time consuming. Hence, the need for fast and cheap wettability characterization technique. Erzuah et al. (2017b) estimated the wettability of dominant sandstone reservoir rock minerals notably; quartz, kaolinite and calcite via Surface Complexation Modelling (SCM). Research has shown that the surface charge, the ionic composition of the formation water (FW) and the polar oil components in the crude oil control the wetting preferences of reservoir rocks. For example, during crude oil/brine/rock (COBR) interactions, the rock/brine and the oil/brine interfaces exhibit different charges ranging from anionic to cationic resulting in diverse chemical interactions. This study seeks to extend the existing SCM technique to predict the wettability of the reservoir rock by capturing the intrinsic properties of the individual mineral in the model via a geochemical simulator (PHREEQ-C).

The SCM technique of characterizing the wettability is a fast and cheap wettability characterization approach in the absence of materials for conventional wettability estimation such as reservoir core sample and Stock Tank Oil (STO, stabilized crude oil). SCM is a powerful technique of modelling surface reactions and it relies on the thermodynamic properties of the aqueous species (Brady and Krumhansl 2012a; Goldberg 2013; Koretsky 2000). Constant capacitance, diffuse-layer, triple-layer and two-pK models are the most commonly employed surface complexation models reported in literature (Goldberg 2013; Koretsky 2000). Sverjensky and Sahai (1996) attributed the differences in the surface complexation models to the description of the electric double layer, the electric potential (Ψ) calculation and the assumptions surrounding the choice of surface sites. i.e. the surface sites can be treated as either completely homogeneous or heterogeneous as depicted by the single-site and multi-site models respectively. The rationale behind the SCM technique of characterizing wettability was to assess the COBR interactions during reservoir filling. Site densities, surface area, equilibrium constant for protonation, deprotonation and adsorption reactions are some of the parameters required during surface complexation modelling (Brady et al. 2012; Koretsky 2000). In

2

addition, the type of SCM employed may require one or more additional capacitance values before the surface interactions can be modelled (Goldberg 2013; Koretsky 2000).

To accomplish this, the surface reactions and their reaction constants of the surfaces (oil and minerals) cannot be ignored. Numerous chemical reactions are bound to take place in the reservoir prior to and after the crude oil accumulation. Since reservoir rocks are composed of different minerals, the mineral/brine interactions prior to the crude oil accumulation have also been studied by numerous authors. For instance, surface reactions and their reaction constants for the different mineral-brine systems have been reported in literature (Brady and Krumhansl 2012a; Brady and Krumhansl 2012b; Brady et al. 2012; Gu and Evans 2007; Van Cappellen et al. 1993; Wolthers et al. 2008). To add to the above, comprehensive surface complexation studies on kaolinite, quartz, goethite, magnetite, talc, muscovite, montmorillonite, albite, anorthite, rutile and gibbsite have also been reported by several authors (Chen and Brantley 1997; Sverjensky and Sahai 1996, 1998; Wieland et al. 1994). Wolthers et al. (2008) also carried out an in-depth review on Surface Complexation Modelling of carbonate minerals such as calcite, rhodochrosite, siderite, magnesite and dolomite. In addition, Brady and Krumhansl (2012b) have also reported on the possible oil-brine interactions and their reaction constants. Several developments have been made in recent years by numerous authors to capitalize on these existing SCM data from literature to better understand experimental results. For example, zeta potential measurements have successfully been modelled via SCM (Erzuah et al. 2018a; Song et al. 2017). In addition, research has shown that the SCM technique is capable of modelling polymer interactions such as precipitation reactions at high surface coverage (Katz and Hayes 1995). Erzuah et al. (2017b) used surface complexation data of quartz, kaolinite and calcite from literature to estimate their wettability via SCM. They accomplished this by evaluating the attractive electrostatic forces existing between the mineral-brine and the oil-brine interfaces via a geochemical simulator; PHREEQ-C. This presented study seeks to characterize the wettability of reservoir rocks and mineral mixtures via SCM.

To extend the existing SCM technique to estimate the wettability of reservoir rocks, the individual properties of the minerals needed to be captured in the model. Minerals have diverse properties such as surface area, surface charge and site densities. Since reservoir rocks/mineral mixtures have varying mineralogical compositions, the plan was to evaluate the wetting preferences of the rocks by understanding the crude oil/brine/rock (COBR) interactions. To accomplish this, two techniques were employed namely the flotation test and SCM technique. The flotation experiments were modelled via a geochemical simulator (PHREEQ-C) using similar quantities and qualities of the materials as used in the experiments. The aim of this presented study was to assess the effect of the intrinsic properties of the reservoir rock minerals on the wettability of the rock via SCM. The SCM technique of estimating wettability was compared with their corresponding flotation test results before meaningful conclusions could be drawn. The flotation test characterizes the wettability by relying on the affinity of the reservoir rock (minerals) to either the oil or brine phase during COBR interactions (Erzuah et al. 2017a). These COBR interactions were modelled via SCM to better understand their wetting preferences. To evaluate the effect of the intrinsic properties of the individual minerals on the wetting preferences of the reservoir rock, the flotation tests were also performed for the dominant minerals in the two sandstone reservoir rocks (SRR) prior to evaluating their contribution to the rock wettability. In addition, the flotation tests were performed for four mineral-mixtures (pseudo-sandstone reservoir rock, PSR) designed to assess specific properties such as increasing surface area or increasing the hydrophobicity of the mixture.

2. Method

The flotation test and the Surface Complexation Modelling (SCM) techniques were employed in this study. The SCM technique was also used to assess the COBR interactions during spontaneous imbibition of formation water and CO_2-saturated brine in carbonate rock (Fjelde et al. 2011).

Flotation test procedure

The rationale behind the flotation test is to replicate the wetting preferences of the reservoir rock prior to and after the crude oil accumulation in the reservoirs. The chosen reservoir rocks were crushed and sieved through 53μm mesh. A known weight (0.20g) of the sieved reservoir rock was then aged in a given volume (10.0ml) of the desired brine at the designated reservoir temperature (80°C) for 2 days (Section I of Figure 1). The brine phase was then separated and stored for later use while the wet rock was aged in a known volume (3.0ml) of the STO at reservoir temperature (80°C) for 2 days with intermittent stirring (Section II of Figure 1) to represent the rock-fluid interactions in the reservoir during the accumulation of crude oil. At the end of the ageing period, the separated brine was added to the aged rock-oil to mimic COBR interactions in the reservoir (Section III of Figure 1). The rock-brine-oil mixtures were thoroughly shaken and allowed to settle for approximately 24 hours at 80°C. The wettability was characterized based on the concentration of the rock sample in each fluid phase. Since it is difficult to separate the oil from the oil-wet particles unlike the water-wet samples, the oil phase was discarded while the brine phase was filtered using 0.22μm filter (Section IV of Figure 1). The filter cake was then dried until a constant weight was achieved. The concentration of the oil-wet particles was calculated from the difference between the initial weight of the rock (0.20g) and that of the dried water-wet rock. Like the reservoir rock flotation tests, the minerals and mineral mixtures flotation experiments were also carried out using a similar procedure as described above. A more detailed flotation test procedure can be obtained from literature (Dubey and Doe 1993; Erzuah et al. 2017a; Mwangi et al. 2013).
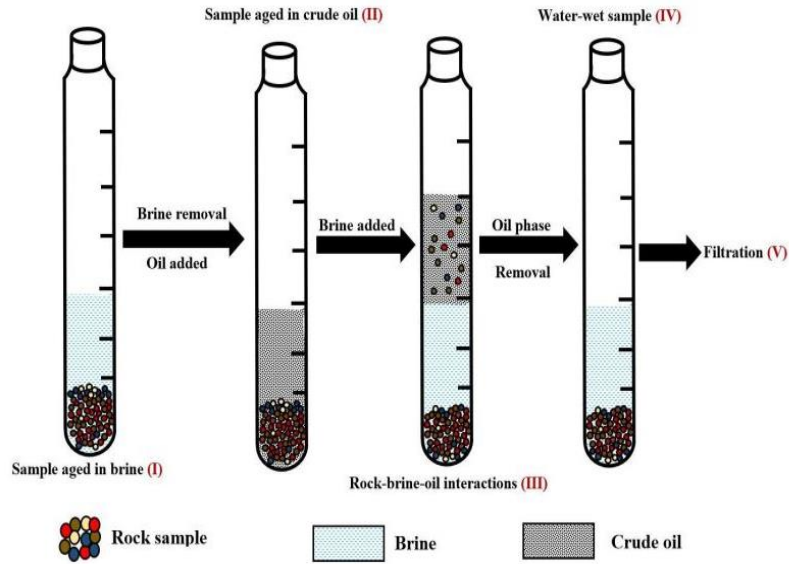
Figure 1 – Flow chart of the flotation experiment. The different colours represent the different minerals constituting the reservoir rock.

Materials used in the flotation test

Flotation tests were performed for five dominant minerals in two sandstone reservoir rocks (SRR) prior to evaluating the reservoir rocks. The minerals considered include; quartz, albite, illite, montmorillonite and calcite. Throughout this study, the two Sandstone Reservoir Rocks will be denoted by SRR #1 and SRR #2 respectively. In addition, mineral-mixtures/ Pseudo-Sandstone Rocks (PSR) were also designed to evaluate the effect of increasing surface area and calcite content. To evaluate the effect of the surface area on wettability, mineral-mixtures/Pseudo-Sandstone Rocks (PSR) were obtained by increasing the content of the desired mineral (illite) in the Sandstone Reservoir Rock #1 (SRR #1). In other words, the effect of the effective surface area on wettability was evaluated by replacing 25% and 50% of the SRR #1 rock mass with illite in PSR #1 and PSR#2 respectively. The PSR #3 and PSR #4 were also prepared in a similar approach as in the PSR #1 and PSR#2 but using calcite. The mineralogical compositions of the Sandstone Reservoir Rocks (SRR) and the mineral mixtures (PSR) are given in Table 1. In addition, the compositions of the Stock Tank Oil (STO) and the Formation Water (FW) employed in this study are also given in Tables 2 and 3 respectively.

Table 1 – Mineralogical composition (weight percent) of the reservoir rocks and the mineral mixtures.

Quartz	83.7	94.9	62.8	41.9	62.8	41.9
Albite	3.3	4.0	2.5	1.6	2.5	1.6
Montmorillonite	3.9	0.0	2.9	1.9	2.9	1.9
Illite	8.8	0.4	31.6	54.4	6.6	4.4
Siderite	0.0	0.5	0.0	0.0	0.0	0.0
Calcite	0.3	0.2	0.2	0.2	25.2	50.2

Note: SRR and PSR represents the sandstone reservoir rock and the pseudo-sandstone rock (mineral mixtures) respectively. PSR #1 and PSR #2 were obtained by replacing 25% and 50% respectively of SRR #1 rock mass with illite. PSR #3 and PSR #4 were also obtained by increasing the calcite content in a similar proportion.

Table 2 – Composition of the stock tank oil (STO).

STO#1	0.86	0.10	1.90
STO#2	0.90	0.38	2.30

Table 3 – Ionic composition of the brine.

Na^+	1326.16	701.88
K^+	5.62	7.11
Mg^{2+}	17.46	23.90
Ca^{2+}	147.94	72.85
Sr^{2+}	8.44	1.65
Ba^{2+}	0.00	0.04
Cl^-	1677.67	898.69
SO_4^{2-}	0.89	3.59
Density (g/cm^3) at 20°C	1.07	1.04

Flotation test prediction via Surface Complexation Modelling (SCM)

To better understand the COBR interactions during the flotation test, the mineral-fluid interactions via SCM as reported by Erzuah et al. (2017b) have been extended to capture that of the rock-fluid interactions. The oil adhesion resulting from the attractive electrostatic forces existing between the rock-brine and the oil-brine interfaces is represented by the Bond Product (BP). BP is the product of the mole fractions of the oil (O_i) and mineral (m_i) sites with unlike charges and it is given by the relation;

$$BP = O_i m_i \qquad (1)$$

For a given mineral or rock, the sum of all the BP is the Total Bond Product (TBP). The flotation test estimates the wettability by measuring the affinity of the mineral (rock) to either brine or oil. The SCM on the other hand, characterizes the wettability by predicting the tendency of oil to be adsorbed onto the mineral surface via TBP (Figure 2). The ">" in Figure 2 represents the oil and mineral surface groups. The TBP can also be written as;

$$TBP = \sum_i^n BP_i \qquad (2)$$
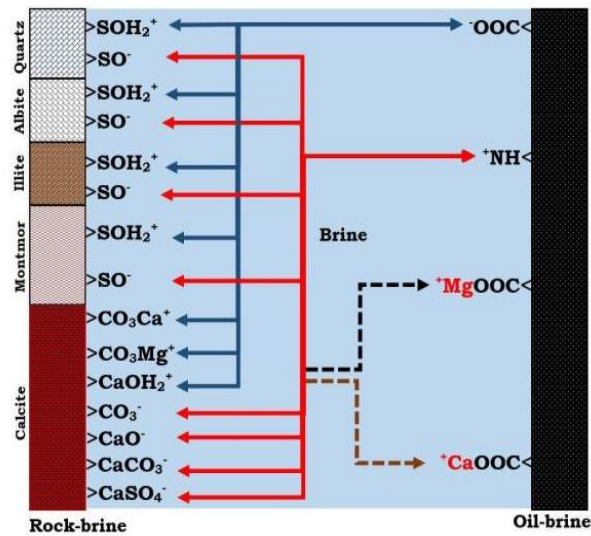
Figure 2 – The electrostatic pair linkages existing between the rock-brine and oil-brine interfaces with unlike charges. Direct adsorption of carboxylate (>COO⁻) onto the positive mineral sites (>SOH₂⁺, >CO₃Ca⁺, >CO₃Mg⁺, >CaOH₂⁺) can lead to oil adsorption. For the carboxylate (>COO⁻) and the negative mineral surfaces (>SO⁻, >CO₃⁻, >CaO⁻, CaCO₃⁻, >CaSO₄⁻) bridging by divalent cations (Ca²⁺ and Mg²⁺) can also lead to oil adsorption.

Surface Complexation Modelling (SCM) input

To predict the mineral-brine and oil-brine interactions during the flotation test, the compositions and properties of the materials used in the flotation experiments were also used as input in the SCM (Erzuah et al. 2017b). The oil and minerals used in the flotation tests were incorporated into the model by their respective surface group. For instance, the surface-active components in the crude oil were depicted by their respective acidic (>COOH) and basic

(>NH$^+$) oil group. The minerals (rocks) were also represented by their respective mineral sites (e.g. >Si-O-H, >CO$_3$H and >CaOH). The oil surface reactions and their reaction constants were obtained from a similar reaction by Brady & Krumhansl (2012a). For the quartz and albite, the surface area and site densities were obtained from Sverjensky and Sahai (1996) while the enthalpy used was from a similar reaction as kaolinite (Sverjensky and Sahai 1998). For the illite, the surface area and site density were obtained from Gu and Evans (2007) while that of montmorillonite were obtained from Wieland et al (1994). In addition, the temperature dependent reaction constants for illite and montmorillonite were obtained from a similar reaction as kaolinite (Sverjensky and Sahai 1998). For the calcite, the surface area was obtained from Hjuler & Fabricius (2009) while its site density was obtained from Wolthers et al. (2008). In addition, the reaction constants were obtained from Van Cappellen et al. (1993). For the reservoir rock (mineral mixtures) of varying mineralogical compositions, the surface reactions and their reaction constants of the individual minerals in the rock were used. Nevertheless, the effective surface area (A$_{eff}$) of the rock (mineral-mixture) was used as input into the SCM and it is given by the relation;

$$A_{eff} = \sum_{n=1}^{\infty} m_i A_i \tag{3}$$

Where,

A$_{eff}$	= Effective surface area (m^2/g)	
mi	= Mass fraction of mineral i (dimensionless)	
A$_i$	= Intrinsic surface area of mineral i (m^2/g)	

Erzuah et al. (2017) reported that the STO can be incorporated into the SCM by converting the total acid number (TAN) and total base number (TBN) into their respective acidic and basic components. They also reported that the oil site densities were estimated from the TAN and TBN by assuming that the surface area of the oil is the same as that of the mineral. Nonetheless, for the reservoir rock (mineral mixtures) the effective surface area of the rock was used. Hence, the extended oil site density is given by the relation;

$$\text{Oil Site Density (site/nm}^2) = \frac{\text{TAN or TBN(mg KOH/g oil)}}{\text{Mw KOH (g/mol)}} \times \frac{\text{Avogadros Constant}}{\text{Effective Surface Area (m}^2/\text{g)}} \tag{4}$$

The SCM input parameters such as surface reactions and their reaction constants of the minerals can be obtained from Table 4. The intrinsic properties of the minerals/rocks such as site densities and the effective surface area (A$_{eff}$) can also be obtained from Table 5. Table 6 gives the estimated oil site densities of the STO employed in this study.

Table 4 – SCM input parameters.

^{a}Oil Surface		
>NH$^+$ ↔ >N + H$^+$	-6.0	34.0
>COOH ↔ >COO$^-$ + H$^+$	-5.0	0.0
>COOH + Ca^{2+} ↔ >COOCa$^+$ + H$^+$	-3.8	1.2
>COOH + Mg^{2+} ↔ >COOMg$^+$ + H$^+$	-4.0	1.2^g
^{b}Quartz		
>Si-O-H + H$^+$ ↔ >Si-O-H$_2^+$	-1.1	-26.4
>Si-O-H ↔ >Si-O- + H$^+$	-8.1	8.4
^{c}Albite		
>Si-O-H + H$^+$ ↔ >Si-O-H$_2^+$	1.9	16.3
>Si-O-H ↔ >Si-O- + H$^+$	-8.5	1.3
^{d}Illite		
>Si-O-H + H$^+$ ↔ >Si-O-H$_2^+$	7.43	24.3^h
>Si-O-H ↔ >Si-O- + H$^+$	-8.99	18.8^i
H$^+$ + NaX$_{ill}$ ↔ HX$_{ill}$ + Na$^+$	1.58	
^{e}Montmorillonite		
>Si-O-H + H$^+$ ↔ >Si-O-H$_2^+$	5.4	24.3^h
>Si-O-H ↔ >Si-O- + H$^+$	-6.7	18.8^i
H$^+$ + NaX$_m$ ↔ HX$_m$ + Na$^+$	4.6	
^{f}Calcite		
>CO$_3$H ↔ >CO$_3^-$ + H$^+$	-4.9	-5.0
>CO$_3$H + Ca^{2+} ↔ >CO$_3$Ca$^+$ + H$^+$	-2.8	25.7
>CO$_3$H + Mg^{2+} ↔ >CO$_3$Mg$^+$ + H$^+$	-2.2	4.5
>CaOH + H$^+$ ↔ >CaOH$_2^+$	12.2	-77.5
>CaOH ↔ >CaO$^-$ + H$^+$	-17.0	116.4
>CaOH + 2H$^+$ + CO$_3^{2-}$ ↔ >CaHCO$_3$ + H$_2$O	24.2	-90.7
>CaOH + CO$_3^{2-}$ + H$^+$ ↔ >CaCO$_3^-$ + H$_2$O	15.5	-61.6
>CaOH + SO$_4^{2-}$ + H$^+$ ↔ >CaSO$_4^-$ + H$_2$O	13.9	-72.0

^{a} after Brady and Krumhansl (2012b).
^{b} and ^{c} after Sverjensky and Sahai (1996, 1998).
^{d} after Gu and Evans (2007)
^{e} after Wieland et al. (1994)
^{f} after Wolthers et al. (2008)
^{g} Enthalpy during Mg^{2+} reaction with >COOH was assumed to be the same as that of Ca^{2+}
^{h} and ^{i} assumed to be the same as similar reactions as kaolinite.
Note. X$_{ill}$ and X$_m$ depicts the exchange sites of illite and montmorillonite respectively.

Table 5 – Intrinsic properties of the mineral/reservoir rock and STO.

Quartz	10.00	1.20
Albite	1.155	1.20
Illite	1.37	66.8
Montmorillonite	5.7	3.0
Calcite	4.90	2.00
SRR #1		7.0
SRR #2		1.5
PSR #1		22.0
PSR #2		36.9
PSR #3		5.8
PSR #4		4.5

Note: For the SRR and PSR, the effective surface area and the site densities of the individual mineralogical compositions were used.

Table 6 – Estimated oil site densities of the STO used.

Quartz	>COOH	0.89	3.40	1.20
	>NH+	16.99	20.56	1.20
Albite	>COOH	0.89	3.40	1.20
	>NH+	16.99	20.56	1.20
Illite	>COOH	0.02	0.06	66.8
	>NH+	0.31	0.37	66.8
Montmorillonite	>COOH	0.36	1.36	3.0
	>NH+	6.79	8.23	3.0
Calcite	>COOH	0.54	2.04	2.00
	>NH+	10.20	12.34	2.00
SRR #1	>COOH	0.15	0.58	7.0
	>NH+	2.89	3.50	7.0
SRR #2	>COOH	0.73	2.77	1.5
	>NH+	13.85	16.76	1.5
PSR #1	>COOH	0.05	0.19	22.0
	>NH+	0.93	1.12	22.0
PSR #2	>COOH	0.03	0.11	36.9
	>NH+	0.55	0.67	36.9
PSR #3	>COOH	0.19	0.70	5.8
	>NH+	3.52	4.27	5.8
PSR #4	>COOH	0.24	0.90	4.5
	>NH+	4.51	5.46	4.5

The effective surface area (A_{eff}) and the oil site densities were calculated using Equations 3 and 4 respectively. NB. Equation 4 assumes that the effective surface area (A_{eff}) of the rock (mineral-mixtures) is the same as their respective oil surface.

3. Results

The flotation test results for the dominant minerals in the sandstone reservoir rocks (SRR #1 and SRR #2) were presented first to investigate the wetting preferences of the individual minerals prior to evaluating their effect on the reservoir rock wettability. The results of the predicted flotation test were then presented. Note that, the flotation test results of quartz and calcite have already been presented (Erzuah et al. 2017b). To add to the above, the oil-brine and mineral-brine interactions that led to the adhesion of oil onto the mineral surfaces were also assessed via SCM. The flotation test results of the reservoir rock and mineral-mixtures (SRR and PSR) were presented first before that of their simulated counterparts. To understand the oil adhesion tendencies in the sandstone reservoir rocks (SRR #1 and SRR #2) during the flotation tests, their oil adhesion mechanisms were also assessed via SCM. The effect of increasing the effective surface areas and the hydrophobic mineral contents were studied by adding illite (PSR #1 and PSR#2) and calcite (PSR #3 and PSR #4) respectively. In addition, the oil adhesion mechanisms in the mineral-mixtures (PSR #1, PSR #2, PSR #3 and PSR #4) were also evaluated to better understand the effect of the intrinsic properties of the minerals on oil adsorption. Finally, the correlation between the intrinsic properties of the reservoir rock minerals and their wetting preferences were assessed via SCM before meaningful conclusions could be drawn.

Flotation test results
It can be observed from Figure 3 that, quartz is strongly hydrophilic (oil-wet fraction < 0.1) while calcite is strongly hydrophobic (oil-wet fraction > 0.7). Montmorillonite on the other hand was more hydrophobic than both illite and albite. Hence, increasing order of the mineral hydrophobicity is given as quartz < albite < illite < montmorillonite < calcite.
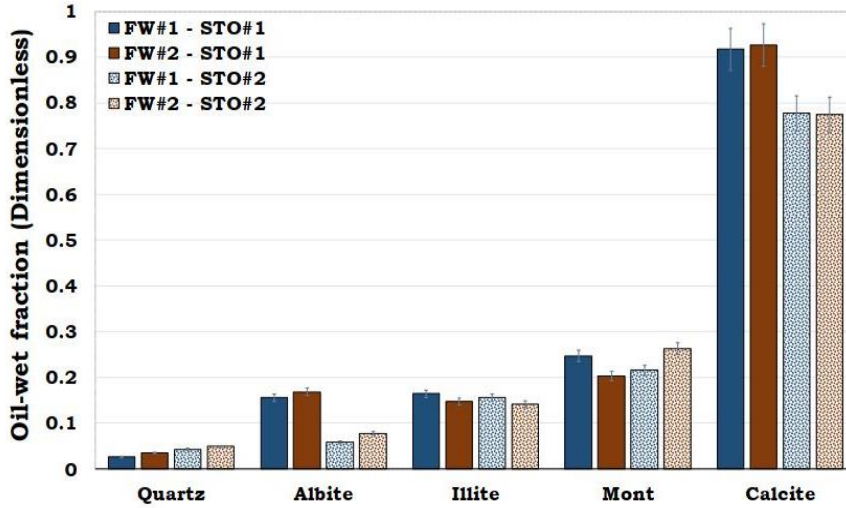
Figure 3 – Wettability characterization of the reservoir rock mineral using the flotation tests. It can be observed that quartz is strongly hydrophilic while calcite is strongly hydrophobic.

Prediction of the flotation tests via SCM

It can be observed that the SCM could capture the trend of the flotation test results. In other words, the ranking of the minerals in the simulations was similar as observed in the flotation tests.
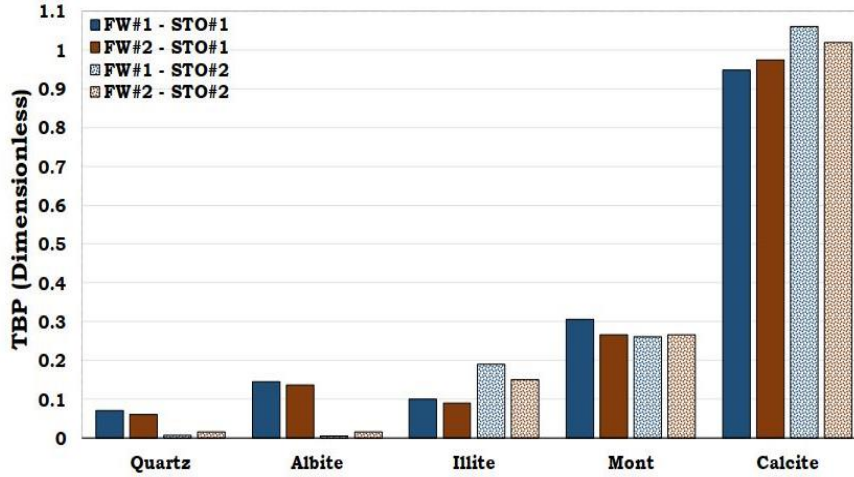
Figure 4 – Prediction of the oil adhesion tendencies of the dominant reservoir rock minerals during the flotation test.

Mechanisms of oil adhesion during the flotation test via SCM

To understand the wetting preferences of the minerals during the flotation test, the attractive electrostatic interactions existing between the mineral-brine and oil-brine interfaces were studied using SCM.

Mechanisms of oil adhesion in quartz

It can be observed that the tendency of oil to be adsorbed onto quartz surface is very small as depicted by its low dominant BP (< 0.1). In addition, considering the quartz-brine and oil-brine interactions, it can be observed that bridging of the two negatively charged surfaces by divalent cations (Ca^{2+} and Mg^{2+}) dominated the oil adhesion mechanisms. Considering the acidic (COO^-) and basic components (NH^+) in the STO, it can be observed that the effect of the NH^- is not pronounced as compared to the COO^-.

8
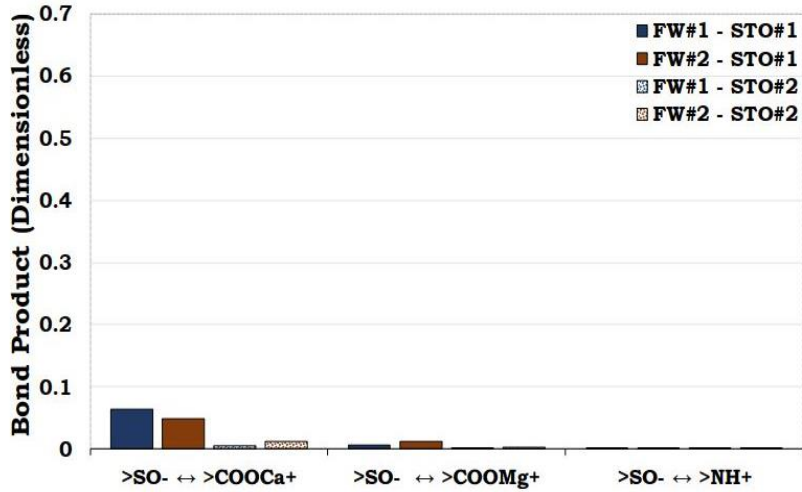
Figure 5 – Depicts the electrostatic pair linkages existing between the quartz-brine and the oil-brine interface with unlike charges. It is estimated that quartz is strongly hydrophilic due to negligible Bond Product (<0.1).

Mechanisms of oil adhesion in albite

Albite was slightly more oil-wet than quartz as depicted by their BP (≈ 0.1 and < 0.1 in Figures 6 and 5 respectively). Similar to the quartz, the interactions in the albite-brine and oil-brine interfaces were also dominated by cation bridging mechanisms. As observed for quartz, the oil adhesion mechanism in albite also recorded insignificant contribution from the basic components in the oil (NH^+) as compared to the acidic component (COO^-).
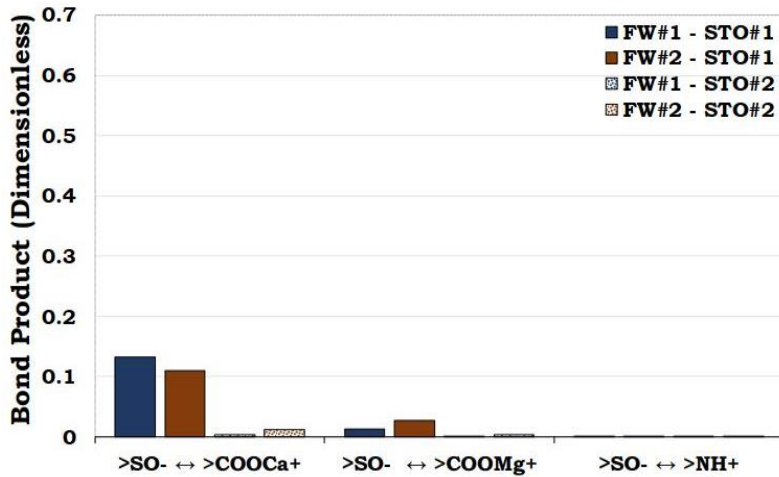
Figure 6 – Oil adhesion due to the electrostatic pair linkages existing between the albite-brine and oil-brine interfaces with unlike charges. Albite is relatively less hydrophilic (i.e. BP ≈ 0.1) than quartz (< 0.1, see Figure 5).

Mechanisms of oil adhesion in illite

It can be observed from Figure 7 that illite is less hydrophilic (BP ≈ 0.2) than albite and quartz (BP ≈ 0.1 and BP < 0.1 respectively). Contrary to the oil adhesion mechanisms in quartz and albite, the interactions in the illite-brine and oil-brine interfaces were dominated by the direct adhesion of carboxylate (COO^-) onto the positive illite surface ($>SOH_2^+$). In addition, bridging of the negative illite surface (SO^-) and the negative oil surface (COO^-) by divalent cations such as Ca^{2+} and Mg^{2+} also occurred. As observed in the earlier results (Figures 5 and 6), the contributions from the basic components in the oil (NH^+) was also negligible as compared to the acidic component (COO^-).
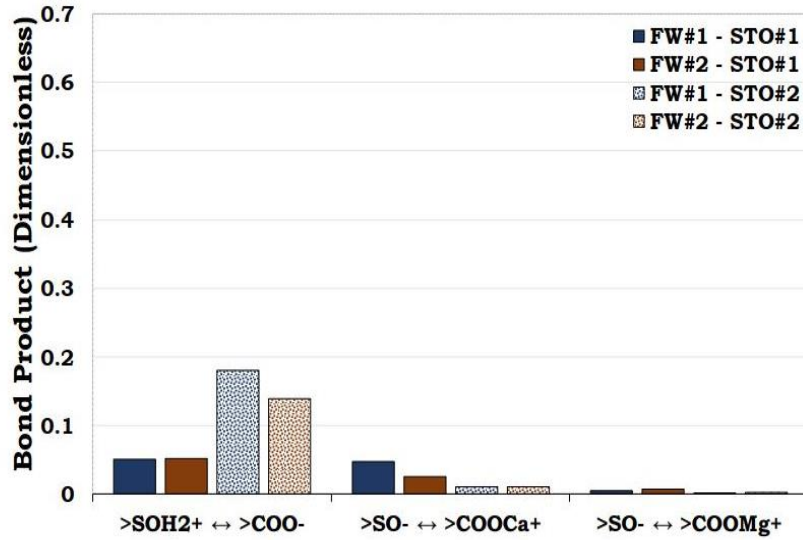
Figure 7 – The electrostatic pair linkages existing between the illite-brine and oil-brine interfaces with unlike charges. Illite is more hydrophobic (BP ≈ 0.2) as compared to quartz (BP < 0.1, Figure 5) and albite (BP ≈ 0.1, Figure 6).

Mechanisms of oil adhesion in montmorillonite
From Figure 8, it can be observed that the montmorillonite was more hydrophobic (BP ≈ 0.25) than illite (BP ≈ 0.2), albite (BP ≈ 0.1) and quartz (BP < 0.1). Unlike the oil adhesion onto illite which was dominated by direct adhesion of carboxylate (Figure 7), the oil adhesion in montmorillonite was dominated by cation bridging (Figure 8). In other words, the dominant oil adhesion mechanisms in montmorillonite was due to the bridging of the negative montmorillonite sites (>SO$^-$) and the carboxylate (COO$^-$) by divalent cations (Ca^{2+} and Mg^{2+}). To add to the above, the influence of the basic components in the oil (NH$^+$) was not significant as compared to the acidic component (COO$^-$) as confirmed by Figures 5 and 6.
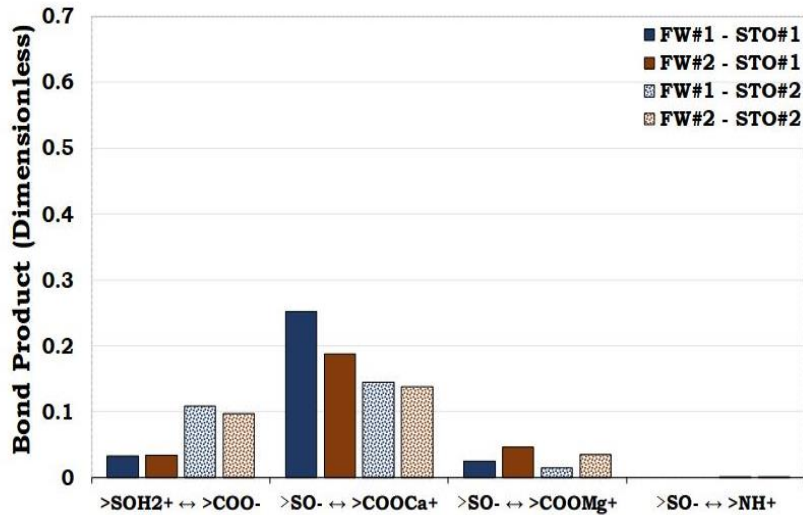
Figure 8 – The electrostatic pair linkages existing between the montmorillonite-brine and oil-brine interface with unlike charges. Montmorillonite is more hydrophobic (BP ≈ 0.3) than quartz (BP < 0.1, Figure 5), albite (BP ≈ 0.1, Figure 6) and illite (BP ≈ 0.2, Figure 7).

Mechanisms of oil adhesion in calcite

From Figure 9, it can be observed that calcite is more hydrophobic (BP ≈ 0.6) than montmorillonite (BP ≈ 0.25), illite (BP ≈ 0.2), albite (BP ≈ 0.1) and quartz (BP < 0.1). Like the direct adhesion of carboxylate (>COO⁻) onto illite (>SOH₂⁺) and montmorillonite (>SOH₂⁺), direct adhesion of carboxylate onto the positively calcite site (>CaOH₂⁺) also took place. However, the BP for the calcite (>CaOH₂⁺ ↔ >COO⁻) was more distinct than that observed in the illite and montmorillonite (>SOH₂⁺ ↔ >COO⁻) thus confirming the hydrophobic nature of the former. Furthermore, oil adhesion resulting from cation bridging also occurred as observed in the other minerals. As seen in the other mineral/brine/oil interaction, effect of the basic components (NH⁺) in the oil adhesion was also negligible as compared to the acidic component (COO⁻).
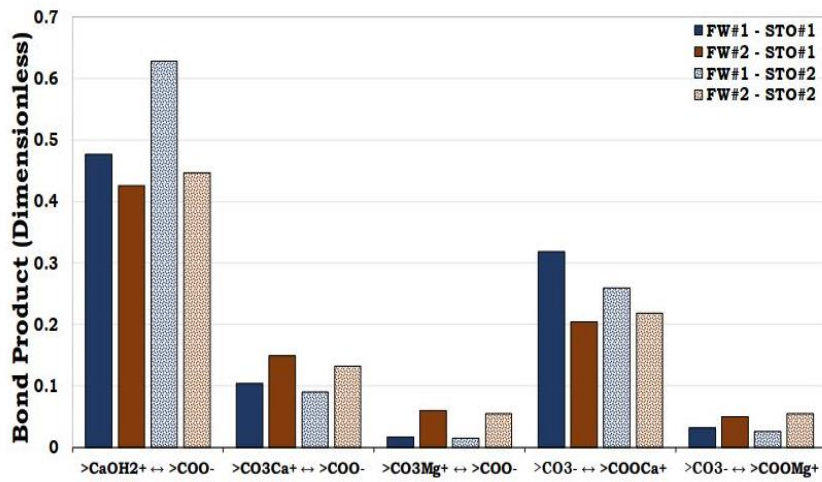

Figure 9 – The electrostatic pair linkages existing between the calcite-brine and oil-brine interfaces with unlike charges. Calcite is strongly oil-wet due to its high BP (≈ 0.6) as compared to quartz (BP < 0.1, Figure 5), albite (BP ≈ 0.1, Figure 6), illite (BP ≈ 0.2, Figure 7) and montmorillonite (BP ≈ 0.3, Figure 8).

Reservoir rock flotation test results

From both the Sandstone Reservoir Rock (SRR) and the Pseudo-Sandstone Rock (PSR) flotation test results (Figure 10), it can be observed that the surface area and wetting state of the individual minerals dictate the wetting preferences of the rocks. For instance, the wettability of the PSR #1 and PSR #2 were dominated by their effective surface area (21.98 m²/g and 36.92 m²/g respectively). Nevertheless, the mass fraction of PSR #1 was dominated by quartz (62.8%) while that of the PSR #2 was dominated by illite (54.4%). Since both quartz and illite were hydrophilic under the studied conditions (Figure 3), it was not surprising that the wetting preferences of PSR #1 and PSR #2 were similar to the wetting state of the mineral with the dominant effective surface area (illite). The effective surface area of PSR #3 and PSR #4 were also dominated by illite (4.40 m²/g and 2.94 m²/g respectively). However, the dominant mass fraction of the minerals in the PSR #3 composition were quartz (62.8%) and calcite (25.2%) while that of the PSR #4 were calcite (50.2%) and quartz (41.9%). Though, the surface area and the mass fraction of the PSR #3 were dominated by hydrophilic minerals (illite and quartz), the wetting state of PSR #3 was observed to be less hydrophilic as compared to SRR #1. This was linked to the high contents of calcite in PSR #3 as compared to SRR #1 (Table 1). On the other hand, though the effective surface area of PSR #4 was dominated by illite, the flotation test results (Figure 10) depict relatively high oil-wet state. This shows that the calcite content has a strong influence on the wetting state of sandstone reservoir rock than the clay minerals. In other words, if the effective surface area of a reservoir rock is dominated by hydrophilic minerals (e.g. illite) but its mineralogical composition is also dominated by the hydrophobic minerals (e.g. calcite), the latter will dictate the wetting state of the rock as confirmed by both the flotation and SCM results (Figures 10 and 11).
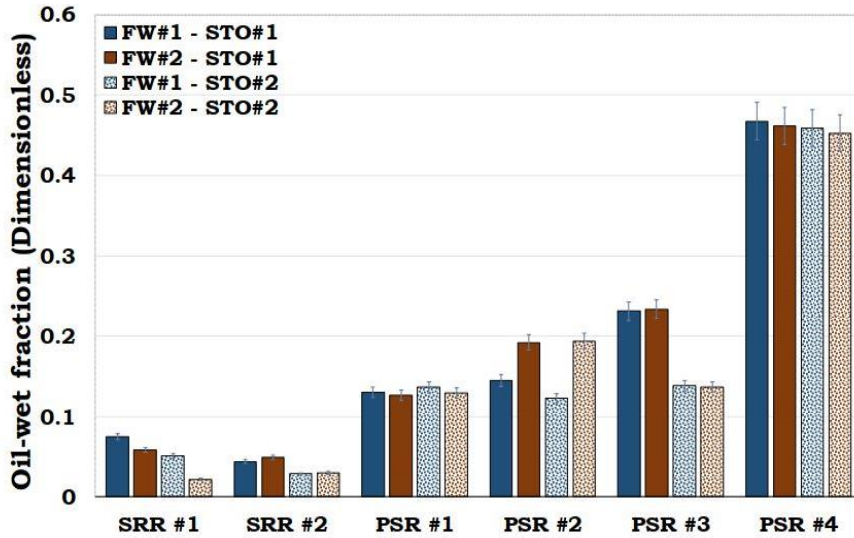
Figure 10 – Flotation tests results of the Sandstone Reservoir Rock (SRR #1 & SRR #2) and the Pseudo Sandstone Rocks (PSR #1, PSR #2, PSR #3 & PSR #4). It can be observed that SRR #1 & SRR #2 were strongly hydrophilic while PSR #4 was observed to be hydrophobic.

Prediction of the reservoir rock flotation test results

Like the prediction of the flotation test of the individual minerals with the SCM (Figure 4), it can be observed from Figure 11 that the SCM could capture the main trends in the flotation test results for the SRR and the PSR.
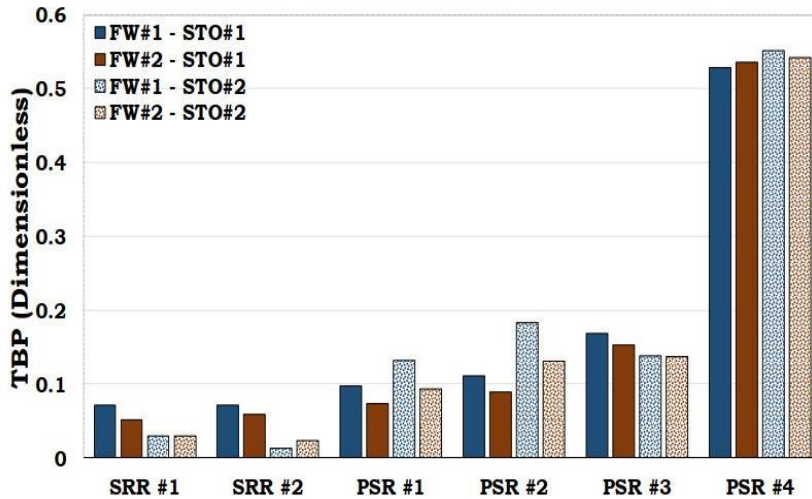
Figure 11 – Oil adhesion tendencies of the Sandstone Reservoir Rock (SRR) and the Pseudo-Sandstone Rock (PSR) via TBP. It can be observed that the SCM could capture the trend of the flotation test results of the SRR and the PSR.

Mechanisms of oil adhesion in sandstone reservoir rock #1 (SRR #1)

It can be observed from Figure 12 that quartz dominated the composition of the SRR#1 (83.7%), its dominant BP was in the same order (< 0.1) as observed for 100% quartz sample (Figure 5). In addition, though the content of illite in the SRR #1 was small (8.8%), its contribution to the rock wettability was

relatively significant compared to the other minerals due to its large surface area. Thus, confirming that the intrinsic properties of the minerals dictate the wettability.
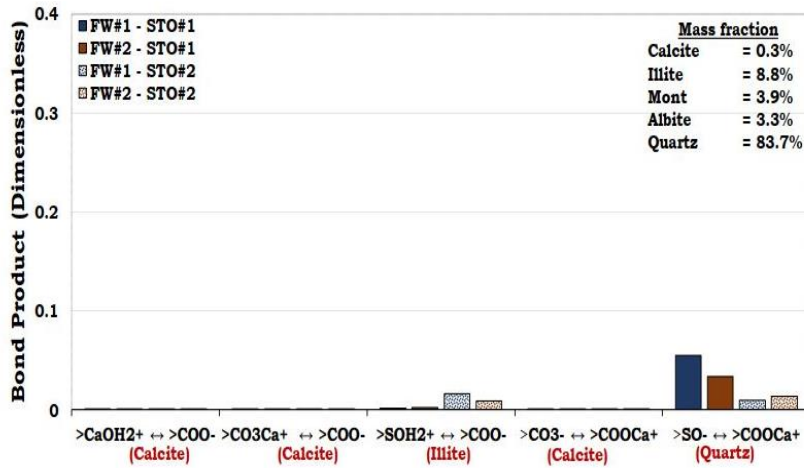
Figure 12 – The electrostatic pair linkages existing between the SRR #1-brine and oil-brine interfaces with unlike charges. It can be concluded that the SRR #1 is strongly hydrophilic due to its low oil adhesion tendencies.

Mechanisms of oil adhesion in sandstone reservoir rock #2 (SRR #2)

Similar to the composition of SRR #1 (Table 1) with high quartz content (83.7%), the SRR #2 composition (Table 1) was also dominated by quartz (94.9%). Hence, the electrostatic pair linkages existing between the SRR #2-brine and oil-brine interfaces also resulted in approximately the same order of oil adhesion (BP < 0.1) as observed in the SRR #1. It can also be observed that unlike SRR#1 composition with high illite content (8.8%), the SRR#2 composition on the other hand has relatively low content of illite (0.4%). Hence, direct adsorption of carboxylate onto the positive illite sites (>SOH$_2^-$) was not distinct in the latter as compared to the former. This is due to the smaller effective illite surface area to be bonded by the oil in the SRR #2 resulting from the lower illite content (0.4%) than in the SRR #1 (8.8%) though the intrinsic surface area remains the same. This shows that the effective surface area of the individual minerals constituting the reservoir rock has a profound effect on the wettability. The dominant electrostatic pair linkage for oil adsorption onto the SRR#2 was due to cation bridging (Ca^{2+}) of the two negatively charged surfaces namely, quartz (>SO$^-$) and carboxylate (>COO$^-$). In addition, direct adsorption of carboxylate (>COO$^-$) onto the positive sites on the SRR #2 minerals such as calcite (>CaOH$_2^-$) and illite (>SOH$_2^-$) also took place but was not distinct. This can be attributed to their negligible effective surface area available for the polar components in the oil to be bonded onto it due to their less dominance in the rock (i.e. low mass fractions).
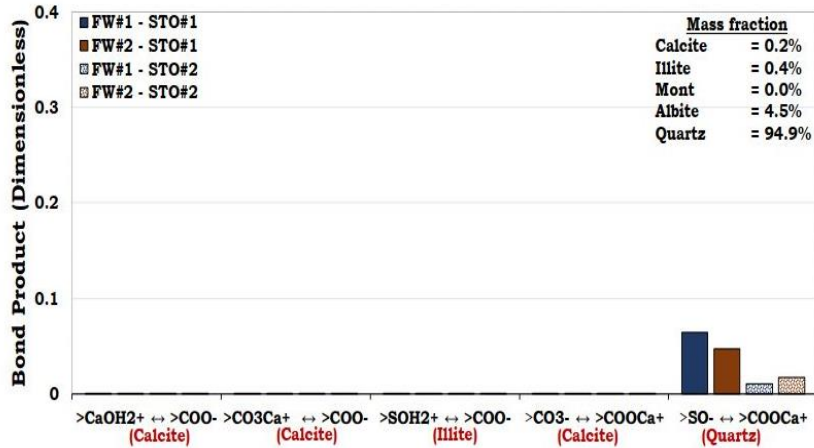
Figure 13 – The electrostatic pair linkages existing between SRR #2-brine and oil-brine interfaces with unlike charges. Similar to the SRR #1, the SRR #2 was also strongly hydrophilic as depicted by both the flotation test and SCM results.

Mechanisms of oil adhesion in Pseudo Sandstone Rock #1 and #2 (PSR #1 and PSR#2)

Unlike SRR#1 and SRR#2 with quartz dominating the composition of the sandstone reservoir rocks (83.7% and 94.9% respectively), the compositions of PSR#1 and PSR#2 were designed to evaluate the effect of increasing the surface area of the mixture by adding illite. For the PSR #1 with approximately 32% illite, it can be observed that direct adhesion of carboxylate ($>COO^-$) onto the positive illite surfaces ($>SOH_2^+$) dominated the oil adhesion (Figure 14). In addition, bridging by divalent cation (e.g. Ca^{2+}) also took place between the negatively oil ($>COO^-$) and quartz ($>SO^-$) surfaces.
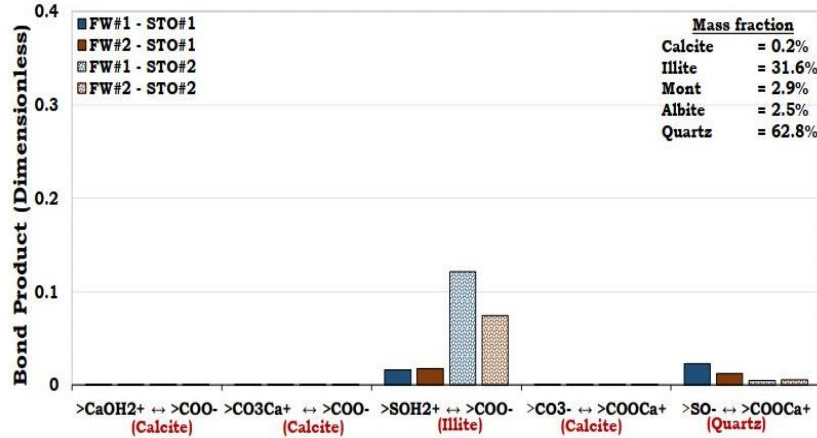
Figure 14 – The electrostatic pair linkages existing between PSR #1-brine and oil-brine interfaces with unlike charges. It can be observed that the surface area of the minerals has an overriding effect on the wetting preferences of the reservoir rock.

In a similar vein, direct adsorption of carboxylate ($>COO^-$) onto the positively charged illite sites ($>SOH_2^+$) also dominated the oil adhesion mechanisms in the PSR #2. From Figure 14, it can be observed that though illite was the second dominant mineral (~ 31.6%) in the mineral mixture, its interaction was stronger than that of quartz (~ 62.8%). It can also be observed from Figure 15 that though, quartz was the second dominant mineral in the PSR#2 (41.85%), the quartz-brine and oil-brine interaction was not distinct. This was attributed to its small intrinsic surface area thereby leading to negligible effective surface area as compared to illite. In other words, the illite overshadowed the contributions of the quartz due to its large effective surface area.
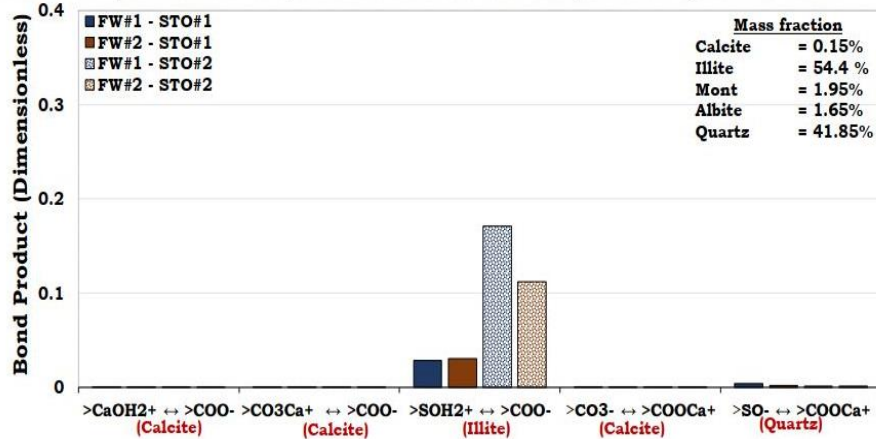

Figure 15 – The electrostatic pair linkages existing between PSR #2-brine and oil-brine interfaces with unlike charges. It can be observed that the surface area of the minerals has an overriding effect on the wetting preferences of the reservoir rock.

Mechanisms of oil adhesion in Pseudo Sandstone Rock #3 and #4 (PSR #3 and PSR#4)

Unlike PSR#1 and PSR#2 with illite dominated contents, PSR#3 and PSR#4 on the other hand were designed to be dominated by the hydrophobic mineral (calcite). This was to evaluate the effect of increasing the calcite content on the wetting preferences of the mineral mixtures. The dominant electrostatic pair linkages existing between the PSR #3-brine and the oil-brine interfaces was less than 0.1 (Figure 16).
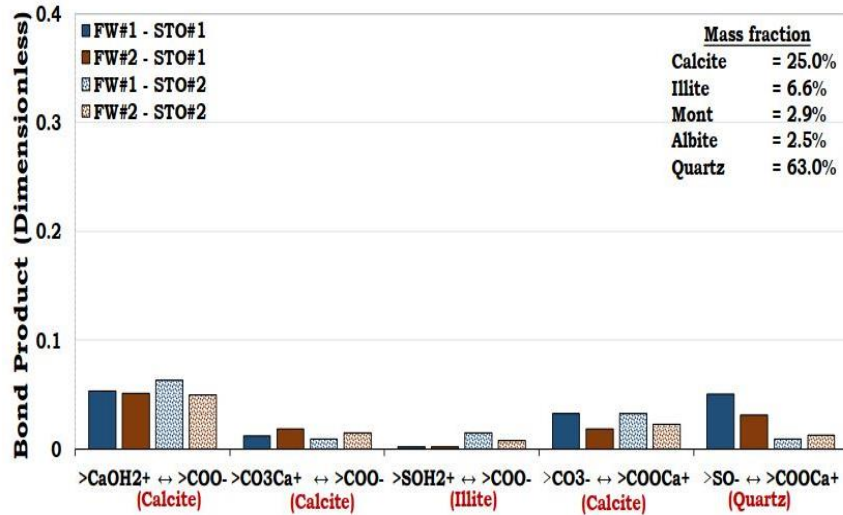
Figure 16 – The electrostatic pair linkages existing between PSR #3-brine and oil-brine interfaces with unlike charges. It can be inferred that increasing the contents of the hydrophobic mineral increases the hydrophobicity of the rock resulting from increase in its effective surface area

It can be observed from Figure 17 that the BP for the dominant electrostatic pair linkage in PSR #4 was approximately 0.3. Thus, confirming that increasing the calcite content of the sandstone rock increases its hydrophobicity as observed in PSR#4 (Figure 17). It can be observed that even with the same content of quartz (41.85%) in both the PSR#2 and PSR#4 (Figures 15 and 17 respectively), the adhesion of oil onto the latter was more distinct than the former. This was confirmed by the indistinct cation bridging (Ca^{2+}) existing between quartz-brine ($>SO^-$) and the oil-brine ($>COO^-$) interfaces in the PSR #2 as compared to PSR #4. This was due to the fact that the contributions from the quartz in PSR #2 was overshadowed by the minerals with large surface such as illite, hence the observed results. In other words, due to the small effective surface area of the PSR#4, the contribution from the quartz become more distinct than in PSR #2. It can also be observed that, even though the content of the illite in PSR#4 was negligible (4.4%), its presence was still felt due to its large effective surface area. Hence, confirming that the intrinsic surface area of the mineral has a pronounced effect on the wettability of the reservoir rock.
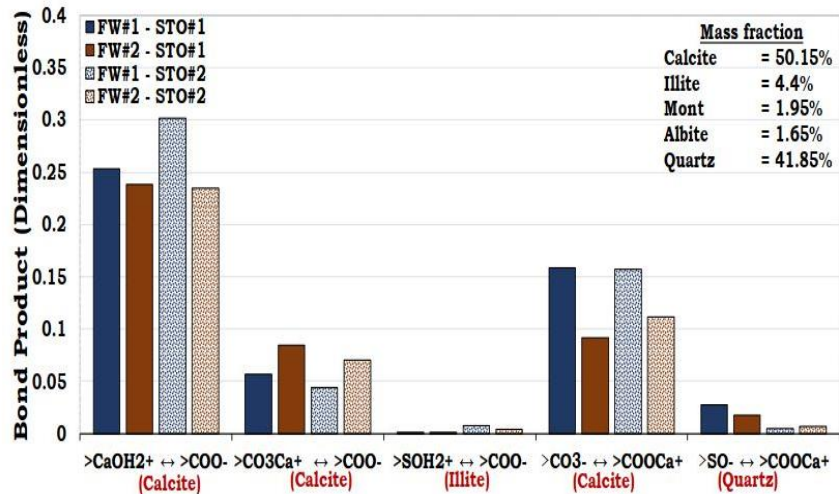
Figure 17 – The electrostatic pair linkages existing between PSR #4-brine and oil-brine interfaces with unlike charges. It can be inferred that increasing the contents of the hydrophobic mineral increases the hydrophobicity of the rock resulting from increase in its effective surface area

MINERAL-BRINE AND OIL-BRINE SURFACE CHARGE PREDICTION VIA SCM

To better understand the flotation test results for SRR and PSR, the mineral-brine and the oil-brine interface charges were also predicted via SCM for the individual minerals to evaluate the effect of the intrinsic surface charge on the wettability of the rock (SRR and PSR).

Mineral-brine interface charge estimation

From Figure 18, the surface charge of the illite-brine and the calcite-brine interface were positively charged. This was attributed to the dominant positive sites in both illite ($>SOH_2^+$) and calcite ($>CaOH_2^+$). Hence, increasing the content of these minerals in the PSR increases their tendencies to adsorb the carboxylate components in the oil ($>COO^-$) and hence, the observed results. On the other hand, the negative mineral-brine interface charge was attributed to the dominance of $>SO^-$ sites in quartz, albite and montmorillonite.
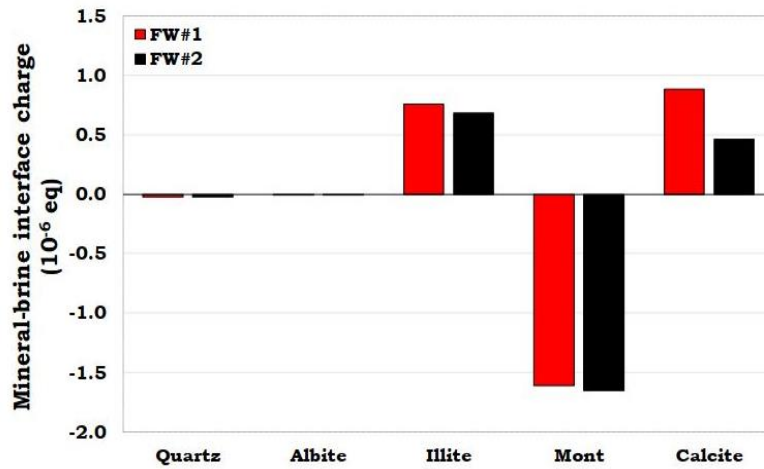
Figure 18 – Mineral-brine interface charge prediction.

Oil-brine interface charge estimation

The oil-brine interfaces were predominantly negatively charged with the exception of the STO#2-FW#1 interfaces of quartz, albite and calcite. This was attributed to the positive oil-complex formed by the divalent cation such as Ca^{2+} and Mg^{2+} in brine with carboxylate ($>COO^-$). Since the concentration of Ca^{2+} in the FW#1 was higher than FW#2 (Table 3), it can be concluded that more divalent cations are available to be bonded to the carboxylate ($>COO^-$) to form the positive oil complexes ($>COOCa^+$ and $>COOMg^-$).
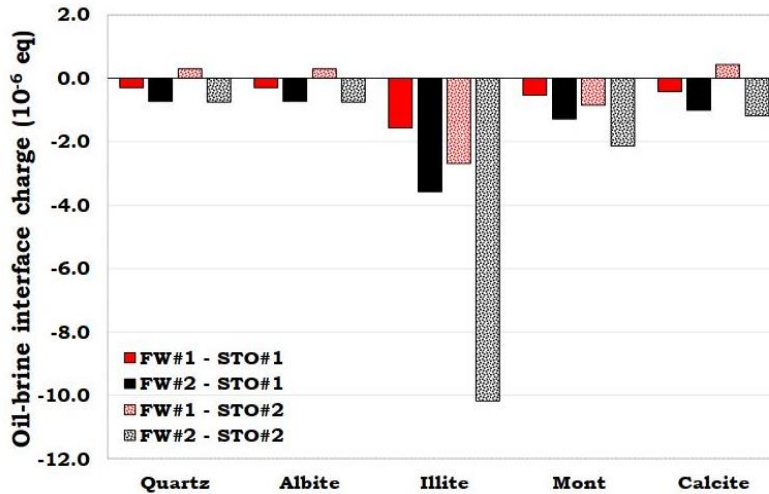
Figure 19 – Prediction of the oil-brine interface charges

Effect of the intrinsic properties on wettability; Flotation test versus effective surface area

The aim of this presented study has been to investigate the effect of increasing illite and calcite contents in the sandstone reservoir rock (SRR #1). It can be inferred from Figure 20 that the wetting preferences of the reservoir rocks were dictated by either the surface area or calcite content. In other words, PSR #1 and PSR #2 were illite dominated while the PSR #3 and PSR #4 were calcite dominated. Based on mass fraction, the dominant minerals in the studied SRR and PSR were quartz, illite and calcite with surface area 1.2 m^2/g, 66.8 m^2/g and 2 m^2/g respectively. For the SRR #1, its effective surface area (7.0 m^2/g) was illite dominated (5.88 m^2/g) and the second dominant mineral being quartz (1.00 m^2/g). Though the mass fraction of illite in the SRR #1 was relatively small (8.8%) compared to the quartz (83.7%), the inherent surface area of illite (66.8 m^2/g) was higher than quartz (1.2 m^2/g) and hence, the observed results. Since the wetting preferences of the two dominant minerals in the SRR #1 notably quartz (~0.05) and illite (~0.15) were both hydrophilic (Figure 3), it was not surprising that SRR #1 was also observed to be hydrophilic (Figure 20). Unlike the illite dominated SRR #1 with relatively high effective surface area (7.0 m^2/g), the SRR #2 on the other hand was quartz dominated and hence relatively small effective surface area (1.5 m^2/g). The effective surface area of the two dominant minerals in the SRR #2 were 1.14 m^2/g (quartz) and 0.27 m^2/g (illite). Though the mass fraction of illite in SRR #2 was negligible (0.4%) as compared to quartz (94.9%), the former also contributed meaningfully to the effective surface area of SRR #2 due to its relatively large intrinsic surface area (66.8 m^2/g) as compared to quartz (1.2 m^2/g). It was not surprising that the SRR #2 was hydrophilic since the dominant minerals in its composition such as quartz (~0.05) and illite (~0.15) were also observed to be strongly hydrophilic as depicted by the flotation tests results (Figure 3). Hence, it can be concluded that the wettability of the reservoir rocks (SRR #1 and SRR #2) were dictated by their effective surface area.
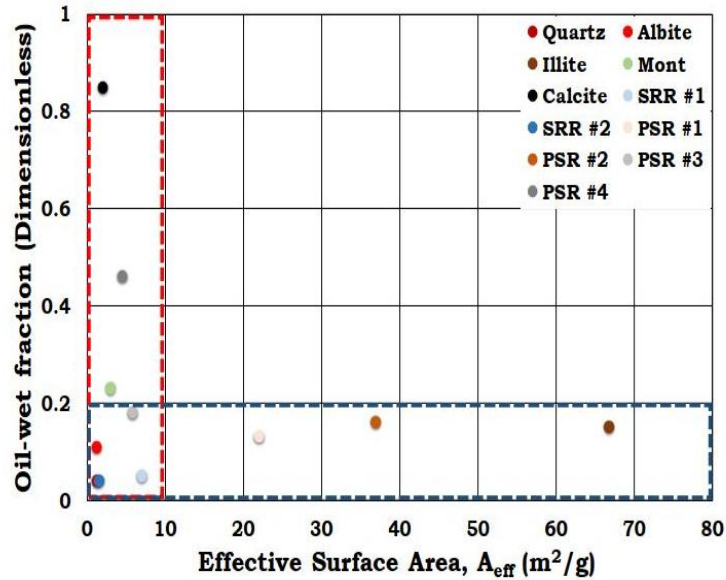
Figure 20 – Effect of the intrinsic surface area on wettability

Considering the mineral-mixtures with high illite contents (PSR #1 and PSR#2), it can be concluded that the wettability of the reservoir rock was dictated by the surface area of illite. In other words, the wettability of the pseudo-sandstone rocks (PSR #1 and PSR#2) were observed to be in the same order as the mineral with predominant surface area. Though the mass fraction of the illite in the PSR #1 was relatively small (31.6%) as compared to that of quartz (62.8%), its contribution to the effective surface area of the PSR #1 (22.0 m^2/g) was 21.11m^2/g as compared to quartz (0.75 m^2/g). As discussed earlier since both the SCM and the flotation test results revealed that illite and quartz were hydrophilic at the studied conditions, the wetting preference of the PSR #1 was as expected. Like the PSR #1, the effective surface area of the PSR #2 (36.9 m^2/g) was dominated by illite (36.34 m^2/g) while the contribution from quartz was negligible (0.5 m^2/g). This was attributed to the mass fraction of the constituent minerals (Table 1) and their intrinsic surface areas (Table 5). Finally, since the effective surface area of PSR #3 (5.8 m^2/g) and PSR#4 (4.5 m^2/g) were dictated by the illite (4.41 m^2/g and 2.94 m^2/g respectively), quartz (0.75 m^2/g and 0.50 m^2/g respectively) and calcite (0.50 m^2/g and 1.0 m^2/g respectively), it can be concluded that the calcite content play a more important role in the wetting preference of sandstone than that of the clay. In other words, unlike the PSR #1 and PSR #2 which were dominated by hydrophilic minerals (illite and quartz), the PSR #3 and PSR #4 were dominated by both hydrophilic (illite and quartz) and hydrophobic (calcite) minerals. Nonetheless, the flotation test and the SCM results reveal that the hydrophobic minerals have pronounced effect on wettability of the sandstone reservoir rock than the hydrophilic counterparts and hence, the observed results.

Understanding IOR mechanisms via the SCM technique

Fjelde et al. (2011) assessed the effect of both carbonated water (CW) and formation water (FW) on the oil recovery efficiency. They reported that the CW was found to improve the spontaneous imbibition of an outcrop chalk at realistic reservoir conditions.
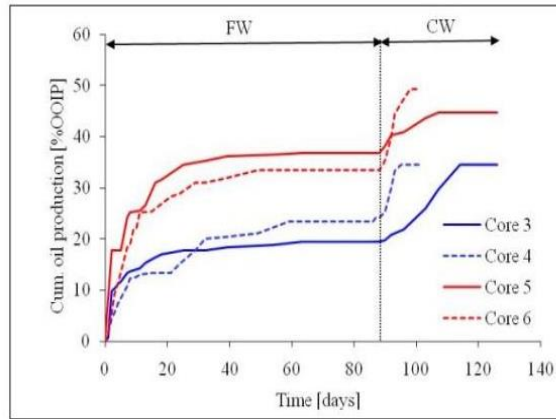
Figure 21 – Result of the spontaneous imbibition experiment in chalk from literature (Fjelde et al. 2011).

Prediction of COBR interactions during carbonated water (CW) imbibition in chalk

To understand the mechanisms during the FW and CW imbibition, the COBR interactions during the spontaneous imbibition experiments (Fjelde et al. 2011) were investigated. This was achieved by modelling the chalk-brine and oil-brine interactions during the spontaneous imbibition experiment via SCM. To accomplish this, the properties of the surfaces (oil and chalk) used in the spontaneous imbibition experiment were also used as input into the SCM. Since calcite is the dominant mineral in the chalk, the surface reactions and the reaction constants of the former were used as analogous for the latter. The Total Acid Number (TAN) and Total Base Number (TBN) of the Stock Tank Oil (STO) employed were 0.1 mg KOH/g oil and 1.3 mg KOH/g respectively. Table 7 gives the ionic composition of the brine used during the spontaneous imbibition experiment. From Figure 22, it can be observed that the dominant oil adhesion mechanism in the chalk exists between the positive chalk site ($>CaOH_2^+$) and the carboxylate ($>COO^-$). The SCM results revealed that the CW has the potential to alter the wettability of the chalk from more oil-wet to less oil-wet (Figure 22). In other words, the tendency of oil to be adsorbed onto the chalk surface as depicted by the Bond Product was observed to be higher for the FW (≈ 0.7) than CW (≈ 0.4). Hence, it can be concluded that the CW has the potential to desorb some of the adsorbed oil from the pore walls of the rock so that it can be mobilized to flow with the injected brine.

Table 7 – Ionic composition of the FW used in the studied spontaneous imbibition experiment in chalk (Fjelde et al. 2011).

Na^+	629.85
K^+	4.16
Mg^{2+}	22.03
Ca^{2+}	226.16
Cl^-	1130.40
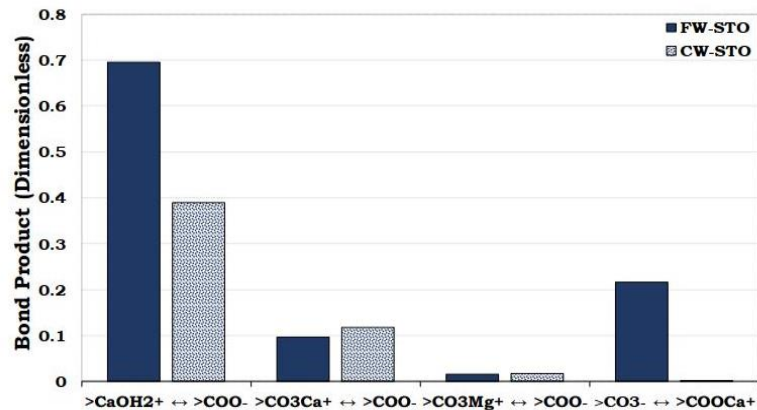
Figure 22 – SCM predictions of the chalk/CW/oil interactions during spontaneous imbibition experiment (Fjelde et al. 2011)

18

Discussions

The SCM technique of estimating wettability is a fast and cheap approach of characterizing wettability of minerals and reservoir rock via a geochemical simulator, PHREEQ-C. One striking advantage of the SCM technique over the existing wettability estimation techniques (e.g. the Amott and the USBM) is that, the SCM technique can predict the wetting tendencies of the minerals (rock). In addition, the SCM can estimate the mechanisms that led to the oil adhesion. Hence, it has the potential to be used in the design of wettability alteration processes for improving the oil recovery. The properties and quantities of the surfaces involved are used as input into the SCM and hence less time consuming unlike the conventional experimental techniques. Some of the SCM input parameters are the ionic composition of the brine, the surface reactions and the reaction constants of the surfaces involved (minerals and oil), the surface area and the site densities. Though, the SCM accounts for the effect of the mineralogical compositions in the model; nonetheless, the effect of the mineral distribution is yet to be captured as compared to the Amott and the USBM techniques. This is because the Amott and the USBM techniques estimate the wettability of the bulk rock while the flotation test estimates the wettability of crushed rock samples. The SCM estimates the wettability by assuming that all mineral surfaces are available for the reaction. The mineral surfaces available for the mineral-fluids interactions are determined by the mineral distribution. Nevertheless, the mineral distributions were not accounted for in both the SCM and the flotation test.

To add to the above, the Quartz Crystal Microbalance with Dissipation (QCM-D) technique characterizes the wettability by measuring the magnitude of oil adsorption onto mineral surfaces (Erzuah et al. 2018b). Unlike the Amott and the USBM techniques, the QCM-D wettability characterization technique is based on surface-surface interactions. In other words, the QCM-D approach relies on the mineral-fluids interactions at the contact surface area. The SCM technique of characterizing wettability is also based on the oil and mineral interactions at the contact surface area. The contact surface area of the mineral-brine and the oil-brine interactions during the flotation tests were higher than in core plugs during the Amott and USBM tests since crushed rocks were used. The tendency of the rock (minerals) to adsorb oil during COBR interactions were incorporated into the SCM using their effective surface area. Since the SCM wettability prediction is based on the attractive electrostatic pair linkages, the maximum surface area for oil adsorption was assumed to be the same as the effective surface area of the rock (mineral). Currently, the SCM technique is based on batch reactions, the plan is to extend the existing model to predict the in-situ reservoir wettability by incorporating into the model the kinetics and the mineral distributions.

---

4. Conclusions

The SCM could capture the trend in the flotation test results. Hence, a fast and cheap technique of characterizing the wettability of both minerals and reservoir rocks (mineral-mixtures) has been presented.

- o The ranking of the hydrophobicity of the dominant minerals in the studied sandstone reservoir rocks during the flotation test is given as quartz < albite < illite < Montmorillonite < calcite as confirmed by the its simulated counterparts.
- o For the studied sandstone rocks and pseudo-sandstone rocks, both the SCM and the flotation test results revealed that the wettability was inclined towards the minerals with highest effective surface area, except for rocks with high calcite content. Hence, it can be concluded that the calcite content has a strong influence on the wetting preferences of the studied sandstone rocks than that of the clay.
- o Unlike the flotation test, the SCM technique can predict both the wetting preferences and the oil adhesion mechanisms such as cation bridging and direct adhesion of carboxylate ($>COO^-$). For instance, cation bridging was the main oil adhesion mechanism in the studied sandstone reservoir rock-fluid systems.
- o For the carbonate minerals (calcite and pseudo-sandstone rocks with high calcite content), it was observed that direct adhesion of carboxylate was the main oil adhesion mechanisms. Nonetheless, oil adhesion by cation bridging mechanisms also occurred.

Nomenclature

BP	Bond Product
COBR	Crude oil/brine/rock
FW	Formation Water
QCM-D	Quartz Crystal Microbalance with Dissipation
SCM	Surface Complexation Modelling
SRR	Sandstone Reservoir Rock
STO	Stock Tank Oil
PSR	Pseudo-Sandstone Rock
TBP	Total Bond Product
Ψ	Electric potential

REFERENCES

Anderson, W. G. [1987]. Wettability Literature Survey Part 5: The Effects of Wettability on Relative Permeability. *Journal of Petroleum Technology* **39** (11): 1453 -1468. SPE-16323-PA.

Brady, P. V. and Krumhansl, J. L. [2012a]. A Surface Complexation Model of Oil–brine–sandstone Interfaces at 100° C: Low Salinity Waterflooding. *Journal of Petroleum Science and Engineering* **81**: 171-176.

Brady, P. V. and Krumhansl, J. L. [2012b]. Surface Complexation Modeling for Waterflooding of Sandstones. *SPE Journal,* **18** (02): 214 - 218. SPE-163053-PA.

Brady, P. V., Krumhansl, J. L. and Mariner, P. E. [2012]. Surface Complexation Modeling for Improved Oil Recovery. SPE IOR Symposium, Tulsa, Oklahoma, USA, Society of Petroleum Engineers. SPE-153744-MS.

Chen, Y. and Brantley, S. L. [1997]. Temperature-and pH-dependence of Albite Dissolution Rate at Acid pH. *Chemical Geology* **135** (3-4): 275-290.

Cockcroft, P., Guise, D. and Waworuntu, I. [1989]. The Effect of Wettability on Estimation of Reserves. SPE Asia-Pacific Conference, Sydney, Australia, Society of Petroleum Engineers. SPE-19484-MS.

Craig, F. J., [1971]. *The Reservoir Engineering Aspect of Waterflooding*. SPE Monograph Series. Dallas, Texas, Society of Petroleum Engineering of AIME.

Dubey, S. and Doe, P. [1993]. Base Number and Wetting Properties of Crude Oils. *SPE Reservoir Engineering* **8** (03): 195-200. SPE-22598-PA.

Erzuah, S., Fjelde, I. and Omekeh, A. [2017a]. Wettability Characterization Using the Flotation Technique Coupled with Geochemical Simulation. 19th European Symposium on Improved Oil Recovery, Norway.

Erzuah, S., Fjelde, I. and Omekeh, A. V. [2017b]. Wettability Estimation by Surface Complexation Simulations. SPE Europec featured at 79th EAGE Conference and Exhibition, Paris, France. SPE-185767-MS.

Erzuah, S., Fjelde, I. and Omekeh, A. V. [2018a]. Wettability Estimation by Surface Complexation Simulations. *SPE Reservoir Evaluation & Engineering-Formation Evaluation*. Accepted.

Erzuah, S., Fjelde, I. and Voke Omekeh, A. [2018b]. Wettability Estimation by Oil Adsorption Using Quartz Crystal Microbalance with Dissipation QCM-D. SPE Europec featured at 80th EAGE Conference and Exhibition, Copenhagen, Denmark. SPE-190882-MS.

Fjelde, I., Aasen, S. and Zuta, J. [2011]. Improvement of Spontaneous Imbibition in Carbonate Rocks by CO2-saturated Brine. 16th European Symposium on Improved Oil Recovery, Cambridge, UK.

Goldberg, S. [2013]. Surface Complexation Modeling. *Reference Module in Earth Systems and Environmental Sciences*.

Gu, X. and Evans, L. J. [2007]. Modelling the Adsorption of Cd (II), Cu (II), Ni (II), Pb (II), and Zn (II) onto Fithian Illite. *Journal of Colloid and Interface Science* **307** (2): 317-325.

Hjuler, M. and Fabricius, I. L. [2009]. Engineering Properties of Chalk Related to Diagenetic Variations of Upper Cretaceous Onshore and Offshore Chalk in the North Sea Area. *Journal of Petroleum Science and Engineering,* **68** (3-4): 151 - 170.

Katz, L. E. and Hayes, K. F. [1995]. Surface Complexation Modeling: I. Strategy for Modeling Monomer Complex Formation at Moderate Surface Coverage. *Journal of Colloid and Interface Science* **170** (2): 477-490.

Koretsky, C. [2000]. The Significance of Surface Complexation Reactions in Hydrologic Systems: a Geochemist's Perspective. *Journal of Hydrology* **230** (3-4): 127-171.

Morrow, N. R. [1990]. *Interfacial Phenomena in Petroleum Recovery*. CRC Press.

Mwangi, P., Thyne, G. and Rao, D. [2013]. Extensive Experimental Wettability Study in Sandstone and Carbonate-Oil-Brine Systems: Part 1–Screening Tool Development. International Symposium of the Society of Core Analysts, Napa Valley, California, USA. SCA3013-84.

Song, J., Zeng, Y., Wang, L., Duan, X., Puerto, M., Chapman, W. G., Biswal, S. L. and Hirasaki, G. J. [2017]. Surface Complexation Modeling of Calcite Zeta Potential Measurements in Brines with Mixed Potential Determining Ions (Ca^{2+}, CO_3^{2-}, Mg^{2+}, SO_4^{2-}) for Characterizing Carbonate Wettability. *Journal of Colloid and Interface Science* **506**: 169-179.

Sverjensky, D. A. and Sahai, N. [1996]. Theoretical Prediction of Single-site Surface-Protonation Equilibrium Constants for Oxides and Silicates in Water. *Geochimica et Cosmochimica Acta,* **60** (20): 3773 - 3797.

Sverjensky, D. A. and Sahai, N. [1998]. Theoretical Prediction of Single-site Enthalpies of Surface Protonation for Oxides and Silicates in Water. *Geochimica et Cosmochimica Acta,* **62** (23-24): 3703 - 3716.

Van Cappellen, P., Charlet, L., Stumm, W. and Wersin, P. [1993]. A Surface Complexation Model of the Carbonate Mineral-aqueous Solution Interface. *Geochimica et Cosmochimica Acta* **57** (15): 3505-3518.

Wieland, E., Wanner, H., Albinsson, Y., Wersin, P. and Karnland, O. [1994]. A Surface Chemical Model of the Bentonite-Water Interface and Its Implications for Modelling the Near Field Chemistry in a Repository for Spent Fuel. Swedish Nuclear Fuel and Waste Management Co.

Wolthers, M., Charlet, L. and Van Cappellen, P. [2008]. The Surface Chemistry of Divalent Metal Carbonate Minerals; A Critical Assessment of Surface Charge and Potential Data Using the Charge Distribution Multi-site Ion Complexation Model. *American Journal of Science* **308** (8): 905 - 941.

Paper VI

Surface Complexation Modelling (SCM) as a New Wettability Screening Tool versus the Existing Techniques. *Manuscript.*

Erzuah, Samuel; Fjelde, Ingebret; Omekeh, Aruoture Voke.

Paper VI

174

Paper VI

Surface Complexation Modelling (SCM) as a New Wettability Screening Tool versus the Existing Techniques

Samuel Erzuah[a,b], Ingebret Fjelde[a,b,c], Aruoture Voke Omekeh[a, c]

[a]The National IOR Centre of Norway, N-4036 Stavanger, Norway
[b]University of Stavanger (UiS), N-4036 Stavanger, Norway
[c]NORCE Norwegian Research Centre AS, P. O. Box 8046, N-4068 Stavanger, Norway

ABSTRACT

Since wettability controls the fluid phase distribution and flow properties such as capillary pressure and interfacial properties in reservoir multiphase flow, numerous existing techniques of estimating the wettability have been developed. The Amott and the United State Bureau of Mines (USBM) methods are the accepted wettability estimation techniques in the oil and gas industry. To add to the above, the flotation test, imbibition rate method, Nuclear Magnetic Resonance (NMR) are some of the qualitative wettability characterization techniques reported in literature. A remarkable feature that spans through all these existing wettability estimation techniques is that each technique characterizes the wettability based on a specific observed output but does not evaluate the crude oil/brine/rock (COBR) interaction mechanisms that triggered the observed outputs. For instance, the Amott test estimates the wettability by relying on the total volume of the fluids (i.e. imbibing and displacing fluids) that can be spontaneously and forcefully imbibed by the core. However, the COBR interactions that led to the measured volumes were not assessed. To add to the above, the flotation test characterizes the wettability by estimating the concentration of the particles in the fluid phases (oil and brine) but does not evaluate the COBR interactions that triggered the observed wetting preferences. Since wettability controls the fluid phase distribution and flow properties in the oil reservoir, it can be concluded that the measured outputs reported by the existing wettability estimation techniques were triggered by the COBR interactions on the pore walls of the rock. The aim of this presented study was to estimate the wettability by evaluating the COBR interactions via Surface Complexation Modelling (SCM) and compared with the wettability measurements from other existing techniques. Since the contact angle measurement technique is a fast wettability characterization approach, it was employed in this study. The contact angle measurements were carried out using the Drop Shape Analyzer (DSA) device. The substrates considered during the contact angle measurement includes; quartz, kaolinite, calcite and Bentheimer sandstone. Amott and USBM wettability measurements from literature were also predicted via SCM.

Both the contact angle measurements and their simulated counterparts reveal that the ranking of the hydrophilicity of the studied substrates was given as calcite < kaolinite < quartz < sandstone. In addition, the SCM technique could capture the main trends during Amott and USBM wettability measurements of the North Sea sandstone reservoir rocks in a study reported in the literature. The SCM results reveal that the mineralogy of the rock dictates the wetting preferences of the sandstone rock. For instance, the predicted SCM results for Amott and USBM wettability measurements from literature revealed that, the less water-wet state of the North Sea sandstone reservoir rock with higher calcite content was attributed to the direct adhesion of carboxylate ($>COO^-$) onto the positive calcite site ($CaOH_2^+$), i.e. $CaOH_2^+ \leftrightarrow >COO^-$. Thereby, increasing the hydrophobicity of the sandstone rock. Hence, the SCM technique is a promising wettability characterization tool.

1. Introduction

Wettability is the tendency of a fluid to spread on or adhere to the surface of a solid in the presence of other immiscible fluids (Craig 1971). Research has shown that wettability, capillary pressure, fluid-fluid and rock-fluid interfacial properties are indispensable parameters in order to accurately predict reservoir behaviour during both primary and secondary recovery (Torsaeter 1988). It has also been reported in literature that wettability is an inevitable parameter due to its pronounced effect on fluid phase distribution and flow properties in oil reservoirs (Anderson 1986b; Anderson 1987a, b; Radke et al. 1992). For instance the driving force during spontaneous imbibition is the capillary pressure (Ma et al. 1999). In multiphase flow, it has been shown that the wetting fluid occupies the smallest pore channels which is the most hydrodynamically resistive pore channels while the non-wetting fluid occupies the largest pore channel which is the least hydrodynamically resistive pore channel (Radke et al. 1992). Hence, wettability is an essential parameter due to its effect on rock-fluid properties such as relative permeability, capillary pressure and residual oil saturation (Anderson 1987a, b; Busireddy and Rao 2004; Radke et al. 1992; Torsaeter 1988). In addition, Hirasaki (1991) reported that the electrostatic force is controlled by the mineralogy, the composition of the crude oil, the salinity and pH of the brine. The composition of the crude oil dictates the wetting preferences of the rocks/minerals. Saturates, Aromatic, Resins and Asphaltenes (SARA) contents are the compositions of the crude oil with the heavy end fractions of the crude oil concentrated in the asphaltenes and resins (Dubey and Waxman 1991; Fan et al. 2002). It has also been reported by numerous authors that surface forces such as structural, van der Waals and electrostatic forces dictate the wetting of mineral/rock surface by either oil or water (Busireddy and Rao 2004; Hirasaki 1991; Wu et al. 2017). However, in this study the emphasis was placed on the role of the electrostatic forces on oil adhesion during Crude oil/Brine/Rock (COBR) interactions via a geochemical simulator, PHREEQ-C.

There are numerous existing techniques of estimating wettability, such as the Amott test, the United State Bureau of Mine (USBM) method, the contact angle measurements, the flotation test and the imbibition rate method (Anderson 1986a; Donaldson et al. 1969; Mwangi et al. 2013). In addition, wettability has also been characterized by measuring the magnitude of the adsorbed oil during the crude-oil/brine/rock (COBR) interactions via Quartz Crystal Micro-

balance with Dissipation (Erzuah et al. 2018b). However, each technique estimates the wetting preference based on a specific measured output. Hence, the various techniques might estimate different wetting preference for the same rock-fluid systems due to differences in the measured outputs. The contact angle measurement technique is one of the fastest and most common wettability characterization technique. The contact angle estimates the wettability of the rock/mineral by measuring the angle subtended by the rock/mineral substrate and the adsorbed oil at the three-phase contact region (Figure 1A). If the measured contact angle is less than 90°, the surface is preferentially water-wet while it is preferential oil-wet if the contact angle is greater than 90° (Anderson 1986a). However, the limitation of the contact angle method is that it measures the wettability on a polished mineral surface (Anderson 1986a). The COBR interactions at the three-phase contact region are dictated by the oil adhesion tendencies of the substrates (Figure 1B). For instance, lack of adhesion of the oil droplet onto the substrate depicts strongly hydrophilic medium and hence, the contact angle is negligible (≈0). Hence, understanding the COBR interactions at the contact surface can be used to characterize the wetting preferences. For the contact angle technique, the angle made by the adsorbed oil on mineral/rock surfaces is controlled by numerous factors such as the mineralogy of the rock, surface roughness, composition of the brine and composition of the oil.
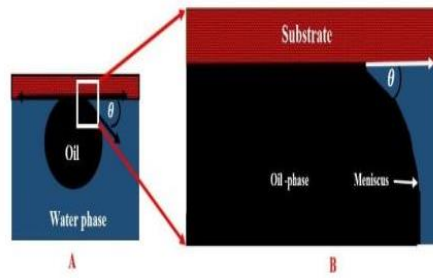

Figure 1 – Analogy of contact angle measurement of an oil/water/solid interfaces

Contrary to the contact angle measurement that estimates the wettability on a mineral substrate, the Amott and the USBM estimate the average wettability of porous medium such as core plugs (Anderson 1986a; Ma et al. 1999). Ma et al. (1999) reported that the Amott and USBM methods depend on capillary pressure and microscopic displacement efficiency. Numerous authors have estimated the wettability of core samples using the Amott technique (Amott 1959; Torsaeter 1988). The Amott wettability test is based on both spontaneous imbibition and forced displacement. The Amott-Harvey wettability index (I_{AH}) is given by the relation;

$$I_{AH} = \frac{V_{osp}}{V_{osp} + V_{od}} - \frac{V_{wsp}}{V_{wsp} + V_{wd}} \qquad (1)$$

Where

V_{osp} = Volume of oil produced after spontaneous imbibition of water into the core
V_{od} = Volume of oil produced after force imbibition of water into the core
V_{wsp} = Volume of water produced after spontaneous imbibition of oil into the core
V_{wd} = Volume of water produced after force imbibition of oil into the core

Since the measured volumes spontaneously and forcefully imbibed by the core during the Amott test are influenced by the COBR interactions on the pore walls, it can be inferred that the estimated wettability is dictated by rock-brine and oil-brine interactions. For instance, though both Amott and USBM technique measure different outputs (i.e. total volume imbibed by a core and area under the capillary pressure curve respectively), their wettability measurements might be different even for the same rock-fluid systems. Research has shown that the adsorption of high-molecular-weight surface-active compounds in the crude oil (e.g. asphaltene) onto the surface of the rock can lead to less water-wet state (Buckley and Liu 1998; Hui and Blunt 2000). Hence, if the oil adhesion tendencies of the rock can be estimated during the COBR interactions, the wetting preferences of the rock can be inferred. To add to the above, if the COBR interactions can be simulated, their wetting state can also be determined. Erzuah et al. (2017) predicted the oil/brine and mineral/brine interactions that can results in the adhesion of oil onto reservoir rock surface via SCM. Erzuah et al. (2018) estimated the wetting preferences of minerals and mineral mixtures based on their interactions with the flowing fluids phases. This was accomplished by estimating the oil adhesion tendencies of the individual minerals. For water-wet system, the water phase adheres to the pore walls and occupies the smallest pore channel while the non-wetting fluid (oil) occupies the largest pore channels (Figure 2). Considering the Amott test, imbibing the water-wet system with the wetting phase (water) leads to increase in saturation of the wetting phase (S_w) while the saturation of the non-wetting phase (oil) decreases ($S_o = 1 - S_w$). In other words, the change in saturation of the wetting and non-wetting phase inside the core is depicted by their respective produced volumes during the Amott and USBM.
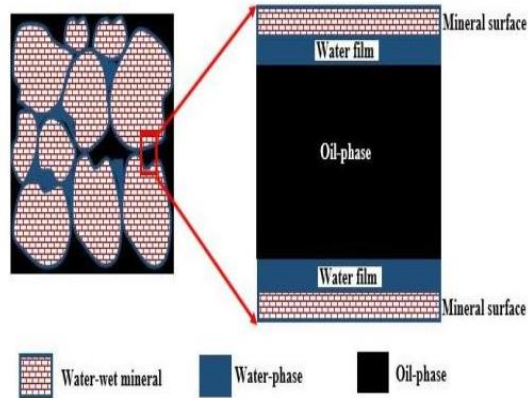
Figure 2 – Illustrates the mechanisms of oil adsorption onto the pore walls of a water-wet core plug during the Amott and the USBM wettability tests. The blue colour depicts water (brine) whiles the black depicts oil.

Oil-wet systems on the other hand has the largest pore channels occupied by the non-wetting fluid (water) while the wetting phase (oil) adheres to the surface of the pore walls and occupies the smallest pore channels (Figure 3). Hence, high spontaneous imbibition of oil in an oil-wet system is due to the displacement of the non-wetting phase (water) with the wetting phase (oil). In other words, if a medium spontaneously imbibe one fluid over the other, then the wetting preferences is inclined towards that fluid. All these observations are activated by the COBR interactions that is taking place on the pore walls.
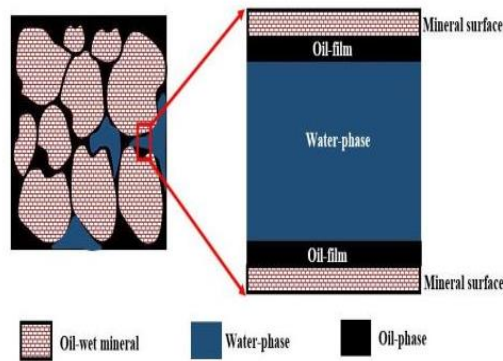
Figure 3 - Oil adsorption mechanisms onto the pore walls of an oil-wet core plug during the Amott and the USBM wettability tests. The blue colour depicts water (brine) whiles the black depicts oil.

To accomplish this, contact angle measurements for some dominant minerals in the sandstone reservoir rock notably quartz, kaolinite and calcite were carried out using Drop Shape Analyzer (DSA) device. In addition, the contact angle measurement was also carried out on sandstone substrate to assess the effect of the different mineralogical composition on wettability. The contact angle measurements were also predicted using the SCM technique. The Amott and USBM wettability data from literature (Torsaeter 1988) were also predicted using the SCM approach. The SCM estimates the wettability based on the mineral-fluid interactions by estimating the oil adhesion tendencies.

2. Method

The captive drop contact angle measurement technique was employed using a Drop Shape Analyzer (DSA) device. Quartz, kaolinite, calcite and Bentheimer sandstone rock were the substrates employed during the contact angle measurements. The SCM wettability characterization technique was also used to predict the oil adhesion tendencies of the substrate-fluid systems during the contact angle measurement. Finally, the Amott and USBM wettability estimation data from literature (Torsaeter 1988) were also predicted using the SCM techniques.

Materials used in the contact angle measurements and the existing wettability estimation techniques from literature

Three mineral substrates (quartz, kaolinite, calcite) and the outcrop sandstone rock (Bentheimer) were utilized in the contact angle measurements. Two oils (n-decane and stock tank oil, STO) and one Formation Water (FW) compositions were used as the fluid phases during the contact angle measurement. N-decane was used as the reference oil due to its non-polar nature. The Total Acid Number (TAN) and Total Base Number (TBN) of the STO used in the contact angle measurement were 0.06 mg KOH/g oil and 0.78 mg KOH/g oil respectively. The composition of the Bentheimer sandstone rock substrate used in the contact angle measurements was similar to the one reported in literature (Peksa et al. 2017) as provided in Table 1. Table 2 gives the ionic composition of the brine.

Table 1 – Mass composition of the Bentheimer sandstone substrate used in the contact angle measurements (Peksa et al. 2017)

Mineral	Bentheimer (%)
Quartz	91.7
Feldspar	4.9
Illite	1.0
Kaolinite	1.7
Iron hydroxide	0.3
Calcite	0.4

Table 2 – Ionic composition of the brine employed in the contact angle measurements.

ION	FW (mmol/L)
Na^+	1326.16
K^+	5.62
Mg^{2+}	17.46
Ca^{2+}	147.94
Sr^{2+}	8.44
Cl^-	1677.67
SO_4^{2-}	0.89

Contact angle measurement Procedure

To replicate the rock-fluid interactions in the reservoir prior to the crude oil accumulation, the mineral sample was aged in a known volume of the brine (20 ml) at the desired reservoir temperature (65°C) for 48 hours. At the end of the ageing period, the brine phase was separated and discarded while the excess brine on the mineral substrate was removed by centrifugation at 1000 rpm for barely 15minutes. The mineral substrate was then aged in a known volume (20 ml) of the desired oil at 65°C for 48 hours with back pressure to prevent the boiling out of the lighter components. The oil phase was removed and discarded while the excess oil on the mineral substrate was removed by centrifugation at 1000 RPM for 15 minutes. The prepared mineral was then mounted on its holder and placed in a pre-cleaned captive drop-cell (Drop Shape Analyzer, DSA, Krüss, Hamburg, Germany) while the chosen fluids (brine and oil) were stored in their respective vessels. With all the connections to the captive drop-cell secured and the camera in place, the Sessile drop-cell was then filled with the desired brine until the air in the system was expelled through the relief valve. The temperature and pressure were then set to their designated values (65°C and 5.7 bar respectively) and allowed to stabilize for 15 minutes. The oil droplets were then placed on the mineral surface and the contact angle measured after a stable measurement was attained (45 minutes). The contact angle measurement experimental set-up is illustrated in Figure 4.
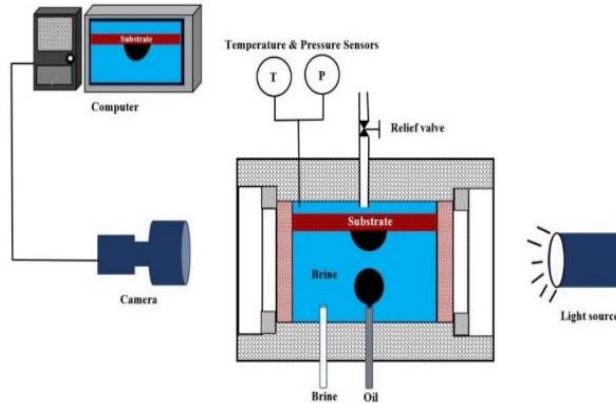

Figure 4 – Contact angle experimental set-up using the Drop Shape Analyzer (DSA) device.

Predicting the oil adhesion tendencies during wettability measurements via Surface Complexation Modelling (SCM)

Erzuah et al. (2018a) estimated the wettability of minerals and rock via SCM and supported by flotation test results. They accomplished this by evaluating the oil adhesion tendencies of the mineral (rock) by capitalizing on the electrostatic pair linkages existing between the oil-brine and the mineral-brine. In other words, since the SCM wettability characterization technique is based on a surface-surface interaction, the polar functional group on the oil and mineral surfaces were incorporated into the model by their representative surface site. For instance, the polar functional group in the crude oil were modelled using their representative acidic (>COOH) and the basic (>NH⁻) oil sites. The ">" denotes the surface sites of both the mineral and the oil surfaces. In addition, the potential oil complexes formed between the oil sites and the ions in the brine (Ca²⁺, Mg²⁺) such as >COOCa⁺ and >COOMg⁺ were also incorporated into the model. Like the oil surfaces, the mineral surfaces were incorporated into the model using their respective surface sites such as >Si-O-H, >Al-O-H and >CaOH. The oil adhesion tendencies of the minerals (rock) during the Amott, the USBM and the contact angle measurement techniques are analogous to Figure 5. The detail SCM procedure can be obtained from literature (Erzuah et al. 2017, 2018a).
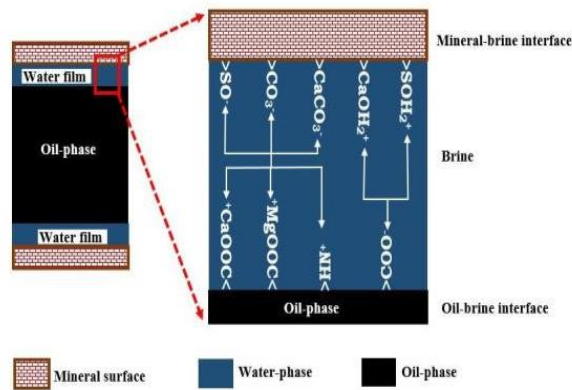

Figure 5 – Illustrates the mechanisms of oil adsorption onto the pore walls of a water-wet core plug during the contact angle, the Amott and the USBM wettability tests. The blue colour depicts water (brine) whiles the black depicts oil.

Surface Complexation Modelling (SCM) input parameters

Since the SCM estimate the oil adhesion tendencies by relying on the attractive electrostatic force existing between the rock-brine and the oil-brine interface, the properties and quantities of the materials were incorporated into the model. In other words, the properties of the rock-fluids system during the wettability measurements such as the contact angle measurements were used as input into the model. The SCM input parameters include the surface area, the composition of the fluid phases (brine and oil), the site densities of the surfaces (mineral and oil). The mineral site densities for numerous minerals have been reported in literature. For the sandstone reservoir rock, the individual minerals sites were used whiles the effective surface area (A$_{eff}$) of the rock was used as input into the SCM. Erzuah et al. (2018a) reported that the effective surface area, A$_{eff}$, (m²/g) of the rock can be calculated based on the mass fraction of the mineral i (dimensionless) and the intrinsic surface area (m²/g) is given by the relation;

$$A_{eff} = \sum_{n=1}^{\infty} m_i A_i \qquad (2)$$

Erzuah et al. (2018a) reported that surface-active components in the crude oil were converted into their representative oil site densities with the assumption that effective surface area of the rock is the same as the respective oil surface. The oil site relation according to Erzuah et al. (2018a) is given as;

$$\text{Oil Site Density (site/nm}^2) = \frac{\text{TAN or TBN(mg KOH/g oil)}}{\text{Mw KOH (g/mol)}} \times \frac{\text{Avogadros Constant}}{\text{Effective Surface Area (m}^2/g)} \qquad (3)$$

The surface sites, surface area and surface reaction of quartz and plagioclase were obtained from Sverjensky and Sahai (1996) while enthalpy used was assumed to be the same as a similar reaction as kaolinite (Sverjensky and Sahai 1998). The surface reactions and the reaction constants for the feldspar used was similar to that of microline while the surface site and surface area were obtained from Sverjensky and Sahai (1996). The SCM input parameters (surface sites and surface area) for illite were obtained from Gu and Evans (2007) while the reaction constants were obtained from similar reaction as kaolinite (Sverjensky and Sahai 1998). The Surface reaction of kaolinite were obtained from Brady & Krumhansl (2012) while its surface area was obtained from (Langmuir 1997). The surface reactions and the reaction constants for iron hydroxide were obtained from Sverjensky and Sahai (1996) while that of calcite were obtained from Van Cappellen et al. (1993). The surface area of calcite (Hjuler and Fabricius 2009) while the site densities were obtained from Wolthers et al. (2008). For the chlorite, the surface reaction and the reaction constants used was similar to that of muscovite (Sverjensky and Sahai 1996) while its surface area after (Jones 1981). Finally, the surface sites and the surface reaction constants of the individual minerals constituting the rock were used as input into the model. The effective surface area and the oil site densities used were as reported by Erzuah et al. (2018). NB. The temperature effect for the surface reaction of plagioclase, feldspar, illite, iron hydroxide and chlorite were assumed to be the same as that of quartz. Detailed description of the SCM technique of wettability characterization can be obtained from literature (Erzuah et al. 2017, 2018a). The oil and minerals site densities are provided in Tables 3 and 4 respectively. The surface reactions and their reaction constants for the various minerals can be obtained from Table 6.

Table 3 – SCM input parameters: Equivalent oil site densities for the surface-active components in the STO.

Surface	Equivalent oil surface	STO Site Density (site/nm^2)	Surface Area (m^2/g)
Quartz	>COOH	0.89	1.20
	>NH$^-$	16.99	1.20
Feldspar	>COOH	10.73	0.1
	>NH$^-$	203.85	0.1
Illite	>COOH	0.02	66.8
	>NH$^-$	0.31	66.8
Kaolinite	>COOH	0.11	10.00
	>NH$^-$	2.04	10.00
Iron hydroxide	>COOH	0.89	1.2
	>NH$^-$	16.99	1.2
Calcite	>COOH	0.54	2.00
	>NH$^-$	10.20	2.00

NB. Both the oil site densities and the effective surface area (A_{eff}) were obtained using Equations 2 and 3 respectively. The effective surface area (A_{eff}) of the oil used in Equation 3 was assumed to be the same as that of the mineral or rock surface.

Table 4 – SCM input parameters for the mineral surfaces

Surface	Site Density (site/nm^2)	Surface Area (m^2/g)
Quartz	10.00[a]	1.20[f]
Plagioclase	1.155[b]	1.20[g]
Feldspar	10.00[*]	0.100[h]
Illite	1.37[c]	66.80[i]
Kaolinite	1.16[d]	10.00[j]
Iron hydroxide	10.00[*]	1.20[k]
Calcite	4.90[e]	2.00[l]
Chlorite	10.00[*]	128.00[m]

[a], [b] and [f], [g] after Sverjensky and Sahai (1996, 1998).
[c] after Gu and Evans (2007)
[d], [i] and [j] after Brady and Krumhansl (2012)
[e] after Wolthers et al. (2008)
[h, k] after Langmuir (1997)
[l] after Hjuler and Fabricius (2009)
[m] after Jones (1981)
[*] Set to a similar reaction as quartz (Sverjensky and Sahai 1996, 1998)

Table 5 – Oil and mineral surfaces reactions and their reaction constants

Surface Reaction	log K @ 25°C	Enthalpy (KJ/mol)
[a]Oil Surface		
$>NH^+ \leftrightarrow >N + H^+$	-6.0	34.0
$>COOH \leftrightarrow >COO^- + H^+$	-5.0	0.0
$>COOH + Ca^{2+} \leftrightarrow >COOCa^+ + H^+$	-3.8	1.2
$>COOH + Mg^{2+} \leftrightarrow >COOMg^+ + H^+$	-4.0	1.2
[b]Quartz		
$>Si\text{-}O\text{-}H + H^+ \leftrightarrow >Si\text{-}O\text{-}H_2^+$	-1.1	-26.4
$>Si\text{-}O\text{-}H \leftrightarrow >Si\text{-}O\text{-} + H^+$	-8.1	8.4
[c]Plagioclase		
$>Si\text{-}O\text{-}H + H^+ \leftrightarrow >Si\text{-}O\text{-}H_2^+$	1.9	-26.4
$>Si\text{-}O\text{-}H \leftrightarrow >Si\text{-}O\text{-} + H^+$	-8.5	8.4
[d]Feldspar		
$>Si\text{-}O\text{-}H + H^+ \leftrightarrow >Si\text{-}O\text{-}H_2^+$	2.5	-26.4
$>Si\text{-}O\text{-}H \leftrightarrow >Si\text{-}O\text{-} + H^+$	-8.9	8.4
[e]Illite		
$>Si\text{-}O\text{-}H + H^+ \leftrightarrow >Si\text{-}O\text{-}H_2^+$	7.43	-26.4
$>Si\text{-}O\text{-}H \leftrightarrow >Si\text{-}O\text{-} + H^+$	-8.99	8.4
$H^+ + NaX_{ill} \leftrightarrow HX_{ill} + Na^+$	1.58	
[f]Kaolinite		
$>Al\text{-}O\text{-}H_2^+ \leftrightarrow >Al\text{-}O\text{-}H + H^+$	-3.0	0.0
$>Al\text{-}O\text{-}H \leftrightarrow >Al\text{-}O^- + H^+$	-3.8	32.0
$>Al\text{-}O\text{-}H + Ca^{2+} \leftrightarrow >Al\text{-}O\text{-}Ca^{2+} + H^+$	-9.7	45.0
$>Al\text{-}O\text{-}H + CaOH+ \leftrightarrow >Al\text{-}O\text{-}CaOH + H^+$	-4.5	45.0
$>Si\text{-}O\text{-}H \leftrightarrow >Si\text{-}O\text{-} + H^+$	-7.0	32.0
$>Si\text{-}O\text{-}H + Ca^{2+} \leftrightarrow >Si\text{-}O\text{-}Ca^{2+} + H^+$	-9.7	45.0
$>Si\text{-}O\text{-}H + CaOH+ \leftrightarrow >Si\text{-}O\text{-}CaOH + H^+$	-4.5	45.0
[g]Iron hydroxide		
$>Si\text{-}O\text{-}H + H^+ \leftrightarrow >Si\text{-}O\text{-}H_2^+$	7.5	-26.4
$>Si\text{-}O\text{-}H \leftrightarrow >Si\text{-}O\text{-} + H^+$	-10.2	8.4
[h]Calcite		
$>CO_3H \leftrightarrow >CO_3^- + H^+$	-4.9	-5.0
$>CO_3H + Ca^{2+} \leftrightarrow >CO_3Ca^+ + H^+$	-2.8	25.7
$>CO_3H + Mg^{2+} \leftrightarrow >CO_3Mg^+ + H^+$	-2.2	4.5
$>CaOH + H^+ \leftrightarrow >CaOH_2^+$	12.2	-77.5
$>CaOH \leftrightarrow >CaO^- + H^+$	-17.0	116.4
$>CaOH + 2H^+ + CO_3^{2-} \leftrightarrow >CaHCO_3 + H_2O$	24.2	-90.7
$>CaOH + CO_3^{2-} + H^+ \leftrightarrow >CaCO_3^- + H_2O$	15.5	-61.6
$>CaOH + SO_4^{2-} + H^+ \leftrightarrow >CaSO_4^- + H_2O$	13.9	-72.0
[i]Chlorite		
$>Si\text{-}O\text{-}H + H^+ \leftrightarrow >Si\text{-}O\text{-}H_2^+$	3.7	-26.4
$>Si\text{-}O\text{-}H \leftrightarrow >Si\text{-}O\text{-} + H^+$	-9.0	8.4

[a] and [f] after (Brady et al. 2012)
[b, c, d, g] and [i] after (Sverjensky and Sahai 1996, 1998)
[e] after (Gu and Evans 2007)
[h] after (Van Cappellen et al. 1993; Wolthers et al. 2008)
Note. The enthalpy of plagioclase, feldspar, illite, iron hydroxide and chlorite were assummed to be same as similar surface reactions in quartz

3. Results

The contact angle measurements will be presented prior to presenting their simulated counterparts. In addition, the electrostatic interactions existing between the mineral-brine and the oil-brine interfaces were also assessed to evaluate their oil adhesion mechanisms via SCM. Finally, the presented SCM technique of estimating wettability was used to predict the Amott and USBM wettability measurements from a study reported in the literature (Torsaeter 1988).

Contact angle measurement results

The contact angle measurement for minerals notably quartz, kaolinite and calcite will be presented in the same order prior to presenting that of the Bentheimer sandstone substrate. For the contact angle measurements, the results of the reference experiments (n-decane) are presented before presenting that of the STO. The experimental error during the contact angle measurements was observed to be ±3°.

Quartz: N-decane & STO

It can be observed from Figure 6 that the contact angle measurement of quartz/n-decane/brine system was approximately 46° and hence preferentially hydrophilic. This can be linked to the absence of surface-active component in the reference oil (n-decane). For the quartz/STO/brine system, the contact angle was measured to be approximately 58°. It can be concluded that the polar oil components in the crude oil had minor effect on the oil adsorption at the three-phase region. Hence, quartz can be said to be strongly hydrophilic.

$\theta \approx 46°$ $\theta \approx 58°$
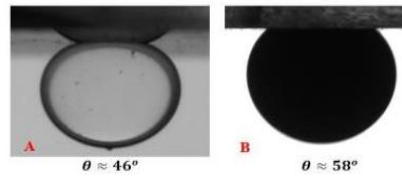
Figure 6 – Contact angle measurement of quartz/oil/brine system using the Sessile drop technique. N-decane was used as the reference oil while the STO was used as the test fluid to evaluate the effect of the polar oil components on the wetting preferences of the quartz substrate.

Kaolinite: N-Decane & STO

Like quartz/n-decane/brine system (Figure 6A), the contact angle measured for the kaolinite/n-decane/brine system (Figure 7A) was also relatively small ($\approx48°$). This can be credited to the absence of polar functional group in the n-decane. For the kaolinite/STO/brine system (Figure 7B), the contact angle was measured to be approximately 64°. Hence, the kaolinite (Figure 7B) was less hydrophilic as compared to quartz (Figure 6B).


$\theta \approx 48°$ $\theta \approx 64°$
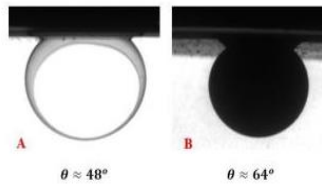
Figure 7 – Contact angle measurement of kaolinite/oil/brine system using the Sessile drop technique. N-decane was used as the reference oil while the STO was used as the test fluid to evaluate the effect of the polar oil components on the wetting preferences of the kaolinite substrate.

Calcite: N-decane & STO

Similar to the quartz/n-decane/brine (Figure 6A) and kaolinite/n-decane/brine (Figure 7A) systems, the calcite/n-decane/brine (Figure 8A) system was also strongly hydrophilic ($\approx47°$) due to lack of surface-active component in the reference oil (n-decane). However, for the calcite/STO/brine interface (Figure 8B), the contact angle was measured to be approximately 121°. This can be attributed to the presence of polar oil component in the STO and the strong hydrophobicity of calcite.

$\theta \approx 47°$ $\theta \approx 121°$
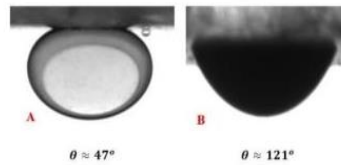
Figure 8 – Contact angle measurement of calcite/oil/brine system using the Sessile drop technique. N-decane was used as the reference oil while the STO was used as the test fluid to evaluate the effect of the polar oil components on the wetting preferences of the calcite substrate.

Sandstone: N-decane & STO

Like the mineral substrates, the contact angle of Bentheimer sandstone measured with the reference oil (n-decane) was also small ($\approx45°$). Since quartz had the dominant mass concentration in the Bentheimer sandstone rock ($\approx 91\%$), it was not surprising that the measured contact angle ($\approx50°$) with the STO was in the same order as the quartz/STO/brine system (Figure 6B).

$\theta \approx 45°$ $\theta \approx 50°$
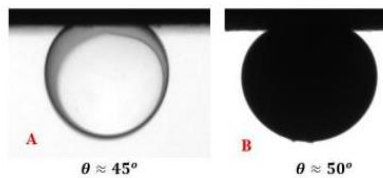
Figure 9 – Contact angle measurement of sandstone (Bentheimer)/oil/brine system using the Sessile drop technique. N-decane was used as the reference oil while the STO was used as the test fluid to evaluate the effect of the polar oil components on the wetting preferences of the sandstone substrate.

Prediction of the oil adhesion tendencies of the rock/mineral substrates via SCM

For the rock/fluids system, the contact angle is governed by the wetting preferences of the minerals/rock at the three-phase region. The mineral/brine/oil interactions during the contact angle measurements were evaluated via SCM. This was achieved by predicting the Total Bond Product (TBP) which is the tendency of oil to be adsorbed onto the mineral/rock surfaces (Erzuah et al. 2017, 2018a). For the simulated mineral/n-decane/brine systems, it can be observed from Figure 10 that the n-decane has negligible effect on the oil adhesion due to lack of polar oil component in the reference oil (n-decane). This was also supported by the low contact angle measurements for the studied mineral (rock)/n-decane/brine (Figures 6, 7, 8 and 9). The simulated mineral (rock)/STO/brine shows that quartz was strongly hydrophilic (TBP < 0.1) while calcite was strongly hydrophobic (TBP ≈ 1). This shows that the tendency of the oil to be adsorbed onto quartz is negligible as compared to calcite. This was also confirmed by the contact angle measurements ($\theta = 58°$ and $\theta = 121°$ respectively) as depicted in Figures 6B and 8B. Hence, for the studied mineral (rock) substrates the wettability in increasing order of hydrophobicity is given as Bentheimer sandstone < quartz < kaolinite < calcite.
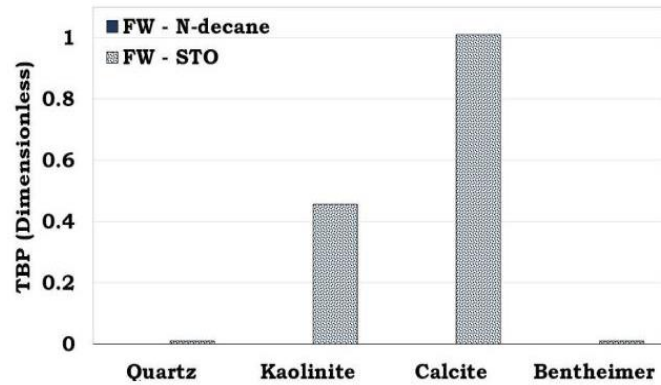

Figure 10 – Predicted oil adhesion tendencies (TBP) of the minerals/rock during the contact angle measurement via SCM. The TBP of FW/n-decane system is zero for all the minerals/rocks due to the non-polar nature of the n-decane.

Considering the oil adhesion mechanisms for calcite/STO/brine interactions, the Bond Product (BP) which measures the electrostatic pair linkages existing between the mineral-brine and oil-brine interfaces was relatively high (BP ≈ 0.58). Hence, calcite can be concluded to be strongly oil-wet as supported by its contact angle measurement (Figures 8B). The major BP for kaolinite and quartz were approximately 0.3 and < 0.1 respectively (Figure 11). This confirms that the tendency for oil to be adsorbed onto kaolinite and quartz is low as compared to calcite (Figure 11). Direct adsorption of carboxylate (>COO⁻) onto the positively charged calcite surface (>CaOH₂⁺) dominated the oil adhesion mechanisms during the calcite/STO/brine system. Nonetheless, divalent cations (Ca²⁺ and Mg²⁺) bridging between the negative calcite (>CO₃⁻) and oil surfaces (>COO⁻) also contributed to the adhesion of oil onto calcite. Cation bridging was the dominant oil adhesion mechanism for kaolinite and it exists between the negative kaolinite sites (>AlO⁻ and >SiO⁻) and that of the carboxylate (>COO⁻). Like the kaolinite, cation bridging was the dominant oil adhesion mechanism for the quartz/STO/brine system. Nonetheless, the cation bridging mechanism was less pronounced in the quartz than in kaolinite. The quartz-brine and the oil-brine electrostatic pair linkage existed between the negative quartz site (>SiO⁻) and carboxylate (>COO⁻) surface. However, the tendency of oil to be adsorbed onto kaolinite (TBP ≈ 0.44) is relatively high as compared to quartz (TBP < 0.1) as depicted in Figure 10.
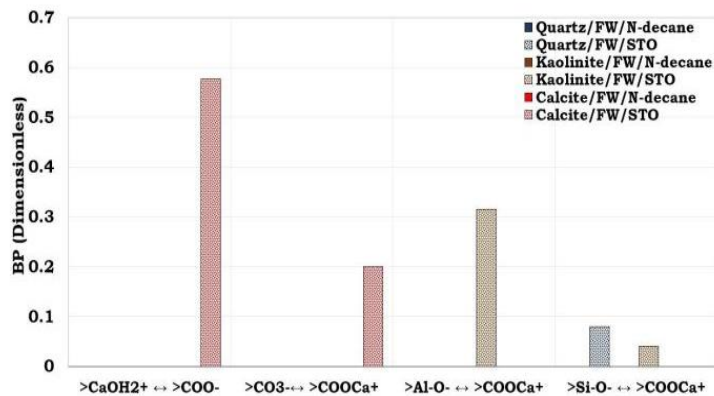

Figure 11 – Simulated crude oil/brine/rock (COBR) interactions at the three-phase region during the contact angle experiments

10

Amott and USBM wettability measurement from literature (Torsaeter 1988)

The Amott and USBM wettability measurements on sandstone reservoir rocks from the North Sea (Torsaeter 1988) exhibited varying degree of water-wetness (Figure 12). The sandstone reservoir rocks samples from first coring depth intervals (A and B) were relatively strongly hydrophilic as compared to the second (C and D) and third (E and F) coring intervals for both the Amott and USBM (Figure 12). However, the sandstone reservoir rocks from the second coring depth were the least hydrophilic.
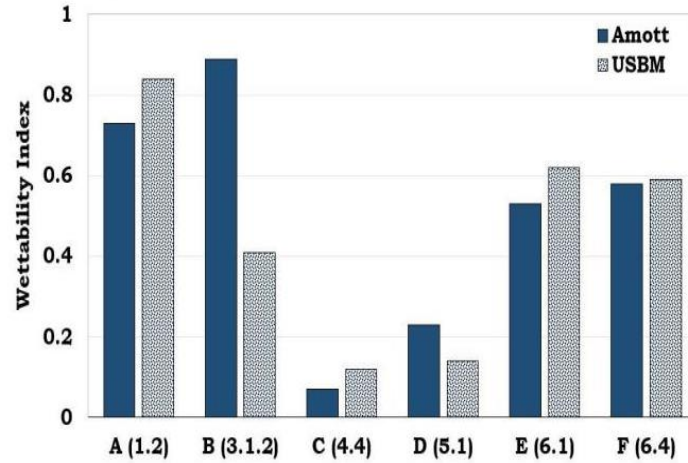

Figure 12 – Amott and USBM wettability measurement results from literature (Torsaeter 1988). The sandstone core plugs from first (A and B), second (C and D) and third (E and F) intervals.

Simulated Amott and USBM wettability measurements from literature (Torsaeter 1988) via SCM

To predict the Amott and USBM wettability measurement from literature (Torsaeter 1988), the properties of the materials in the wettability experimental work was used as input into the model. The Total Acid Number (TAN) and the Total Base Number (TBN) of the STO used in the Amott and USBM wettability measurements were 0.02 mg KOH/g oil and 1.1 mg KOH/g oil respectively. The TAN and TBN were converted to their effective oil site densities using Eqn (3) as suggested by Erzuah et al. (2017, 2018a). The estimated oil site densities are given in Table 6.

Table 6 – Estimated oil site densities of the STO used in the Amott and USBM wettability measurement after Torsaeter (1988)

Surface	Equivalent oil surface	STO Site Density (site/nm^2)	Effective Surface Area (m^2/g)
Quartz	>COOH	0.18	1.20
	>NH$^+$	9.83	1.20
Plagioclase	>COOH	0.18	1.20
	>NH$^+$	9.83	1.20
Feldspar	>COOH	2.15	0.1
	>NH$^+$	118.02	0.1
Illite	>COOH	0.003	66.8
	>NH$^+$	0.18	66.8
Kaolinite	>COOH	0.02	10.00
	>NH$^+$	1.18	10.00
Iron hydroxide	>COOH	0.18	1.2
	>NH$^+$	9.83	1.2
Calcite	>COOH	0.11	2.00
	>NH$^+$	5.90	2.00
Chlorite	>COOH	0.002	128
	>NH$^+$	0.09	128

NB. Equations 2 and 3 were used to estimate the oil site densities and the effective surface area (A$_{eff}$) respectively. However, Equation 3 is base on the assumption that the effective surface area (A$_{eff}$) of the oil was the same as its respective mineral or rock surface.

The mineralogical composition of the North Sea Sandstone employed by Torsaeter (1988) in the wettability measurements are given in Table 7. The surface reactions and the reaction constant of the North Sea Sandstone are similar to the one reported for Bentheimer sandstone substrate in Table 5 during the contact angle measurements. Hence, the ionic composition of the brine (Table 8), the oil site density (Table 6) and mineral site density (Table 4) were used as input into the SCM to predict the oil adhesion tendencies during the Amott and USBM wettability measurements.

Table 7 – Composition of the North Sea Sandstone used in the Amott and USBM wettability measurement after Torsaeter (1988).

Mineral	Field S_1 (%)	Field S_2 (%)	Field S_3 (%)
Quartz	53.2	63.8	52.0
Plagioclase	19.2	15.0	17.7
Feldspar	16.0	11.4	8.9
Illite	1.7	2.0	4.4
Kaolinite	8.0	6.2	5.5
Calcite	1.4	0.0	9.9
Chlorite	0.5	1.6	1.6

NB. Field S_1, Field S_2 and Field S_3 depicts the first, second and third coring depth respectively.

Table 8 – Ionic composition of the brine used in the Amott and USBM wettability measurement after Torsaeter (1988).

ION	FW (mmol/L)
Na^+	533.61
K^+	3.07
Mg^{2+}	6.66
Ca^{2+}	28.00
Cl^-	599.75
HCO_3^-	6.26

The COBR interactions during the Amott and USBM wettability measurements (Torsaeter 1998) can now be estimated using the SCM input parameters (Tables 4, 5, 6 and 8) of the surfaces as used in the experiments. The SCM results could capture the main trends during the Amott and USBM wettability measurements (Torsaeter 1998) except the core plugs retrieved from the second depth interval (i.e. Cores C and D). From Figure 13, it can be observed that the tendency of oil to be adsorbed onto the Core A and B were relatively low (< 0.02) as compared to Cores E and F ($\approx$ 0.04). This confirms the strongly hydrophilic nature of the Cores A and B as depicted in Figure 12. Unlike Cores A and B, the oil adhesion onto Cores E and F were relatively high (Figure 13) as confirmed by the Amott and USBM wettability measurements (Figure 12). However, the predicted wettability measurement of Cores C and D were on the same order as Cores A and B (Figure 13) though their wettability measurements suggested otherwise (Figure 12). This is because, the SCM wettability technique is based on the rock-fluids (crude oil/brine/rock) interactions. Hence, since the rock-fluids systems in both the first and second coring depth were similar i.e. less calcite contents (Tables 7, 8 and STO composition), it was not surprising that the SCM method predicted approximately the same results for the first and second coring depths (Figure 13).
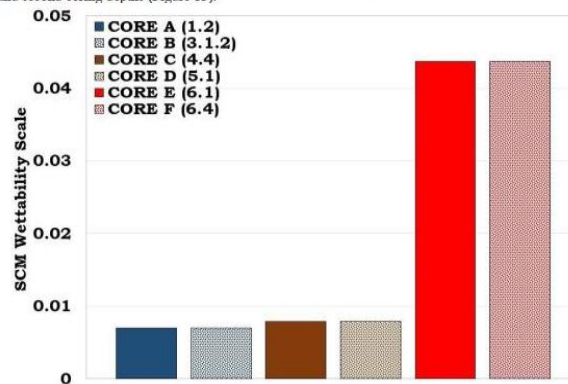

Figure 13 – Prediction of the Amott and USBM wettability results from literature (Torsaeter 1988) via SCM. Note that for strongly water-wet medium, the tendency of oil to be adhere onto the solid surface (SCM wettability scale) is 0 while it is 1 if the medium is strongly oil-wet.

Mechanisms of oil adhesion onto the pore wall of the reservoir rock
The mechanisms during the oil adsorption were also evaluated to better understand the wetting preferences of the North Sea sandstone reservoir rocks employed by Torsaeter (1998). It can be concluded that direct adsorption of carboxylate ($>COO^-$) onto the positive calcite and chlorite sites ($>CaOH_2^+$ and $>SOH_2^+$ respectively) dominated the adhesion of oil onto the Cores E and F (Figure 14). From Figure 13, the relatively high oil adhesion tendencies of the third coring depth interval (Cores E and F) were linked to their high calcite contents (9.9%) as compared to the first (1.4%) and the second (0.0%) coring depth intervals (Table 7). Hence, it can be concluded that the wetting preferences of the sandstone rocks used by Torsaeter (1998) in Figure 12, are dictated by the calcite content as predicted by SCM results (Figures 13 and 14). In addition, cation (Ca^{2+}) bridging mechanisms also dominated the oil adhesion mechanism in the studied North Sea sandstone rocks. However, the cation bridging mechanisms were only prominent in Cores E and F unlike Cores A, B, C and D. In other words, the bridging of the negative calcite site ($>CO_3^-$) and the carboxylate ($>COO^-$) surface by divalent cation such as Ca^{2+} and Mg^{2+} led to the adhesion of oil onto the rock surface (Figure 14). Hence, the results were expected since the content of calcite in core plugs retrieved from the third depth interval (Cores E and F) were relatively high (9.9%) as compared to the other intervals as depicted in Table 7. In addition, though, the content of chlorite in the three intervals were relatively small (0.5%, 1.6% and 1.6% respectively), the electrostatic pair linkages existing between the chlorite-brine ($>SOH_2^+$) and the carboxylate ($>COO^-$) were relatively high due to its large surface area (128 m²/g) compared to the other mineralogical constituents in the sandstone rock.

12
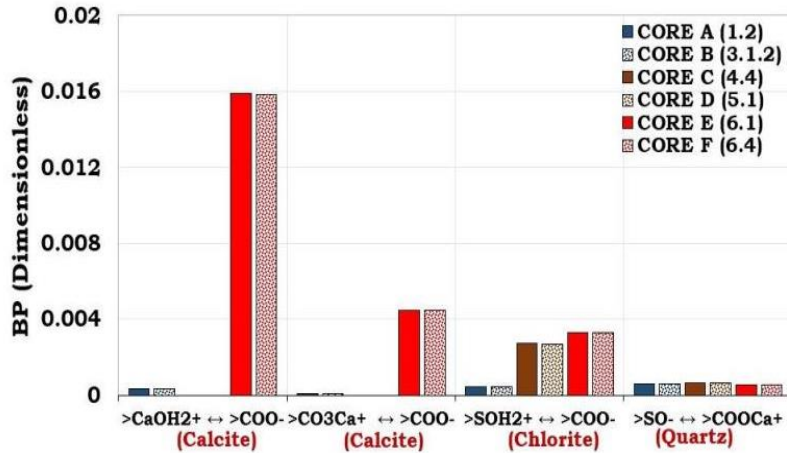
Figure 14 – Mechanisms of oil adhesion onto the pore walls of the sandstone reservoir core plugs during the Amott and USBM wettability measurements via SCM. Note that the low BP is attributed to the hydrophilicity of sandstone rocks as reported in literature.

Discussions

The SCM technique is a fast approach of screening the wettability of reservoir rocks and fluids (brine and oil) of varying compositions by capitalizing on the attractive electrostatic forces existing between the rock-brine and oil-brine interfaces via a geochemical simulator, PHREEQ-C. Unlike the existing wettability estimation techniques, the SCM approach can predict the wetting preferences of the rock in addition to the mechanisms that led to their wetting properties. For example, direct adhesion of carboxylate ($>COO^-$) onto the positive rock-brine interface was observed in calcite. However, if the rock-brine and oil-brine interfaces were both negatively charged, the wetting preferences of the rock will be less water-wet if divalent cations (Ca^{2+} and Mg^{2+}) in the brine bridge the two surfaces leading to oil adhesion. Hence, the SCM technique can be used in the design of injection brine for EOR processes. The existing wettability estimation techniques such as the Amott and the USBM estimates the wettability by measuring a specific output such as the total volume imbibed by the core (Amott test) and the area under the capillary pressure curve (USBM method). Hence, Amott and the USBM wettability techniques might estimate different wetting state even for the same rock-fluid systems. The SCM technique estimates the tendency for oil to be adsorbed onto the rock during the COBR interactions and it is dictated by only the rock and fluids (oil and brine) properties. For instance, for a given core plug (e.g. Core B) the Amott test described it to be strongly hydrophilic state (I_{AH} = 0.89) while the USBM technique suggested a relatively less hydrophilic state (USBM = 0.41) for the same rock-fluids system as depicted in Figure 12. The SCM results depicts that tendency for the oil to be adsorbed onto the pore walls of the cores (e.g. Core B) was low and hence hydrophilic (Figure 13) as confirmed by the Amott and USBM wettability measurements (Figure 12). Note that, it was not surprising that the SCM wettability prediction for the core plug retrieved from the first (Cores A and B) and second (Cores C and D) depth intervals were approximately the same due to their similar mineralogical (Table 7) and fluids (oil and brine) compositions. Nevertheless, the results of the Amott and USBM wettability measurements carried out by Torsaeter (1998) reported otherwise. Though, wettability governs the fluid phase distribution and flow properties (capillary pressure and relative permeability), nonetheless the pore geometry, pore size and mineral distributions in the core will also influence the flow properties and the measured volumes for the more traditional Amott and USBM methods. Hence, the plan is to extend the existing SCM technique to capture these effects. Thereby, improving the accuracy of the SCM wettability predictions.

4. Conclusions

It can be concluded that the SCM wettability approach could capture the trend in the existing experimental wettability data. One important advantage of the SCM technique over the existing techniques is that it does not only characterize the wetting state but also it unravels the mechanisms that led to the observed wetting state such as cation bridging and direct adhesion of carboxylate. Hence, the SCM technique can be used to screen potential injection water compositions to assess their potential to optimize oil recovery. Some of the advantages of the SCM technique over the existing techniques include;

- o The SCM technique is a fast and cheap wettability characterization approach as compared to the experimental wettability measurements. This is due to the fact that the inputs into the SCM are the properties and quantities of the studied rock-fluids system via a geochemical simulator (PHREEQ-C).
- o SCM can help to get better understanding of the wettability especially if there are some deviations in the Amott and USBM results. Nonetheless, the distribution of minerals in the rock and the kinetics of the minerals are yet to be incorporated into the SCM simulator.
- o The SCM results reveals that the mineralogical compositions of the reservoir rock dictate the wettability. For example, the sandstone reservoir rock with relatively high calcite content was less hydrophilic due to the adhesion of carboxylate ($>COO^-$) onto the positive calcite site ($>CaOH_2^+$). To add to the above, the contact angle measurements confirm the SCM results.
- o The ranking of the hydrophobicity of the substrates during the contact angle measurements and their simulated counterparts is given as Bentheimer sandstone rock < quartz < kaolinite < calcite.
- o The SCM technique could capture the trends in the Amott and USBM wettability measurements for the studied sandstone core plugs from literature, except the core plugs retrieved from the second depth intervals (Cores C and D). The SCM wettability predictions for the Core plugs C and D were in the same order as Core plugs A and B due to similar mineralogical compositions of the core (i.e. low contents of calcite). Hence, it can be concluded that the calcite content is very important for the wetting preferences in sandstone rocks.

Nomenclature

A_{eff}	Effective surface area of the rock
BP	Bond Product
COBR	Crude oil/brine/rock
DSA	Drop Shape Analyser
FW	Formation Water
I_{AH}	Amott-Harvey Index
SCM	Surface Complexation Modelling
STO	Stock Tank Oil
TAN	Total Acid Number
TBN	Total Base Number
TBP	Total Bond Product
USBM	United Bureau of Mines
V_{osp}	Volume of oil produced after spontaneous imbibition of water into the core
V_{od}	Volume of oil produced after force imbibition of water into the core
V_{wsp}	Volume of water produced after spontaneous imbibition of oil into the core
V_{wd}	Volume of water produced after force imbibition of oil into the core
θ	Contact angle

Acknowledgements

REFERENCES

Amott, E. [1959]. Observations Relating to the Wettability of Porous Rock. Fall Meeting of Los Angeles Basin Section, Los Angeles, California, Society of Petroleum Engineers. SPE-1167-G.

Anderson, W. [1986a]. Wettability Literature Survey-Part 2: Wettability Measurement. *Journal of Petroleum Technology* **38** (11): 1246 - 1262.

Anderson, W. G. [1986b]. Wettability Literature Survey- Part 1: Rock/Oil/Brine Interactions and the Effects of Core Handling on Wettability. *Journal of Petroleum Technology* **38** (10): 20. SPE-13932-PA.

Anderson, W. G. [1987a]. Wettability Literature Survey-Part 4: Effects of Wettability on Capillary Pressure. *Journal of Petroleum Technology* **39** (10): 1283-1300. SPE- 15271-PA

Anderson, W. G. [1987b]. Wettability Literature Survey Part 5: The Effects of Wettability on Relative Permeability. *Journal of Petroleum Technology* **39** (11): 1453 -1468. SPE-16323-PA.

Brady, P. V., Krumhansl, J. L. and Mariner, P. E. [2012]. Surface Complexation Modeling for Improved Oil Recovery. SPE IOR Tulsa, Oklahoma, USA., Society of Petroleum Engineers. SPE-153744-MS.

Buckley, J. and Liu, Y. [1998]. Some Mechanisms of Crude Oil/Brine/Solid Interactions. *J Pet Sci and Eng* **20** (3 - 4): 155 -160.

Busireddy, C. and Rao, D. N. [2004]. Application of DLVO Theory to Characterize Spreading in Crude oil-Brine-Rock Systems. SPE/DOE Symposium on Improved Oil Recovery, Tulsa, Oklahoma, Society of Petroleum Engineers. SPE-89425-MS.

Craig, F. J., [1971]. *The Reservoir Engineering Aspect of Waterflooding*. SPE Monograph Series. Dallas, Texas, Society of Petroleum Engineering of AIME.

Donaldson, E. C., Thomas, R. D. and Lorenz, P. B. [1969]. Wettability Determination and its Effect on Recovery Efficiency. *Society of Petroleum Engineers Journal* **9** (01): 13-20. SPE-2338-PA.

Dubey, S. and Waxman, M. [1991]. Asphaltene Adsorption and Desorption from Mineral Surfaces. *SPE Reservoir Engineering* **6** (03): 389-395.

Erzuah, S., Fjelde, I. and Omekeh, A. V. [2017]. Wettability Estimation by Surface Complexation Simulations. SPE Europec featured at 79th EAGE Conference and Exhibition, Paris, France. SPE-185767-MS.

Erzuah, S., Fjelde, I and Omekeh, A. V. [2018a]. Wettability Estimation by Surface Complexation Simulations. *SPE Reservoir Evaluation & Engineering-Formation Evaluation*. SPE-185767-PA. Accepted.

Erzuah, S., Fjelde, I. and Voke Omekeh, A. [2018b]. Wettability Estimation by Oil Adsorption Using Quartz Crystal Microbalance with Dissipation QCM-D. SPE Europec featured at 80th EAGE Conference and Exhibition, Copenhagen, Denmark. SPE-190882-MS.

Paper VI

14

Fan, T., Wang, J. and Buckley, J. S. [2002]. Evaluating Crude Oils by SARA Analysis. SPE/DOE Improved Oil Recovery Symposium, Society of Petroleum Engineers. SPE-75228-MS.

Gu, X. and Evans, L. J. [2007]. Modelling the Adsorption of Cd (II), Cu (II), Ni (II), Pb (II), and Zn (II) onto Fithian Illite. *Journal of Colloid and Interface Science* **307** (2): 317-325.

Hirasaki, G. [1991]. Wettability: Fundamentals and Surface Forces. *SPE Formation Evaluation* **6** (02): 217-226. SPE- 17367-PA

Hjuler, M. and Fabricius, I. L. [2009]. Engineering properties of chalk related to diagenetic variations of Upper Cretaceous onshore and offshore chalk in the North Sea area. *Journal of Petroleum Science and Engineering* **68** (3-4): 151-170.

Hui, M.-H. and Blunt, M. J. [2000]. Effects of Wettability on Three-Phase Flow in Porous Media. *Journal of Physical Chemistry,* **104** (16): 3833 - 3845.

Jones, A. A. [1981]. Charges on the surfaces of two chlorites. *Clay Miner* **16** (4): 347-359.

Langmuir, D. [1997]. *Aqueous environmental*. Prentice Hall.

Ma, S., Zhang, X., Morrow, N. and Zhou, X. [1999]. Characterization of Wettability from Spontaneous Imbibition Measurements. *Journal of Canadian Petroleum Technology* **38** (13).

Mwangi, P., Thyne, G. and Rao, D. [2013]. Extensive Experimental Wettability Study in Sandstone and Carbonate-Oil-Brine Systems: Part 1–Screening Tool Development. International Symposium of the Society of Core Analysts held in Napa Valley, California, USA. SCA3013-84.

Peksa, A. E., Wolf, K.-H. A., Slob, E. C., Chmura, Ł. and Zitha, P. L. [2017]. Original and Pyrometamorphical Altered Bentheimer Sandstone; Petrophysical Properties, Surface and Dielectric Behavior. *Journal of Petroleum Science and Engineering* **149**: 270-280.

Radke, C., Kovscek, A. and Wong, H. [1992]. A Pore-Level Scenario for the Development of Mixed Wettability in Oil Reservoirs. SPE Annual Technical Conference and Exhibition, Washington, D.C. Society of Petroleum Engineers. SPE-24880-MS.

Sverjensky, D. A. and Sahai, N. [1996]. Theoretical Prediction of Single-site Surface-Protonation Equilibrium Constants for Oxides and Silicates in Water. *Geochimica et Cosmochimica Acta,* **60** (20): 3773 - 3797.

Sverjensky, D. A. and Sahai, N. [1998]. Theoretical Prediction of Single-site Enthalpies of Surface Protonation for Oxides and Silicates in Water. *Geochimica et Cosmochimica Acta,* **62** (23-24): 3703 - 3716.

Torsaeter, O. [1988]. A Comparative Study of Wettability Test Methods Based on Experimental Results From North Sea Reservoir Rocks. SPE Annual Technical Conference and Exhibition, Houston, Texas, Society of Petroleum Engineers. SPE-18281-MS.

Van Cappellen, P., Charlet, L., Stumm, W. and Wersin, P. [1993]. A Surface Complexation Model of the Carbonate Mineral-aqueous Solution Interface. *Geochimica et Cosmochimica Acta* **57** (15): 3505-3518.

Wolthers, M., Charlet, L. and Van Cappellen, P. [2008]. The Surface Chemistry of Divalent Metal Carbonate Minerals; A Critical Assessment of Surface Charge and Potential Data Using the Charge Distribution Multi-site Ion Complexation Model. *American Journal of Science* **308** (8): 905 - 941.

Wu, J., Liu, F., Yang, H., Xu, S., Xie, Q., Zhang, M., Chen, T., Hu, G. and Wang, J. [2017]. Effect of Specific Functional Groups On Oil Adhesion From Mica Substrate: Implications For Low Salinity Effect. *Journal of Industrial and Engineering Chemistry* **56**: 342-349.